Fall 2009

Optimization-based dynamic prediction of 3D human running

Hyun-Joon Chung
University of Iowa

OPTIMIZATION-BASED DYNAMIC PREDICTION OF 3D HUMAN RUNNING

by

Hyun-Joon Chung

An Abstract

Of a thesis submitted in partial fulfillment of the
requirements for the Doctor of Philosophy degree
in Mechanical Engineering
in the Graduate College of
The University of Iowa

December 2009

Thesis Supervisors: Professor Jasbir S. Arora
Professor Karim Abdel-Malek

ABSTRACT

Mathematical modeling of human running is a challenging problem from analytical and computational points of view. Purpose of the present research is to develop and study formulations and computational procedures for simulation of natural human running. The human skeletal structure is modeled as a mechanical system that includes link lengths, mass moments of inertia, joint torques, and external forces. The model has 55 degrees of freedom, 49 for revolute joints and 6 for global translation and rotation. Denavit-Hartenberg method is used for kinematics analysis and recursive Lagrangian formulation is used for the equations of motion. The dynamic stability is achieved by satisfying the zero moment point (ZMP) condition during the ground contact phase. B-spline interpolation is used for discretization of the joint angle profiles. The joint torque square, impulse at the foot strike, and yawing moment are included in the performance measure. A minimal set of constraints is imposed in the formulation of the problem to simulate natural running motion. Normal running with arm fixed, slow jog along curves, and running with upper body motion are formulated. Simulation results are obtained for various cases and discussed. The cases are running with different foot locations, running with backpack, and running with different running speeds. Also, extreme cases are performed. Each case gives reasonable cause and effect results. Furthermore, sparsity of the formulation is studied. The results obtained with the formulation are validated with the experimental data. The proposed formulation is robust and can predict natural motion of human running.

Abstract Approved:

_____
Thesis Supervisor

_____
Title and Department

_____
Date

_____
Thesis Supervisor

_____
Title and Department

_____
Date

OPTIMIZATION-BASED DYNAMIC PREDICTION OF 3D HUMAN RUNNING

by

Hyun-Joon Chung

A thesis submitted in partial fulfillment of the
requirements for the Doctor of Philosophy degree
in Mechanical Engineering
in the Graduate College of
The University of Iowa

December 2009

Thesis Supervisors: Professor Jasbir S. Arora
Professor Karim Abdel-Malek

Graduate College
The University of Iowa
Iowa City, Iowa

CERTIFICATE OF APPROVAL

_____

PH.D. THESIS

_____

This is to certify that the Ph.D. thesis of

Hyun-Joon Chung

has been approved by the Examining Committee
for the thesis requirement for the Doctor of Philosophy
degree in Mechanical Engineering at the December 2009 graduation.

Thesis Committee: _____
Jasbir S. Arora, Thesis Supervisor

_____
Karim Abdel-Malek, Thesis Supervisor

_____
Salam Rahmatalla

_____
Jia Lu

_____
Shaoping Xiao

To my parents

ACKNOWLEDGMENTS

First of all, I thank my advisor Professor Jasbir Arora for his guidance and supervision to my Ph.D. study. Not only his academic knowledge but also attitude to the research influenced and improved my study a lot. And also, I thank my co-advisor Professor Karim Abdel-Malek for giving me opportunity of this work and encouraging me in everything. Thank to Professor Salam Rahmatalla for the motion capture data and the validation of running simulation. I thank to Professor Jia Lu and Shaoping Xiao for serving as committee of my dissertation.

I also thank all my friends in virtual soldier research lab, Yujiang Xiang, Anith Mathai, Joo Hyun Kim, Rajan Bhatt, Tim Marler, Steve Beck, Chris Murphy, Kim Farrell, Andy Taylor, Hyun Jung Kwon, Katha Sheth, Mahdiar Hariri, and Jun Hyuk Choi for their help.

Finally, I thank to my parents with all my love. This work is dedicated to them.

ABSTRACT

Mathematical modeling of human running is a challenging problem from analytical and computational points of view. Purpose of the present research is to develop and study formulations and computational procedures for simulation of natural human running. The human skeletal structure is modeled as a mechanical system that includes link lengths, mass moments of inertia, joint torques, and external forces. The model has 55 degrees of freedom, 49 for revolute joints and 6 for global translation and rotation. Denavit-Hartenberg method is used for kinematics analysis and recursive Lagrangian formulation is used for the equations of motion. The dynamic stability is achieved by satisfying the zero moment point (ZMP) condition during the ground contact phase. B-spline interpolation is used for discretization of the joint angle profiles. The joint torque square, impulse at the foot strike, and yawing moment are included in the performance measure. A minimal set of constraints is imposed in the formulation of the problem to simulate natural running motion. Normal running with arm fixed, slow jog along curves, and running with upper body motion are formulated. Simulation results are obtained for various cases and discussed. The cases are running with different foot locations, running with backpack, and running with different running speeds. Also, extreme cases are performed. Each case gives reasonable cause and effect results. Furthermore, sparsity of the formulation is studied. The results obtained with the formulation are validated with the experimental data. The proposed formulation is robust and can predict natural motion of human running.

TABLE OF CONTENTS

LIST OF TABLES

LIST OF FIGURES

CHAPTER 1

INTRODUCTION

1.1. Motivation

Major motivation of this research is to study the human running problem with digital human models. A digital human is a human-like character in the physics-based world. Therefore, a digital human can perform different tasks such as walking, running, and stair climbing in the virtual environment. Nowadays, people want to have an interface for design of any product that is related to human factors. A virtual prototype may decrease development costs or reduce any risk that exists in the real-world environment. Therefore, digital human dynamics simulation is a new frontier and a hot area of research at the present time.

In many multi-body dynamics commercial codes, the numerical integration solver has been used to solve equations of motion for a physical system (forward dynamics). However, this method does not have the capability to predict how a human moves. Therefore, we somehow need to solve the equations of motion in a way that predicts how humans move. Moreover, the kinetics and physiological parameters need to be monitored in addition to the kinematical parameters because the user needs to monitor all forces, such as joint torques. Therefore, we introduce the method of predictive dynamics. It is a new method that can predict the human motion that satisfies the dynamics equations of motion. It is an optimization-based approach with physics-based constraints. One does not have to integrate the dynamics equations of motion.

There has been some research on human running motion and the running of robots, but there has not been much work on the simulation of human running. Some running simulation work in the robotics area or computer animation area is available in the literature. Hodgins (1996) simulated 3D digital human motion of running, but it was done for animation purpose. Therefore, 3D stability or joint torque limits of a human were not considered because animators are more interested in high-level behavior and are not interested in kinetics of the model. Looking at the robotics area, we observe that two robots are available: the Honda ASIMO and the Sony QRIO. However, they have fewer degrees of freedom than a human and the anthropometric data of the mechanical models are not close to that of a human. It is concluded that a full body 3D dynamics simulation of human running is not available in the literature. Thus, this topic (optimization-based dynamic prediction of 3D human running) of the thesis is quite new in the sense of dynamics and digital human models.

1.2. Research Objectives

1.2.1. Description of the Research Problem

The main objective of this study is the prediction of 3D human running motion. Therefore, the research focuses on the following:

- The joint angle and joint torque profiles will be calculated for the full body model.
- Recursive Lagrangian equations of motion with external forces will be derived and used.
- Dynamic stability for the running problem—zero moment point—will be investigated.
- Ground reaction forces will be determined.

- Methods to include impact in the model at foot strike will be investigated.
- Optimization method for sparse problems will be investigated.
- Various constraints and performance measures for natural human running, such as for the upper-body motion, will be investigated.
- Simulations will be validated using the running determinants.

1.2.2. How are the Research Objectives to be accomplished?

The basic hypothesis of solving the running problem is to formulate it as an optimization problem. An algorithm based on the sequential quadratic programming approach is used to solve the nonlinear optimization problem. The digital human is modeled as a mechanical system that includes link lengths, mass moments of inertia, joint torques, and external forces. Denavit-Hartenberg method is used for kinematics analysis of open loop chains. In this approach, a degree of freedom characterizes relative rotation of two body segments that are assumed to be connected by revolute joints. The recursive Lagrangian formulation is used for the equations of motion which can be derived using the energy methods. For efficiency of calculations, we have to consider the number of additions and multiplications of the transformation matrices since the optimization method can take several iterations to converge. From this point of view, recursive Lagrangian formulation is quite efficient. To verify the recursive equation of motion, commercial general-purpose multi-body dynamics software is used. B-spline interpolation is used for time discretization and the control points for the joint angle profiles are treated as design variables. Also, the running motion is assumed to be completely periodic. For the performance measure in the optimization problem, the

dynamic effort that is represented as the integral of the sum of the squares of all the joint torques is minimized. A minimal set of constraints is imposed in the formulation of the problem to simulate natural running motion. The dynamic stability is achieved by satisfying the zero moment point (ZMP) constraint in the support phase. The impulse at the foot strike is included in the performance measure; therefore, the problem is treated as a multi-objective optimization problem. Load carrying, such as a backpack or hand load, and the motion for different running speeds are simulated as case studies.

1.3. Literature Review

Very few researchers have worked on mathematical modeling of digital human running simulation. Therefore, there is scarcity of literature that is directly related to digital human running simulation. However, we can review papers in several areas that give us some ideas about the running problem. These areas are sports, biomechanics, robotics, and computer graphics animation.

1.3.1. General Description and Review of Human Running

There are several review papers related to the biomechanics of human running (Cavanagh, 1990; Dillman, 1975; Alexander, 1984; Ounpuu, 1994; Novacheck, 1998). Generally, they describe the terminology of running, the kinematics results, the kinetics results, and the ground reaction forces. Cavanagh (1990) provided a very good reference not only for historical perspective, but also for the study of human running. Dillman (1975) provided a general summary of the biomechanics of human running from the view point of sports activities. Kinematical factors of human running were described such as

stride length, running velocity, and stride rate (stride frequency; the number of strides per second). He also explained the relationship between anthropometric factors and stride length. Alexander (1984) explained walking and running in terms of energy costs, force patterns, and elastic mechanics. The paper explained that the locomotion was adapted to minimize energy costs. He further explained the change from walking to running in terms of cheaper consumption of gait energy. For example, walkers used less energy than runners did when their speed was less than 2.3 m/sec and vice versa when their speed was more than 2.3 m/sec. Ounpuu (1994) described the terminology, kinematics, and kinetics of human walking and running. The general terminology of gait, such as gait cycle, step length, and stride length, was defined. Joint kinematics, joint kinetics, and ground reaction force of human walking and running were also summarized. Novacheck (1998) reviewed the biomechanics of human running. He discussed gait cycle, EMG, kinematics, kinetics, and potential and kinetic energy of running. It was noted that 80% of distance runners were rear foot strikers and the rest of them were mid foot strikers. He also distinguished distance running and sprinting at the point of the change from hindfoot to forefoot initial contact. He explained that for distance running the body moves at a more controlled rate in relation to the energy demand. On the contrary, during sprinting the body moves as rapidly as possible through the entire race.

1.3.2. Step Length and Time Duration

Step length and time duration, such as stance time or flight time, are important to formulate the problem. In biomechanics, sports and clinical areas, there are many papers that discuss or measure step length and time duration of human running. This is also

discussed in the computer graphics area because they want to animate the human running motion. Högberg (1952) measured stride length, stride frequency, flight period, and maximum distance between the feet during running. He used two subjects who were well-trained runners. He used a treadmill to perform the experiments and measured stride length and stride frequency at different speeds. He also measured flight period and foot contact at different speeds. Dillman (1975) discussed about stride length, stride frequency and running velocity. He noted that the better runners (or more skilled runners) had a greater length of stride than the poor runners (or less skilled runners). He also noted that better runners have a lower stride frequency than poor runners. Cavanagh and Kram (1990) performed experiments to study the relationship between stride length in distance running and running velocity, the relationship between stride length and anthropometric variables, and the effects of added mass on stride length. From the experimental results, they obtained an equation for stride length with respect to running velocity and the equation for stride length with respect to running velocity and leg length. Bruderlin and Calvert (1996) introduced a high-level motion control system for human running animation. In their paper, they gave equations for step length, which is a function of running speed, the height of the runner, and the runner's skill. The flight time is also formulated as a function of step frequency. The step frequency is a function of step length and running speed.

1.3.3. Kinematics and Kinetics of Human Running

In the biomechanics area, experiments have been performed and the joint angle profiles and joint torque profiles of human running have been measured. These

kinematics and kinetics results of running play an important role in the validation of digital human simulation. Milliron and Cavanagh (1990) synthesized the data available in the literature for the lower extremity for planar motion (sagittal plane) and showed how such data can be extended to obtain insights for mechanics of running. They also performed their own experiments for lower extremity kinematics for a small group of subjects running on a treadmill to present a coherent set of new data. Simpson and Bates (1990) experimented with the effect of running speed on joint moments in the support phase using the motion captured method. They calculated lower extremity joint moments using the data from motion capture and the ground reaction force from force plate. Then, the effects of running speed on joint moments were investigated. Four skilled runners tried eight trials at four target speeds (3.06, 3.57, 4.09, 4.60 m/s). Experimental setup was a force platform and a set of high-speed movie cameras. A side view of the right leg support phase on the platform was filmed. From the side view movie, they digitized 17 anatomical landmarks for the kinematics data. A Newtonian model was used for the calculation of joint moments of the support leg. In review papers, Ounpuu (1994) and Novacheck (1998) reviewed and summarized the joint angles and joint torques during human running.

1.3.4. Ground Reaction Forces

Cavanagh and Lafortune (1980) studied ground reaction forces in distance running for 17 subjects. From the experiments, they classified the pattern of center of pressure on the foot. The results showed that the rear-foot striker and the mid-foot striker had different mean center of pressure locations. They also obtained all the x-, y-, and z-

directional force components in the Cartesian coordinates. Munro et al. (1987) examined ground reaction forces for twenty male subjects. Running speeds ranged from 2.5 to 5.5 m/s. They classified foot strike type, and seventeen of them were rear-foot strikers. They also measured the stance time. Then, they obtained antero-posterior, vertical, and medial-lateral ground reaction forces. Williams and Cavanagh (1987) compared distance running mechanics, running economy, and performance. One result of their research was the vertical component of the ground reaction force as a function of time. Miller (1990) discussed general issues in ground reaction forces. In the review paper, Ounpuu (1994) and Novacheck (1998) summarized ground reaction forces in graphs.

1.3.5. Optimization-based Motion Prediction

There is a great deal of research in different areas using the optimization technique. Research in the areas of biomechanics, robotics, and computer graphics is discussed in this section. Even though some of the research is not directly related to the simulation of human running, it gives us some helpful information such as what kind of objective function was used, how the constraints were applied, what assumptions were made, and so on. Witkin and Kass (1988) developed a new method for creating character animation. This was the first optimization-based physical motion prediction method. They used SQP optimization to simulate Pixar animation Luxo Jr. – a four links table lamp. The objective function was to minimize the multiplication of the force and joint angle velocity. The force term was modeled by the character's muscle. For the equations of motion, a Lagrangian formulation was used. They used only kinetic energy for the Lagrangian formulation, so the gravitational force was not involved. As constraints, they

specified initial and final poses and constrained the force of contact with the floor on landing. Roussel et al. (1998) simulated planar four-degree–of-freedom biped walking robots with an optimization approach. The formulation included both the double support phase and the single support phase. The objective function was the joint torques, which quantifies the injected energy into the robot. The interesting thing in the formulation was that they had an impulse term in the objective function to handle the impact issue. Therefore, the objective function was the combination of joint torques and impulse. This idea is used to handle the impact issue in the present study as well. Lo et al. (2002) simulated human motion-planning problem with a quasi-Newton nonlinear programming technique. The problem addressed was controlling a simulated human figure (from 6 to 12 degrees of freedom) to perform given tasks such as leg lifting, weight lifting, and chin-ups. The recursive Newton-Euler dynamics formula was used for equations of motion. For explicit analytical gradients of dynamics, they used a matrix exponential formulation and Lie algebra. Cubic B-spline was used for function approximation. Fujimoto (2004) presented a method to generate the trajectory of a biped running robot. Basically, he used an optimization technique to minimize energy consumption during running. The simulation was performed with a five-link planar biped robot. The performance measure for optimization was the multiplication of joint torque and joint angle velocity. The problem was stated as symmetric and periodic running motion. In the formulation, there were two phases: the support phase and the flight phase.

1.3.6. Robotics and Biped Robots

Many researchers have worked on the locomotion of biped robots. Of course, there are certain differences between robotics and digital human simulation, such as number of degrees of freedom and the anthropometric data. However, there are many similarities in terms of dynamics because both are locomotion problems. Therefore, we review the studies of biped robots in this section. Honda has been developing humanoid robots since 1986, and their robot Advanced Step in Innovative Mobility (ASIMO) is the most advanced running robot to date. Hirai et al. (1998) have published their work which gives some idea about how to impose dynamics constraints such as zero moment point (ZMP). However, their running technology is not completely known at the present time. Currently, ASIMO has 34 degrees of freedom and can run at 6 km/h in a straight line and 5 km/h in a circular path of radius 2.5 m. SONY has developed a small bipedal entertainment robot QRIO (Nagasaka et al., 2004). Even though it is small (58 cm, 7 kg) and its degrees of freedom are thirty eight, it performs with good stability in its walking and running motion. The key constraints they have used are ZMP and conservation of angular momentum. Therefore, the ZMP is applied in the stance phase of QRIO and the conservation of angular momentum is applied in the flight phase. As other work in the robotics area, Nagasaki et al. (2003) generated the running pattern by using the angular momentum and the control theory. Park and Kwon (2003) developed a biped robot's running motion by using the impedance control. Hybrid Zero Dynamics (HZD) was presented by Westervelt and Grizzle (2003). The robot has quite a natural motion with that method, but it does not have 3D stability. Kajita et al. (2007) generated the running motion and applied it to a humanoid robot. First, they generated running motion for a

simple inverted pendulum. Then, they transformed the running motion into a running pattern for a humanoid robot, HRP-2LR. The robot performed 0.16 m/s running with a flight phase (0.06 second) and a support phase (0.3 second). Shin and Park (2008) proposed a method to generate the running trajectory of a biped robot. The trajectory was generated based on an inverted pendulum, and constant ground reaction force was proposed with ZMP. Results were shown by a 7-DOF biped robot simulation. Hodgins (1996) published a paper about the control of a simulated three-dimensional model of a human running for animation. She modeled 17 segments of the rigid body as a mechanical structure. The equations of motion were used in this digital human running simulation. She used robotics control theory for human animation and used commercial dynamics software to solve the problem. Then, the locomotion control algorithms that allowed the model to run were developed. Since the purpose of the simulation was the animation of digital human running, it did not have any 3D stability issue.

1.3.7. Kinematics, Dynamics, and Stability

Denavit and Hartenberg (1955) present kinematic symbolic notation for lower-pair mechanisms based on matrices, which is called the Denavit-Hartenberg method. This provides a powerful and reliable analytical procedure for the analysis of kinematics as well as computational implementation. Uicker (1965) derived the standard formulation for a general linkage problem. He set up the Lagrangian-based dynamics by using 4×4 matrices. Since this formulation has the order $O(n^4)$, where n is the number of degrees of freedom, it is not efficient in terms of computational time. Hollerbach (1980) proposed the recursive Lagrangian formulation of manipulator dynamics based on matrix algebra.

This is the formulation with the order $O(n)$, so the calculation time is significantly decreased compared to the calculation time of the formulation from Uicker. The recursive Lagrangian formulation is not more efficient than the Newton-Euler formulation. However, this dynamic formulation has both convenience and efficiency. Vukobratović and Borovac (2004) explained the concept and notion of zero moment point (ZMP), and Sardain and Bessonnet (2004) compared center of pressure (COP) and zero moment point (ZMP).

1.3.8. Upper-Body Motion

Kim et al. (2005) studied yawing moment cancelation and ZMP compensation for the humanoid robot (HanSaRam) to avoid the possible slipping on the ground caused by the yawing moment. So, they postulated that the upper-body motion of the robot should compensate for the yawing moment. Collins et al. (2009) studied arm swing motion in human walking. Their hypothesis was that the reduction of ground reaction moment may explain the physiological benefit of arm swinging. From the experimental measurements of humans, they observed the arm swinging motion most affected by the vertical ground reaction moment.

1.4. Scope of the Dissertation

In Chapter 2, a kinematic model of the human body based on the Denavit-Hartenberg (DH) method is discussed, and recursive formulas for kinematic analysis and analytical gradients are provided. Analytical gradients help in efficient solution of the nonlinear optimization problem. In Chapter 3, dynamics equilibrium based on a recursive

Lagrange dynamics formulation is discussed. The recursive Lagrange dynamics formulation is derived from kinetic energy and potential energy with external force, and its analytical gradients are also derived. In Chapter 4, dynamic stability is discussed. The zero moment point (ZMP) method is used for dynamic stability of human running. The zero moment point (ZMP) formula and rate of angular momentum are derived in recursive form, and analytical gradients are also derived for optimization. In Chapter 5, function approximation for time discretization is discussed. The B-spline method is used for function approximation, and the basis function, clamped B-spline curves, and properties of B-spline are studied. Also, other function approximations are discussed and compared to B-spline. In Chapter 6, the concept of predictive dynamics is presented. The basic notion and formulation of predictive dynamics is defined, and numerical examples are solved to provide some insight for predictive dynamics. The numerical examples are solved for a simple pendulum with external sinusoidal torque. In Chapter 7, the formulation of a running problem is discussed. The model of running is described, and the formulation of the impact in running is discussed. Then, design variables, performance measures, and constraints are discussed, and the gradients for constraints are presented. In Chapter 8, the results of various simulations are provided. In Chapter 9, the formulation and results of a slow jog along curvilinear paths are presented. In Chapter 10, upper-body motion is studied and a modified performance measure is presented for upper-body yawing motion. In Chapter 11, the sparsity of the formulation is analyzed and discussed. In Chapter 12, conclusions and future research are discussed.

CHAPTER 2

KINEMATIC MODEL OF THE HUMAN BODY

Digital human is modeled as a mechanical system that includes link lengths, mass moments of inertia, joint torques, and external forces. The entire model has 55 degrees of freedom—6 degrees of freedom for global translation and rotation, and 49 degrees of freedom for the body. A degree of freedom in this case characterizes a jointed pair in the kinematics sense, where various segments of the body are assumed to be connected by revolute joints. The Denavit-Hartenberg (DH) method is applied for the kinematics analysis.

2.1. Denavit-Hartenberg Method

Denavit and Hartenberg (1955) proposed a matrix transformation method to describe the translational and rotational relationship systematically between adjacent links in articulated chains. This matrix transformation representation is called the DH method. The transformation matrix is a 4×4 homogeneous matrix. This method represents each link coordinate system in terms of the previous link coordinate system. Any local coordinate system (including the end-effector of the manipulator or serial chain) can be expressed in global reference frame by the DH method. So, basically, the method represents a vector in one coordinate frame in terms of another coordinate frame. This method has its base in the field of robotics, but it can be used for modeling human kinematics as well.

Consider an articulated chain depicted in Figure 2.1.

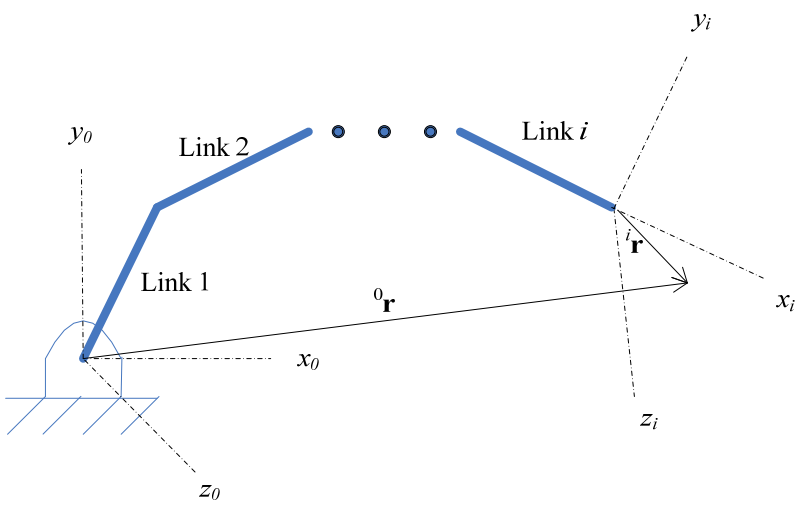

Figure 2.1 Articulated chain

Any point of interest in the i^{th} frame $^i\mathbf{x}$ can be transferred to the global reference frame $^0\mathbf{r}$:

$$^0\mathbf{r} = {}^0\mathbf{T}_i \, {}^i\mathbf{r} \tag{2.1}$$

where $^i\mathbf{r}$ is a 4×1 vector in terms of the i^{th} reference frame and $^0\mathbf{T}_i$ is a 4×4 homogeneous transformation matrix from the i^{th} reference frame to the global reference frame. The format of the vector $^i\mathbf{r}$ is

$$^i\mathbf{r} = \begin{bmatrix} r_x \\ r_y \\ r_z \\ 1 \end{bmatrix} \tag{2.2}$$

where r_x, r_y, and r_z represent any point of interest in the i^{th} frame in terms of the Cartesian coordinates.

Here the transformation of a vector to the global reference frame is simply the multiplication of transformation matrices, which is given as:

$$ {}^{0}\mathbf{T}_{i} = {}^{0}\mathbf{T}_{1}\,{}^{1}\mathbf{T}_{2}\cdots{}^{i-1}\mathbf{T}_{i} = \prod_{n=1}^{i} {}^{n-1}\mathbf{T}_{n} \tag{2.3} $$

The transformation matrix of this vector is a 4×4 matrix that includes 4 DH parameters, which are described in Figure 2.2.

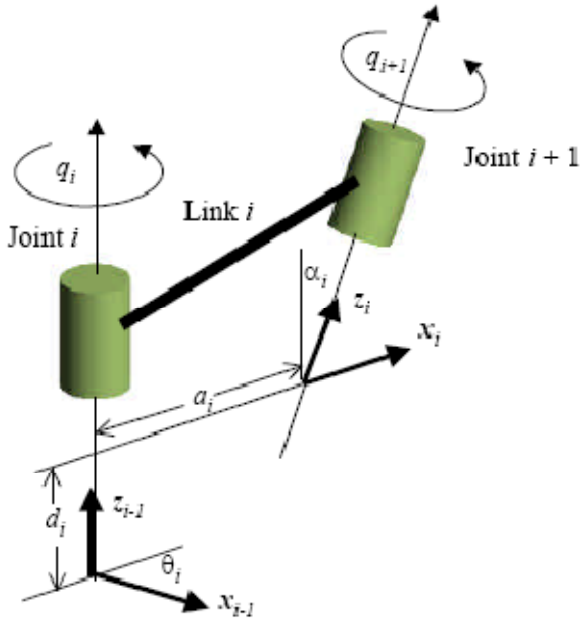

Figure 2.2 DH parameters

According to the DH method, the four DH parameters in Figure 2.2 are defined as follows:

1) θ_i is the joint angle between the x_{i-1} axis and the x_i axis about the z_{i-1} axis according to the right-hand rule.
2) d_i is the distance between the origin of the i–1th coordinate frame and the intersection of the z_{i-1} axis with the x_i axis along the z_{i-1}axis.
3) a_i is the distance between the intersection of the z_{i-1} axis with the x_i axis and the

origin of the i^{th} frame along the x_i axis. Or, the shortest distance between the z_{i-1} and z_i axes.

4) α_i is the angle between the z_{i-1} axis and the z_i axis about the x_i axis according to the right-hand rule.

Then, the transformation matrix ${}^{i-1}\mathbf{T}_i$ is composed in the following sequence of transformations:

$$ {}^{i-1}\mathbf{T}_i = \mathbf{R}_z(\theta_i)\mathbf{Trans}_z(d_i)\mathbf{Trans}_x(a_i)\mathbf{R}_x(\alpha_i) \tag{2.4} $$

where $\mathbf{R}_z$ and $\mathbf{R}_x$ represent rotation about the z and x axes, respectively, and $\mathbf{Trans}_z$ and $\mathbf{Trans}_x$ represent translations along the z and x axes, respectively. In other words, Equation 2.4 represents the following:

1) first, the i–1^{th} frame is rotated by angle θ about the z axis;
2) second, the rotated frame is translated by distance d along the z axis;
3) third, the translated frame is translated again by distance a along the x axis; and
4) fourth, the translated frame is rotated by angle α about the x axis.

This allows us to establish the home configuration, which is the starting configuration of the mechanical linkage; a suitable home configuration must be established in order to use the DH transformation method. In summary, to use the DH method, the coordinates system must satisfy the following two conditions:

1) The axis x_i is perpendicular to the axis z_{i-1}.
2) The axis x_i must intersect the axis z_{i-1}.

The DH transformation matrix from the i^{th} frame to the i–1^{th} frame is then given as:

$$ {}^{i-1}\mathbf{T}_i = \begin{bmatrix} \cos\theta_i & -\cos\alpha_i \sin\theta_i & \sin\alpha_i \sin\theta_i & a_i \cos\theta_i \\ \sin\theta_i & \cos\alpha_i \cos\theta_i & -\sin\alpha_i \cos\theta_i & a_i \sin\theta_i \\ 0 & \sin\alpha_i & \cos\alpha_i & d_i \\ 0 & 0 & 0 & 1 \end{bmatrix} \tag{2.5} $$

In the case of a rotational joint, the joint parameters d_i, a_i, and α_i are constant (which means they are fixed). Only θ_i is treated as a rotational degree of freedom, q_i. In a mechanical model, q_i is the vector of generalized coordinates, and each transformation matrix has one degree of freedom.

Note that the local coordinate system is located at the end of the link in this DH representation. For example, consider that there is a one-degree-of-freedom manipulator as shown in Figure 2.3 and the global reference frame is x_0, y_0, z_0 (z axis is perpendicular to the paper). Then the local reference frame x_1, y_1, z_1, is located at the end of the linkage, according to the DH method.

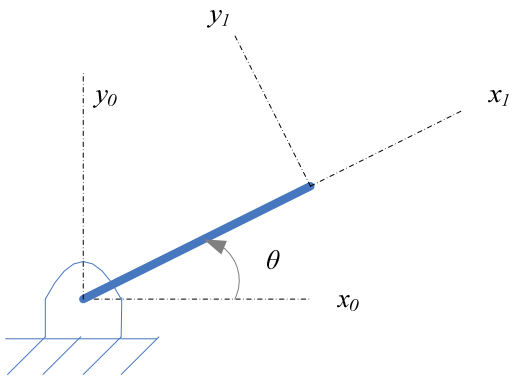

Figure 2.3 Local reference frame in DH method

2.2. Kinematic Modeling of the Digital Human

The digital human is modeled as a mechanical system that includes link lengths and mass moments of inertia. Figure 2.4 depicts the modeling of a human using a series of rigid links connected by joints; the light blue circles represent kinematic joints.

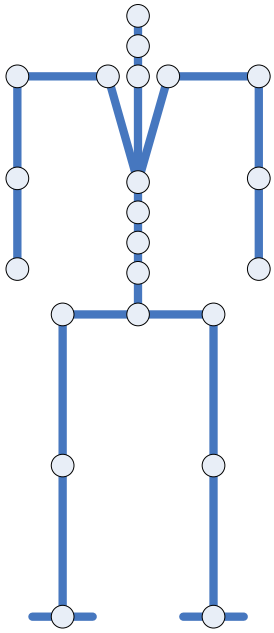

Figure 2.4 Digital human modeling using a series of rigid links connected by joints

The body segments are assumed to be connected by rotational (revolute) joints. For instance, consider the right knee joint of a human, shown in Figure 2.5. The knee joint is composed of ligaments and tendons between two segments, which are the femur and the tibia. Since the knee is bent in one direction, it is assumed to be a one-degree-of-freedom revolute joint as shown in Figure 2.6.

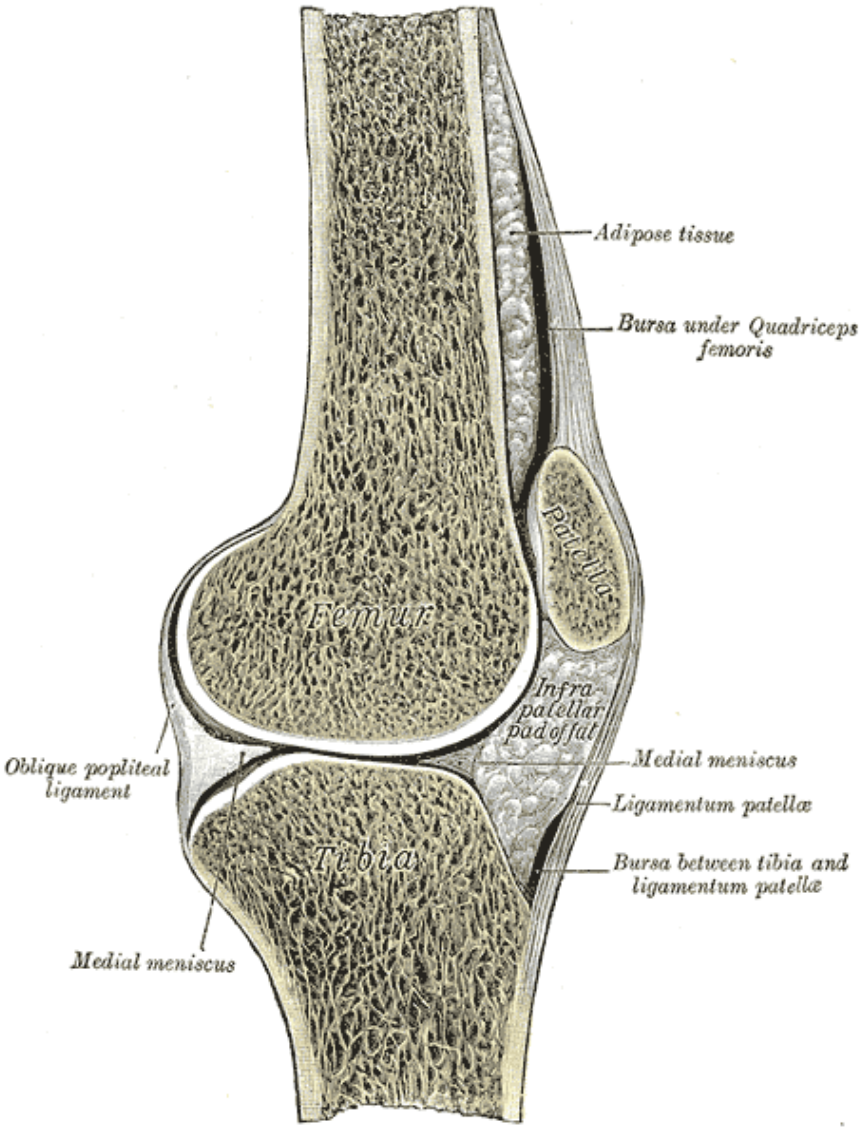

Figure 2.5 Right knee joint (Gray's anatomy)

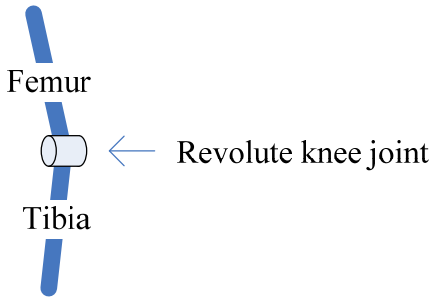

Figure 2.6 Knee joint modeling using revolute joint

A more complicated joint can be modeled in the same manner. Figure 2.7 depicts human hip joint anatomy and its mechanical model.

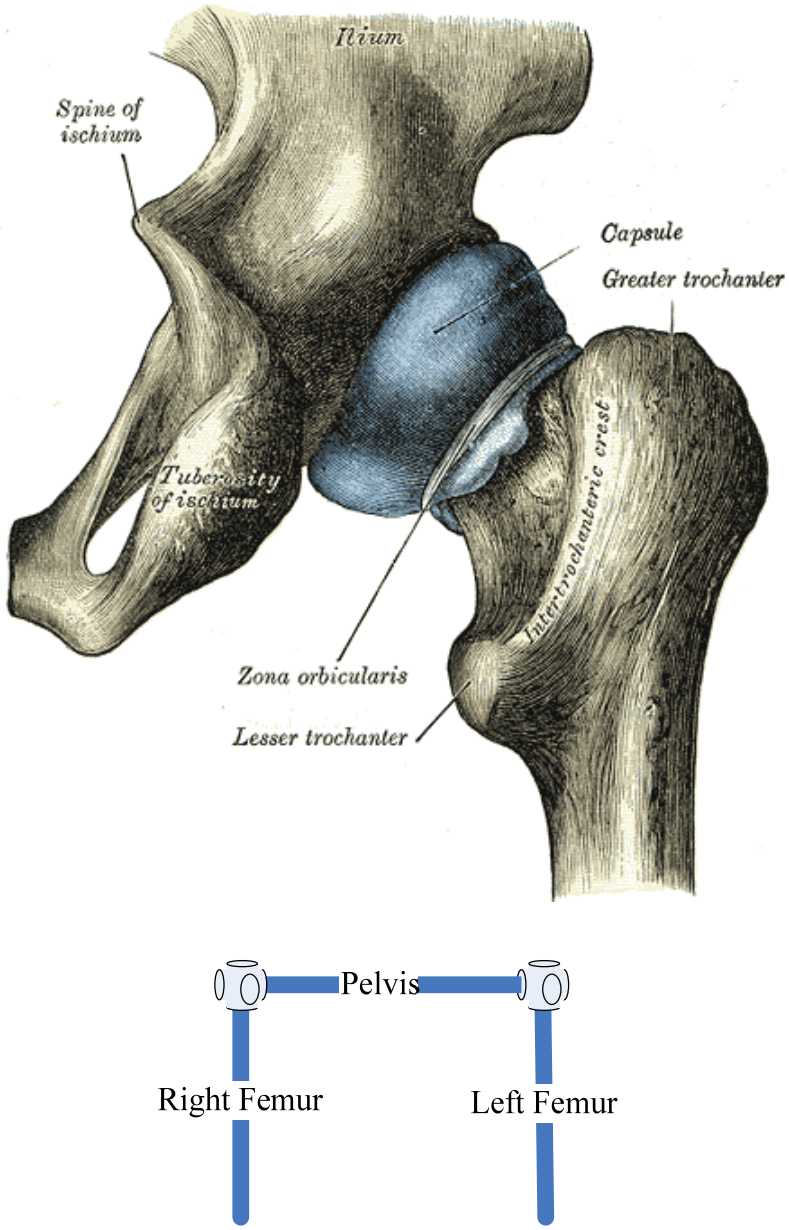

Figure 2.7 Left hip joint anatomy (Gray's anatomy) and its mechanical model

Since the hip joint can rotate in any direction, it is assumed to be a universal joint, which has three degrees of freedom. Similarly, the shoulder and spine joints are also treated as universal joints. The knee and toe joints are assumed to be one-degree-of-freedom rotational (revolute) joints. The elbow, wrist, and ankle joints are to be two-degree-of-freedom rotational joints. The entire Santos joint description is displayed in Figure 2.8.

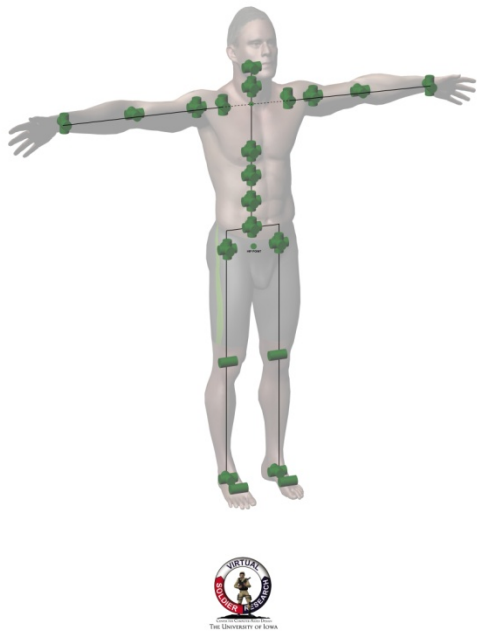

Figure 2.8 Santos kinematic joints description

2.3. DH Structure for the Digital Human

2.3.1. Global Degree of Freedom and Branches in Local Body Frame

In general, human locomotion means the body moves around. In other words, the global degree of freedom exists with respect to an inertial reference frame in the mathematical sense. The global degrees of freedom are composed of three translational (prismatic) joints and three rotational (revolute) joints. Figure 2.9 depicts how the global

degrees of freedom are set up in the DH method. The degree of freedom is given in the *z*-direction in both the translational joint and the rotational joint. The last degree of freedom (third global rotation, GR3) must satisfy the DH condition discussed in the previous section to any local body frame. Table 2.1 presents the DH table for the global degrees of freedom.

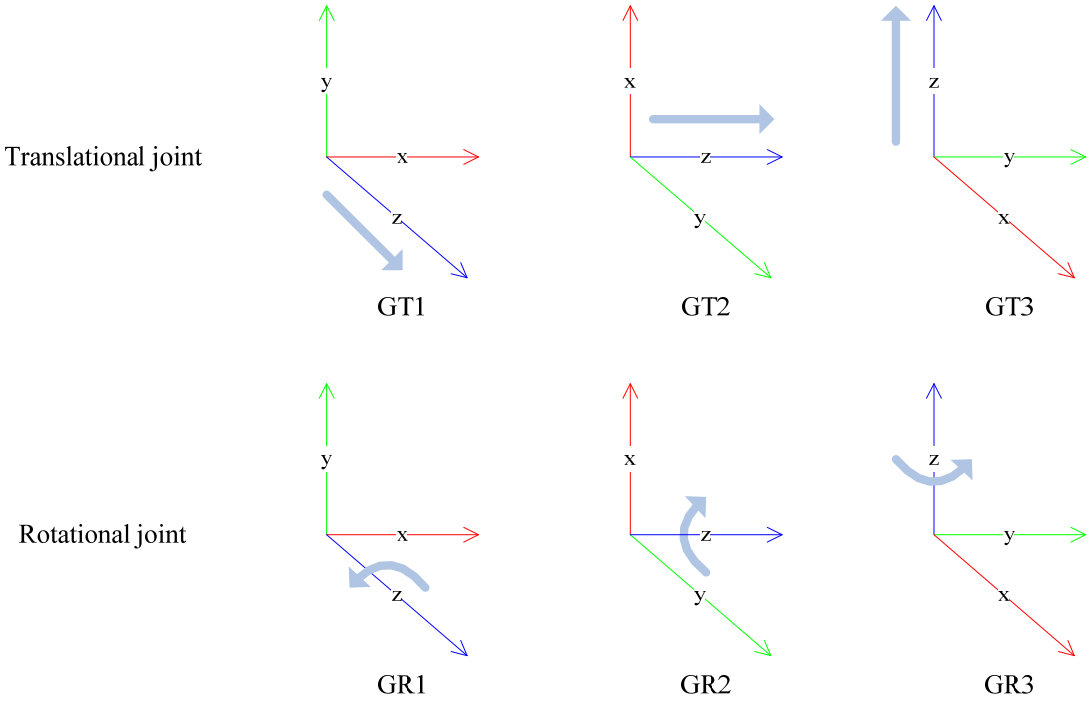

Figure 2.9 Global degree of freedom description

Table 2.1 DH table for global degrees of freedom

DOF Joint type	θ	d	a	α
Prismatic	$\pi/2$	0	0	$\pi/2$
Prismatic	$\pi/2$	0	0	$\pi/2$
Prismatic	$\pi/2$	$L_{19}+L_{20}$	0	$\pi/2$
Rotational	$\pi/2$	0	0	$\pi/2$
Rotational	$\pi/2$	0	0	$\pi/2$
Rotational (to right leg branch)	$-\pi/2$	0	L_{17}	$-\pi/2$
Rotational (to left leg branch)	$\pi/2$	0	L_{22}	$-\pi/2$
Rotational (to spine branch)	$\pi/2$	L_{18}	0	$\pi/2$

* L_{17}, L_{18}, L_{19}, L_{20} and L_{22} are defined in Figure 2.11

There are six branches in the body frame. The first branch is the right leg, the second is the left leg, and the third is the spine. In the spine branch, there are three child branches—the right arm branch, left arm branch, and neck branch (Figure 2.10). Each branch has a starting local frame that differs from its parent branch. Therefore, the DH table should have different values for the parent branch and its child branches. This branch concept causes some difficulty when the gradients for equations of motion are programmed; this is discussed in the dynamics section.

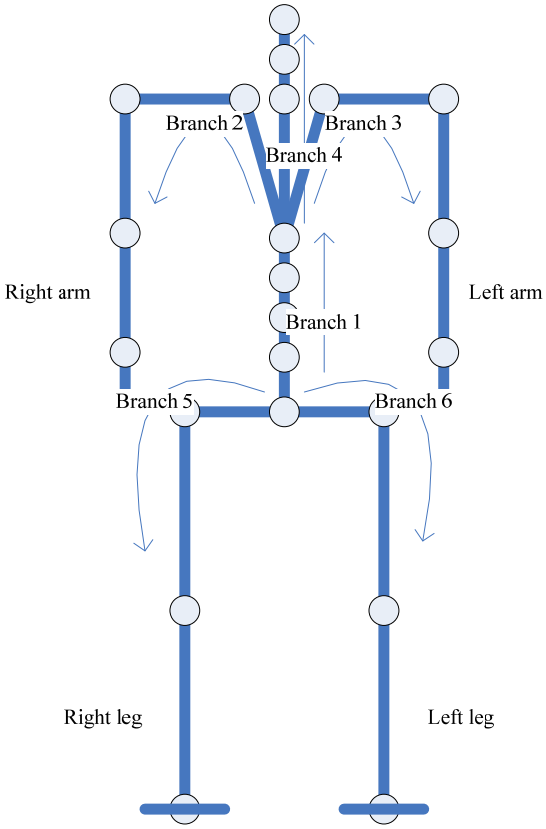

Figure 2.10 Branch description in body frame

2.3.2. DH Table for Local Body Frame

The current digital human model Santos has 49 degrees of freedom for the local body frame according to the DH method. The 6 global degrees of freedom bring the total to 55 degrees of freedom. A full-body digital human model is described in Figure 2.11 and Tables 2.2-2.4.

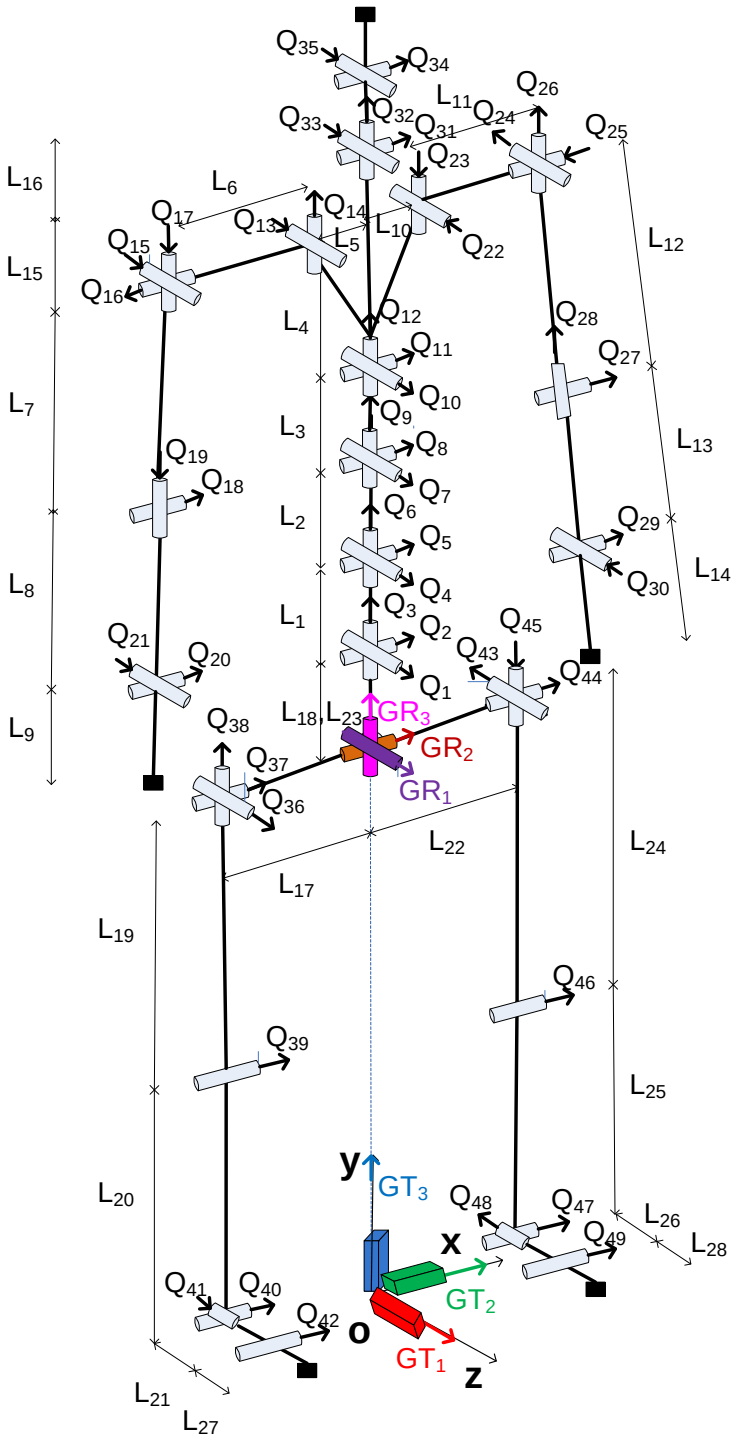

Figure 2.11 Local coordinate system of Santos based on DH method

Table 2.2 Link length of Santos (cm)

L_1	5.6267	L_{15}	4.4081
L_2	5.44274	L_{16}	17.0596
L_3	5.99962	L_{17}	8.5142
L_4	17.3856	L_{18}	9.0000
L_5	1.70799	L_{19}	38.2615
L_6	15.057	L_{20}	39.4626
L_7	25.8638	L_{21}	9.0165
L_8	24.7374	L_{22}	8.5142
L_9	16.5099	L_{23}	9.0000
L_{10}	1.70799	L_{24}	38.2615
L_{11}	14.175	L_{25}	39.4625
L_{12}	25.9194	L_{26}	9.0165
L_{13}	24.7482	L_{27}	6.0000
L_{14}	17.1041	L_{28}	6.0000

Table 2.3 DH table for upper body

DOF	θ	d	a	α	Segment
Q1	$\pi/2$	0	0	$\pi/2$	spine
Q2	$\pi/2$	0	0	$\pi/2$	
Q3	$\pi/2$	L_1	0	$\pi/2$	
Q4	$\pi/2$	0	0	$\pi/2$	
Q5	$\pi/2$	0	0	$\pi/2$	
Q6	$\pi/2$	L_2	0	$\pi/2$	
Q7	$\pi/2$	0	0	$\pi/2$	
Q8	$\pi/2$	0	0	$\pi/2$	
Q9	$\pi/2$	L_3	0	$\pi/2$	
Q10	$\pi/2$	0	0	$\pi/2$	
Q11	$\pi/2$	0	0	$\pi/2$	
Q12(to right arm)	$-\pi/2$	L_4	L_5	$-\pi/2$	
Q12(to left arm)	$\pi/2$	L_4	L_{10}	$-\pi/2$	
Q12(to head)	$\pi/2$	L_4+L_{15}	0	$\pi/2$	
Q13	0	0	0	$\pi/2$	right arm
Q14	0	0	L_6	$-\pi/2$	
Q15	0	0	0	$\pi/2$	
Q16	$\pi/2$	0	0	$\pi/2$	
Q17	$\pi/2$	L_7	0	$\pi/2$	
Q18	0	0	0	$-\pi/2$	
Q19	0	L_8	0	$\pi/2$	
Q20	$\pi/2$	0	0	$\pi/2$	
Q21	0	0	L_9	0	
Q22	0	0	0	$-\pi/2$	left arm
Q23	0	0	L_{11}	$\pi/2$	
Q24	0	0	0	$-\pi/2$	
Q25	$-\pi/2$	0	0	$\pi/2$	
Q26	$\pi/2$	$-L_{12}$	0	$\pi/2$	
Q27	0	0	0	$-\pi/2$	
Q28	0	$-L_{13}$	0	$\pi/2$	
Q29	$-\pi/2$	0	0	$-\pi/2$	
Q30	0	0	L_{14}	0	
Q31	$\pi/2$	0	0	$\pi/2$	head
Q32	$\pi/2$	0	0	$\pi/2$	
Q33	$\pi/2$	L_{16}	0	$\pi/2$	
Q34	$\pi/2$	0	0	$\pi/2$	
Q35	0	0	0	0	

Table 2.4 DH table for lower body

DOF	θ	d	a	α	Segment
Q36	$\pi/2$	0	0	$-\pi/2$	right leg
Q37	$-\pi/2$	0	0	$\pi/2$	
Q38	0	$-L_{19}$	0	$-\pi/2$	
Q39	$\pi/2$	0	L_{20}	0	
Q40	0	0	0	$\pi/2$	
Q41	0	L_{21}	0	$-\pi/2$	
Q42	$-\pi/2$	0	L_{27}	0	
Q43	$-\pi/2$	0	0	$-\pi/2$	left leg
Q44	$-\pi/2$	0	0	$\pi/2$	
Q45	0	L_{24}	0	$-\pi/2$	
Q46	$\pi/2$	0	$-L_{25}$	0	
Q47	0	0	0	$\pi/2$	
Q48	0	$-L_{26}$	0	$-\pi/2$	
Q49	$\pi/2$	0	L_{28}	0	

2.4. Kinematic Analysis of the Human Body

The kinematics analysis in the recursive form leads to a simpler form for the transformation matrix $\mathbf{A}_i$. The time derivatives of the transformation matrix $\mathbf{A}_i$ can be obtained in the recursive form as well:

$$\mathbf{A}_i = \mathbf{A}_{i-1}\mathbf{T}_i \tag{2.6.a}$$

$$\mathbf{B}_i = \dot{\mathbf{A}}_i = \mathbf{B}_{i-1}\mathbf{T}_i + \mathbf{A}_{i-1}\frac{\partial \mathbf{T}_i}{\partial q_i}\dot{q}_i \tag{2.6.b}$$

$$\mathbf{C}_i = \dot{\mathbf{B}}_i = \mathbf{C}_{i-1}\mathbf{T}_i + 2\mathbf{B}_{i-1}\frac{\partial \mathbf{T}_i}{\partial q_i}\dot{q}_i + \mathbf{A}_{i-1}\frac{\partial^2 \mathbf{T}_i}{\partial q_i^2}\dot{q}_i^2 + \mathbf{A}_{i-1}\frac{\partial \mathbf{T}_i}{\partial q_i}\ddot{q}_i \tag{2.6.c}$$

where q_i is the joint angle and $\mathbf{T}_i$ is the link transformation matrix. The derivatives of the transformation matrices with respect to joint angles, joint angle velocities and joint angle accelerations are

$$\frac{\partial \mathbf{A}_i}{\partial q_k} = \begin{cases} \mathbf{A}_{i-1} \dfrac{\partial \mathbf{T}_i}{\partial q_k} & (k = i) \\ \dfrac{\partial \mathbf{A}_{i-1}}{\partial q_k} \mathbf{T}_i & (k < i) \end{cases} \tag{2.7.a}$$

$$\frac{\partial \mathbf{B}_i}{\partial q_k} = \begin{cases} \mathbf{B}_{i-1} \dfrac{\partial \mathbf{T}_i}{\partial q_k} + \mathbf{A}_{i-1} \dfrac{\partial^2 \mathbf{T}_i}{\partial q_k^2} \dot{q}_i & (k = i) \\ \dfrac{\partial \mathbf{B}_{i-1}}{\partial q_k} \mathbf{T}_i + \dfrac{\partial \mathbf{A}_{i-1}}{\partial q_k} \dfrac{\partial \mathbf{T}_i}{\partial q_i} \dot{q}_i & (k < i) \end{cases} \tag{2.7.b}$$

$$\frac{\partial \mathbf{B}_i}{\partial \dot{q}_k} = \begin{cases} \mathbf{A}_{i-1} \dfrac{\partial \mathbf{T}_i}{\partial q_k} & (k = i) \\ \dfrac{\partial \mathbf{B}_{i-1}}{\partial \dot{q}_k} \mathbf{T}_i & (k < i) \end{cases} \tag{2.7.c}$$

$$\frac{\partial \mathbf{C}_i}{\partial q_k} = \begin{cases} \mathbf{C}_{i-1} \dfrac{\partial \mathbf{T}_i}{\partial q_k} + 2\mathbf{B}_{i-1} \dfrac{\partial^2 \mathbf{T}_i}{\partial q_k^2} \dot{q}_i + \mathbf{A}_{i-1} \dfrac{\partial^3 \mathbf{T}_i}{\partial q_k^3} \dot{q}_i^2 + \mathbf{A}_{i-1} \dfrac{\partial^2 \mathbf{T}_i}{\partial q_k^2} \ddot{q}_i & (k = i) \\ \dfrac{\partial \mathbf{C}_{i-1}}{\partial q_k} \mathbf{T}_i + 2 \dfrac{\partial \mathbf{B}_{i-1}}{\partial q_k} \dfrac{\partial \mathbf{T}_i}{\partial q_i} \dot{q}_i + \dfrac{\partial \mathbf{A}_{i-1}}{\partial q_k} \dfrac{\partial^2 \mathbf{T}_i}{\partial q_i^2} \dot{q}_i^2 + \dfrac{\partial \mathbf{A}_{i-1}}{\partial q_k} \dfrac{\partial \mathbf{T}_i}{\partial q_i} \ddot{q}_i & (k < i) \end{cases} \tag{2.7.d}$$

$$\frac{\partial \mathbf{C}_i}{\partial \dot{q}_k} = \begin{cases} 2\mathbf{B}_{i-1} \dfrac{\partial \mathbf{T}_i}{\partial q_k} + 2\mathbf{A}_{i-1} \dfrac{\partial^2 \mathbf{T}_i}{\partial q_k^2} \dot{q}_i & (k = i) \\ \dfrac{\partial \mathbf{C}_{i-1}}{\partial \dot{q}_k} \mathbf{T}_i + 2 \dfrac{\partial \mathbf{B}_{i-1}}{\partial \dot{q}_k} \dfrac{\partial \mathbf{T}_i}{\partial q_i} \dot{q}_i & (k < i) \end{cases} \tag{2.7.e}$$

$$\frac{\partial \mathbf{C}_i}{\partial \ddot{q}_k} = \begin{cases} \mathbf{A}_{i-1} \dfrac{\partial \mathbf{T}_i}{\partial q_k} & (k = i) \\ \dfrac{\partial \mathbf{C}_{i-1}}{\partial \ddot{q}_k} \mathbf{T}_i & (k < i) \end{cases} \tag{2.7.f}$$

CHAPTER 3

DYNAMIC EQUILIBRIUM

Dynamic equations of motion are important constraints in the optimization-based predictive dynamics problem of human running. The problem involves a large number of calculations because there are many matrix multiplications and additions during the solution process. Also, the optimization process can take many iterations. These issues are discussed in this section.

Denavit and Hartenberg (1955) developed a method referred as DH method for kinematics of manipulators. Uicker (1965) derived the standard formulation for manipulator dynamics based on Lagrangian dynamics using 4×4 DH matrix transformations. However, that formulation takes order n^4 calculations. In 1979, Waters noticed that a simpler formulation can be derived that takes order n^2 calculations. After that, Hollerbach (1980) derived a recursive formulation from the Waters formula that takes order n calculations. Since we are solving an optimization problem, the numbers of multiplications and additions that need to be taken into consideration are significant. Therefore we adopt Hollerbach's (1980) approach in the present work and extend it to include external forces and torques on the links.

3.1. Lagrange's Equation and Lagrangian Dynamics Formulation

The Lagrange's equation is given as

$$Q_i = \frac{d}{dt}\left(\frac{\partial L}{\partial \dot{q}_i}\right) - \frac{\partial L}{\partial q_i}, \tag{3.1}$$

where the Lagrangian $L = K - V$ (kinetic energy – potential energy), q_i is the generalized coordinate vector (joint angles), and Q_i is the generalized force vector (joint torque). Using Equation (3.1), Uicker (1965) derived the following equation for dynamics of a manipulator using the DH method:

$$\tau_i = \sum_{j=i}^{n}\left[\sum_{k=1}^{j}\left(tr\left(\frac{\partial \mathbf{A}_j}{\partial q_i}\mathbf{J}_j\frac{\partial \mathbf{A}_j^T}{\partial q_k}\right)\right)\ddot{q}_k + \sum_{k=1}^{j}\sum_{l=1}^{j}\left(tr\left(\frac{\partial \mathbf{A}_j}{\partial q_i}\mathbf{J}_j\frac{\partial^2 \mathbf{A}_j^T}{\partial q_k \partial q_l}\right)\dot{q}_k\dot{q}_l\right) - m_j\mathbf{g}^T\frac{\partial \mathbf{A}_j}{\partial q_i}{}^j\mathbf{r}_j\right], \quad (3.2)$$

where

τ_i : Joint torque of the link expressed in the i^{th} reference frame

$\mathbf{A}_j$: DH transformation matrix from the j^{th} reference frame to the global reference frame

$\mathbf{J}_j$: Inertia matrix for the j^{th} link

m_j : Mass of the link expressed in the j^{th} reference frame

$\mathbf{g}$: Gravity vector

${}^j\mathbf{r}_j$: Center of mass of the link expressed in the j^{th} reference frame

As noted before, the order of calculations for the formulation of Equation (3.2) is n^4. Waters (1979) developed (also based on Lagrange's equation) a simpler form for the governing equations, as follows:

$$\tau_i = \sum_{j=i}^{n}\left[tr\left(\frac{\partial \mathbf{A}_i}{\partial q_i}{}^i\mathbf{T}_j\mathbf{J}_j\ddot{\mathbf{A}}_j^T\right) - m_j\mathbf{g}^T\frac{\partial \mathbf{A}_j}{\partial q_i}{}^i\mathbf{T}_j{}^j\mathbf{r}_j\right], \quad (3.3)$$

where ${}^i\mathbf{T}_j$ is the DH transformation matrix from the j^{th} reference frame to the i^{th} reference frame. The order of calculations for this formulation is n^2.

3.2. Recursive Lagrangian Dynamics Formulation

The order of calculations in Equation (3.3) can be reduced to n by transcribing the equation to a recursive form (Hollerbach, 1980). Even though the original formulation does not include external forces, we can re-derive it using the Lagrange's equation to include external forces.

3.2.1. Lagrangian Formulation with DH Transformations

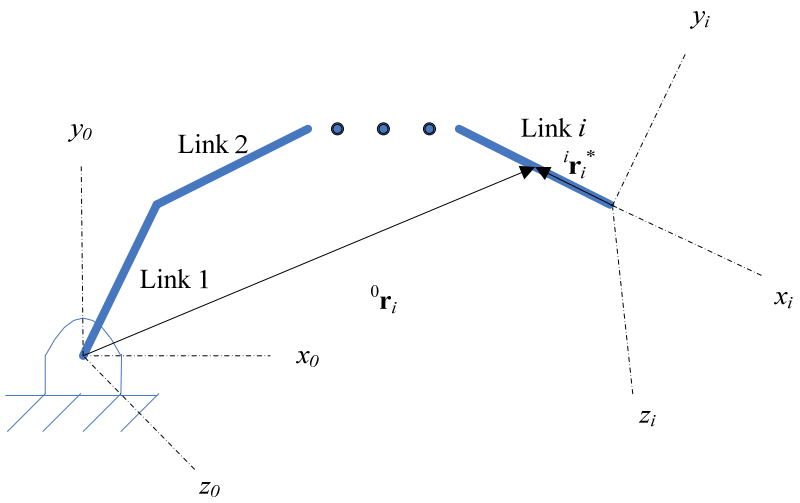

Figure 3.1 Articulated chain

From Figure 3.1, let ${}^i\mathbf{r}_i^* = \begin{bmatrix} x_i^* & y_i^* & z_i^* & 1 \end{bmatrix}^T$ be a vector to some particle of the i^{th} link expressed in the i^{th} reference frame. The vector to the particle ${}^0\mathbf{r}_i$ in the global reference frame is

$$ {}^0\mathbf{r}_i = \mathbf{A}_i \, {}^i\mathbf{r}_i^* . \tag{3.4}$$

Then, the velocity for the particle is

$$ {}^{0}\dot{\mathbf{r}}_i = \dot{\mathbf{A}}_i \, {}^{i}\mathbf{r}_i^*, \tag{3.5} $$

where $\mathbf{A}_i$ is a DH transformation matrix from the i^{th} reference frame to the global reference frame. The kinetic energy for the particle is

$$ \begin{aligned} dK_i &= \frac{1}{2} tr\left({}^{0}\dot{\mathbf{r}}_i \, {}^{0}\dot{\mathbf{r}}_i^T \right) dm \\ &= \frac{1}{2} tr\left(\dot{\mathbf{A}}_i \, {}^{i}\mathbf{r}_i^* \, {}^{i}\mathbf{r}_i^{*T} \dot{\mathbf{A}}_i^T \right) dm. \end{aligned} \tag{3.6} $$

Since the inertia matrix is

$$ \mathbf{J}_i = \int {}^{i}\mathbf{r}_i^* \, {}^{i}\mathbf{r}_i^{*T} dm \, , \tag{3.7} $$

the kinetic energy for the i^{th} linkage is given as

$$ K_i = \frac{1}{2} tr\left(\dot{\mathbf{A}}_i \mathbf{J}_i \dot{\mathbf{A}}_i^T \right). \tag{3.8} $$

Therefore, the total kinetic energy is given as

$$ K = \sum_{j=1}^{n} K_j = \frac{1}{2} \sum_{i=1}^{n} tr\left(\dot{\mathbf{A}}_i \mathbf{J}_i \dot{\mathbf{A}}_i^T \right), \tag{3.9} $$

where n is the number of local reference frames.

The potential energy for the system is given as

$$ V = -\sum_{j=1}^{n} m_j \mathbf{g}^T \mathbf{A}_j \, {}^{j}\overline{\mathbf{r}}_j - \sum_{j=1}^{n} \mathbf{f}_k^T \mathbf{A}_j \, {}^{k}\mathbf{r}_f \delta_{jk} \, , \tag{3.10} $$

where the variables are defined as follows:

m_j is the mass of the link expressed in the j^{th} reference frame

$\mathbf{g}$ is the gravity vector

${}^{j}\overline{\mathbf{r}}_j$ is the center of mass of the link expressed in the j^{th} reference frame

$\mathbf{f}_k$ is an external force defined in the global reference frame and acting on the link expressed in the k^{th} reference frame

${}^k\mathbf{r}_f$ is the location of external force acting on the link expressed in the k^{th} reference frame

δ_{jk} is the Kronecker delta

From Lagrange's equation in Equation (3.1), the first term of the right-hand side is

$$\frac{\partial L}{\partial \dot{q}_i} = \sum_{j=i}^{n} tr\left(\frac{\partial \dot{\mathbf{A}}_j}{\partial \dot{q}_i}\mathbf{J}_j\dot{\mathbf{A}}_j^T\right) \tag{3.11a}$$

$$\frac{d}{dt}\left(\frac{\partial L}{\partial \dot{q}_i}\right) = \sum_{j=i}^{n} tr\left(\frac{\partial \dot{\mathbf{A}}_j}{\partial \dot{q}_i}\mathbf{J}_j\ddot{\mathbf{A}}_j^T + \frac{d}{dt}\left(\frac{\partial \dot{\mathbf{A}}_j}{\partial \dot{q}_i}\right)\mathbf{J}_j\dot{\mathbf{A}}_j^T\right). \tag{3.11b}$$

Then, the second term of the right-hand side becomes

$$\begin{aligned}\frac{\partial L}{\partial q_i} &= \frac{\partial K}{\partial q_i} - \frac{\partial V}{\partial q_i} \\ &= \sum_{j=i}^{n} tr\left(\frac{\partial \dot{\mathbf{A}}_j}{\partial q_i}\mathbf{J}_j\dot{\mathbf{A}}_j^T\right) - \left(-\sum_{j=i}^{n} m_j\mathbf{g}^T\frac{\partial \mathbf{A}_j}{\partial q_i}{}^j\overline{\mathbf{r}}_j - \sum_{j=i}^{n}\mathbf{f}_k^T\frac{\partial \mathbf{A}_j}{\partial q_i}{}^k\mathbf{r}_f\delta_{jk}\right).\end{aligned} \tag{3.12}$$

The following relationships can be shown:

$$\frac{\partial \dot{\mathbf{A}}_j}{\partial \dot{q}_i} = \frac{\partial \mathbf{A}_j}{\partial q_i} \tag{3.13a}$$

$$\frac{\partial \dot{\mathbf{A}}_j}{\partial q_i} = \frac{d}{dt}\left(\frac{\partial \dot{\mathbf{A}}_j}{\partial \dot{q}_i}\right) \tag{3.13b}$$

$$\mathbf{A}_j = \mathbf{A}_i{}^i\mathbf{T}_j, \tag{3.13c}$$

where ${}^i\mathbf{T}_j$ is the DH transformation matrix from the j^{th} reference frame to the i^{th} reference frame.

Therefore, Equation (3.1) becomes

$$Q_i = \sum_{j=i}^{n} tr\left(\frac{\partial \mathbf{A}_i}{\partial q_i}\,{}^{i}\mathbf{T}_j \mathbf{J}_j \ddot{\mathbf{A}}_j^T\right) - \sum_{j=i}^{n} m_j \mathbf{g}^T \frac{\partial \mathbf{A}_i}{\partial q_i}\,{}^{i}\mathbf{T}_j\,{}^{j}\bar{\mathbf{r}}_j - \sum_{j=i}^{n} \mathbf{f}_k^T \frac{\partial \mathbf{A}_i}{\partial q_i}\,{}^{i}\mathbf{T}_j\,{}^{k}\mathbf{r}_f \delta_{jk} \,. \quad (3.14)$$

Now, the generalized force can be decomposed into non-conservative force (τ_i) and conservative force ($\tilde{\tau}_i$), such as

$$Q_i = \tau_i + \tilde{\tau}_i \,. \quad (3.15)$$

Then, Equation (3.14) can be rewritten as

$$\tau_i = tr\left(\frac{\partial \mathbf{A}_i}{\partial q_i} \sum_{j=i}^{n} {}^{i}\mathbf{T}_j \mathbf{J}_j \ddot{\mathbf{A}}_j^T\right) - \mathbf{g}^T \frac{\partial \mathbf{A}_i}{\partial q_i} \sum_{j=i}^{n} m_j\,{}^{i}\mathbf{T}_j\,{}^{j}\bar{\mathbf{r}}_j - \mathbf{f}_k^T \frac{\partial \mathbf{A}_i}{\partial q_i} \sum_{j=i}^{n} {}^{i}\mathbf{T}_j\,{}^{k}\mathbf{r}_f \delta_{jk} - \tilde{\tau}_i \,. \quad (3.16)$$

Since the generalized coordinates q_i represent joint angle, $\tilde{\tau}_i$ is the summation of moments applied to the link expressed in the i^{th} reference frame. Let $\mathbf{G}_i$ be the summation of moments defined in the global reference frame and apply it to the link expressed in the i^{th} reference frame. $\mathbf{G}_i$ is defined in the global reference frame, and $\tilde{\tau}_i$ is defined in the local reference frame. Thus, $\mathbf{G}_i$ has to be transferred into the local reference frame. Recall that the only rotational degree of freedom is allowed along the z-axis in the mechanical system, according to the DH method. Therefore, we have the following relationship between $\tilde{\tau}_i$ and $\mathbf{G}_i$:

$$\tilde{\tau}_i = \mathbf{G}_i \mathbf{A}_{i-1} \mathbf{z}_0 \,, \quad (3.17)$$

where $\mathbf{z}_0$ is $\begin{bmatrix} 0 & 0 & 1 & 0 \end{bmatrix}^T$. The term $\mathbf{A}_{i-1}\mathbf{z}_0$ means that the local reference frame, which corresponds to the degrees of freedom ($\mathbf{z}_0$), is represented in the global reference frame. Then, the moment value along that local axis ($\mathbf{z}_0$) can be obtained by the inner product of

$\mathbf{G}_i$ and $\mathbf{A}_{i-1}\mathbf{z}_0$ as in Equation (3.17). Finally, Equation (3.16) is rewritten as

$$\tau_i = tr\left(\frac{\partial \mathbf{A}_i}{\partial q_i}\sum_{j=i}^{n} {}^{i}\mathbf{T}_j \mathbf{J}_j \ddot{\mathbf{A}}_j^T\right) - \mathbf{g}^T \frac{\partial \mathbf{A}_i}{\partial q_i}\sum_{j=i}^{n} m_j {}^{i}\mathbf{T}_j {}^{j}\bar{\mathbf{r}}_j - \mathbf{f}_k^T \frac{\partial \mathbf{A}_i}{\partial q_i}\sum_{j=i}^{n} {}^{i}\mathbf{T}_j {}^{k}r_f \delta_{jk} - \mathbf{G}_i \mathbf{A}_{i-1}\mathbf{z}_0 . \quad (3.18)$$

3.2.2. Recursive Lagrangian Formulation

The first term of Equation (3.18) can be represented as

$$\begin{aligned}
\mathbf{D}_i &= \sum_{j=i}^{n} {}^{i}\mathbf{T}_j \mathbf{J}_j \ddot{\mathbf{A}}_j^T \\
&= {}^{i}\mathbf{T}_i \mathbf{J}_i \ddot{\mathbf{A}}_i^T + \sum_{j=i+1}^{n} {}^{i}\mathbf{T}_j \mathbf{J}_j \ddot{\mathbf{A}}_j^T \\
&= \mathbf{J}_i \ddot{\mathbf{A}}_i^T + {}^{i}\mathbf{T}_{i+1} \sum_{j=i+1}^{n} {}^{i+1}\mathbf{T}_j \mathbf{J}_j \ddot{\mathbf{A}}_j^T \\
&= \mathbf{J}_i \ddot{\mathbf{A}}_i^T + {}^{i}\mathbf{T}_{i+1}\mathbf{D}_{i+1}.
\end{aligned} \quad (3.19)$$

The second term of Equation (3.18) can be represented as

$$\begin{aligned}
\mathbf{E}_i &= \sum_{j=i}^{n} m_j {}^{i}\mathbf{T}_j {}^{j}\bar{\mathbf{r}}_j \\
&= m_i {}^{i}\mathbf{T}_i {}^{i}\bar{\mathbf{r}}_i + \sum_{j=i+1}^{n} m_j {}^{i}\mathbf{T}_j {}^{j}\bar{\mathbf{r}}_j \\
&= m_i {}^{i}\bar{\mathbf{r}}_i + {}^{i}\mathbf{T}_{i+1} \sum_{j=i+1}^{n} m_j {}^{i+1}\mathbf{T}_j {}^{j}\bar{\mathbf{r}}_j \\
&= m_i {}^{i}\bar{\mathbf{r}}_i + {}^{i}\mathbf{T}_{i+1}\mathbf{E}_{i+1}.
\end{aligned} \quad (3.20)$$

The third term of Equation (3.18) can be represented as

$$\begin{aligned}\mathbf{F}_i &= \sum_{j=i}^{n} {}^{i}\mathbf{T}_j \, {}^{k}\mathbf{r}_f \delta_{jk} \\ &= {}^{i}\mathbf{T}_i \, {}^{k}\mathbf{r}_f \delta_{ik} + \sum_{j=i+1}^{n} {}^{i}\mathbf{T}_j \, {}^{k}\mathbf{r}_f \delta_{jk} \\ &= {}^{k}\mathbf{r}_f \delta_{ik} + {}^{i}\mathbf{T}_{i+1} \sum_{j=i+1}^{n} {}^{i+1}\mathbf{T}_j \, {}^{k}\mathbf{r}_f \delta_{jk} \\ &= {}^{k}\mathbf{r}_f \delta_{ik} + {}^{i}\mathbf{T}_{i+1} \mathbf{F}_{i+1}.\end{aligned} \tag{3.21}$$

The last term of Equation (3.18) can be represented as

$$\mathbf{G}_i = \mathbf{h}_k \delta_{ik} + \mathbf{G}_{i+1}, \tag{3.22}$$

where $\mathbf{h}_k$ is an external moment vector defined in the global reference frame and acting on the link expressed in the k^{th} reference frame.

Therefore, Equation (3.18) becomes

$$\tau_i = tr\left(\frac{\partial \mathbf{A}_i}{\partial q_i}\mathbf{D}_i\right) - \mathbf{g}^T \frac{\partial \mathbf{A}_i}{\partial q_i}\mathbf{E}_i - \mathbf{f}_k^T \frac{\partial \mathbf{A}_i}{\partial q_i}\mathbf{F}_i - \mathbf{G}^T{}_i \mathbf{A}_{i-1}\mathbf{z}_0 \tag{3.23}$$

in recursive form, where $\mathbf{D}_{n+1} = \mathbf{E}_{n+1} = \mathbf{F}_{n+1} = \mathbf{G}_{n+1} = \mathbf{0}$.

3.2.3. Sensitivity Analysis

The sensitivity analysis should be carefully derived for the optimization process. The sensitivities of Equation (3.23) are

$$\frac{\partial \tau_i}{\partial q_k} = \begin{cases} tr\left(\dfrac{\partial^2 \mathbf{A}_i}{\partial q_i \partial q_k}\mathbf{D}_i + \dfrac{\partial \mathbf{A}_i}{\partial q_i}\dfrac{\partial \mathbf{D}_i}{\partial q_k}\right) - \mathbf{g}^T \dfrac{\partial^2 \mathbf{A}_i}{\partial q_i \partial q_k}\mathbf{E}_i - \mathbf{f}_k^T \dfrac{\partial^2 \mathbf{A}_i}{\partial q_i \partial q_k}\mathbf{F}_i - \mathbf{G}_i^T \dfrac{\partial \mathbf{A}_{i-1}}{\partial q_k}\mathbf{z}_0 & (k \le i) \\ tr\left(\dfrac{\partial \mathbf{A}_i}{\partial q_i}\dfrac{\partial \mathbf{D}_i}{\partial q_k}\right) - \mathbf{g}^T \dfrac{\partial \mathbf{A}_i}{\partial q_i}\dfrac{\partial \mathbf{E}_i}{\partial q_k} - \mathbf{f}_k^T \dfrac{\partial \mathbf{A}_i}{\partial q_i}\dfrac{\partial \mathbf{F}_i}{\partial q_k} & (k > i) \end{cases} \tag{3.24a}$$

$$\frac{\partial \tau_i}{\partial \dot{q}_k} = tr\left(\frac{\partial \mathbf{A}_i}{\partial q_i}\frac{\partial \mathbf{D}_i}{\partial \dot{q}_k}\right) \tag{3.24b}$$

$$\frac{\partial \tau_i}{\partial \ddot{q}_k} = tr\left(\frac{\partial \mathbf{A}_i}{\partial q_i}\frac{\partial \mathbf{D}_i}{\partial \ddot{q}_k}\right). \tag{3.24c}$$

where

$$\frac{\partial \mathbf{A}_i}{\partial q_i} = \mathbf{A}_{i-1}\frac{\partial {}^{i-1}\mathbf{T}_i}{\partial q_i} \tag{3.24d}$$

$$\frac{\partial^2 \mathbf{A}_i}{\partial q_k \partial q_i} = \begin{cases} \dfrac{\partial \mathbf{A}_{i-1}}{\partial q_k}\dfrac{\partial {}^{i-1}\mathbf{T}_i}{\partial q_i} + \mathbf{A}_{i-1}\dfrac{\partial^2 {}^{i-1}\mathbf{T}_i}{\partial q_k \partial q_i} = \dfrac{\partial \mathbf{A}_{i-1}}{\partial q_k}\dfrac{\partial {}^{i-1}\mathbf{T}_i}{\partial q_i} & (k<i) \\ \dfrac{\partial \mathbf{A}_{i-1}}{\partial q_k}\dfrac{\partial {}^{i-1}\mathbf{T}_i}{\partial q_i} + \mathbf{A}_{i-1}\dfrac{\partial^2 {}^{i-1}\mathbf{T}_i}{\partial q_k \partial q_i} = \mathbf{A}_{i-1}\dfrac{\partial^2 {}^{i-1}\mathbf{T}_i}{\partial q_i^2} & (k=i) \end{cases} \tag{3.24e}$$

$$\frac{\partial \mathbf{D}_i}{\partial q_k} = \begin{cases} \mathbf{J}_i\dfrac{\partial \ddot{\mathbf{A}}_i^T}{\partial q_k} + \dfrac{\partial {}^{i}\mathbf{T}_{i+1}}{\partial q_k}\mathbf{D}_{i+1} + {}^{i}\mathbf{T}_{i+1}\dfrac{\partial \mathbf{D}_{i+1}}{\partial q_k} = \mathbf{J}_i\dfrac{\partial \ddot{\mathbf{A}}_i^T}{\partial q_k} + {}^{i}\mathbf{T}_{i+1}\dfrac{\partial \mathbf{D}_{i+1}}{\partial q_k} & (k<i+1) \\ \dfrac{\partial {}^{i}\mathbf{T}_{i+1}}{\partial q_k}\mathbf{D}_{i+1} + {}^{i}\mathbf{T}_{i+1}\dfrac{\partial \mathbf{D}_{i+1}}{\partial q_k} & (k=i+1) \\ \dfrac{\partial {}^{i}\mathbf{T}_{i+1}}{\partial q_k}\mathbf{D}_{i+1} + {}^{i}\mathbf{T}_{i+1}\dfrac{\partial \mathbf{D}_{i+1}}{\partial q_k} = {}^{i}\mathbf{T}_{i+1}\dfrac{\partial \mathbf{D}_{i+1}}{\partial q_k} & (k>i+1) \end{cases} \tag{3.24f}$$

$$\frac{\partial \mathbf{D}_i}{\partial \dot{q}_k} = \begin{cases} \mathbf{J}_i\dfrac{\partial \ddot{\mathbf{A}}_i^T}{\partial \dot{q}_k} + {}^{i}\mathbf{T}_{i+1}\dfrac{\partial \mathbf{D}_{i+1}}{\partial \dot{q}_k} & (k<i+1) \\ {}^{i}\mathbf{T}_{i+1}\dfrac{\partial \mathbf{D}_{i+1}}{\partial \dot{q}_k} & (k\geq i+1) \end{cases} \tag{3.24g}$$

$$\frac{\partial \mathbf{D}_i}{\partial \ddot{q}_k} = \begin{cases} \mathbf{J}_i \dfrac{\partial \ddot{\mathbf{A}}_i^T}{\partial \ddot{q}_k} + {}^i\mathbf{T}_{i+1} \dfrac{\partial \mathbf{D}_{i+1}}{\partial \ddot{q}_k} & (k < i+1) \\ {}^i\mathbf{T}_{i+1} \dfrac{\partial \mathbf{D}_{i+1}}{\partial \ddot{q}_k} & (k \geq i+1) \end{cases} \tag{3.24h}$$

$$\frac{\partial \mathbf{E}_i}{\partial q_k} = \begin{cases} \cancel{\dfrac{\partial {}^i\mathbf{T}_{i+1}}{\partial q_k}} \mathbf{E}_{i+1} + {}^i\mathbf{T}_{i+1} \cancel{\dfrac{\partial \mathbf{E}_{i+1}}{\partial q_k}} = \mathbf{0} & (k < i+1) \\ \dfrac{\partial {}^i\mathbf{T}_{i+1}}{\partial q_k} \mathbf{E}_{i+1} + {}^i\mathbf{T}_{i+1} \dfrac{\partial \mathbf{E}_{i+1}}{\partial q_k} & (k = i+1) \\ \cancel{\dfrac{\partial {}^i\mathbf{T}_{i+1}}{\partial q_k}} \mathbf{E}_{i+1} + {}^i\mathbf{T}_{i+1} \dfrac{\partial \mathbf{E}_{i+1}}{\partial q_k} = {}^i\mathbf{T}_{i+1} \dfrac{\partial \mathbf{E}_{i+1}}{\partial q_k} & (k > i+1) \end{cases} \tag{3.24i}$$

$$\frac{\partial \mathbf{F}_i}{\partial q_k} = \begin{cases} \mathbf{0} & (k < i+1) \\ \dfrac{\partial {}^i\mathbf{T}_{i+1}}{\partial q_k} \mathbf{F}_{i+1} + {}^i\mathbf{T}_{i+1} \dfrac{\partial \mathbf{F}_{i+1}}{\partial q_k} & (k = i+1) \\ {}^i\mathbf{T}_{i+1} \dfrac{\partial \mathbf{F}_{i+1}}{\partial q_k} & (k > i+1) \end{cases} \tag{3.24j}$$

$$\frac{\partial \mathbf{G}_i^T}{\partial q_k} = \mathbf{0} \tag{3.24k}$$

3.2.4. Inertia Matrix

The inertia $\mathbf{J}_i$ for Equation (3.7) is

$$\mathbf{J}_i = \int {}^i\mathbf{r}_i^* \, {}^i\mathbf{r}_i^{*T} dm = \begin{bmatrix} \int x_i^{*2} dm & \int x_i^* y_i^* dm & \int x_i^* z_i^* dm & \int x_i^* dm \\ \int x_i^* y_i^* dm & \int y_i^{*2} dm & \int y_i^* z_i^* dm & \int y_i^* dm \\ \int x_i^* z_i^* dm & \int y_i^* z_i^* dm & \int z_i^{*2} dm & \int z_i^* dm \\ \int x_i^* dm & \int y_i^* dm & \int z_i^* dm & \int dm \end{bmatrix}. \tag{3.25}$$

By using inertia tensor $I_{xx}, I_{yy}, I_{zz}, I_{xy}, I_{yz}, I_{xz}$, Equation (3.25) can be rewritten as

$$\mathbf{J}_i = \begin{bmatrix} \dfrac{-I_{xx}+I_{yy}+I_{zz}}{2} & I_{xy} & I_{xz} & m_i\bar{x}_i \\ I_{xy} & \dfrac{I_{xx}-I_{yy}+I_{zz}}{2} & I_{yz} & m_i\bar{y}_i \\ I_{xz} & I_{yz} & \dfrac{I_{xx}+I_{yy}-I_{zz}}{2} & m_i\bar{z}_i \\ m_i\bar{x}_i & m_i\bar{y}_i & m_i\bar{z}_i & m_i \end{bmatrix}, \tag{3.26}$$

where ${}^i\bar{\mathbf{r}}_i = \begin{bmatrix} \bar{x}_i & \bar{y}_i & \bar{z}_i & 1 \end{bmatrix}^T$ is the center of mass vector of the link that is expressed in the i^{th} reference frame.

3.3. Computational Consideration

The number of multiplications and additions for each formulation are summarized in Table 3.1. The order of calculations for the three formulations noted previously can be observed in the table. For a system with small degrees of freedom, the total computational time with the three formulations may not be too different. However, for a model with a large number of degrees of freedom (such as the Santos model's 55 degrees of freedom), the number of calculations can be significantly different. This can have a significant impact on the efficiency of the entire optimization process. It is clear that the recursive formulation is the most suitable for digital human modeling, and it is used for the running problem.

Table 3.1 Number of multiplication and additions (*n*: number of transformation matrices)

Method	Multiplications	Additions
Uicker (1965)	32 1/2 n^4+86 5/12 n^3 +171 1/4 n^2 + 5 1/3 n -128	25 n^4 + 66 1/3 n^3 +129 1/2 n^2 +42 1/3 n -96
Waters (1979)	106 1/2 n^2 + 620 1/2 n – 512	82 n^2 + 514 n – 384
Hollerbach (1980)	830 n - 592	675 n - 464

Table 3.2 Number of multiplications and additions for *n*=55

Method	Multiplications	Additions	Total
Uicker (1965)	312293722	240195803	552489525
Waters (1979)	355778	275936	631714
Hollerbach (1980)	45058	36661	81719

3.4. Pendulum Example with Recursive Lagrange EOM Module

The equations of motion were verified by the forward dynamics process using a commercial general-purpose multi-body dynamics software code (ADAMS). The simple pendulum problem was solved for this process.

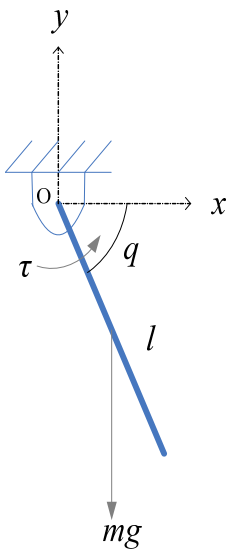

Figure 3.2 Simple pendulum

Figure 3.2 depicts the simple pendulum model in which mass is 0.5 kg, length is 0.4 m, and it is assumed to be a slender bar. The equation of motion is given as

$$I\ddot{q} + mg\frac{l}{2}\cos q = \tau \,. \tag{3.27}$$

The initial position is $q = 0$, the joint torque is $\tau = 0$, and the ADAMS results are shown in Figure3.3.

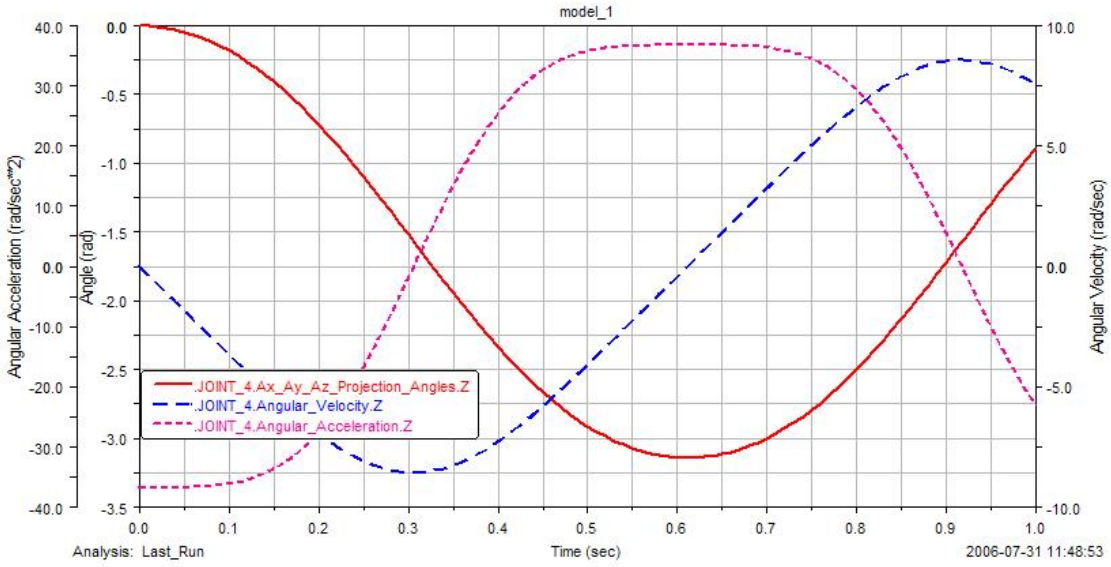

Figure 3.3 Joint angle, angular velocity, and angular acceleration of simple pendulum

To verify EOM module, first, the joint angel, joint angle velocity, and joint angle acceleration is obtained by ADAMS (Figure 3.3). These obtained data - joint angle, joint angle velocity, and joint angle acceleration is imposed to EOM module. Then, the joint torque from EOM module is checked (inverse dynamics). The joint torque is indeed obtained as zero, thus verifying the current EOM module. As same manner, it is verified for the case of external joint torque ($\tau \neq 0$).

CHAPTER 4

DYNAMIC STABILITY

Much research has been done in the area of biped robots. Dynamic stability is an important consideration in the gait problem. There are many concepts related to stability, such as center of pressure, foot rotation index, and zero moment point (ZMP). Zero moment point is the key constraint, or most popular technique, for handling the stability of the biped robot. In 1968 and 1969, Vukobratović presented this concept for synthesis of biped gait. Waseda University in Japan has applied this technique to their walking robot, WL-10RD. It was the first practical demonstration of ZMP. The ZMP concept is more than thirty years old, and many researchers have applied it to their biped robots; an example is the Honda's ASIMO robot.

4.1. Zero Moment Point

An important consideration for the running problem is the dynamic stability of the motion. The most common constraint for achieving stability for biped gait analysis is the ZMP constraint in the support phase. Zero moment point can be derived by using the following steps (Sardin and Bessonnet, 2004).

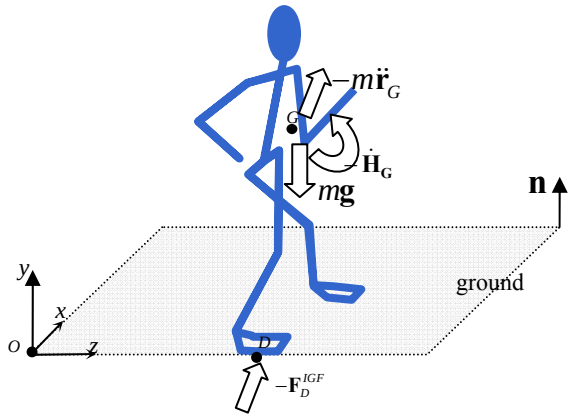

Figure 4.1 Description of ZMP

In Figure 4.1, point *D* is the ZMP, which needs to be determined; *m* is the total mass of the body; $\mathbf{g}$ is the gravitational acceleration; *G* is the center of mass of the body; $\ddot{\mathbf{r}}_G$ is the acceleration of *G*; and $\dot{\mathbf{H}}_G$ is the rate of angular momentum about *G*. The resultant force due to inertia and gravity forces at point *D* is written as

$$\mathbf{F}_D^{IGF} = m\mathbf{g} - m\ddot{\mathbf{r}}_G . \tag{4.1}$$

The resultant moment about the ZMP by inertia, gravity, and external force (IGF) is given as

$$\mathbf{M}_D^{IGF} = \mathbf{r}_{DG} \times \mathbf{F}_D^{IGF} - \dot{\mathbf{H}}_G \tag{4.2a}$$

$$\mathbf{M}_D^{IGF} = \mathbf{r}_{DG} \times m\mathbf{g} - \mathbf{r}_{DG} \times m\ddot{\mathbf{r}}_G - \dot{\mathbf{H}}_G . \tag{4.2b}$$

The resultant moment about the fixed point *O* is

$$\mathbf{M}_O^{IGF} = \mathbf{r}_{OG} \times \mathbf{F}_D^{IGF} - \dot{\mathbf{H}}_G \tag{4.3a}$$

$$\mathbf{M}_O^{IGF} = \mathbf{r}_{OG} \times m\mathbf{g} - \mathbf{r}_{OG} \times m\ddot{\mathbf{r}}_G - \dot{\mathbf{H}}_G . \tag{4.3b}$$

Since

$$\mathbf{r}_{DG} = \mathbf{r}_{OG} - \mathbf{r}_{OD} , \tag{4.4}$$

Equation (4.2b) can be written as

$$\mathbf{M}_D^{IGF} = \mathbf{M}_O^{IGF} - \mathbf{r}_{OD} \times \mathbf{F}_D^{IGF} . \tag{4.5}$$

Note the condition to determine ZMP is that the tipping moment by the IGF measured at *D* should be zero. Therefore, we have

$$\begin{aligned} \mathbf{n} \times \mathbf{M}_D^{IGF} &= \mathbf{n} \times \mathbf{M}_O^{IGF} - \mathbf{n} \times (\mathbf{r}_{OD} \times \mathbf{F}_D^{IGF}) \\ &= \mathbf{n} \times \mathbf{M}_O^{IGF} - (\mathbf{n} \cdot \mathbf{F}_D^{IGF})\mathbf{r}_{OD} + (\mathbf{n} \cdot \mathbf{r}_{OD})\mathbf{F}_D^{IGF} \\ &= \mathbf{0} \end{aligned} \tag{4.6}$$

where **n** is a unit vector that is normal to ground plane. Since

$$\mathbf{n} \cdot \mathbf{r}_{OD} = 0 , \tag{4.7}$$

ZMP location is obtained from Equation (4.6) as follows:

$$\mathbf{r}_{OD} = \frac{\mathbf{n} \times \mathbf{M}_O^{IGF}}{\mathbf{n} \cdot \mathbf{F}_D^{IGF}} . \tag{4.8}$$

Summation of the inertia forces acting on each segment gives the resulting inertia forces acting on the center of mass of the body ($-\dot{\mathbf{H}}_G$ and $m_i \ddot{\mathbf{r}}_{Gi}$). Therefore, the resultant reaction force by the inertial and gravitational forces that are acting on the body can be calculated as

$$\mathbf{F}_D^{IGF} = \sum_i^n (m_i \mathbf{g} - m_i \ddot{\mathbf{r}}_{Gi}) , \tag{4.9}$$

where n is the number of body segments and $\ddot{\mathbf{r}}_{Gi}$ is the acceleration of the i^{th} body segment's center of mass. The resultant moment $\mathbf{M}_O^{IGF}$ can be calculated in a similar way using Equations (4.3a) and (4.9):

$$\mathbf{M}_O^{IGF} = \sum_i^n \left[\mathbf{r}_{OGi} \times \left(m_i \mathbf{g} - m_i \ddot{\mathbf{r}}_{Gi} \right) \right] - \dot{\mathbf{H}}_G , \tag{4.10}$$

where $\mathbf{r}_{OGi}$ is the location vector of the i^{th} body segment's center of mass in the global

reference frame and $\dot{\mathbf{H}}_G$ is the rate of angular momentum about the center of mass of the body—point *G* in Figure 4.1. Let the components of $\dot{\mathbf{H}}_G$ be

$$\dot{\mathbf{H}}_G = \begin{bmatrix} \dot{H}_{Gx} \\ \dot{H}_{Gy} \\ \dot{H}_{Gz} \end{bmatrix}. \tag{4.11}$$

The vector $\mathbf{n}$ (unit normal vector) can be expressed as its components, n_x, n_y, n_z:

$$\mathbf{n} = \frac{1}{\sqrt{n_x^2 + n_y^2 + n_z^2}} \begin{bmatrix} n_x \\ n_y \\ n_z \end{bmatrix}. \tag{4.12}$$

Then the ZMP from Equations (4.8), (4.9) and (4.10) is

$$\mathbf{x}_{OD} = \begin{bmatrix} x_{zmp} \\ y_{zmp} \\ z_{zmp} \end{bmatrix} \tag{4.13a}$$

$$x_{zmp} = \frac{\sum_i^n \left[m_i(-\ddot{y}_i x_i n_y - g x_i n_y - \ddot{z}_i x_i n_z + \ddot{x}_i y_i n_y + \ddot{x}_i z_i n_z) \right] - \dot{H}_{Gz} n_y + \dot{H}_{Gy} n_z}{\sum_i^n m_i(-\ddot{x}_i n_x - \ddot{y}_i n_y - g n_y - \ddot{z}_i n_z)} \tag{4.13b}$$

$$y_{zmp} = \frac{\sum_i^n \left[m_i(\ddot{y}_i n_x x_i + g n_x x_i - \ddot{x}_i y_i n_x - \ddot{z}_i y_i n_z + \ddot{y}_i z_i n_z + g n_z z_i) \right] + \dot{H}_{Gz} n_x - \dot{H}_{Gx} n_z}{\sum_i^n m_i(-\ddot{x}_i n_x - \ddot{y}_i n_y - g n_y - \ddot{z}_i n_z)} \tag{4.13c}$$

$$z_{zmp} = \frac{\sum_i^n \left[m_i(-\ddot{x}_i z_i n_x - g z_i n_y - \ddot{y}_i z_i n_y + \ddot{z}_i x_i n_x + \ddot{z}_i y_i n_y) \right] - \dot{H}_{Gy} n_x + \dot{H}_{Gx} n_y}{\sum_i^n m_i(-\ddot{x}_i n_x - \ddot{y}_i n_y - g n_y - \ddot{z}_i n_z)} \tag{4.13d}$$

If the *x*-*z* plane is considered as the ground as shown in Figure 4.1, the normal vector $\mathbf{n}$ is $[0 \quad 1 \quad 0]^T$. Then, the ZMP can be calculated as

$$z_{zmp} = \frac{\sum_{i}^{n}\left[m_i(-\ddot{y}_i - g)z_i + m_i\ddot{z}_i y_i\right] + \dot{H}_{Gx}}{\sum_{i}^{n} m_i(-\ddot{y}_i - g)} \tag{4.14a}$$

$$x_{zmp} = \frac{\sum_{i}^{n}\left[m_i(-\ddot{y}_i - g)x_i + m_i\ddot{x}_i y_i\right] - \dot{H}_{Gz}}{\sum_{i}^{n} m_i(-\ddot{y}_i - g)}. \tag{4.14b}$$

4.2. Rate of Angular Momentum in ZMP

The classical method to find the rate of angular momentum $\dot{\mathbf{H}}_G$ at G is

$$\dot{\mathbf{H}}_G = \sum_{i}^{n} \mathbf{R}_i(\mathbf{J}_i\dot{\boldsymbol{\omega}}_i - (\mathbf{J}_i\boldsymbol{\omega}_i)\times\boldsymbol{\omega}_i), \tag{4.15}$$

where the variables are defined as follows:

$\mathbf{R}_i$ is the rotation matrix from the i^{th} link frame to the global reference frame

$\mathbf{J}_i$ is the mass moment of the inertia matrix of the i^{th} link about its center of mass

$\boldsymbol{\omega}_i$ is the angular velocity vector of the i^{th} link.

Since $\boldsymbol{\omega}_i$ is an absolute value, Equation (4.15) is very difficult to implement in the Denavit-Hartenberg method. The reason is that the generalized coordinate (joint angles) q_i and angular velocities $\dot{q}_i$ in the Denavit-Hartenberg method are relative values (and local). For example, to transfer the relative values to the absolute values, those values have to be written in global coordinate system. Otherwise, there is no way to calculate the absolute value. Once they are transferred to absolute values, they must be rewritten in local form because the mass moment of inertia is in local form. Even though there is a way to calculate the mass moment of inertia in terms of the global reference frame, it

takes too much calculation time because the mass moment of inertia is no longer in data form and must be calculated with the integral formula at every time segment.

4.2.1. Generalized Momentum

To overcome the foregoing difficulty, we can use the generalized momentum. The components of the rate of angular momentum can be obtained by taking derivative of the generalized momentum with respect to time. The generalized momentum p_i is defined as

$$p_i = \frac{\partial L}{\partial \dot{q}_i}, \tag{4.16}$$

where L is the Lagrangian and q_i is the generalized coordinate. Note that the notation of angular momentum p_i is usually used in Lagrangian mechanics, and the notation of angular momentum $\mathbf{H}$ is usually used in Newtonian mechanics. If the generalized coordinate q_i is a linear displacement, p_i is the linear momentum. If the generalized coordinate q_i is an angular displacement, p_i is the angular momentum (Greenwood, 1977). The derivative of the Lagrangian L with respect to $\dot{q}_i$ has already been derived in Chapter 3:

$$\frac{\partial L}{\partial \dot{q}_i} = \sum_{j=i}^{n} tr\left(\frac{\partial \dot{\mathbf{A}}_j}{\partial \dot{q}_i} \mathbf{J}_j \dot{\mathbf{A}}_j^T \right). \tag{4.17}$$

4.2.2. Rate of Angular Momentum in Recursive Form

The rate of angular momentum is the derivative of Equation (4.17) with respect to time, which can be obtained as

$$\frac{d}{dt}\left(\frac{\partial L}{\partial \dot{q}_i}\right)=\sum_{j=i}^{n} tr\left(\frac{\partial \dot{\mathbf{A}}_j}{\partial \dot{q}_i}\mathbf{J}_j\ddot{\mathbf{A}}_j^T+\frac{d}{dt}\left(\frac{\partial \dot{\mathbf{A}}_j}{\partial \dot{q}_i}\right)\mathbf{J}_j\dot{\mathbf{A}}_j^T\right). \tag{4.18}$$

The following relationship can be shown:

$$\frac{\partial \dot{\mathbf{A}}_j}{\partial \dot{q}_i}=\frac{\partial \mathbf{A}_j}{\partial q_i} \tag{4.19a}$$

$$\frac{\partial \dot{\mathbf{A}}_j}{\partial q_i}=\frac{d}{dt}\left(\frac{\partial \dot{\mathbf{A}}_j}{\partial \dot{q}_i}\right) \tag{4.19b}$$

$$\mathbf{A}_j=\mathbf{A}_i\,{}^i\mathbf{T}_j \tag{4.19c}$$

$$\dot{\mathbf{A}}_j=\dot{\mathbf{A}}_i\,{}^i\mathbf{T}_j+\mathbf{A}_i\,{}^i\dot{\mathbf{T}}_j\,. \tag{4.19d}$$

Then, Equation (4.18) can be rewritten as

$$\begin{aligned}\frac{d}{dt}\left(\frac{\partial L}{\partial \dot{q}_i}\right)&=\sum_{j=i}^{n} tr\left(\frac{\partial \mathbf{A}_j}{\partial q_i}\mathbf{J}_j\ddot{\mathbf{A}}_j^T+\frac{\partial \dot{\mathbf{A}}_j}{\partial q_i}\mathbf{J}_j\dot{\mathbf{A}}_j^T\right)\\&=\sum_{j=i}^{n} tr\left(\frac{\partial \mathbf{A}_i}{\partial q_i}\,{}^i\mathbf{T}_j\mathbf{J}_j\ddot{\mathbf{A}}_j^T+\frac{\partial \dot{\mathbf{A}}_i}{\partial q_i}\,{}^i\mathbf{T}_j\mathbf{J}_j\dot{\mathbf{A}}_j^T+\frac{\partial \mathbf{A}_i}{\partial q_i}\,{}^i\dot{\mathbf{T}}_j\mathbf{J}_j\dot{\mathbf{A}}_j^T\right)\\&=tr\left(\frac{\partial \mathbf{A}_i}{\partial q_i}\sum_{j=i}^{n}\,{}^i\mathbf{T}_j\mathbf{J}_j\ddot{\mathbf{A}}_j^T\right)+tr\left(\frac{\partial \dot{\mathbf{A}}_i}{\partial q_i}\sum_{j=i}^{n}\,{}^i\mathbf{T}_j\mathbf{J}_j\dot{\mathbf{A}}_j^T\right)+tr\left(\frac{\partial \mathbf{A}_i}{\partial q_i}\sum_{j=i}^{n}\,{}^i\dot{\mathbf{T}}_j\mathbf{J}_j\dot{\mathbf{A}}_j^T\right)\end{aligned} \tag{4.20}$$

The first term of Equation (4.20) can be represented as

$$\begin{aligned}\mathbf{D}_i&=\sum_{j=i}^{n}\,{}^i\mathbf{T}_j\mathbf{J}_j\ddot{\mathbf{A}}_j^T\\&={}^i\mathbf{T}_i\mathbf{J}_i\ddot{\mathbf{A}}_i^T+\sum_{j=i+1}^{n}\,{}^i\mathbf{T}_j\mathbf{J}_j\ddot{\mathbf{A}}_j^T\\&=\mathbf{J}_i\ddot{\mathbf{A}}_i^T+\,{}^i\mathbf{T}_{i+1}\sum_{j=i+1}^{n}\,{}^{i+1}\mathbf{T}_j\mathbf{J}_j\ddot{\mathbf{A}}_j^T\\&=\mathbf{J}_i\ddot{\mathbf{A}}_i^T+\,{}^i\mathbf{T}_{i+1}\mathbf{D}_{i+1}\end{aligned} \tag{4.21}$$

The second term of Equation (4.20) can be represented as

$$\begin{aligned}\mathbf{D}_i^{'} &= \sum_{j=i}^{n} {}^{i}\mathbf{T}_j \mathbf{J}_j \dot{\mathbf{A}}_j^T \\ &= {}^{i}\mathbf{T}_i \mathbf{J}_i \dot{\mathbf{A}}_i^T + \sum_{j=i+1}^{n} {}^{i}\mathbf{T}_j \mathbf{J}_j \dot{\mathbf{A}}_j^T \\ &= \mathbf{J}_i \dot{\mathbf{A}}_i^T + {}^{i}\mathbf{T}_{i+1} \sum_{j=i+1}^{n} {}^{i+1}\mathbf{T}_j \mathbf{J}_j \dot{\mathbf{A}}_j^T \\ &= \mathbf{J}_i \dot{\mathbf{A}}_i^T + {}^{i}\mathbf{T}_{i+1} \mathbf{D}_{i+1}^{'}\end{aligned} \tag{4.22}$$

The third term of Equation (4.20) can be represented as

$$\begin{aligned}\mathbf{D}_i^{''} &= \sum_{j=i}^{n} {}^{i}\dot{\mathbf{T}}_j \mathbf{J}_j \dot{\mathbf{A}}_j^T \\ &= {}^{i}\dot{\mathbf{T}}_i \mathbf{J}_i \dot{\mathbf{A}}_i^T + \sum_{j=i+1}^{n} {}^{i}\dot{\mathbf{T}}_j \mathbf{J}_j \dot{\mathbf{A}}_j^T \\ &= {}^{i}\dot{\mathbf{T}}_{i+1} \sum_{j=i+1}^{n} {}^{i+1}\dot{\mathbf{T}}_j \mathbf{J}_j \dot{\mathbf{A}}_j^T \\ &= {}^{i}\dot{\mathbf{T}}_{i+1} \mathbf{D}_{i+1}^{''}\end{aligned} \tag{4.23}$$

Therefore, Equation (4.20) becomes

$$\begin{aligned}\dot{p}_i &= tr\left(\frac{\partial \mathbf{A}_i}{\partial q_i}\mathbf{D}_i\right) + tr\left(\frac{\partial \dot{\mathbf{A}}_i}{\partial q_i}\mathbf{D}_i^{'}\right) + tr\left(\frac{\partial \mathbf{A}_i}{\partial q_i}\mathbf{D}_i^{''}\right) \\ &= tr\left(\frac{\partial \mathbf{A}_i}{\partial q_i}(\mathbf{D}_i + \mathbf{D}_i^{''}) + \frac{\partial \dot{\mathbf{A}}_i}{\partial q_i}\mathbf{D}_i^{'}\right)\end{aligned} \tag{4.24}$$

in recursive form, where $\mathbf{D}_{n+1} = \mathbf{D}_{n+1}^{'} = \mathbf{D}_{n+1}^{''} = \mathbf{0}$.

4.2.3. Sensitivity of Rate of Angular Momentum

The analytical sensitivity analysis should be carefully derived for the optimization process. The sensitivity of Equation (4.21) is

$$\frac{\partial \mathbf{D}_i}{\partial q_k} = \begin{cases} \mathbf{J}_i \dfrac{\partial \ddot{\mathbf{A}}_i^T}{\partial q_k} + {}^i\mathbf{T}_{i+1} \dfrac{\partial \mathbf{D}_{i+1}}{\partial q_k} & (k < i+1) \\ \dfrac{\partial {}^i\mathbf{T}_{i+1}}{\partial q_k} \mathbf{D}_{i+1} + {}^i\mathbf{T}_{i+1} \dfrac{\partial \mathbf{D}_{i+1}}{\partial q_k} & (k = i+1) \\ {}^i\mathbf{T}_{i+1} \dfrac{\partial \mathbf{D}_{i+1}}{\partial q_k} & (k > i+1) \end{cases} \tag{4.25a}$$

$$\frac{\partial \mathbf{D}_i}{\partial \dot{q}_k} = \begin{cases} \mathbf{J}_i \dfrac{\partial \ddot{\mathbf{A}}_i^T}{\partial \dot{q}_k} + {}^i\mathbf{T}_{i+1} \dfrac{\partial \mathbf{D}_{i+1}}{\partial \dot{q}_k} & (k < i+1) \\ {}^i\mathbf{T}_{i+1} \dfrac{\partial \mathbf{D}_{i+1}}{\partial \dot{q}_k} & (k \geq i+1) \end{cases} \tag{4.25b}$$

$$\frac{\partial \mathbf{D}_i}{\partial \ddot{q}_k} = \begin{cases} \mathbf{J}_i \dfrac{\partial \ddot{\mathbf{A}}_i^T}{\partial \ddot{q}_k} + {}^i\mathbf{T}_{i+1} \dfrac{\partial \mathbf{D}_{i+1}}{\partial \ddot{q}_k} & (k < i+1) \\ {}^i\mathbf{T}_{i+1} \dfrac{\partial \mathbf{D}_{i+1}}{\partial \ddot{q}_k} & (k \geq i+1) \end{cases} \tag{4.25c}$$

The sensitivity of Equation (4.22) is

$$\frac{\partial \mathbf{D}'_i}{\partial q_k} = \begin{cases} \mathbf{J}_i \dfrac{\partial \dot{\mathbf{A}}_i^T}{\partial q_k} + {}^i\mathbf{T}_{i+1} \dfrac{\partial \mathbf{D}'_{i+1}}{\partial q_k} & (k < i+1) \\ \dfrac{\partial {}^i\mathbf{T}_{i+1}}{\partial q_k} \mathbf{D}'_{i+1} + {}^i\mathbf{T}_{i+1} \dfrac{\partial \mathbf{D}'_{i+1}}{\partial q_k} & (k = i+1) \\ {}^i\mathbf{T}_{i+1} \dfrac{\partial \mathbf{D}'_{i+1}}{\partial q_k} & (k > i+1) \end{cases} \tag{4.26a}$$

$$\frac{\partial \mathbf{D}'_i}{\partial \dot{q}_k} = \begin{cases} \mathbf{J}_i \dfrac{\partial \dot{\mathbf{A}}_i^T}{\partial \dot{q}_k} + {}^i\mathbf{T}_{i+1} \dfrac{\partial \mathbf{D}'_{i+1}}{\partial \dot{q}_k} & (k < i+1) \\ \dfrac{\partial {}^i\mathbf{T}_{i+1}}{\partial \dot{q}_k} \mathbf{D}'_{i+1} + {}^i\mathbf{T}_{i+1} \dfrac{\partial \mathbf{D}'_{i+1}}{\partial \dot{q}_k} & (k = i+1) \\ {}^i\mathbf{T}_{i+1} \dfrac{\partial \mathbf{D}'_{i+1}}{\partial \dot{q}_k} & (k > i+1) \end{cases} \tag{4.26b}$$

$$\frac{\partial \mathbf{D}_i^{'}}{\partial \ddot{q}_k}=\begin{cases}\mathbf{J}_i\dfrac{\partial \dot{\mathbf{A}}_i^T}{\partial \ddot{q}_k}+{}^i\mathbf{T}_{i+1}\dfrac{\partial \mathbf{D}_{i+1}^{'}}{\partial \ddot{q}_k}={}^i\mathbf{T}_{i+1}\dfrac{\partial \mathbf{D}_{i+1}^{'}}{\partial \ddot{q}_k} & (k<i+1)\\ \dfrac{\partial {}^i\mathbf{T}_{i+1}}{\partial \ddot{q}_k}\mathbf{D}_{i+1}^{'}+{}^i\mathbf{T}_{i+1}\dfrac{\partial \mathbf{D}_{i+1}^{'}}{\partial \ddot{q}_k} & (k=i+1)\\ {}^i\mathbf{T}_{i+1}\dfrac{\partial \mathbf{D}_{i+1}^{'}}{\partial \ddot{q}_k} & (k>i+1)\end{cases} \tag{4.26c}$$

The sensitivity of Equation (4.23) is

$$\frac{\partial \mathbf{D}_i^{''}}{\partial q_k}=\begin{cases}{}^i\dot{\mathbf{T}}_{i+1}\dfrac{\partial \mathbf{D}_{i+1}^{''}}{\partial q_k} & (k<i+1)\\ \dfrac{\partial {}^i\dot{\mathbf{T}}_{i+1}}{\partial q_k}\mathbf{D}_{i+1}^{''}+{}^i\dot{\mathbf{T}}_{i+1}\dfrac{\partial \mathbf{D}_{i+1}^{''}}{\partial q_k} & (k=i+1)\\ {}^i\dot{\mathbf{T}}_{i+1}\dfrac{\partial \mathbf{D}_{i+1}^{''}}{\partial q_k} & (k>i+1)\end{cases} \tag{4.27a}$$

$$\frac{\partial \mathbf{D}_i^{''}}{\partial \dot{q}_k}=\begin{cases}{}^i\dot{\mathbf{T}}_{i+1}\dfrac{\partial \mathbf{D}_{i+1}^{''}}{\partial \dot{q}_k} & (k<i+1)\\ \dfrac{\partial {}^i\dot{\mathbf{T}}_{i+1}}{\partial \dot{q}_k}\mathbf{D}_{i+1}^{''}+{}^i\dot{\mathbf{T}}_{i+1}\dfrac{\partial \mathbf{D}_{i+1}^{''}}{\partial \dot{q}_k}=\dfrac{\partial {}^i\mathbf{T}_{i+1}}{\partial q_k}\mathbf{D}_{i+1}^{''}+{}^i\dot{\mathbf{T}}_{i+1}\dfrac{\partial \mathbf{D}_{i+1}^{''}}{\partial \dot{q}_k} & (k=i+1)\\ {}^i\dot{\mathbf{T}}_{i+1}\dfrac{\partial \mathbf{D}_{i+1}^{''}}{\partial \dot{q}_k} & (k>i+1)\end{cases} \tag{4.27b}$$

$$\frac{\partial \mathbf{D}_i^{''}}{\partial \ddot{q}_k}=\begin{cases}{}^i\dot{\mathbf{T}}_{i+1}\dfrac{\partial \mathbf{D}_{i+1}^{''}}{\partial \ddot{q}_k} & (k<i+1)\\ \dfrac{\partial {}^i\dot{\mathbf{T}}_{i+1}}{\partial \ddot{q}_k}\mathbf{D}_{i+1}^{''}+{}^i\dot{\mathbf{T}}_{i+1}\dfrac{\partial \mathbf{D}_{i+1}^{''}}{\partial \ddot{q}_k}={}^i\dot{\mathbf{T}}_{i+1}\dfrac{\partial \mathbf{D}_{i+1}^{''}}{\partial \ddot{q}_k} & (k=i+1)\\ {}^i\dot{\mathbf{T}}_{i+1}\dfrac{\partial \mathbf{D}_{i+1}^{''}}{\partial \ddot{q}_k} & (k>i+1)\end{cases} \tag{4.27c}$$

where

$${}^{i-1}\dot{\mathbf{T}}_i=\frac{\partial {}^{i-1}\mathbf{T}_i}{\partial q_i}\frac{dq_i}{dt}=\frac{\partial {}^{i-1}\mathbf{T}_i}{\partial q_i}\dot{q}_i \tag{4.27d}$$

$$
\begin{aligned}
\frac{\partial^{i-1}\dot{\mathbf{T}}_i}{\partial q_k} &= \frac{\partial}{\partial q_k}\left(\frac{\partial^{i-1}\mathbf{T}_i}{\partial q_i}\dot{q}_i\right) \\
&= \frac{\partial^{2\ i-1}\mathbf{T}_i}{\partial q_k \partial q_i}\dot{q}_i + \frac{\partial^{i-1}\mathbf{T}_i}{\partial q_i}\frac{\partial \dot{q}_i}{\partial q_k} \\
&= \frac{\partial^{2\ i-1}\mathbf{T}_i}{\partial q_k \partial q_i}\dot{q}_i \qquad \left(\because \frac{\partial \dot{q}_i}{\partial q_k} = 0\right) \\
&= \begin{cases} \dfrac{\partial^{2\ i-1}\mathbf{T}_i}{\partial q_i^2}\dot{q}_i & (k = i) \\ 0 & (k \neq i) \end{cases}
\end{aligned}
\tag{4.27e}
$$

$$
\begin{aligned}
\frac{\partial^{i-1}\dot{\mathbf{T}}_i}{\partial \ddot{q}_k} &= \frac{\partial}{\partial \ddot{q}_k}\left(\frac{\partial^{i-1}\mathbf{T}_i}{\partial q_i}\dot{q}_i\right) \\
&= \frac{\partial^{2\ i-1}\mathbf{T}_i}{\partial \ddot{q}_k \partial q_i}\dot{q}_i + \frac{\partial^{i-1}\mathbf{T}_i}{\partial q_i}\frac{\partial \dot{q}_i}{\partial \ddot{q}_k} \\
&= \frac{\partial}{\partial q_i}\left(\frac{\partial^{i-1}\mathbf{T}_i}{\partial \ddot{q}_k}\right)\dot{q}_i \qquad \left(\because \frac{\partial \dot{q}_i}{\partial \ddot{q}_k} = 0\right) \\
&= 0 \qquad \left(\because \frac{\partial^{i-1}\mathbf{T}_i}{\partial \ddot{q}_k} = 0\right)
\end{aligned}
\tag{4.27f}
$$

Finally, the sensitivity of Equation (4.24) is

$$
\frac{\partial \dot{p}_i}{\partial q_k} = \begin{cases} tr\left(\dfrac{\partial^2 \mathbf{A}_i}{\partial q_k \partial q_i}(\mathbf{D}_i + \mathbf{D}_i^{''}) + \dfrac{\partial \mathbf{A}_i}{\partial q_i}\dfrac{\partial(\mathbf{D}_i + \mathbf{D}_i^{''})}{\partial q_k} + \dfrac{\partial^2 \dot{\mathbf{A}}_i}{\partial q_k \partial q_i}\mathbf{D}_i^{'} + \dfrac{\partial \dot{\mathbf{A}}_i}{\partial q_i}\dfrac{\partial \mathbf{D}_i^{'}}{\partial q_k}\right) & (k \leq i) \\ tr\left(\dfrac{\partial \mathbf{A}_i}{\partial q_i}\dfrac{\partial(\mathbf{D}_i + \mathbf{D}_i^{''})}{\partial q_k} + \dfrac{\partial \dot{\mathbf{A}}_i}{\partial q_i}\dfrac{\partial \mathbf{D}_i^{'}}{\partial q_k}\right) & (k > i) \end{cases}
\tag{4.28a}
$$

$$
\frac{\partial \dot{p}_i}{\partial \dot{q}_k} = tr\left(\frac{\partial \mathbf{A}_i}{\partial q_i}\frac{\partial(\mathbf{D}_i + \mathbf{D}_i^{''})}{\partial \dot{q}_k} + \frac{\partial \dot{\mathbf{A}}_i}{\partial q_i}\frac{\partial \mathbf{D}_i^{'}}{\partial \dot{q}_k}\right)
\tag{4.28b}
$$

$$
\frac{\partial \dot{p}_i}{\partial \ddot{q}_k} = tr\left(\frac{\partial \mathbf{A}_i}{\partial q_i}\frac{\partial(\mathbf{D}_i + \mathbf{D}_i^{''})}{\partial \ddot{q}_k} + \frac{\partial \dot{\mathbf{A}}_i}{\partial q_i}\frac{\partial \mathbf{D}_i^{'}}{\partial \ddot{q}_k}\right)
\tag{4.28c}
$$

where

$$\mathbf{A}_i = \mathbf{A}_{i-1}\,{}^{i-1}\mathbf{T}_i \tag{4.28d}$$

$$\mathbf{B}_i = \dot{\mathbf{A}}_i = \mathbf{B}_{i-1}\,{}^{i-1}\mathbf{T}_i + \mathbf{A}_{i-1}\frac{\partial\,{}^{i-1}\mathbf{T}_i}{\partial q_i}\dot{q}_i \tag{4.28e}$$

$$\frac{\partial \mathbf{A}_i}{\partial q_i} = \mathbf{A}_{i-1}\frac{\partial\,{}^{i-1}\mathbf{T}_i}{\partial q_i} \tag{4.28f}$$

$$\frac{\partial^2 \mathbf{A}_i}{\partial q_k \partial q_i} = \begin{cases} \mathbf{A}_{i-1}\dfrac{\partial^2\,{}^{i-1}\mathbf{T}_i}{\partial q_k \partial q_i} = \mathbf{A}_{i-1}\dfrac{\partial^2\,{}^{i-1}\mathbf{T}_i}{\partial q_i^2} & (k=i) \\ \dfrac{\partial \mathbf{A}_{i-1}}{\partial q_k}\dfrac{\partial\,{}^{i-1}\mathbf{T}_i}{\partial q_i} + \mathbf{A}_{i-1}\dfrac{\partial^2\,{}^{i-1}\mathbf{T}_i}{\partial q_k \partial q_i} = \dfrac{\partial \mathbf{A}_{i-1}}{\partial q_k}\dfrac{\partial\,{}^{i-1}\mathbf{T}_i}{\partial q_i} & (k<i) \end{cases} \tag{4.28g}$$

$$\frac{\partial \mathbf{B}_i}{\partial q_i} = \frac{\partial \dot{\mathbf{A}}_i}{\partial q_i} = \mathbf{B}_{i-1}\frac{\partial\,{}^{i-1}\mathbf{T}_i}{\partial q_i} + \mathbf{A}_{i-1}\frac{\partial^2\,{}^{i-1}\mathbf{T}_i}{\partial q_i^2}\dot{q}_i \tag{4.28h}$$

$$\frac{\partial^2 \dot{\mathbf{A}}_i}{\partial q_k \partial q_i} = \begin{cases} \mathbf{B}_{i-1}\dfrac{\partial^2\,{}^{i-1}\mathbf{T}_i}{\partial q_k \partial q_i} + \mathbf{A}_{i-1}\dfrac{\partial^3\,{}^{i-1}\mathbf{T}_i}{\partial q_k \partial q_i^2}\dot{q}_i = \mathbf{B}_{i-1}\dfrac{\partial^2\,{}^{i-1}\mathbf{T}_i}{\partial q_i^2} + \mathbf{A}_{i-1}\dfrac{\partial^3\,{}^{i-1}\mathbf{T}_i}{\partial q_i^3}\dot{q}_i & (k=i) \\ \dfrac{\partial \mathbf{B}_{i-1}}{\partial q_k}\dfrac{\partial\,{}^{i-1}\mathbf{T}_i}{\partial q_i} + \mathbf{B}_{i-1}\dfrac{\partial^2\,{}^{i-1}\mathbf{T}_i}{\partial q_k \partial q_i} + \dfrac{\partial \mathbf{A}_{i-1}}{\partial q_k}\dfrac{\partial^2\,{}^{i-1}\mathbf{T}_i}{\partial q_i^2}\dot{q}_i + \mathbf{A}_{i-1}\dfrac{\partial^3\,{}^{i-1}\mathbf{T}_i}{\partial q_k \partial q_i^2}\dot{q}_i + \mathbf{A}_{i-1}\dfrac{\partial^2\,{}^{i-1}\mathbf{T}_i}{\partial q_i^2}\dfrac{\partial \dot{q}_i}{\partial q_k} & \\ = \dfrac{\partial \mathbf{B}_{i-1}}{\partial q_k}\dfrac{\partial\,{}^{i-1}\mathbf{T}_i}{\partial q_i} + \dfrac{\partial \mathbf{A}_{i-1}}{\partial q_k}\dfrac{\partial^2\,{}^{i-1}\mathbf{T}_i}{\partial q_i^2}\dot{q}_i & (k<i) \end{cases} \tag{4.28i}$$

CHAPTER 5

FUNCTION APPROXIMATION

5.1. Introduction

Discretization of time domain is an important part of the formulation since we are solving a dynamic response optimization problem. Therefore, understanding function approximation is a necessary step before formulating the problem. There are many function approximation methods, such as the spline interpolation function approximation, the Hermite function approximation, and the least square function approximation. Each method has its own merits and demerits. For example, spline functions have proved very useful with data fitting problems and curve fitting, and Lagrange and Hermite functions are more useful for analytical approximations in solving integral and differential equations, respectively (Atkinson, 1988). The B-spline function approximation has been chosen for the predictive dynamics problem for certain reasons that will be explained in later sections.

The B-spline (or basis spline) function approximation is the linear combination of the B-spline basis functions. The curves pass through the data points in the spline interpolation functions. However, the B-spline curves do not pass through the control points. The joint angle profiles of the human model are interpolated using these control points. In the optimization process, the control points have the role of design variables. In terms of differentiability, C^2 functions are desirable for optimization. Therefore, the cubic B-spline basis functions are adopted for the joint angle profile approximation.

5.2. B-spline Approximation

Given control points $\hat{q}_0$, $\hat{q}_1$, $\hat{q}_2$,..., $\hat{q}_n$ and a knot vector $\mathbf{t} = \{t_0, t_1, t_2, \cdots, t_m\}$, which are non-decreasing real numbers, the B-spline approximation is defined as

$$q(t) = \sum_{i=0}^{n} \hat{q}_i N_{i,p}(t) \tag{5.1}$$

where $\hat{q}_i$ represents given control points ($\hat{q}_0$, $\hat{q}_1$, $\hat{q}_2$,..., $\hat{q}_n$), and $N_{i,p}(t)$ represents the i^{th} B-spline basis function of degree *p*. B-spline function approximation has the following important properties. Some more details are presented in later sections.

- The B-spline curve is a piecewise curve. Each component is a composite curve of degree *p*.
- The following equation must be satisfied:

  $$m = n + p + 1 \tag{5.2}$$

  where $m + 1$ is the number of knots, $n + 1$ is the number of control points, and *p* is degree.
- The clamped B-spline curve passes through the two end control points $\hat{q}_0$ and $\hat{q}_n$.
- B-spline curves are C^{p-k} continuous at a knot that has multiplicity *k*.
- When the position of the i^{th} control point is changed, it only affects the curve on interval $t_i \le t < t_{i+p+1}$.
- Bezier curves are special cases of B-spline curves.

5.3. B-spline Basis Function

The basis function $N_{i,p}(t)$ is given as

$$N_{i,p}(t) = \frac{t - t_i}{t_{i+p} - t_i} N_{i,p-1}(t) + \frac{t_{i+p+1} - t}{t_{i+p+1} - t_{i+1}} N_{i+1,p-1}(t) \tag{5.3}$$

where

$$N_{i,0}(t) = \begin{cases} 1 & (t_i \le t < t_{i+1}) \\ 0 & \text{otherwise} \end{cases}.$$

Equation (5.3) is usually referred to as the Cox–der Boor recursion formula. The following diagram (Figure 5.1) helps in understanding of this recursion formula:

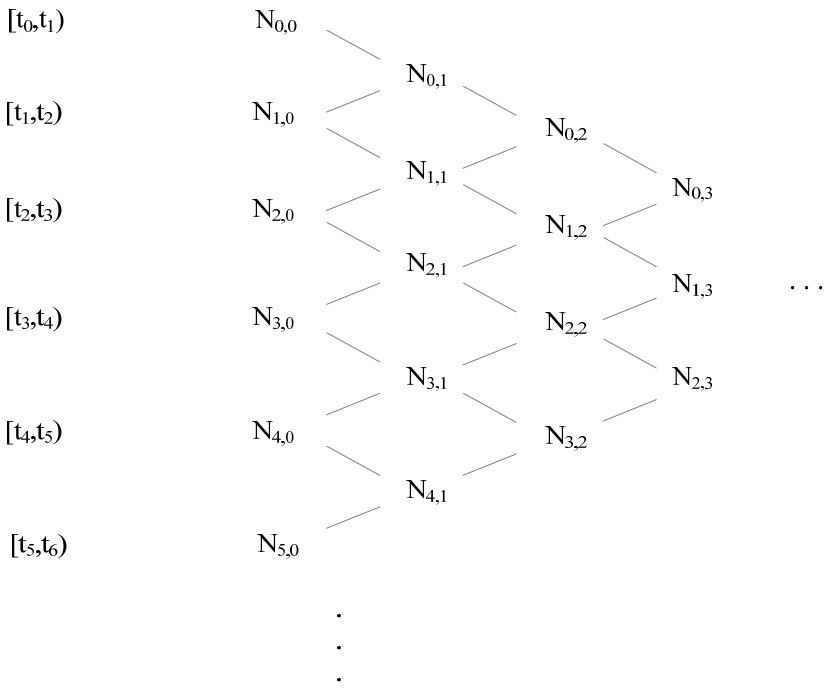

Figure 5.1 Diagram of Cox–der Boor recursion formula

From Figure 5.1, it is clear that $N_{i,0}(t)$ and $N_{i+1,0}(t)$ are required to compute $N_{i,1}(t)$. Also, $N_{i,1}(t)$ and $N_{i+1,1}(t)$ are required to compute $N_{i,2}(t)$. In a similar way, $N_{i,p-1}(t)$ and $N_{i+1,p-1}(t)$ are required for the basis function of degree p – $N_{i,p}(t)$. For example, let us assume we have a knot vector **t** = {0, 1, 2, 3}. We can write the 0 degree basis functions $N_{0,0}(t)$, $N_{1,0}(t)$, and $N_{2,0}(t)$ quite easily. Then we have the basis function of degree of 1, as follows:

$$N_{0,1}(t) = \frac{t - t_0}{t_1 - t_0} N_{0,0}(t) + \frac{t_2 - t}{t_2 - t_1} N_{1,0}(t) \tag{5.4a}$$

$$N_{1,1}(t) = \frac{t - t_1}{t_2 - t_1} N_{1,0}(t) + \frac{t_3 - t}{t_3 - t_2} N_{2,0}(t). \tag{5.4b}$$

Since $t_0 = 0$, $t_1 = 1$ and $t_2 = 2$, Equation (5.4a) becomes

$$N_{0,1}(t) = tN_{0,0}(t) + (2 - t)N_{1,0}(t), \tag{5.5a}$$

and Equation (5.4b) becomes

$$N_{1,1}(t) = (t - 1)N_{1,0}(t) + (3 - t)N_{2,0}(t). \tag{5.5b}$$

$N_{0,0}(t)$ is non-zero on $0 \le t < 1$ and $N_{1,0}(t)$ is non-zero on $1 \le t < 2$. Therefore, $N_{0,1}(t)$ is as shown in Figure 5.2.

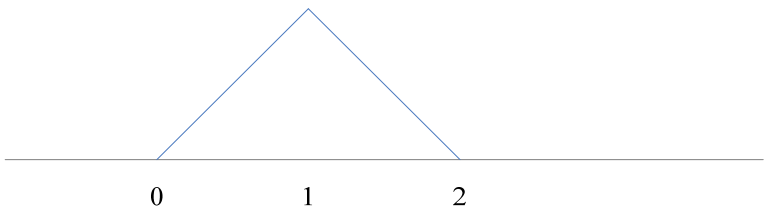

Figure 5.2 Basis function, $N_{0,1}(t)$

In the same way, $N_{1,1}(t)$ is as shown in Figure 5.3.

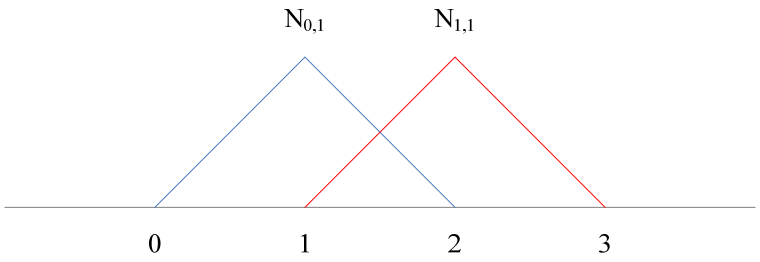

Figure 5.3 Basis function, $N_{0,1}(t)$ and $N_{1,1}(t)$

Similarly, the B-spline basis functions of degree 2 with knot vector $\mathbf{t} = \{t_i, t_{i+1}, t_{i+2}, t_{i+3}, t_{i+4}\}$ are

$$N_{i,2}(t) = \frac{t - t_i}{t_{i+2} - t_i} N_{i,1}(t) + \frac{t_{i+3} - t}{t_{i+3} - t_{i+1}} N_{i+1,1}(t) \tag{5.6}$$

The blue line is $N_{i,2}(t)$, and the red line is $N_{i+1,2}(t)$ in Figure 5.4.

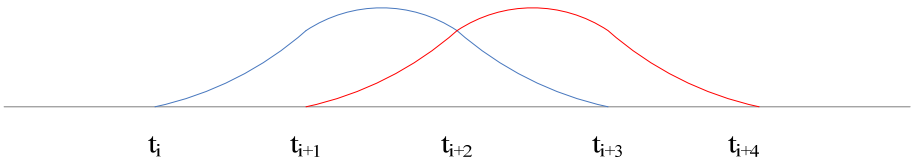

Figure 5.4 Basis function, $N_{i,2}(t)$ and $N_{i+1,2}(t)$

Finally, the B-spline basis function of degree 3 (cubic B-spline basis function) with knot vector $\mathbf{t} = \{t_i, t_{i+1}, t_{i+2}, t_{i+3}, t_{i+4}\}$ is

$$N_{i,3}(t) = \frac{t - t_i}{t_{i+3} - t_i} N_{i,2}(t) + \frac{t_{i+4} - t}{t_{i+4} - t_{i+1}} N_{i+1,2}(t) \tag{5.7}$$

and its shape is shown in Figure 5.5.

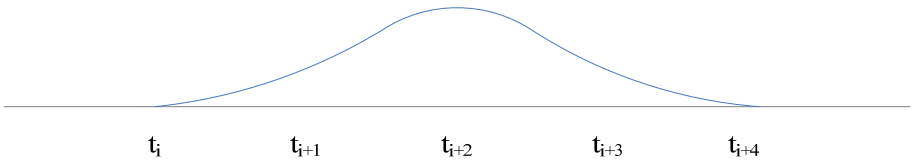

Figure 5.5 Basis function, $N_{i,3}(t)$

B-spline basis functions have the following properties:

- $N_{i,p}(t)$ is a polynomial in t with degree p.
- $N_{i,p}(t)$ is a combined curve by degree p polynomials (e.g., Equations (5.5a) and (5.5b))
- $N_{i,p}(t)$ is non-negative for all i, p, and t.
- $N_{i,p}(t)$ is a non-zero polynomial on $t_i \le t < t_{i+p+1}$.
- $N_{i,p}(t)$ is C^{p-k} at a knot that has multiplicity k.
- On $t_i \le t < t_{i+1}$, the sum of all degree p basis functions is 1.

5.4. Open B-spline Curves vs. Clamped B-spline Curves

If there is not any particular structure in a knot vector, the curves will not pass the first and last control points. These kinds of B-spline curves are called *open* B-spline curves. If the B-spline curves touch the first and last control points, they are called

clamped B-spline curves. Usually, we want clamped B-spline curves. To generate clamped B-spline curves, the first knot and the last knot must be of multiplicity p+1.

5.5. Continuity Property

The B-spline approximation function $q(t)$ is C^{p-k} continuous at a knot of multiplicity k. For example, consider the following clamped knot vector (Figure 5.6).

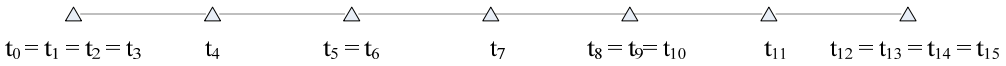

Figure 5.6 Clamped knot vector

In Figure 5.6, t_5 is a double knot and t_8 is a triple knot. Therefore, the above knot vector has the following continuity at each knot position:

- The $q(t)$ is C^3 continuous at any point that is not a knot.
- The $q(t)$ is C^2 continuous at t_4, t_7, and t_{11}.
- The $q(t)$ is C^1 continuous at t_5 (and t_6).
- The $q(t)$ is C^0 continuous at t_8 (and t_9, t_{10}).

For these reasons, cubic B-spline approximations are used for the current running problem formulation. The second derivative of joint angle profiles is joint angle acceleration. Therefore, the continuity condition is needed in C^2. Once there are non-repeated increasing knots, cubic B-spline curves have at least C^2 continuity at any point. The degree more than three ($p > 3$) might be considered. However, the B-spline curves

tend to move closer to the control polyline (the linear line connecting control points) as the degree decreases. Therefore, degree three (cubic; $p = 3$) is the best choice in terms of differentiability and controllability.

5.6. Cubic B-spline Approximation

Since the dynamics formulation needs C^2 continuity, we should focus on the cubic B-spline function approximation with a degree of three. Consider the knot span (time interval) on $t_i \le t < t_{i+1}$, which is depicted as a red line in Figure 5.7. For the cubic B-spline functions, there are four B-spline basis functions (the blue lines in Figure 5.7) that contribute to the function approximation.

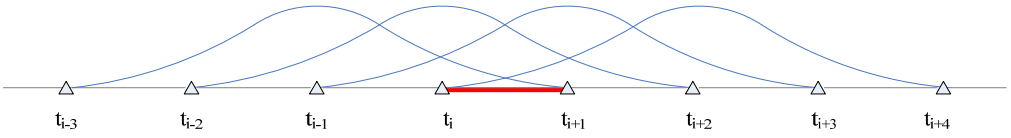

Figure 5.7 Cubic B-spline basis functions

Using Equation (5.2), the basis function are obtained as

$$N_{i-3,3} = \frac{(t_{i+1} - t)^3}{(t_{i+1} - t_i)(t_{i+1} - t_{i-1})(t_{i+1} - t_{i-2})} \tag{5.8a}$$

$$N_{i-2,3} = \frac{(t - t_{i-2})(t_{i+1} - t)^2}{(t_{i+1} - t_{i-2})(t_{i+1} - t_{i-1})(t_{i+2} - t_i)} + \frac{(t - t_{i-1})(t_{i+1} - t)(t_{i+2} - t)}{(t_{i+1} - t_{i-1})(t_{i+1} - t_i)(t_{i+2} - t_{i-1})} + \frac{(t - t_i)(t_{i+2} - t)^2}{(t_{i+1} - t_i)(t_{i+2} - t_{i-1})(t_{i+2} - t_i)} \tag{5.8b}$$

$$N_{i-1,3} = \frac{(t-t_{i-1})^2(t_{i+1}-t)}{(t_{i+1}-t_{i-1})(t_{i+1}-t_i)(t_{i+2}-t_{i-1})} + \frac{(t-t_{i-1})(t-t_i)(t_{i+2}-t)}{(t_{i+1}-t_i)(t_{i+2}-t_{i-1})(t_{i+2}-t_i)} + \frac{(t-t_i)^2(t_{i+3}-t)}{(t_{i+1}-t_i)(t_{i+2}-t_i)(t_{i+3}-t_i)} \tag{5.8c}$$

$$N_{i,3} = \frac{(t-t_i)^3}{(t_{i+1}-t_i)(t_{i+2}-t_i)(t_{i+3}-t_i)} \tag{5.8d}$$

Note that t_{i-3} and t_{i+4} do not appear in the cubic B-spline basis functions, Equations (5.8a-5.8d), for this interval. Note that the number of knots and the number of control points should satisfy the consistency condition in Equation (5.2). Therefore, even though only six knots appear in Equations (5.8a-5.8d), the number of knots *m* in Equation (5.2) is eight (4+3+1), including t_{i-3} and t_{i+4}. Expanding Equation (5.1) with cubic B-spline basis functions in $t_i \le t < t_{i+1}$, the function approximation for the running problem formulation becomes

$$q(t) = \hat{q}_{i-3}N_{i-3,3}(t) + \hat{q}_{i-2}N_{i-2,3}(t) + \hat{q}_{i-1}N_{i-1,3}(t) + \hat{q}_i N_{i,3}(t) \qquad i \ge 3 \tag{5.9}$$

For clamped B-spline curves, knots at the beginning and end must satisfy multiplicity of $p+1$; it is four for the cubic B-splines. Therefore, the knots in Equation (5.9) should be

$$t_0 = t_1 = t_2 = t_3 \tag{5.10a}$$

$$t_4 = t_5 = t_6 = t_7 . \tag{5.11b}$$

Again, t_0 and t_7 do not appear in the cubic B-spline basis functions.

5.7. Why B-spline? Comparison to Other Function Approximations

There might be a question as to why the B-spline curves are chosen as function approximation instead of other popular function approximation methods such as spline

interpolation or least square approximation. In this section, these other popular approximation methods are described briefly, and then the reason for selecting the B-spline function approximation is explained.

5.7.1. Cubic Spline Interpolation

Let s(x) be a spline function with knot points $x_0<x_1<x_2<...<x_n$. The spline function that interpolates y_0, y_1,..., y_n, is s(x_i) = y_i for i = 0, 1, 2,..., n. On an interval [x_i, x_{i+1}], s(x)=p_i(x), where $p_i(x)$ is a cubic polynomial in x. A cubic polynomial is given as $p_i(x) = a_i x^3 + b_i x^2 + c_i x + d_i$. For each interval, four unknown coefficients exist, and so to define s(x), there are 4n parameters. Interpolation conditions are

$$p_i(x_i) = y_i \qquad i = 0,1,...,n-1 \tag{5.12a}$$

$$p_i(x_{i+1}) = y_{i+1} \qquad i = 0,1,...,n-1. \tag{5.12b}$$

The continuity of the first derivative is

$$p_{i-1}'(x_i) = p_i'(x_i) \qquad i = 1,2,...,n-1. \tag{5.12c}$$

The continuity of the second derivative is

$$p_{i-1}''(x_i) = p_i''(x_i) \qquad i = 1,2,...,n-1. \tag{5.12d}$$

Therefore, the number of coefficients is 4n, and the number of equations is 4n – 2. For the extra two equations, the following equations are used in each case.

Natural spline: $s''(x_0) = s''(x_n) = 0$ (5.13a)

Clamped spline: $s'(x_0) = y_0'$, $s'(x_n) = y_n'$ (5.13b)

Periodic spline: $s'(x_0) = s'(x_n)$, $s''(x_0) = s''(x_n)$ (5.13c)

Let $M_i = s''(x_i)$ and $h_i = x_{i+1} - x_i$. Then, we have

$$p_i(x) = s(x)$$
$$= \frac{(x_{i+1}-x)^3 M_i + (x-x_i)^3 M_{i+1}}{6h_i} + \left(\frac{y_i}{h_i} - \frac{h_i}{6}M_i\right)(x_{i+1}-x) + \left(\frac{y_{i+1}}{h_i} - \frac{h_i}{6}M_{i+1}\right)(x-x_i). \quad (5.14)$$

For the natural spline, the condition is $s''(x_0) = s''(x_n) = 0$, so $M_0 = M_n = 0$. Therefore, we have a linear system of equations for M_i:

$$\begin{bmatrix} \frac{h_0+h_1}{3} & \frac{h_1}{6} & & & \\ \frac{h_1}{6} & \frac{h_1+h_2}{3} & \frac{h_2}{6} & & \\ & \frac{h_2}{6} & \frac{h_2+h_3}{3} & & \\ & & & \ddots & \\ & & & & \frac{h_{n-2}+h_{n-1}}{3} \end{bmatrix} \begin{bmatrix} M_1 \\ M_2 \\ \vdots \\ \vdots \\ M_{n-1} \end{bmatrix} = \begin{bmatrix} \frac{y_2-y_1}{h_1} - \frac{y_1-y_0}{h_0} \\ \frac{y_3-y_2}{h_2} - \frac{y_2-y_1}{h_1} \\ \frac{y_4-y_3}{h_3} - \frac{y_3-y_2}{h_2} \\ \vdots \\ \frac{y_n-y_{n-1}}{h_{n-1}} - \frac{y_{n-1}-y_{n-2}}{h_{n-2}} \end{bmatrix}. \quad (5.15)$$

To solve Equation (5.15), inverse of the coefficient matrix is needed. Equation (5.15) will be different for different tasks that use different knot sequences. For these reasons, the cubic spline interpolation function approximation is not proper for the predictive dynamics problem.

5.7.2. Least Squares Approximation

Let f be a given function and g be an approximating function. Then, the measure of error is given by

$$\|f-g\|_w = \left[\int_a^b w(x)(f(x)-g(x))^2 dx\right]^{1/2} \quad (5.16)$$

where $w(x)$ is a given positive weight function. Using the inner product, Equation (5.16) becomes

$$\|f-g\|_w = \sqrt{(f-g, f-g)_w}\,. \tag{5.17}$$

Therefore, minimizing Equation (5.16) is same as minimizing the term $(f-g, f-g)_w$. Given f, and ϕ_1, ϕ_2, ..., ϕ_n, we need to find c_1, ..., c_n, where

$$f(x) \approx c_1\phi_1(x) + c_2\phi_2(x) + \cdots + c_n\phi_n(x) \tag{5.18}$$

in the least square sense. That means to minimize $(f-g, f-g)_w$ overall,

$$g(x) = c_1\phi_1(x) + c_2\phi_2(x) + \cdots + c_n\phi_n(x)\,. \tag{5.19}$$

To get the minimizer, take the derivatives of $(f-g, f-g)_w$ with respect to c_1, c_2, ..., c_n and set them to zero.

$$\frac{\partial}{\partial c_k}\left[(f-g, f-g)_w\right] = 0 \tag{5.20}$$

Then, the solution can be obtained as

$$f(x) \approx \sum_{i=1}^{n} c_i\phi_i = \sum_{i=1}^{n} \frac{(f, \phi_i)_w}{(\phi_i, \phi_i)_w}\phi_i(x)\,. \tag{5.21}$$

The coefficients c_i depend on the given value f. Since the analytical solution for derivatives with respect to time is necessary, this is not appropriate for the predictive dynamics approach.

CHAPTER 6

PREDICTIVE DYNAMICS

The term *predictive dynamics* is coined to characterize the prediction of human motion in a physics-based world. Forward dynamics and inverse dynamics are used to solve the mechanical problems in general. In this case, either information about force or information about displacement, velocity, and acceleration is known. However, limited information is available in a bio-system such as human motion; this means both information about force and information about displacement, velocity, and acceleration are unknown in most cases. For example, joint angle profiles and joint torque profiles are unknown, and only a few boundary conditions and state responses are known. Therefore, predictive dynamics is introduced to solve such a problem.

6.1. The Predictive Dynamics Notion

Let a dynamics problem with the boundary $\mathbf{\Gamma}$ over the time domain Ω have the Lagrangian function $L = K - V$ (kinetic energy – potential energy). Then, the governing equation for the dynamics system is given in Lagrange's equation form as:

$$\mathbf{Q} = \frac{d}{dt}\left(\frac{\partial L}{\partial \dot{\mathbf{q}}}\right) - \frac{\partial L}{\partial \mathbf{q}} \tag{6.1}$$

where $\mathbf{q}$ is the generalized coordinate vector, and $\mathbf{Q}$ is the generalized force vector. In general, the right side turns out to be a function of $\mathbf{q}$, $\dot{\mathbf{q}}$, $\ddot{\mathbf{q}}$. Forward dynamics integrates the governing equation, which is in the form of a differential algebraic equation (DAE) with the boundary condition $\mathbf{\Gamma}$ over the time domain Ω. So displacement, velocity, and

acceleration, $\mathbf{q}$, $\dot{\mathbf{q}}$, $\ddot{\mathbf{q}}$, are obtained for given force $\mathbf{Q}$. Inverse dynamics calculates force $\mathbf{Q}$ from given displacement, velocity, and acceleration, $\mathbf{q}$, $\dot{\mathbf{q}}$, $\ddot{\mathbf{q}}$, using the governing equation. However, predictive dynamics handles the case in which both $\mathbf{Q}$ and $\mathbf{q}$, $\dot{\mathbf{q}}$, $\ddot{\mathbf{q}}$ are unknown. Table 6.1 summarizes these concepts.

Table 6.1 Forward, inverse and predictive dynamics concepts

	Known	Unknown
Forward dynamics	$\mathbf{Q}$	$\mathbf{q}$, $\dot{\mathbf{q}}$, $\ddot{\mathbf{q}}$
Inverse dynamics	$\mathbf{q}$, $\dot{\mathbf{q}}$, $\ddot{\mathbf{q}}$	$\mathbf{Q}$
Predictive dynamics	Some available information such as $\mathbf{\Gamma}$, Ω	$\mathbf{q}$, $\dot{\mathbf{q}}$, $\ddot{\mathbf{q}}$, and $\mathbf{Q}$

In general, a bio-system such as a human has many degrees of freedom, and both $\mathbf{Q}$ and $\mathbf{q}$, $\dot{\mathbf{q}}$, $\ddot{\mathbf{q}}$ are unknown. Therefore, either forward dynamics or inverse dynamics cannot be applied to solve the given dynamics problem for a bio-system. However, predictive dynamics can be used to handle such a problem since it determines both unknown $\mathbf{Q}$ and unknown $\mathbf{q}$, $\dot{\mathbf{q}}$, $\ddot{\mathbf{q}}$.

6.2. Formulation of Predictive Dynamics

The predictive dynamics method is based on a novel optimization-based approach in a physics environment (physics-based optimization). Even though it handles such a complicated dynamics problem with large degrees of freedom, certain difficulties need to

be overcome. Since it is an optimization-based approach, a performance measure must be formulated. However, this performance measure is unknown for the bio-system. Therefore, it is inevitable to try to observe several performance measures. Fortunately, literature gives us some appropriate performance measures for general human motion, such as the dynamics effort that is based on energy consumption. It is also necessary to use feasible constant performance measure. This performance measure leads to a feasible solution that satisfies all the constraints of the problem. In practice, it helps not only to test the feasibility of constraints but also to build a good starting point for optimization with a real performance measure. Formulation of constraints is another difficulty. In general, there is little information to use as constraints in human motion. Some conditions may be imposed as constraints based on assumptions, and some may be obtained from motion capture data or earlier research for a specific task. Constraints are usually divided into two kinds: time-dependent constraints and time-independent constraints. Time-dependent constraints must be satisfied over the time domain Ω. Time-independent constraints must be satisfied only at a specific time.

6.3. Numerical Examples

The motion of a non-linear simple pendulum with external joint torque is investigated with predictive dynamics. The predictive dynamics is run with different boundary conditions and state response constraints. Then, the results are compared to results from forward dynamics. The forward dynamics is performed using the commercial software ADAMS Runge-Kutta solver. A simple pendulum pivots at the point O as shown in Figure 6.1. The pendulum is assumed as a rigid slender bar and the

hinge is frictionless.

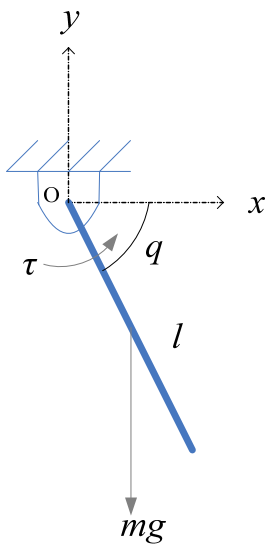

Figure 6.1 Simple pendulum

m is the mass of the pendulum, *l* is the link of the pendulum, *q* is joint angle, *g* is gravity acceleration, and τ is external torque.

6.3.1. Equation of Motion

The equations for the coordinates *x* and *y* are

$$x = \frac{l}{2}\cos q \tag{6.2a}$$

$$y = \frac{l}{2}\sin q \tag{6.2b}$$

Therefore,

$$\dot{x} = -\frac{l}{2}\dot{q}\sin q \tag{6.2c}$$

$$\dot{y} = \frac{l}{2}\dot{q}\cos q \tag{6.2d}$$

Note that q is positive in the counter clockwise direction. The kinetic energy of the pendulum is

$$\begin{aligned} K &= \frac{1}{2}m\left(\dot{x}^2 + \dot{y}^2\right) + \frac{1}{2}J_G\dot{q}^2 \\ &= \frac{1}{2}m\left[\left(\frac{l}{2}\right)^2\dot{q}^2\sin^2 q + \left(\frac{l}{2}\right)^2\dot{q}^2\cos^2 q\right] + \frac{1}{2}J_G\dot{q}^2 \\ &= \frac{1}{8}ml^2\dot{q}^2 + \frac{1}{2}J_G\dot{q}^2 \end{aligned} \tag{6.3}$$

where, J_G is the mass moment of inertia about the center of mass. The potential energy of the pendulum is

$$\begin{aligned} V &= -m\mathbf{g}^T\begin{bmatrix}\frac{l}{2}\cos q \\ \frac{l}{2}\sin q\end{bmatrix} = -m\begin{bmatrix}0 & -g\end{bmatrix}\begin{bmatrix}\frac{l}{2}\cos q \\ \frac{l}{2}\sin q\end{bmatrix} \\ &= mg\frac{l}{2}\sin q \end{aligned} \tag{6.4}$$

The Lagrangian function is

$$L = K - V = \frac{1}{8}ml^2\dot{q}^2 + \frac{1}{2}J_G\dot{q}^2 - mg\frac{l}{2}\sin q \tag{6.5}$$

With Equation (6.1), we can write

$$\begin{aligned} \tau &= \frac{d}{dt}\left(\frac{\partial L}{\partial \dot{q}}\right) - \frac{\partial L}{\partial q} \\ &= \frac{d}{dt}\left(\frac{1}{4}ml^2\dot{q} + J_G\dot{q}\right) - \left(-mg\frac{l}{2}\cos q\right) \\ &= \frac{1}{4}ml^2\ddot{q} + J_G\ddot{q} + mg\frac{l}{2}\cos q \end{aligned} \tag{6.6}$$

Since J_G is $ml^2/12$, the mass moment of inertia of a rigid slender bar with mass m and length l about point O is

$$J_O = \frac{1}{3} m l^2 \tag{6.7}$$

Therefore, the equation of motion of the simple pendulum in Figure 6.1 is

$$J_O \ddot{q} + mg \frac{l}{2} \cos q = \tau \tag{6.8}$$

6.3.2. Forward Dynamics

For numerical calculation, the geometrical and physical parameters of the simple pendulum are m = 0.5 kg, l = 0.4 m, and J_O = 0.0267 kgm^2. Equation (6.8) is a second-order differential equation, so it needs to be converted to a first-order differential equation–differential algebraic equation (DAE) form (Haug, 1989). The state variable vector u is defined as:

$$\mathbf{u} = \begin{bmatrix} u_1 \\ u_2 \end{bmatrix} = \begin{bmatrix} q \\ \dot{q} \end{bmatrix} \tag{6.9}$$

Then, Equation (6.8) is rewritten as a first-order differential equation:

$$\dot{\mathbf{u}} = \begin{bmatrix} \dot{u}_1 \\ \dot{u}_2 \end{bmatrix} = \begin{bmatrix} \dot{q} \\ \ddot{q} \end{bmatrix} = \begin{bmatrix} \dot{q} \\ \dfrac{1}{J_O}\left(\tau - mg\dfrac{l}{2}\cos q\right) \end{bmatrix} \tag{6.10}$$

The initial conditions for forward dynamics are given as

$$q(0) = 0 \tag{6.11a}$$

$$\dot{q}(0) = 0\,. \tag{6.11b}$$

The time step for numerical integration is set to 10^{-3}. The ADAMS results of the forward dynamics of Equation (6.10) with given initial condition are shown in Figures 6.2-6.3. Figure 6.2 is the case without any external force, $\tau = 0$. Figure 6.3 is the case with applied

external force, which is

$$\tau = 0.1 \sin 5t \,. \tag{6.12}$$

These ADAMS results are double-checked by MATLAB ODE solver, ode45 (Figure 6.4).

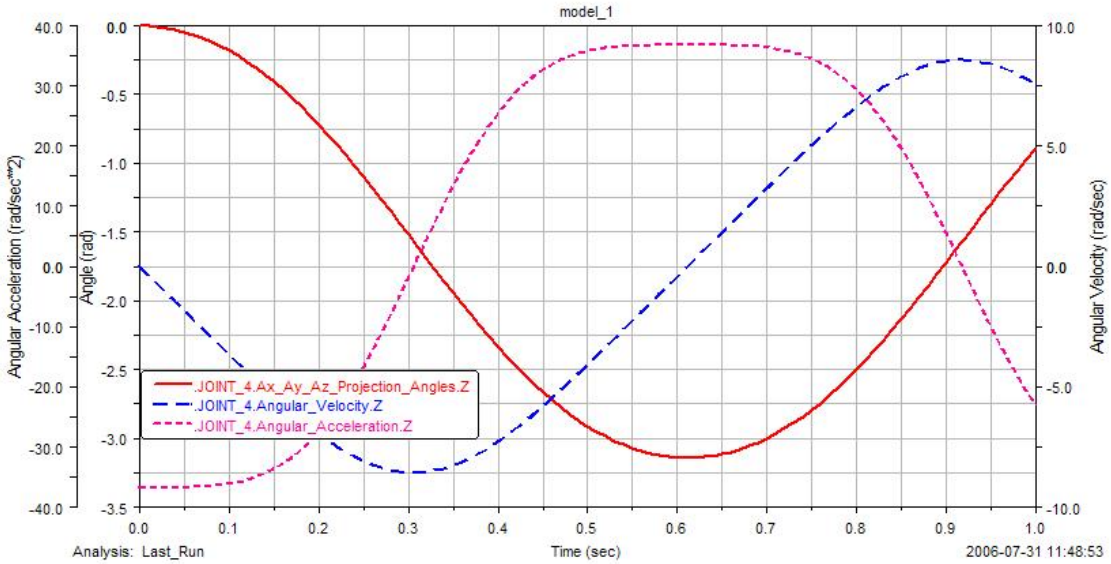

Figure 6.2 ADAMS results for the case without external torque

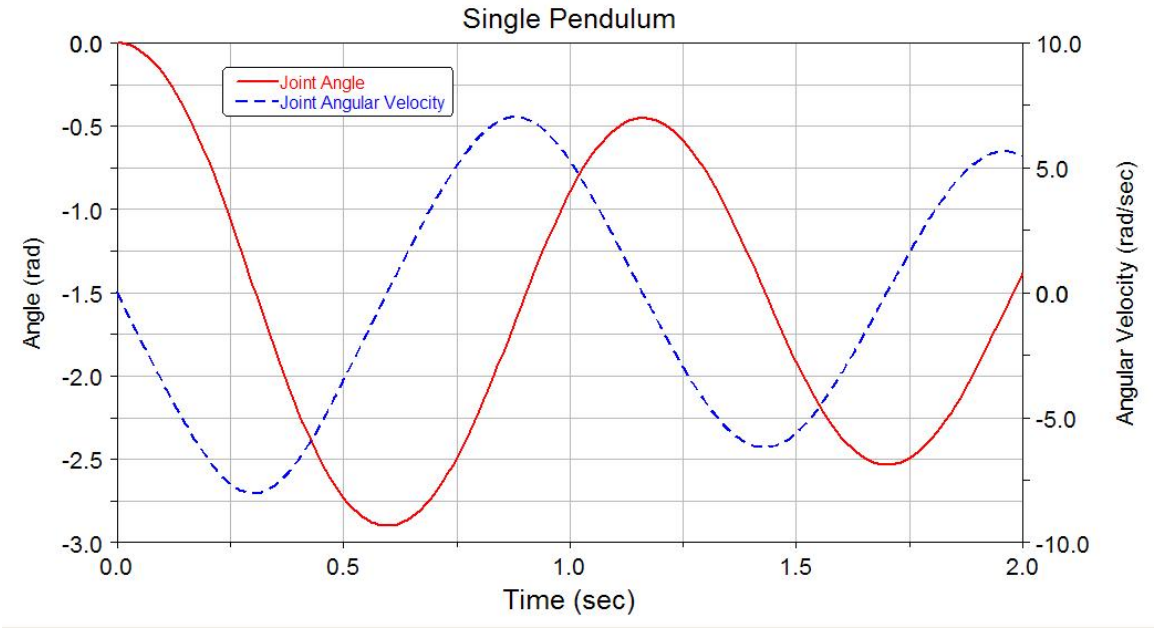

Figure 6.3 ADAMS results for the case with applied external torque

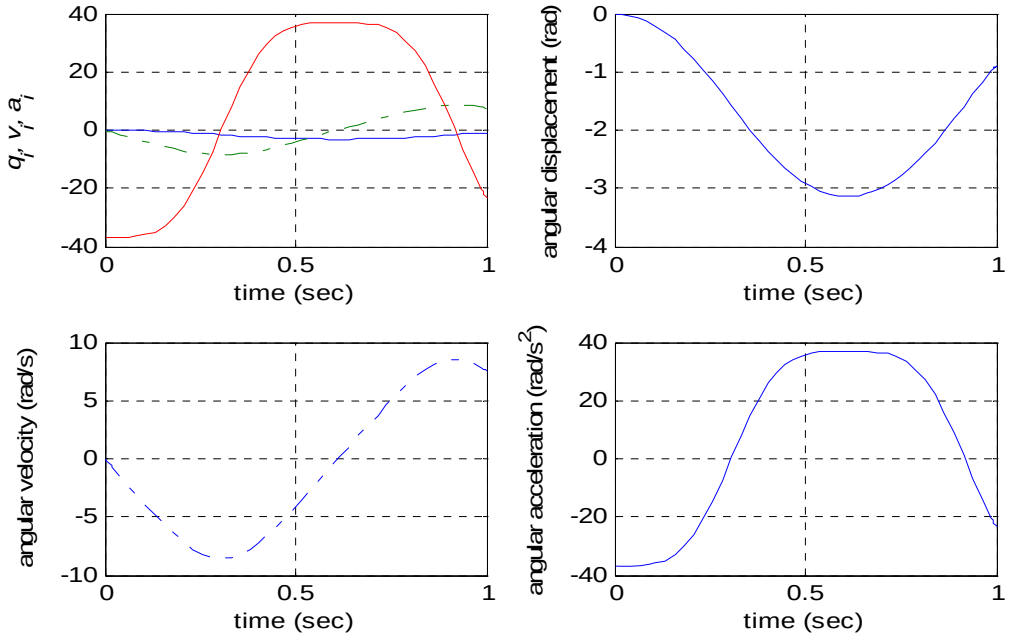

Figure 6.4 Matlab results for the case without external torque

Now we can use the results such as joint angle and joint angular velocity as the

information for predictive dynamics simulation. It could be the boundary conditions and/or state response constraints.

6.3.3. Performance Measure and Constraints for Predictive Dynamics

The joint angle profile q is set as a design variable. Let the time domain of simulation be $t \in [0,T]$. The performance measures that are to be studied in each case are listed in Equations (6.13a-d).

1) Minimize dynamic effort (torque square):

$$\text{Minimize: } f_1 = \int_0^T \tau^2 dt \tag{6.13a}$$

2) Minimize maximum torque:

$$\text{Minimize: } f_2 = \max_{t\in[0,T]} \tau \tag{6.13b}$$

3) Minimize total time:

$$\text{Minimize: } f_3 = T \tag{6.13c}$$

4) Feasible performance measure:

$$\text{Minimize: } f_4 = 0 \tag{6.13d}$$

Constraints for which information is to be taken from forward dynamics are listed as follows.

- Time-dependent constraints:

$$I_O \ddot{q} + mg\frac{l}{2}\cos q = \tau \quad \text{(Embedded)}$$

$$q_{lower} \le q \le q_{upper}$$

$$\tau_{lower} \le \tau \le \tau_{upper}$$

- Time-independent constraints:

$$q(t_{specific}) = q_{specific}$$

$$\dot{q}(t_{specific}) = \dot{q}_{specific}$$

The boundary conditions are included in the time independent constraints. Therefore, specific points could be initial and final points. Also, mid-points, which are somewhere in the profiles from the forward dynamics data, could be the specific points.

6.3.4. Results

Case 1: Simple Swing with Only Boundary Conditions without Applied Torque

The first case is a simple down swing without applied torque ($\tau = 0$). The pendulum does not have any oscillation motion at all in this case, and only the boundary conditions are given. The total simulation time is set to be $T = 0.406$. The formulation of optimization is

Minimize: $f_i \qquad i = 1,...,4$

Subject to: $I_O \ddot{q} + mg\frac{l}{2}\cos q = \tau$ (embedded)

$$-\pi \le q \le \pi$$

$$-10 \le \tau \le 10$$

$$q(0) = 0$$

$$q(T) = -2.37$$

$$\dot{q}(0) = 0$$

$$\dot{q}(T) = -7.13$$

The results of predictive dynamics are depicted in Figures (6.5-6.8)

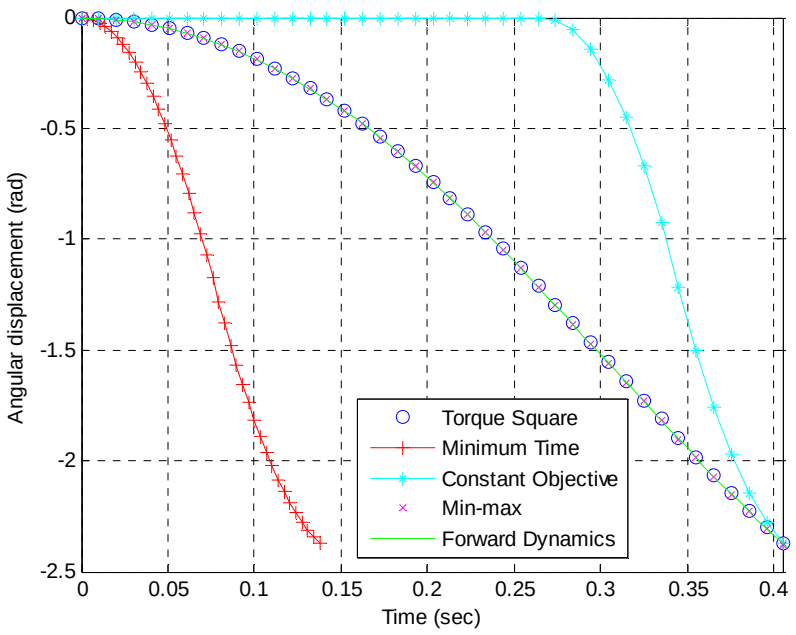

Figure 6.5 Joint angle profiles for Case 1

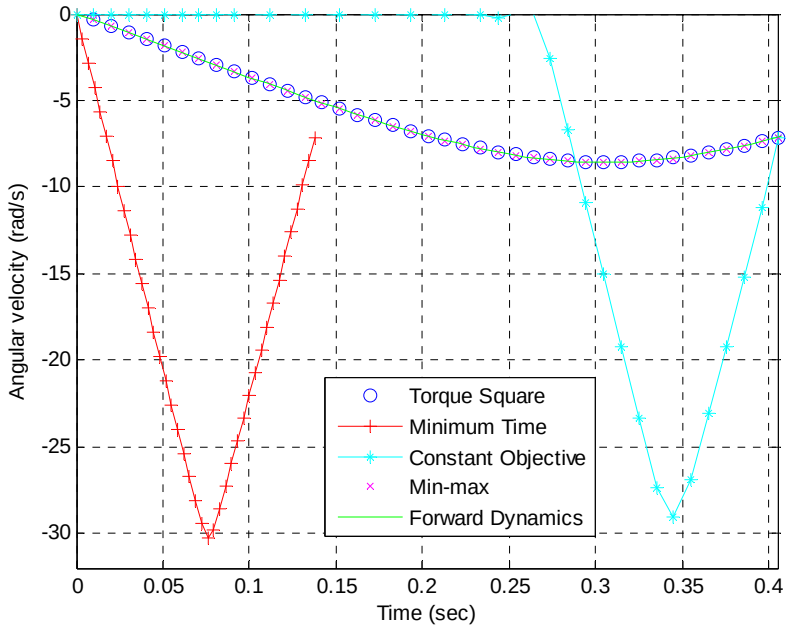

Figure 6.6 Angular velocity profiles for Case 1

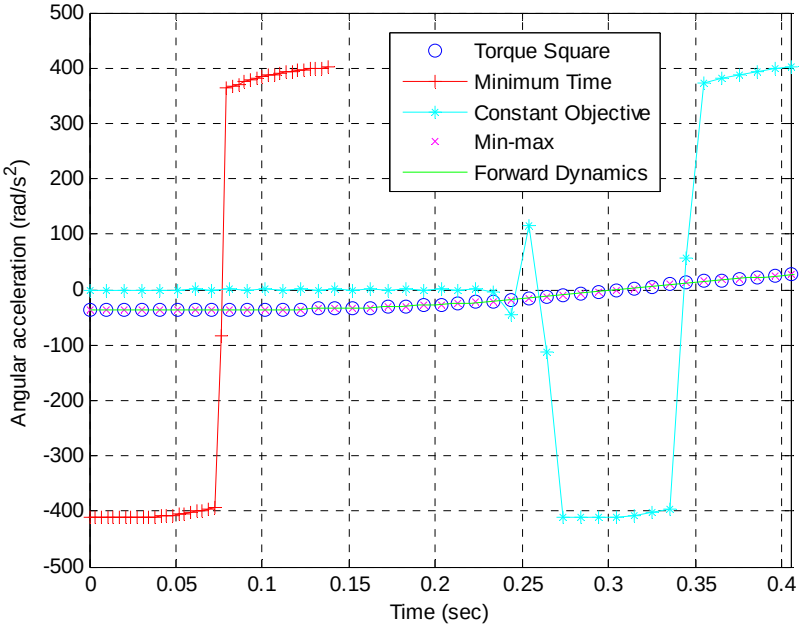

Figure 6.7 Angular acceleration profiles for Case 1

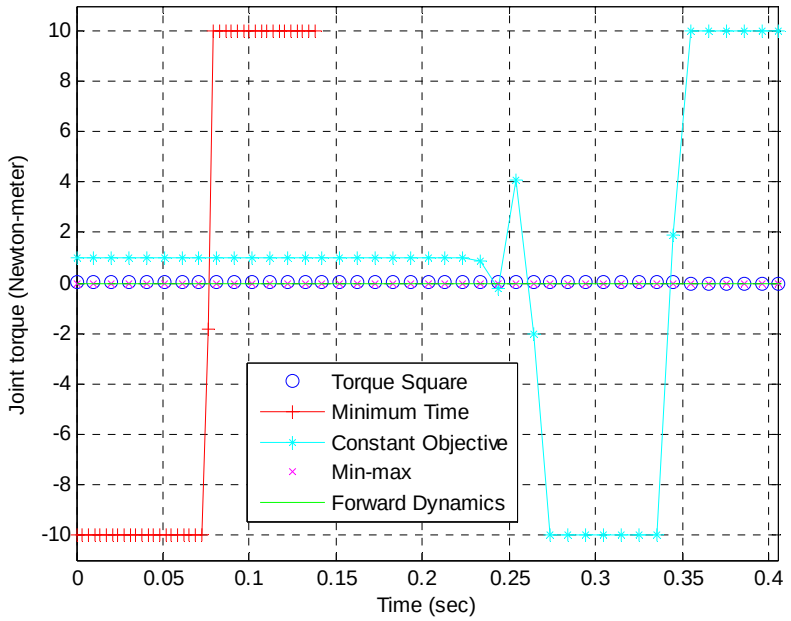

Figure 6.8 Joint torque profiles for Case 1

Case 2: Simple Swing with Only Boundary Conditions with Applied Torque

The second case is a simple down swing without oscillation with applied torque. Only the boundary conditions are given in this case. The total simulation time is set to be $T = 0.43$. The applied external torque is

$$\tau = 0.1 \sin 5t$$

The formulation of optimization is

Minimize: $f_i \qquad i = 1,...,4$

Subject to: $I_O \ddot{q} + mg \frac{l}{2} \cos q = \tau$ (Embedded)

$$-\pi \le q \le \pi$$

$$-10 \le \tau \le 10$$

$$q(0) = 0$$

$$q(T) = -2.40$$

$$\dot{q}(0) = 0$$

$$\dot{q}(T) = -5.86$$

The results of predictive dynamics are depicted in Figures (6.9-6.11)

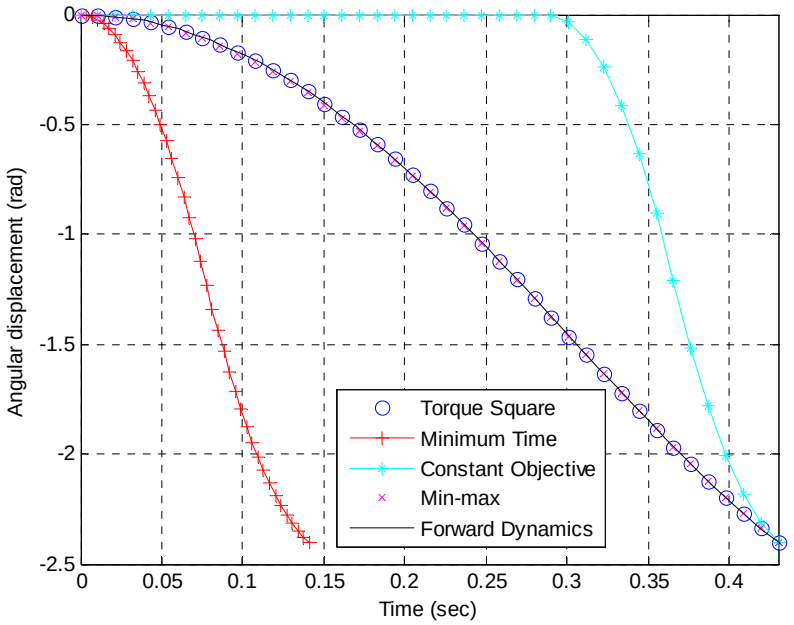

Figure 6.9 Joint angle profiles for Case 2

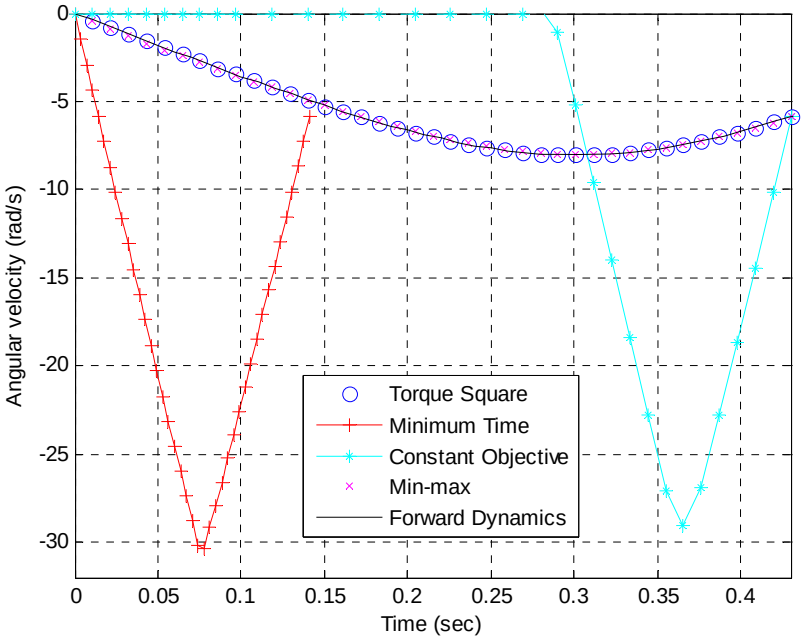

Figure 6.10 Angular velocity profiles for Case 2

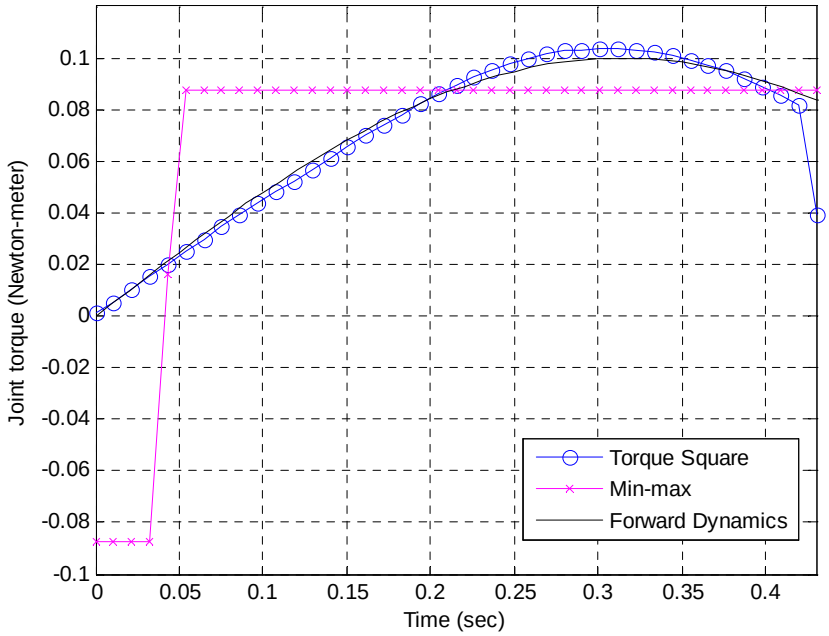

Figure 6.11 Joint torque profiles for Case 2

Case3: Oscillation Swing with Only Boundary Conditions

The third case is an oscillation swing with only boundary conditions and applied torque. The total simulation time is set to be $T = 1.79$. The applied external torque is

$$\tau = 0.1 \sin 5t$$

The formulation of optimization is

Minimize: $f_i \qquad i = 1, 2$

Subject to: $I_O \ddot{q} + mg \frac{l}{2} \cos q = \tau$ (Embedded)

$$-\pi \le q \le \pi$$

$$-10 \le \tau \le 10$$

$$q(0) = 0$$

$$q(T) = -2.40$$

$$\dot{q}(0) = 0$$

$$\dot{q}(T) = 2.85$$

The results of predictive dynamics are depicted in Figures (6.12-6.14)

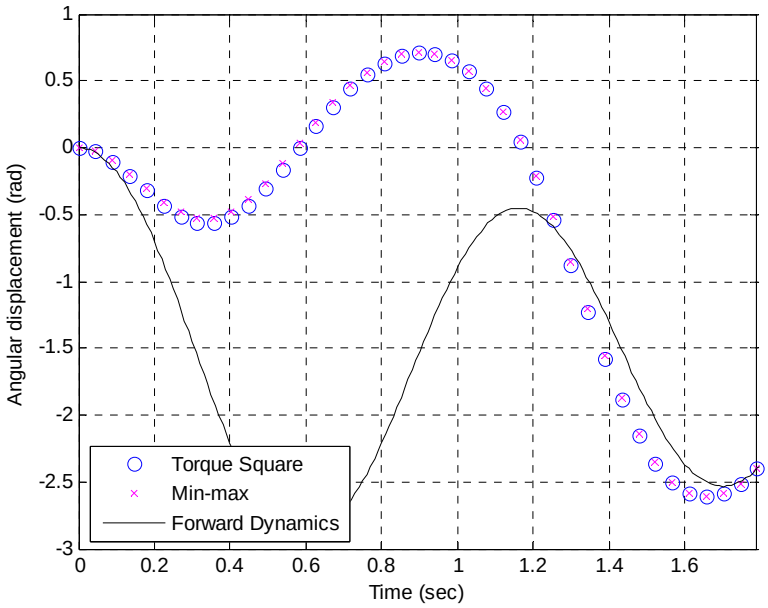

Figure 6.12 Joint angle profiles for Case 3

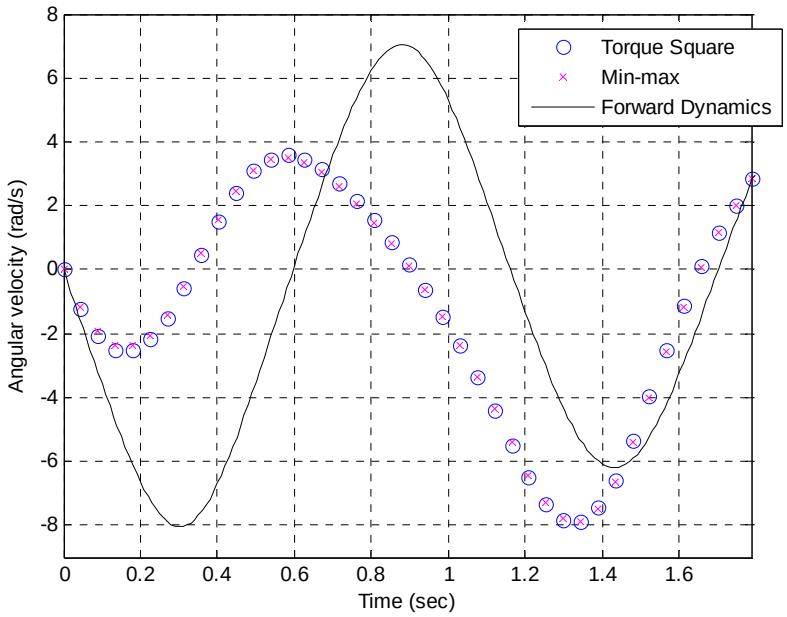

Figure 6.13 Angular velocity profiles for Case 3

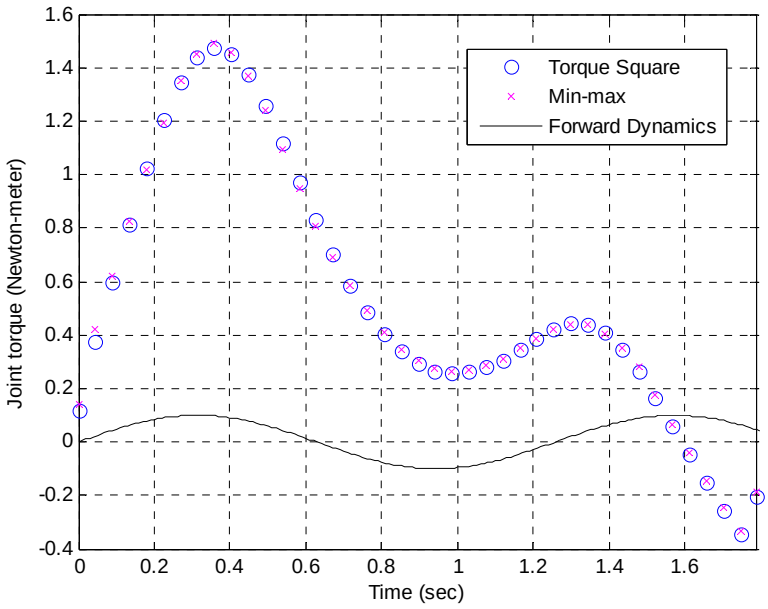

Figure 6.14 Joint torque profiles for Case 3

Case 4: Oscillation Swing with Boundary Conditions and One Mid-constraint

The fourth case is an oscillation swing with boundary conditions and one mid-constraint, and external torque is applied. The mid-constraint is applied at t = 0.76. The total simulation time is also set to be T = 1.79. The applied external torque is

$$\tau = 0.1 \sin 5t$$

The formulation of optimization is

Minimize: $f_i \qquad i = 1,...,4$

Subject to: $I_O \ddot{q} + mg \frac{l}{2} \cos q = \tau$ (Embedded)

$$-\pi \le q \le \pi$$

$$-10 \le \tau \le 10$$

$$q(0) = 0$$

$$q(0.76) = -2.44$$

$$q(T) = -2.40$$

$$\dot{q}(0) = 0$$

$$\dot{q}(T) = 2.85$$

The results of predictive dynamics are depicted in Figures (6.15-6.17)

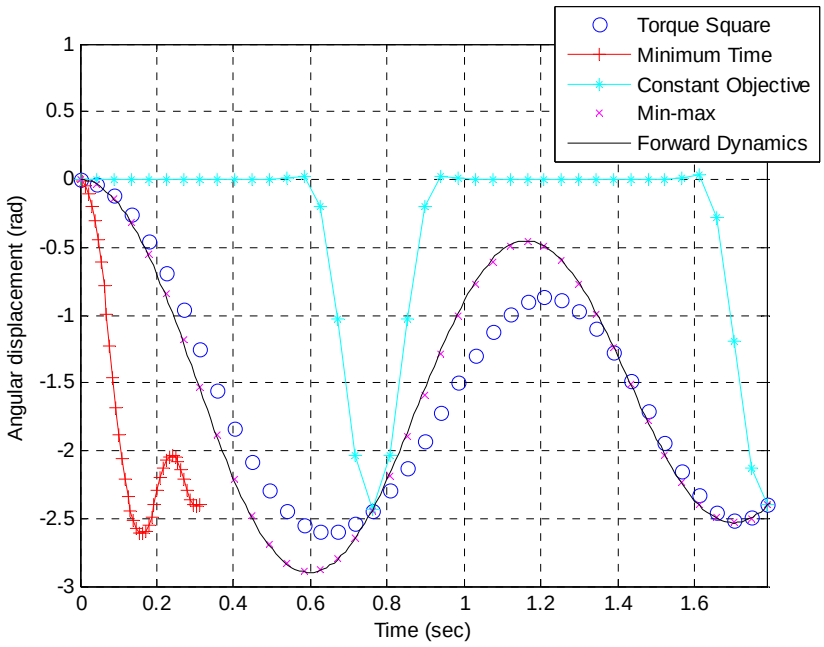

Figure 6.15 Joint angle profiles for Case 4

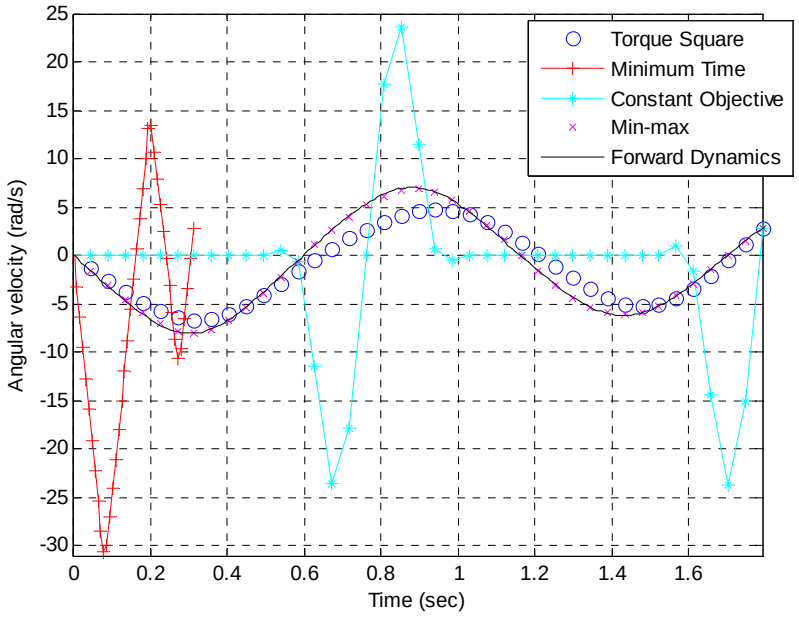

Figure 6.16 Angular velocity profiles for Case 4

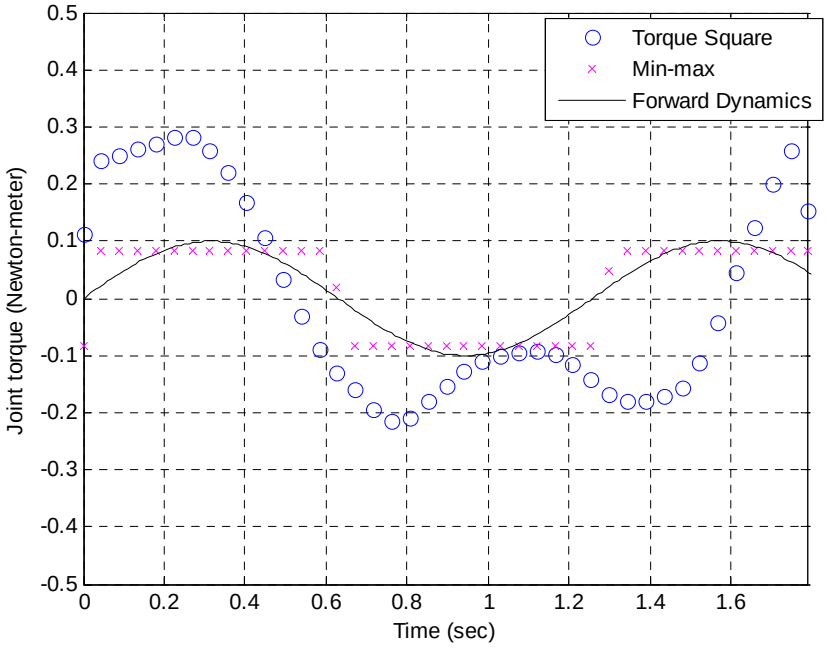

Figure 6.17 Joint torque profiles for Case 4

Case 5: Oscillation Swing with Boundary Conditions and Two Mid-constraints

The last case is an oscillation swing with boundary conditions and two mid-constraints, and external torque is applied. The mid-constraint is applied at $t = 0.76$ and $t = 1.21$. The total simulation time is also set to be $T = 1.79$. The applied external torque is

$$\tau = 0.1 \sin 5t$$

The formulation of optimization is

Minimize: $f_i \qquad i = 1, 2$

Subject to: $I_O \ddot{q} + mg \frac{l}{2} \cos q = \tau$ (Embedded)

$$-\pi \le q \le \pi$$

$$-10 \le \tau \le 10$$

$$q(0) = 0$$

$$q(0.76) = -2.44$$

$$q(1.21) = -0.493$$

$$q(T) = -2.40$$

$$\dot{q}(0) = 0$$

$$\dot{q}(T) = 2.85$$

The results of predictive dynamics are depicted in Figures (6.18-6.20)

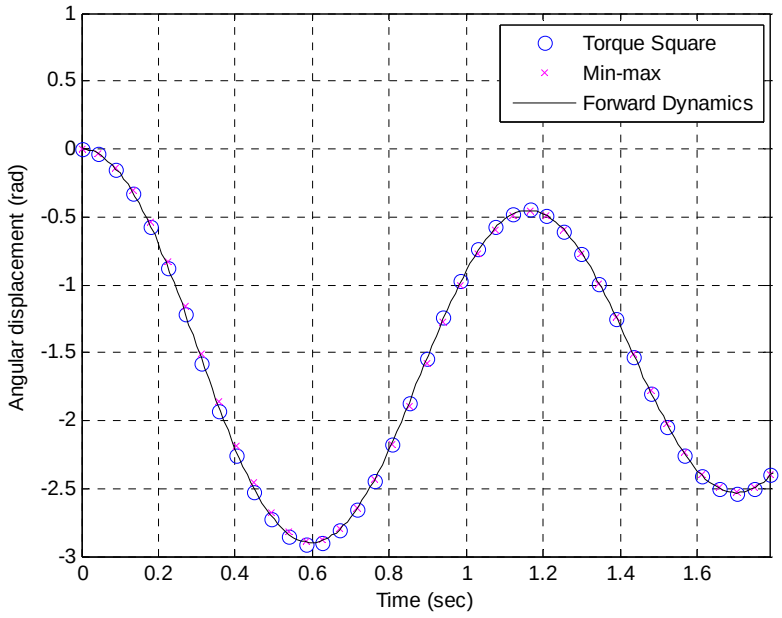

Figure 6.18 Joint angle profiles for Case 5

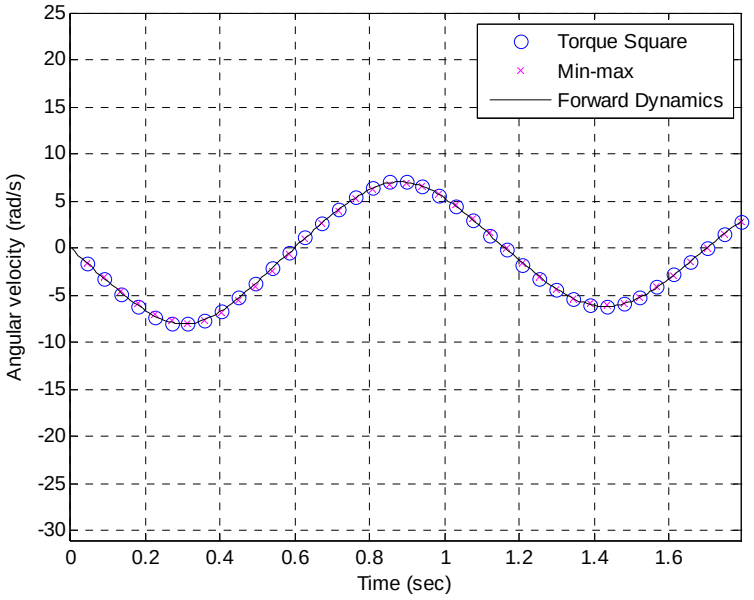

Figure 6.19 Angular velocity profiles for Case 5

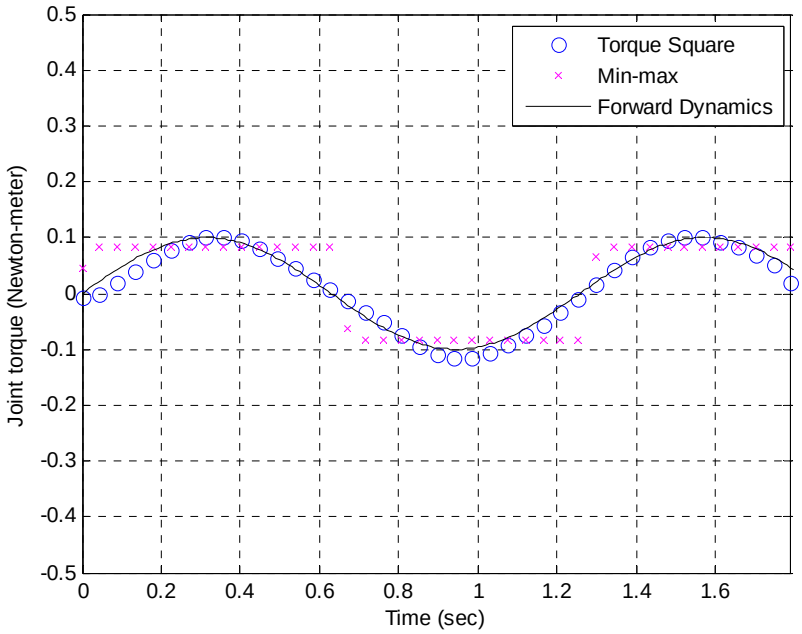

Figure 6.20 Joint torque profiles for Case 5

6.3.5. Discussion

Case 1 and Case 2 show that joint angle profiles, joint angle velocity profiles, and joint torque profiles are well predicted. However, the oscillation case in Case 3 shows that more information has to be provided to predict the motion correctly, Case 4 and Case 5 show how the predicted motions are improved by imposing mid-constraints. It is obvious that Case 5 has a better-predicted solution than Case 4 because of the number of mid-constraint imposed.

As far as the performance measure are concerned, the results show that minimizing total time and using feasible performance measure could not predict the motion well, but that minimizing torque square and minimizing maximum torque could predict the motion well. In terms of joint torque prediction, only minimizing torque square predicts it correctly. In fact, the torque square is proportional to the mechanical energy. In conclusion, the results show that minimal energy consumption is the best performance measure for predictive dynamics.

CHAPTER 7

FORMULATION OF RUNNING PROBLEM

The problem is to determine the joint angle profiles that minimize an energy cost function. It is assumed that the running motion is completely periodic and that there are two phases, support and flight. To solve this optimization problem, a skeletal model of the human and the running speed are needed as input. Through the optimization process, the joint angle profiles, joint torque profiles, and contact force profiles are obtained as output, as shown in Figure 7.1.

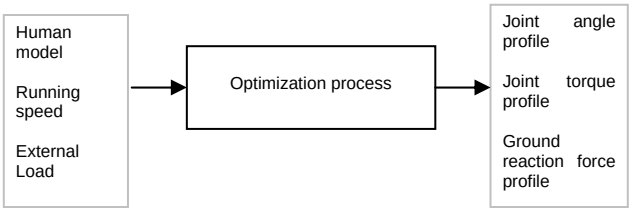

Figure 7.1 Input and output of running problem

7.1. General Description of Human Running

The word “run” is defined as “to go faster than a walk; specifically: to go steadily by springing steps so that both feet leave the ground for an instant in each step” (Merriam-Webster dictionary Online). Therefore, running is basically separated from walking in terms of whether or not both feet are off the ground during a gait cycle. The mechanism of running motion is very complicated. The entire body is involved while running; many muscles get activated during the running motion. Moreover, every human being runs in a slightly different way. Both the upper-body motion and the lower-body

motion differ, and running speeds vary. However, there are some common features in the running motion.

The lower-body motion of running is usually described in two or three phases (sometimes it is described in more than three phases, depending on the researcher or literature). In biomechanics, it is usually divided into three phases: support, drive, and recovery. The support phase is the phase when a foot is touching the ground and supporting the body against the force of gravity. The drive phase is the phase when the leg drives the body so that it maintains forward motion. The leg is extended at the knee and hip, and then the foot pushes backward in this phase. The recovery phase is the phase in between the drive phase and the support phase. Therefore, it is from the time when the toe is no longer contacting the ground to the time when the other foot is contacting the ground. In robotics, running is usually described in two phases: support and flight. As described earlier, biomechanics considers only one foot motion, but in robotics, both foot motions are considered. Therefore, the support phase means that a foot is contacting the ground, and the flight phase means that both feet are off the ground.

In general, *stride* refers to the period from the initial foot contact to the next contact of the same foot, and *step* refers to the period from the initial foot contact to the next contact of the other foot. However, this definition sometimes differs from field to field.

7.2. Model of Running

The running model for the formulation is composed of two phases—the support phase and the flight phase (Figure 7.2).

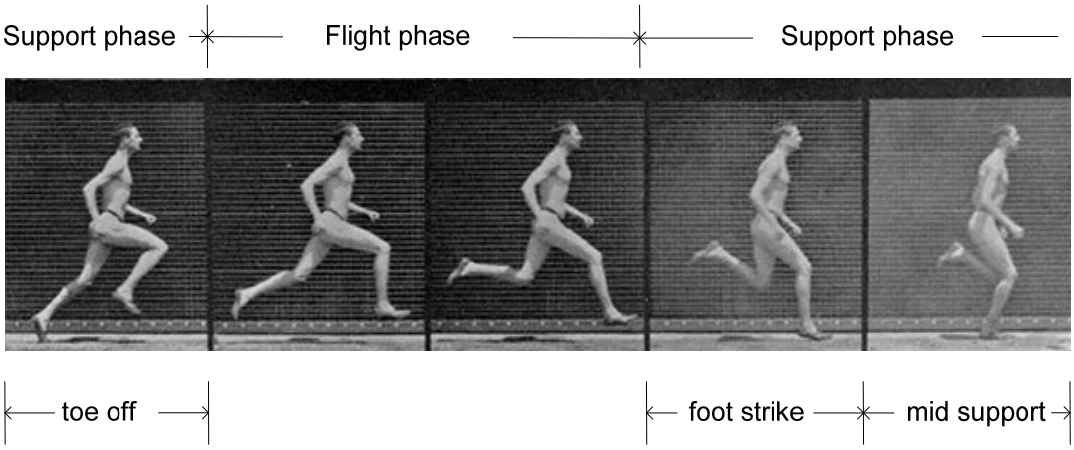

Figure 7.2 Human running (photo by Edward Muybridge)

The support phase is divided into three segments—foot strike, mid-support, and toe off. The terms mid-support and toe off have been adopted from the literature (Williams and Cavanagh, 1987). Figure 7.3 depicts these three segments of the support phase in detail.

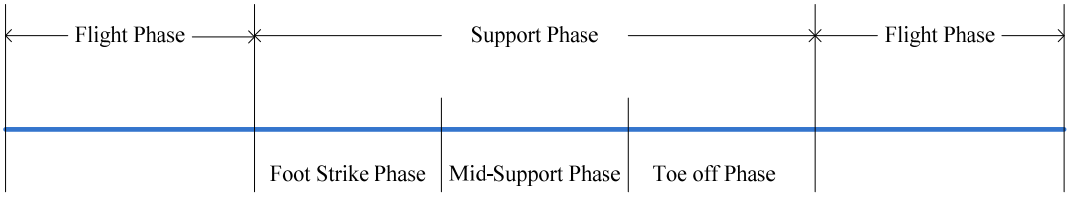

Figure 7.3 Model of running phase

7.2.1. Literature Summary of Lower Extremity Motion at Support Phase

Foot strike phase is the initial stage for the support phase. In the case of distance running, 80% of runners strike rear foot first, and the rest are mid foot strikers (Novacheck, 1998). Usually, when the running speed increases, initial contact is changed

from rear foot to forefoot (Novacheck, 1998). The angle of shank with the vertical is from 5.5 deg to 8.2 deg at this stage with the knee behind the ankle (Williams and Cavanagh, 1987). In mid-support phase, the entire foot area is the support region. As the speed increases, the maximum angle *q* (Figure 7.4) of the swing leg between shank and thigh becomes larger. As the running speed decreases, this angle between shank and thigh becomes smaller. The maximum angle *q* (Figure 7.4) of the swing leg (dashed line) is about 103.9 deg and the maximum angle of the support leg (solid line leg in Figure 7.4) is about 40.6 deg at 3.4 m/s—neutral angle at stance is 16 deg- (Milliron and Cavanagh, 1990).

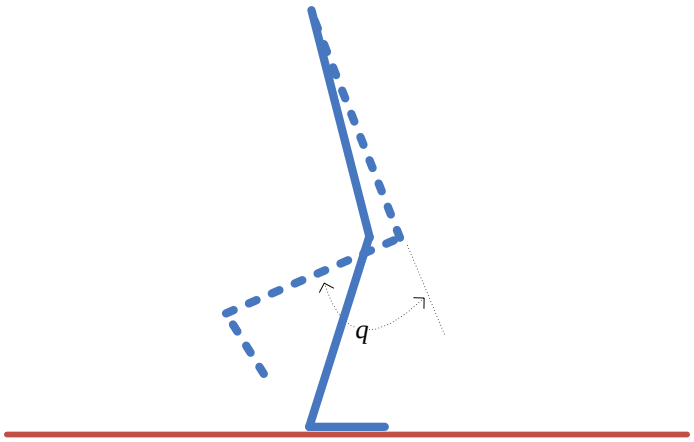

Figure 7.4 Leg motion at mid-support phase

7.2.2. Difficulties of the Running Problem

It is difficult to predict a completely *natural* running motion of human because:

1) No wobbling masses (soft tissues) effect is modeled (rigid body assumption), and mass moment of inertia is approximated.
2) We do not include muscle models.

3) Coupling of joint angles and joint torques are neglected.

4) High-velocity motion makes the dynamic motion very sensitive to variation of parameters (for example, mass moment of inertia); the faster it moves the harder it is to get natural motion for the assumed mechanical structure.

7.2.3. Foot Model

The current foot model is depicted in Figures 7.5 and 7.6. Red balls indicate the ankle joint and toe joint.

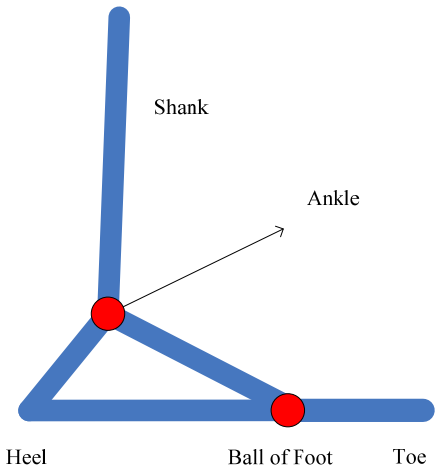

Figure 7.5 Description of foot model – side view

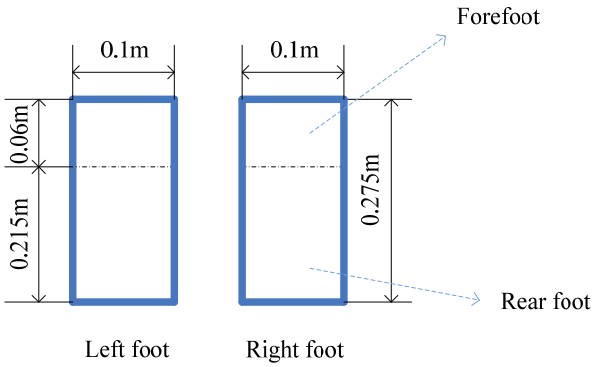

Figure 7.6 Description of foot model – top view

7.2.4. Description of Foot Support Region in Each Phase

Figures 7.7, 7.8 and 7.9 depict that foot support region in the support phase. The support region will be used in the dynamic stability constraint (ZMP constraint) and ground penetration constraint in later sections. The black dashed area is the support region in current formulation. According to the literature, 80% of runners strike rear foot first (Novacheck, 1998). Therefore, it is formulated that the rear foot is the contact area at foot strike phase. Entire foot is support region in mid-support phase and forefoot is the support region in the toe off phase. In the flight phase, there is no constraint on the foot. The only criterion is the conservation of angular momentum, and it is embedded in the equations of motion.

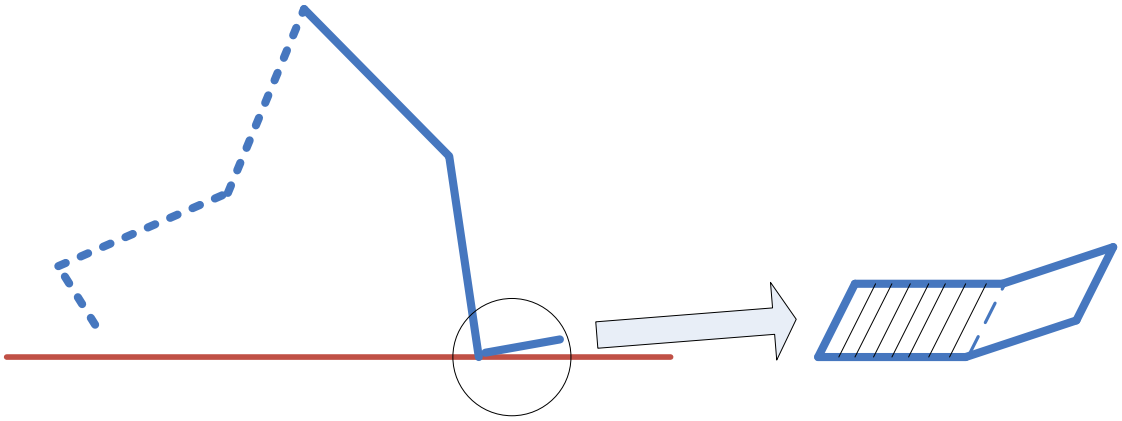

Figure 7.7 Foot strike phase and foot support region

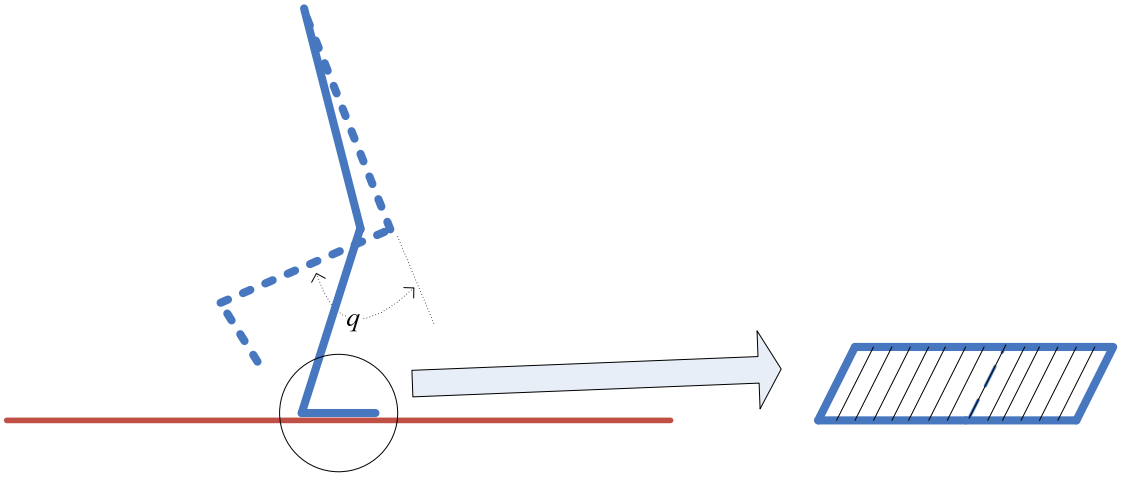

Figure 7.8 Mid-support phase and foot support region

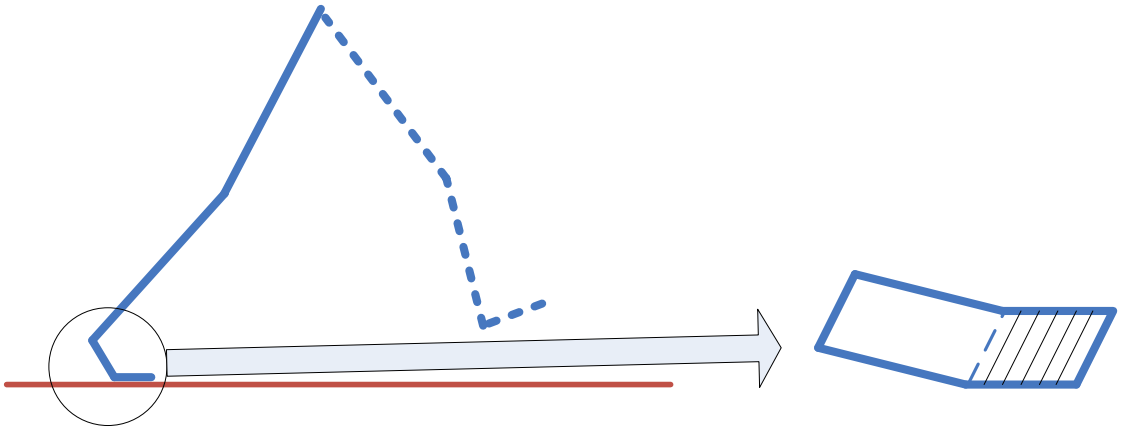

Figure 7.9 Toe off phase and foot support region

7.2.5. Step Length

The step length *sl* has been formulated as a function of running speed and body height in the computer graphics literature (Bruderlin and Calvert, 1996), as

$$sl = 0.1394 + (0.00465 + level)v\sqrt{\frac{body\_height}{1.8}} \text{ ; m} \tag{7.1}$$

where the variables are defined as follows:

v is running speed in m/min,

level is the level of expertise in running (−0.001 as poor ≤ *level* ≤ 0.001 as skilled)

body_height is the height of the human body (in meters).

This formula is applied up to 400 m/min (24 km/h, 6.6667 m/s). If the running speed (*v*) increases further, the step length (*sl*) is kept constant at that for the running speed of 400 m/min (Bruderlin and Calvert, 1996). Table 7.1 shows the step length in terms of the running speed when the *body_height* is 1.5934 m and the *level* is 0.001.

Table 7.1 Running speed vs. step length (*body_height* = 1.5934 *m*, *level* = 0.001)

Running Speed (m/s)	Step Length (meter)
2.5	0.9367
3.0	1.0962
3.5	1.2557
4.0	1.4152
4.5	1.5746
5.0	1.7341
5.5	1.8936
6.0	2.0531
6.5	2.2125

7.2.6. Step Time and Flight Time

7.2.6.1. Step Time

Once step length is obtained, step time is easily calculated from the running speed as:

$$t_{step} = sl / V \tag{7.2}$$

where t_{step} is the time for one step, sl is step length (meter), and V is running speed (m/s).

7.2.6.2. Flight Time

The flight time has been formulated in the computer graphics area, as a function of the running frequency (Bruderlin and Calvert, 1996). The flight time t_{flight} (sec) is given as

$$t_{flight} = -0.675\times10^{-3} - (0.15\times10^{-3} + level_2)sf + 0.542\times10^{-5} sf^2 \quad (0 \le sf \le 180\ steps/\min) \tag{7.3a}$$

$$t_{flight} = -8.925 + (0.131 + level_2)sf - 0.623\times10^{-3} sf^2 + 0.979\times10^{-6} sf^3 \quad (180 < sf \le 320\ steps/\min) \tag{7.3b}$$

where sf is step frequency (steps/min, $sf = v / sl$) and $level_2$ is the level of expertise in running (-0.0001 as poor $\le level_2 \le 0.0001$ as skilled).

The approximated flight time also can be obtained by support time from experimental data (Munro et al, 1987). The flight time is nothing but step time minus the support time:

$$t_{flight} = t_{step} - t_{support} \tag{7.4}$$

where $t_{support}$ is the time for the support phase. Table 7.2 shows support time and flight time with respect to the running speed.

Table 7.2 Time durations in one step ($level_2$ = 0.0001)

Running speed(m/s)	Step time (sec)	Support time (sec)	Flight time (sec)	Support time in gait cycle
2.5	0.3747	0.2764	0.0982	73.7%
3.0	0.3654	0.2610	0.1043	71.4%
3.5	0.3587	0.2496	0.1090	69.5%
4.0	0.3538	0.2409	0.1128	68.1%
4.5	0.3499	0.2341	0.1158	66.9%
5.0	0.3468	0.2285	0.1182	65.8%
5.5	0.3442	0.2239	0.1203	65.0%
6.0	0.3421	0.2200	0.1221	64.3%
6.5	0.3403	0.2167	0.1236	63.6%

The time is distributed uniformly for foot strike phase, mid-support phase, and toe off phase. There is no data from literature for this time distribution. Therefore, it is selected by numerical experimentation.

7.3. Formulation of Ground Reaction Force

Assume that the ground reaction force is acting at the zero moment point (ZMP) *D* in Figure 7.10.

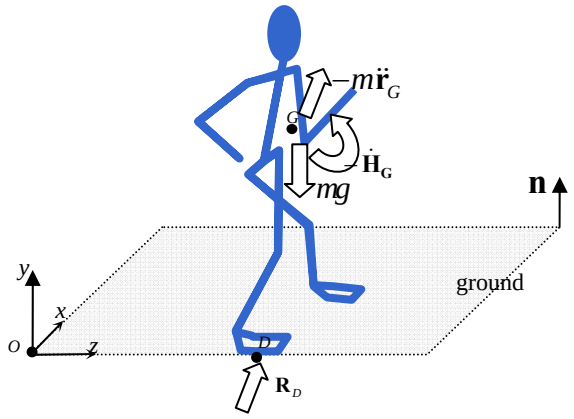

Figure 7.10 Inertia, gravity and resultant force in locomotion

The resultant force due to gravity and inertia at the foot support is

$$\mathbf{F}_D = -m\ddot{\mathbf{r}}_G + m\mathbf{g} \tag{7.5}$$

If the normal vector is $\mathbf{n}= [0,1,0]^T$, the gravity vector is $\mathbf{g}=[0,-g,0]^T$. The center of pressure and zero moment point coincide (Sardain and Bessonnet, 2004). Then, the ground reaction force is written as:

$$\mathbf{R}_D = -\mathbf{F}_D \tag{7.6a}$$

Therefore,

$$\mathbf{R}_D = m\ddot{\mathbf{r}}_G - m\mathbf{g} \tag{7.6b}$$

The general equations of motion of human body is

$$m\ddot{\mathbf{r}}_G = \mathbf{F} + \mathbf{F}_g \tag{7.7a}$$

where $\mathbf{F}$ is generalized force and $\mathbf{F}_g$ is the gravity force

$$\mathbf{F}_g = m\mathbf{g} \tag{7.7b}$$

Thus, from Eqs. (7.6b), (7.7a) and (7.7b), we get

$$\mathbf{F} = \mathbf{R}_D \tag{7.7c}$$

Note that the generalized force **F** is same as the global force due to generalized coordinate (translational q_0, q_1, q_2) in the recursive Lagrange dynamics formula. From Equation (7.7c), we can use generalized force **F** as passive force in our algorithm so that it is treated as ground reaction force (Xiang, 2008). The algorithm consists of two parts. First part is the simulation without ground reaction force. Once the global force is acquired, it is applied to the second simulation part as an external force.

7.4. Formulation of the Impact in Running

7.4.1. Impact Formulation: Basic Idea

Impact at foot strike has been treated in the robotics area by using the angular momentum. For example, Roussel and Goswami (1998) calculated impulse by using the angular momentum as:

$$\mathbf{I} = \mathbf{J}(\mathbf{q})(\dot{\mathbf{q}}^{+} - \dot{\mathbf{q}}^{-}) \tag{7.8}$$

where $\mathbf{q}$ is the joint angle vector, $\dot{\mathbf{q}}^{-}$ is the joint angle velocity vector just before the foot contact, $\dot{\mathbf{q}}^{+}$ is the joint angle velocity vector just after the foot contact, $\mathbf{J}(\mathbf{q})$ is the inertia matrix, and **I** is impulse. Then, they included this impulse in the cost function for the optimization formulation of the biped robot walking problem:

$$f = \int_0^T \boldsymbol{\tau}^T \boldsymbol{\tau}\, dt + \mathbf{I}^T \mathbf{I} \tag{7.9}$$

where $\boldsymbol{\tau}$ is the joint torque vector, and **I** is the impulse at the foot strike phase. Therefore, the impulse at foot strike is minimized while satisfying the impulse and angular momentum equations.

7.4.2. Impact Formulation: Difficulty

Using angular momentum to calculate impulse (Roussel and Goswami's method) is appropriate, but there is one difficulty in using that method. The usual formulation for calculating angular momentum and impulse is

$$\mathbf{H}_0 = \sum_i (\mathbf{r}_i \times m_i \frac{d}{dt}\mathbf{r}_i + {}^0\mathbf{T}_i \mathbf{J}_i \omega_i) \tag{7.10a}$$

$$\mathbf{I} = \mathbf{H}_0^+ - \mathbf{H}_0^- \tag{7.10b}$$

where the variables are defined as follows**:**

$\mathbf{r}_i$ is the center of mass of the *i*-th link

${}^0\mathbf{T}_i$ is the transformation matrix from the *i*-th link to the origin of the inertial reference frame

$\mathbf{J}_i$ is the inertia matrix for the *i*-th link

ω_i is the joint angular velocity

$\mathbf{I}$ is impulse

$\mathbf{H}_O$ is the angular momentum about point *O*

$\mathbf{H}_O^-$ is the angular momentum just before impact

$\mathbf{H}_O^+$ is the angular momentum just after impact

However, there is difficulty in using Equations (7.10a) and (7.10b). The fact is that the angular velocity ω_i is an absolute value (and global). In the current formulation with the Denavit-Hartenberg method, angular velocity ω_i (or $\dot{q}_i$) has been defined as a relative and local value. Therefore, the absolute angular velocity ω_i as well as the global angular

velocity have to be calculated in order to use Equations (7.10a) and (7.10b). This gives difficulties in implementation of the formulation.

7.4.3. Impact Formulation: Linear Impulse

It turns out that there is another way to calculate the impact during the foot contact that does not use velocities of the individual segments of the body. If the ground reaction forces are known then the concept of linear impulse can be used to formulate the impact phenomena. The Newton's second law states that the force acting on a particle is equal to the rate of change of the linear momentum, i.e.,

$$\sum \mathbf{F} = m\frac{d\mathbf{v}}{dt}. \tag{7.11}$$

Integrating the equation with respect to time gives

$$\int_{t_1}^{t_2} \sum \mathbf{F} dt = m\mathbf{v}_2 - m\mathbf{v}_1. \tag{7.12}$$

The term on the left is called *linear impulse*. The average with respect to time of the total force acting on an object from t_1 to t_2 is

$$\sum \mathbf{F}_{average} = \frac{1}{(t_2 - t_1)} \int_{t_1}^{t_2} \sum \mathbf{F} dt. \tag{7.13}$$

So, with Equation (7.12), we can write

$$(t_2 - t_1) \sum \mathbf{F}_{average} = m\mathbf{v}_2 - m\mathbf{v}_1. \tag{7.14}$$

The impulsive force is defined as a force of relatively large magnitude that acts over a small interval of time. Determining the actual history of such a force is often impractical, but its average value can be estimated (Bedford and Fowler, 2002). Therefore, the impulse at foot strike $\mathbf{I}_{strk}$ can be approximated as:

$$\mathbf{I}_{strk} = \Delta t \sum \mathbf{F}_{average} \,. \tag{7.15}$$

The ground reaction force is the resultant external force in the current mechanical model. Therefore, impulse in terms of ground reaction force (resultant external force) is

$$\mathbf{I}_{strk} = \mathbf{R}_D \Delta t \,, \tag{7.16}$$

where D is the zero moment point.

7.5. Optimization Formulation

7.5.1. Design Variables

The design variables are the joint angle profiles $\mathbf{q}(t)$ parameterized using B-spline approximation. As depicted in Figure 7.11, the number of control points in the current formulation is 5 for each joint angle. Since the number of degrees of freedom for the mechanical system is 55, the total number of design variables is 55×5 = 275.

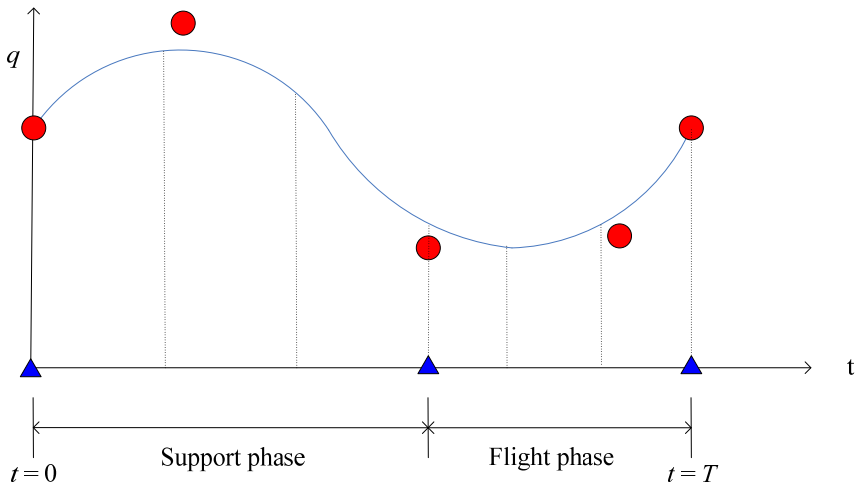

Figure 7.11 Joint angle profiles parameterized in the B-spline

The time is distributed uniformly in the support phase between the foot strike, mid-

support, and toe off phases.

7.5.2. Performance Measure

The first performance measure which is proportional to the mechanical energy is

$$f_\tau = \int_0^T \bar{\boldsymbol{\tau}}^T \bar{\boldsymbol{\tau}} dt \,, \tag{7.17a}$$

where $\bar{\boldsymbol{\tau}}$ contains the weighted joint torques as

$$\bar{\tau}_i = w_i \tau_i \tag{7.17b}$$

where w_i is the weight coefficients. This mechanical energy is a reasonable criterion to minimize as discussed previously (Roussel et al., 1998). The impulse can be calculated from Equation (7.16) once the ground reaction forces have been calculated. Then, we can incorporate the impulse into the performance measure to minimize it. Therefore, the second performance measure is

$$f_I = \mathbf{I}_{strk}^{\mathrm{T}} \mathbf{I}_{strk} \,. \tag{7.17c}$$

Thus, the final performance measure for running formulation is

$$f = w_\tau f_\tau + w_I f_I \,, \tag{7.17d}$$

where w_τ and w_I are the weighting parameters for the two objectives.

7.5.3. Constraints

Most constraints are motivated by the digital human walking formulation (Xiang et al., 2007), listed as follows:

1) Joint angle limits
2) Joint torque limits

3) Ground penetration constraint
4) Foot location constraint - ground contact points
5) Initial posture constraint of foot location - initial rear heel position
6) No slip constraint (zero velocity at foot strike)
7) ZMP constraint during support phase
8) Symmetry condition (step formulation) or continuity condition (stride formulation)

7.6. Description of Constraints

7.6.1. Joint Angle Limits

Joint angle limits for the body are determined based on work by Norkin and White (2003):

$$\mathbf{q}_{lower} \le \mathbf{q}(t) \le \mathbf{q}_{upper} \qquad (0 \le t \le T) \tag{7.18}$$

Some joint angle limits are re-defined by trial and error for better simulation results (task-specific joint angle limits). Some degrees of freedom do not participate significantly in the running motion. Therefore, those degrees of freedom are frozen to avoid redundancy and to facilitate natural motion. The frozen degrees of freedom are the neck bend joint, clavicle joint, elbow joint, wrist joint, shoulder joint, and spine twist of the second, third, and fourth spine joints. Thus, 33 active degrees of freedom are used for the running simulation. Joint angle limits for each degree of freedom are listed in Table 7.3.

Table 7.3 Joint angle limits (degrees)

DOF	Lower	Upper	Motion Direction
Q01	-2.0024	2.0368	Spine joint1 tilt
Q02	1.0027	12.0	Spine joint1 bend
Q03	-15.0177	15.0521	Spine joint1 twist
Q04	-2.0024	2.0425	Spine joint2 tilt
Q05	1.0027	12.0	Spine joint2 bend
Q06	-1.0	1.0	Spine joint2 twist
Q07	-2.0024	2.0368	Spine joint3 tilt
Q08	1.0027	15.0	Spine joint3 bend
Q09	-1.0	1.0	Spine joint3 twist
Q10	-2.0024	2.0368	Spine joint4 tilt
Q11	1.0027	15.0	Spine joint4 bend
Q12	-1.0	1.0	Spine joint4 twist
Q13	-0.0573	0.0573	Right clavicle
Q14	-0.0573	0.0573	Right clavicle
Q15	-0.5730	0.5730	Right shoulder abduction/adduction
Q16	-1.0	1.0	Right shoulder extension/flexion
Q17	-6.5	-5.5	Right shoulder internal rotation/external rotation
Q18	-91.0	-89.9427	Right elbow flexion/extension
Q19	-0.5730	0.5730	Right elbow internal rotation/external rotation
Q20	-0.5730	0.5730	Right wrist radial dev./ulnar dev.
Q21	-0.5730	0.5730	Right wrist extension/flexion
Q22	-0.0573	0.0573	Left clavicle
Q23	-0.0573	0.0573	Left clavicle
Q24	-0.5730	0.5730	Left shoulder abduction/adduction
Q25	-1.0	1.0	Left shoulder extension/flexion

Table 7.3 Continued

Q26	-6.5	-5.5	Left shoulder internal rotation/external rotation
Q27	-91.0	-89.9427	Left elbow flexion/extension
Q28	-0.5730	0.5730	Left elbow internal rotation/external rotation
Q29	-0.5730	0.5730	Left wrist radial dev./ulnar dev.
Q30	-0.5730	0.5730	Left wrist extension/flexion
Q31	-2.0	2.0	Neck joint1 lateral flex-left/lateral flex-right
Q32	-5.0	5.0	Neck joint1 saggital-extension/saggital-flexion
Q33	-5.0	5.0	Neck joint1 transverse-right/transverse-left
Q34	-2.0	2.0	Neck joint2 lateral flex-left/lateral flex-right
Q35	-1.0	1.0	Neck joint2 saggital-extension/saggital-flexion
Q36	-20.0	10.0	Right hip abduction/adduction
Q37	-90.0	90.0	Right hip flexion/extension
Q38	-20.0	20.0	Right hip external rotation/internal rotation
Q39	10.	135.0	Right knee extension/flexion
Q40	-20.1175	54.4721	Right ankle dorsiflexion/plantar flexion
Q41	-10.0	10.0	Right ankle eversion/inversion
Q42	-70.8319	0.0229	Right midfoot dorsiflexion/plantar flexion
Q43	-20.0	10.0	Left hip abduction/adduction
Q44	-90.0	90.0	Left hip hip flexion/extension
Q45	-20.0	20.0	Left hip external rotation/internal rotation
Q46	10.0	135.0	Left knee extension/flexion
Q47	-20.1175	54.4721	Left ankle dorsiflexion/plantar flexion
Q48	-10.0	10.0	Left ankle eversion/inversion
Q49	-70.8319	0.0229	Left midfoot dorsiflexion/plantar flexion

7.6.2. Joint Torque Limits

$$\boldsymbol{\tau}_{lower} \le \boldsymbol{\tau}(t) \le \boldsymbol{\tau}_{upper} \qquad (0 \le t \le T) \tag{7.19}$$

References for each joint torque limit are listed in Table 7.4 and joint torque limits for each degree of freedom are listed in Table 7.5.

Table 7.4 References for joint torque limits

Joint	References
Neck	Seng KY, Lee Peter VS, and Lam PM. (2002)
Torso	Kumar S (1996); Ho CW, Chen LC, Hsu HH, Chiang SL, Li MH, Jiang SH, and Tsai KC (2005); Huang QM and, Thorstensson A (2000); Kumar S, Narayan Y, Garand D (2003)
Shoulder	Mayer F, Horstmann T, Röcker K, Heitkamp HC, Dickhuth HH. (1994)
Wrist	Delp S, Grierson A, and Buchanan T (1996); Marley R and Thomson M (2000); O'Sullivan L and Gallwey T (2005); Forthomme B, Croisier J, Foidart-Dessalle M, and Crielaard J (2002)
Hip	Cahalan TD, Johnson ME, Liu S, and Chao EY. (1989)
Ankle	Kaminski TW, Perrin DH, and Gansneder BM. (1999)

Table 7.5 Joint torque limits (N m)

DOF	Lower	Upper	Motion Direction
Q01	-150	150	Spine joint1 tilt
Q02	-300	300	Spine joint1 bend
Q03	-150	150	Spine joint1 twist
Q04	-40.0	40.0	Spine joint2 tilt
Q05	-300.0	300.0	Spine joint2 bend
Q06	-40.0	40.0	Spine joint2 twist
Q07	-30.0	30.0	Spine joint3 tilt
Q08	-300.0	300.0	Spine joint3 bend
Q09	-30.0	30.0	Spine joint3 twist
Q10	-20.0	20.0	Spine joint4 tilt
Q11	-200.0	200.0	Spine joint4 bend
Q12	-20.0	20.0	Spine joint4 twist
Q13	-50.0	50.0	Right clavicle
Q14	-50.0	50.0	Right clavicle
Q15	-47.0	66.0	Right shoulder abduction/adduction
Q16	-92.0	63.0	Right shoulder extension/flexion
Q17	-27.0	43.0	Right shoulder internal rotation/external rotation
Q18	-58.7	60.3	Right elbow flexion/extension
Q19	-12.0	15.0	Right elbow internal rotation/external rotation
Q20	-11.0	9.1	Right wrist radial dev./ulnar dev.
Q21	-6.0	12.2	Right wrist extension/flexion
Q22	-50.0	50.0	Left clavicle
Q23	-55.0	50.0	Left clavicle
Q24	-47.0	66.0	Left shoulder abduction/adduction
Q25	-92.0	63.0	Left shoulder extension/flexion

Table 7.5 Continued

Q26	-27.0	43.0	Left shoulder internal rotation/external rotation
Q27	-58.7	60.3	Left elbow flexion/extension
Q28	-12.0	15.0	Left elbow internal rotation/external rotation
Q29	-11.0	9.1	Left wrist radial dev./ulnar dev.
Q30	-6.0	12.2	Left wrist extension/flexion
Q31	-27.0	27.2	Neck joint1 lateral flex-left/lateral flex-right
Q32	-45.0	23.0	Neck joint1 saggital-extension/saggital-flexion
Q33	-11.0	10.0	Neck joint1 transverse-right/transverse-left
Q34	-30.0	30.0	Neck joint2 lateral flex-left/lateral flex-right
Q35	-30.0	30.0	Neck joint2 saggital-extension/saggital-flexion
Q36	-120.0	129.0	Right hip abduction/adduction
Q37	-167.0	204.0	Right hip flexion/extension
Q38	-67.0	85.0	Right hip external rotation/internal rotation
Q39	-259.1	103.2	Right knee extension/flexion
Q40	-37.7	85.3	Right ankle dorsiflexion/plantar flexion
Q41	-30.1	30.1	Right ankle eversion/inversion
Q42	-72.0	70.0	Right midfoot dorsiflexion/plantar flexion
Q43	-120.0	129.0	Left hip abduction/adduction
Q44	-167.0	204.0	Left hip hip flexion/extension
Q45	-67.0	85.0	Left hip external rotation/internal rotation
Q46	-259.1	103.2	Left knee extension/flexion
Q47	-37.7	85.3	Left ankle dorsiflexion/plantar flexion
Q48	-30.1	30.1	Left ankle eversion/inversion
Q49	-70.0	70.0	Left midfoot dorsiflexion/plantar flexion

7.6.3. Foot Location of Ground Contact Point

Since the step length can be calculated from the running speed, the location of the foot contact points can be specified.

$$\mathbf{r}_i(t) = \tilde{\mathbf{r}}_i, \qquad (i \in contact) \tag{7.20}$$

where $\tilde{\mathbf{r}}_i$ is the specified foot location. The specified foot location is calculated from the step length formula. Figure 7.12 depicts the key points for the foot location constraint. Also the foot location is 0.01 m away from the center line of the running direction (gap in Figures 7.13, 7.14, and 7.15). This distance has been optimized by trial and error. In the flight phase, this constraint is not applied.

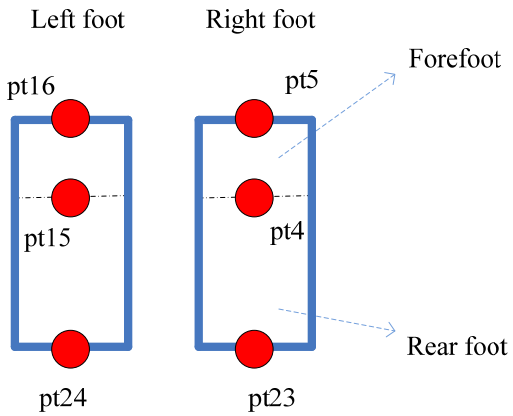

Figure 7.12 Key points for the foot location constraint

pt16: left toe center pt5: right toe center

pt15: left ball center pt4: right ball center

pt24: left heel center pt23: right heel center

7.6.3.1. At foot strike instant

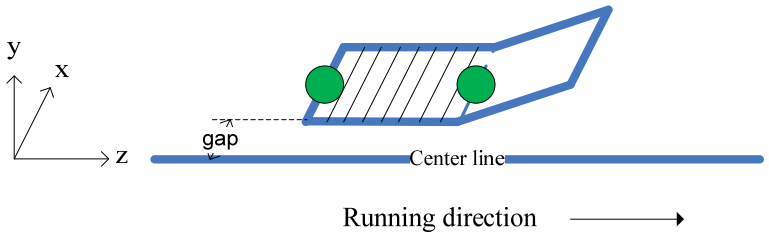

Figure 7.13 Points for the foot location constraint at foot strike instant

The green points (heel center, ball center) are constrained by the foot location constraint into the specified location $\tilde{\mathbf{r}}_i$:

$$\mathbf{r}_i(t) = \tilde{\mathbf{r}}_i, \qquad (i \in contact) \tag{7.21}$$

7.6.3.2. At mid-support instant

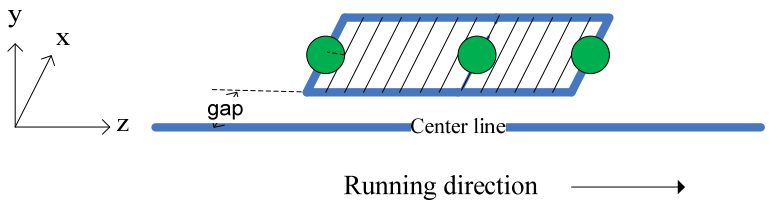

Figure 7.14 Points for the foot location constraint at mid-support instant

All three points (heel center, ball center, toe center) are constrained by the foot location constraint at this instant.

$$\mathbf{r}_i(t) = \tilde{\mathbf{r}}_i, \qquad (i \in contact) \tag{7.22}$$

7.6.3.3. At toe off instant

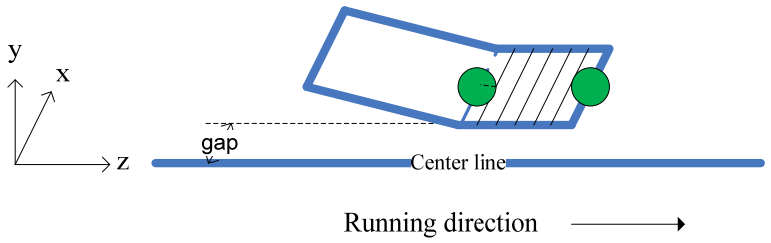

Figure 7.15 Points for the foot location constraint at toe off instant

The green points (ball center, toe center) are constrained by the foot location constraint into the specified location $\tilde{\mathbf{r}}_i$:

$$\mathbf{r}_i(t) = \tilde{\mathbf{r}}_i, \qquad (i \in contact) \tag{7.23}$$

7.6.4. Ground Penetration

While the foot is contacting the ground, the height of the foot from the ground is zero. While the foot is not contacting the ground, the foot should be above the ground. Then, the height of the foot from the ground is greater than zero.

$$\begin{aligned} &y_i(t) = 0, && (i \in contact) \\ &y_i(t) \geq \varepsilon, && (i \notin contact) \\ &\varepsilon = 10^{-3} \end{aligned} \tag{7.24}$$

where *i* refers to the contact point in the set of contact points. In the current formulation, 6 points are used on each foot for the ground penetration constraints (Figure 7.16; the numbers are the assigned point numbers).

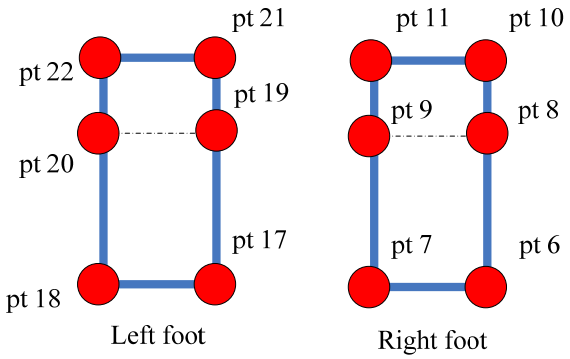

Figure 7.16 Six points of foot for ground penetration constraint

pt22: left toe lateral pt10: right toe lateral

pt20: left ball lateral pt8: right ball lateral

pt18: left heel lateral pt6: right heel lateral

pt21: left toe medial pt11: right toe medial

pt19: left ball medial pt9: right ball medial

pt17: left heel medial pt7: right heel medial

7.6.4.1. <u>At foot strike instant</u>

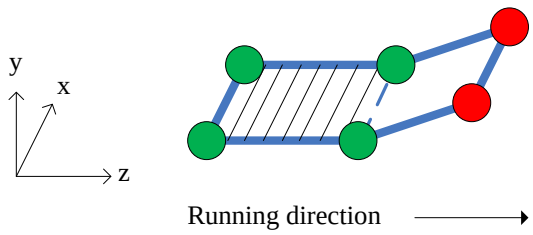

Figure 7.17 Points for ground penetration constraint at foot strike instant

The green points (heel lateral, heel medial, ball lateral, ball medial) are in contact

on the ground:

$$y_i(t) = 0 \tag{7.25a}$$

The red points (toe lateral, toe medial) are not in contact on the ground:

$$y_i(t) \geq \varepsilon, \quad \varepsilon = 10^{-3} \tag{7.25b}$$

7.6.4.2. At mid-support instant

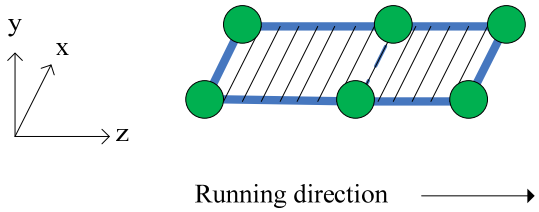

Figure 7.18 Points for ground penetration constraint at mid-support instant

All points are in contact with the ground in this phase (Figure 7.18):

$$y_i(t) = 0 \tag{7.26}$$

7.6.4.3. At toe off instant

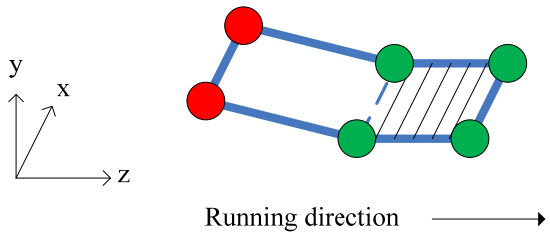

Figure 7.19 Points for ground penetration constraint at toe off phase

The green points (ball lateral, ball medial, toe lateral, toe medial) are in contact on

the ground (Figure 7.19):

$$y_i(t) = 0 \tag{7.27a}$$

The red points (heel lateral, heel medial) are not in contact on the ground:

$$y_i(t) \geq \varepsilon, \quad \varepsilon = 10^{-3} \tag{7.27b}$$

7.6.4.4. In flight phase

All points are off the ground in flight phase:

$$y_i(t) \geq \varepsilon, \quad \varepsilon = 10^{-3} \tag{7.28}$$

7.6.5. Initial Posture Constraint - Initial Rear Heel Position

To avoid redundancy at t = 0, the initial posture constraint is imposed. As an initial posture constraint, the rear foot heel position is controlled at the foot strike phase. And only the z-directional (running direction) position is constrained by an inequality constraint at only the foot strike phase:

$$z_{RFH} \leq \frac{1}{2} sl - L_{shank} \tag{7.29}$$

where z_{RFH} is the point of the rear foot heel (*z*-direction in the inertial reference frame), sl is step length, and L_{shank} is the length of the shank. Figure 7.20 depicts the position z_{RFH} at the foot strike of the opposite foot.

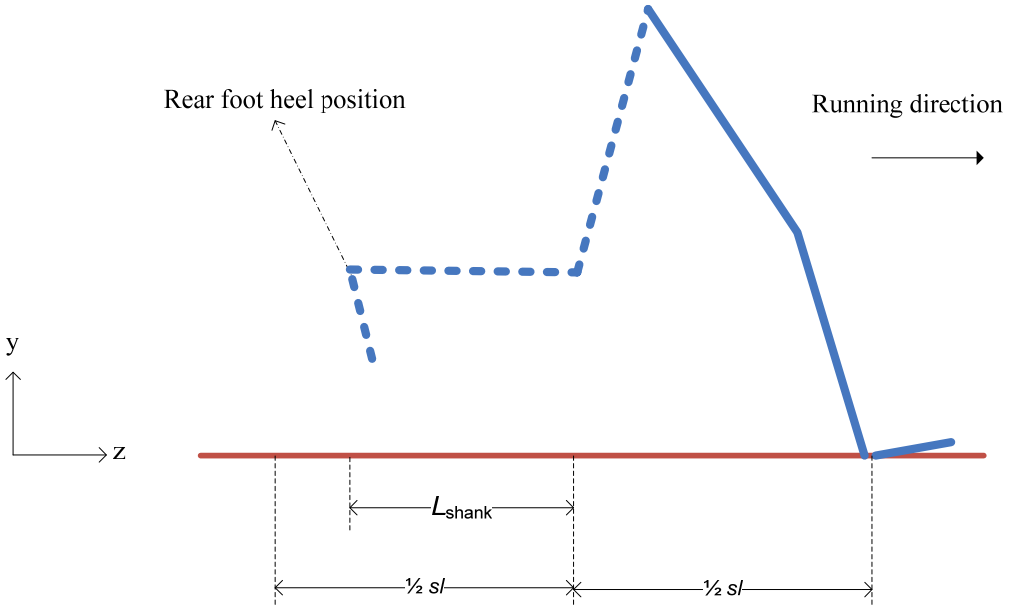

Figure 7.20 Description of initial rear heel position

7.6.6. No Slip Constraint

The velocity of the contacting points at the foot landing instant is set to be zero (soft impact). Therefore, the following constraints are imposed:

$$\dot{\mathbf{r}}_i(t) = 0 \qquad (i \in contact) \tag{7.30}$$

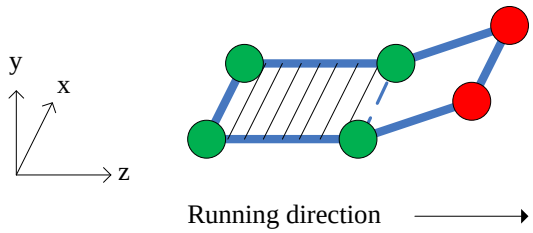

Figure 7.21 Points for no slip constraint

The green points (heel lateral, heel medial, ball lateral, ball medial) are the points where the no slip constraint is imposed.

7.6.7. Zero Moment Point Constraint

7.6.7.1. Zero moment point (ZMP)

To implement the ZMP constraint in the current formulation, we consider the *x*-*z* plane as the ground in Figure 7.10. In other words, the normal vector **n** is $[0 \quad 1 \quad 0]^T$. Again, we can simplify the ZMP calculation from Equation (4.8) in this case as:

$$z_{zmp} = \frac{\sum_i^n m_i(-\ddot{y}_i - g)z_i + m_i\ddot{z}_i y_i + \dot{H}_{ix}}{\sum_i^n m_i(-\ddot{y}_i - g)} \tag{7.31a}$$

$$x_{zmp} = \frac{\sum_i^n m_i(-\ddot{y}_i - g)x_i + m_i\ddot{x}_i y_i - \dot{H}_{iz}}{\sum_i^n m_i(-\ddot{y}_i - g)} \tag{7.31b}$$

Here, the ZMP is simply a point where the moments about the *x* and *z*-axes due to inertia, gravity, and external force (IGF) are zero. Then, the ZMP constraint is

$$z_{zmp} \in \text{FSR}, \; x_{zmp} \in \text{FSR}, \tag{7.31c}$$

where FSR is the foot support region. The foot support region is described in Figure 7.22 for the foot strike instant, in Figure 7.23 for the mid-support instant, and in Figure 7.24 for the toe off instant.

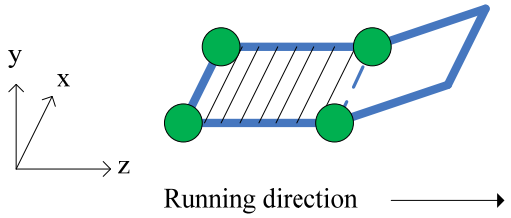

Figure 7.22 Foot support region at foot strike phase

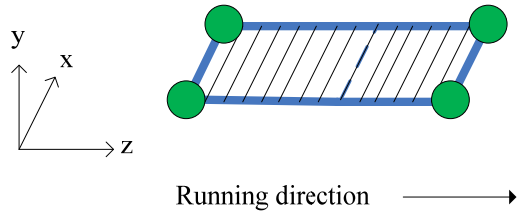

Figure 7.23 Foot support region at mid-support phase

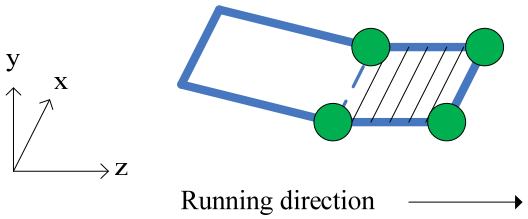

Figure 7.24 Foot support region at toe off phase

7.6.7.2. ZMP constraint

Let the polygon in Figure 7.25 be the foot support region. p_1, p_2, p_3, and p_4 are the vertices of the polygon. The point *D* is the ZMP. Let the vectors from each point p_1, p_2, p_3, p_4 to the zero moment point *D* be $\mathbf{d}_1, \mathbf{d}_2, \mathbf{d}_3$,and $\mathbf{d}_4$, respectively. Also let the polygon line vectors be $\mathbf{L}_1, \mathbf{L}_2, \mathbf{L}_3$,and $\mathbf{L}_4$ as shown in Figure 7.25. Take the cross product of this line vector with the vector to the zero moment point *D*:

$$\mathbf{n}_1 = \mathbf{L}_1 \times \mathbf{d}_1 \tag{7.32a}$$

$$\mathbf{n}_2 = \mathbf{L}_2 \times \mathbf{d}_2 \tag{7.32b}$$

$$\mathbf{n}_3 = \mathbf{L}_3 \times \mathbf{d}_3 \tag{7.32c}$$

$$\mathbf{n}_4 = \mathbf{L}_4 \times \mathbf{d}_4 . \tag{7.32d}$$

If the signs of $\mathbf{n}_1, \mathbf{n}_2, \mathbf{n}_3$, and $\mathbf{n}_4$ are all positive, the zero moment point *D* is in the polygon. The normal in Figure 7.25 has been defined as the positive *y* direction in the current coordinate configuration of the formulation. Therefore, all positive signs of $\mathbf{n}_1$, $\mathbf{n}_2, \mathbf{n}_3$, and $\mathbf{n}_4$ indicate that the zero moment point *D* stays in the foot support region.

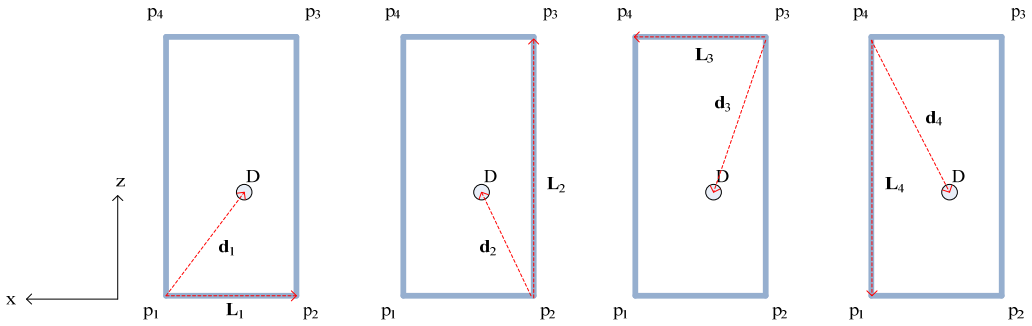

Figure 7.25 ZMP Constraint

7.6.8. Symmetry Constraint - Step Formulation

This constraint is applied according to the assumption that the running motion is symmetric and periodic.

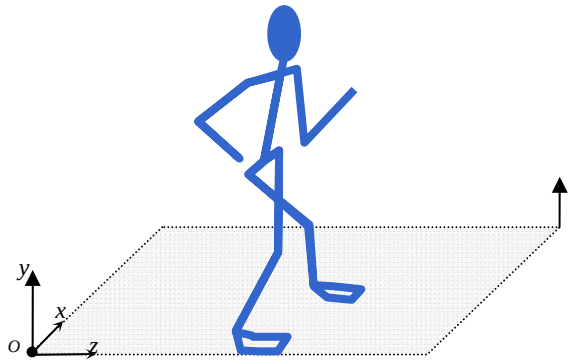

Figure 7.26 Global coordinates for symmetry condition

To have symmetric motion, the joint angles of the left (or right) arm and leg at the initial posture (t = 0) must be the same as the joint angle of the right (or left) arm and leg at the final position posture (t = T). Therefore, the symmetry condition constraint for the arm and leg is

$$\mathbf{x}_{left}(0) = \mathbf{x}_{right}(T)\,. \tag{7.33a}$$

$$\mathbf{x}_{right}(0) = \mathbf{x}_{left}(T) \tag{7.33b}$$

where $\mathbf{x}_{left}(0)$ represents the control points of the left arm and leg at t = 0, $\mathbf{x}_{right}(T)$ represents the control points of the right arm and leg at t = T, $\mathbf{x}_{right}(0)$ represents the control points of the right arm and leg at t = 0, and $\mathbf{x}_{left}(T)$ represents the control points of the arm and leg at t = T. For the spine, head, and rotational global DOF, they must be the same values for the x-axis, but the opposite sign for the y-axis and z-axis. Thus, the symmetry condition constraints for the spine, head, and rotational global DOF are as follows:

$$\mathbf{x}_{x}(0) = \mathbf{x}_{x}(T) \tag{7.33c}$$

$$\mathbf{x}_y(0) = -\mathbf{x}_y(T) \tag{7.33d}$$

$$\mathbf{x}_z(0) = -\mathbf{x}_z(T) \tag{7.33e}$$

where $\mathbf{x}_x(0)$ represents the control points of the spine, head, and rotational global DOF about the *x*-axis at $t = 0$; $\mathbf{x}_x(T)$ represents the control points of the spine, head, and rotational global DOF about the *x*-axis at $t = T$; $\mathbf{x}_y(0)$ represents the control points of the spine, head, and rotational global DOF about the *y*-axis at $t = 0$; $\mathbf{x}_y(T)$ represents the control points of the spine, head, and rotational global DOF about the *y*-axis at $t = T$; $\mathbf{x}_z(0)$ represents the control points of the spine, head, and rotational global DOF about the *z*-axis at $t = 0$; and $\mathbf{x}_z(T)$ represents the control points of the spine, head, and rotational global DOF about the *z*-axis at $t = T$. For the translational global DOF, DOF about the *z*-axis is excluded. However, DOF about the *x*-axis and *y*-axis have symmetry condition as:

$$\mathbf{x}_x(0) = -\mathbf{x}_x(T) \tag{7.34a}$$

$$\mathbf{x}_y(0) = \mathbf{x}_y(T) \tag{7.34b}$$

Here, the control points can be used directly instead of joint angles because of the property of clamped B-spline curves.

7.6.9. Continuity Constraint - Stride Formulation

One stride formulation consists of two optimization problems: right leg swinging and left leg swinging with the continuity condition constraints (no symmetry constraint). We have two optimization problems because we cannot have impact (sudden change of the joint angles velocity field) at the foot strike instant in one optimization of one stride

because of the B-spline property. Figure 7.27 depicts the one stride formulation and the continuity constraint.

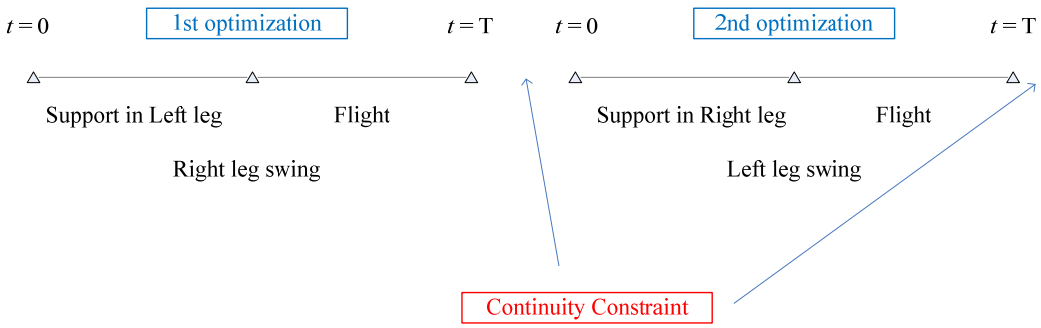

Figure 7.27 One stride formulation and continuity constraint

The continuity constraints are

$$\mathbf{x}_{1st}(T) = \mathbf{x}_{2nd}(0) \tag{7.35a}$$

$$\mathbf{x}_{1st}(0) = \mathbf{x}_{2nd}(T), \tag{7.35b}$$

where $\mathbf{x}_{1st}$ represents the control points of the first optimization problem and $\mathbf{x}_{2nd}$ represents the control points of the second optimization problem. Here, the translational global DOF about the *z*-axis is excluded in Equation (7.35b). Again, the control points are used directly instead of joint angles because of the property of clamped B-spline.

7.7. Gradient Evaluation for Constraints and Performance Measure

The analytical gradient of constraints should be evaluated for the optimization process. The gradient of the constraint with respect to the design variables is

$$\frac{\partial C}{\partial \mathbf{x}} = \begin{bmatrix} \frac{\partial C}{\partial x_1} \\ \frac{\partial C}{\partial x_2} \\ \vdots \\ \frac{\partial C}{\partial x_m} \end{bmatrix}, \tag{7.36}$$

where C is a constraint, $\mathbf{x} = \left[x_1, x_2, \cdots, x_m\right]^T$ represents the design variables (control points), and m is the number of design variables. Since C is the function of the generalized coordinates, the mapping process from the generalized coordinates to the control points (design variables) is needed. Thus, using the chain rule, we have

$$\begin{aligned}
\frac{\partial C}{\partial x_1} &= \frac{\partial C}{\partial q_1}\frac{\partial q_1}{\partial x_1} + \frac{\partial C}{\partial q_2}\frac{\partial q_2}{\partial x_1} + \cdots + \frac{\partial C}{\partial q_n}\frac{\partial q_n}{\partial x_1} + \frac{\partial C}{\partial \dot{q}_1}\frac{\partial \dot{q}_1}{\partial x_1} + \cdots + \frac{\partial C}{\partial \dot{q}_n}\frac{\partial \dot{q}_n}{\partial x_1} + \cdots + \frac{\partial C}{\partial \ddot{q}_n}\frac{\partial \ddot{q}_n}{\partial x_1} \\
\frac{\partial C}{\partial x_2} &= \frac{\partial C}{\partial q_1}\frac{\partial q_1}{\partial x_2} + \frac{\partial C}{\partial q_2}\frac{\partial q_2}{\partial x_2} + \cdots + \frac{\partial C}{\partial q_n}\frac{\partial q_n}{\partial x_2} + \frac{\partial C}{\partial \dot{q}_1}\frac{\partial \dot{q}_1}{\partial x_2} + \cdots + \frac{\partial C}{\partial \dot{q}_n}\frac{\partial \dot{q}_n}{\partial x_2} + \cdots + \frac{\partial C}{\partial \ddot{q}_n}\frac{\partial \ddot{q}_n}{\partial x_2} \\
&\vdots \\
\frac{\partial C}{\partial x_m} &= \frac{\partial C}{\partial q_1}\frac{\partial q_1}{\partial x_m} + \frac{\partial C}{\partial q_2}\frac{\partial q_2}{\partial x_m} + \cdots + \frac{\partial C}{\partial q_n}\frac{\partial q_n}{\partial x_m} + \frac{\partial C}{\partial \dot{q}_1}\frac{\partial \dot{q}_1}{\partial x_m} + \cdots + \frac{\partial C}{\partial \dot{q}_n}\frac{\partial \dot{q}_n}{\partial x_m} + \cdots + \frac{\partial C}{\partial \ddot{q}_n}\frac{\partial \ddot{q}_n}{\partial x_m}
\end{aligned} \tag{7.37a}$$

where q_1, q_2,..., q_n are generalized coordinates, and n is the number of degrees of freedom. In matrix form, we have

$$\begin{bmatrix} \frac{\partial C}{\partial x_1} \\ \frac{\partial C}{\partial x_2} \\ \vdots \\ \frac{\partial C}{\partial x_m} \end{bmatrix} = \begin{bmatrix} \frac{\partial q_1}{\partial x_1} & \frac{\partial q_2}{\partial x_1} & \cdots & \frac{\partial q_n}{\partial x_1} & \frac{\partial \dot{q}_1}{\partial x_1} & \cdots & \frac{\partial \dot{q}_n}{\partial x_1} & \cdots & \frac{\partial \ddot{q}_n}{\partial x_1} \\ \frac{\partial q_1}{\partial x_2} & \frac{\partial q_2}{\partial x_2} & \cdots & \frac{\partial q_n}{\partial x_2} & \frac{\partial \dot{q}_1}{\partial x_2} & \cdots & \frac{\partial \dot{q}_n}{\partial x_2} & \cdots & \frac{\partial \ddot{q}_n}{\partial x_2} \\ \vdots & \vdots & \ddots & \vdots & \vdots & \ddots & \vdots & \ddots & \vdots \\ \frac{\partial q_1}{\partial x_m} & \frac{\partial q_2}{\partial x_m} & \cdots & \frac{\partial q_n}{\partial x_m} & \frac{\partial \dot{q}_1}{\partial x_m} & \cdots & \frac{\partial \dot{q}_n}{\partial x_m} & \cdots & \frac{\partial \ddot{q}_n}{\partial x_m} \end{bmatrix} \begin{bmatrix} \frac{\partial C}{\partial q_1} \\ \frac{\partial C}{\partial q_2} \\ \vdots \\ \frac{\partial C}{\partial q_n} \\ \frac{\partial C}{\partial \dot{q}_1} \\ \vdots \\ \frac{\partial C}{\partial \dot{q}_n} \\ \vdots \\ \frac{\partial C}{\partial \ddot{q}_n} \end{bmatrix} \tag{7.37b}$$

Equations (7.37a) and (7.37b) can be rewritten as

$$\frac{\partial C}{\partial x_k} = \frac{\partial C}{\partial q_j}\frac{\partial q_j}{\partial x_k} + \frac{\partial C}{\partial \dot{q}_j}\frac{\partial \dot{q}_j}{\partial x_k} + \frac{\partial C}{\partial \ddot{q}_j}\frac{\partial \ddot{q}_j}{\partial x_k} \tag{7.38}$$

The terms $\partial q_j / \partial x_k$, $\partial \dot{q}_j / \partial x_k$, and $\partial \ddot{q}_j / \partial x_k$ can be obtained from Equation (5.1) , and the terms $\partial C / \partial q_j$, $\partial C / \partial \dot{q}_j$, and $\partial C / \partial \ddot{q}_j$ are evaluated for each constraint discussed in the previous section. Most constraints need the chain rule process in Equation (7.37a). However, the symmetry condition constraint (or continuity constraint) does not need this process because the symmetry condition constraint is only needed at the beginning of the B-spline curve and at the end of the B-spline curve—it is a *time independent constraint*. Since the clamped B-spline has been adopted, the spline curve passes through the control point exactly at the beginning and the end.

In similar way, the analytical gradient for performance measure can be obtained. The gradient of torque for dynamics effort is

$$\frac{\partial \tau}{\partial x_k} = \frac{\partial \tau}{\partial q_j}\frac{\partial q_j}{\partial x_k} + \frac{\partial \tau}{\partial \dot{q}_j}\frac{\partial \dot{q}_j}{\partial x_k} + \frac{\partial \tau}{\partial \ddot{q}_j}\frac{\partial \ddot{q}_j}{\partial x_k} \tag{7.39a}$$

From Equation (7.16), gradient of the impulse is

$$\frac{\partial \mathbf{I}_{strk}}{\partial x_k} = \left(\frac{\partial \mathbf{R}_D}{\partial q_j}\frac{\partial q_j}{\partial x_k} + \frac{\partial \mathbf{R}_D}{\partial \dot{q}_j}\frac{\partial \dot{q}_j}{\partial x_k} + \frac{\partial \mathbf{R}_D}{\partial \ddot{q}_j}\frac{\partial \ddot{q}_j}{\partial x_k} \right) \Delta t \tag{7.39b}$$

The terms $\partial\tau/\partial q_j$, $\partial\tau/\partial \dot{q}_j$, and $\partial\tau/\partial \ddot{q}_j$ are already evaluated in Equations (3.24a-3.24c). From Equation (7.7c), we know that $\mathbf{R}_D$ is same as global force $\mathbf{F}$. Therefore, $\partial\mathbf{R}_D/\partial q_j$, $\partial\mathbf{R}_D/\partial \dot{q}_j$, and $\partial\mathbf{R}_D/\partial \ddot{q}_j$ also can be obtained from Equations (3.24a-3.24c);

$$\frac{\partial \mathbf{R}_D}{\partial q_j} = \frac{\partial \tau_i}{\partial q_j}, \quad i = 0, 1, 2 \tag{7.40a}$$

$$\frac{\partial \mathbf{R}_D}{\partial \dot{q}_j} = \frac{\partial \tau_i}{\partial \dot{q}_j}, \quad i = 0, 1, 2 \tag{7.40b}$$

$$\frac{\partial \mathbf{R}_D}{\partial \ddot{q}_j} = \frac{\partial \tau_i}{\partial \ddot{q}_j}, \quad i = 0, 1, 2 \tag{7.40c}$$

CHAPTER 8

RUNNING SIMULATION RESULTS

A sequential quadratic programming (SQP) algorithm is adopted to solve the problem and commercial software SNOPT (NPOPT solver) is used (Gill, Murray, and Saunders, 2002). The number of control points in the current formulation is 5 for each joint angle. Since the number of degrees of freedom for the mechanical system is 55, the total number of design variables is 55×5 = 275. The number of constraints is 1,046. The running speed is an input parameter and the step length is determined using the formula described in chapter 7. A feasible solution without dynamic effort performance measure is obtained first. In this process, home configuration of DH table is used as the starting point for optimization which means all generalized coordinates values are equal to zero, $\mathbf{q} = \mathbf{0}$. Once we get a feasible solution, it is used as the starting point for optimization with performance measure from Equation (7.17d). One of the optimal solutions is used as default starting point for various case studies such as different running speed, backpack load, and the restriction on the range of motion due to body armor. The *level* in Equation (7.1) is set to 0.001 and $level_2$ in Equations (7.3a and 7.3b) is set to 0.0001 as a skilled runner. The weight values in performance measure are set to 1.0 for the torque square term and 0.5 for the impulse term. Δt in Equation (7.16) is set to 10% of support time. These values are determined by numerical experimentation.

Figure 8.1 is a snapshot of posture for 3.0 m/s running with 37.04N weapon. The step length for the given running speed is 1.096 m. Pentium 3.20GHz CPU is used to obtain optimal solution. The number of iterations for the feasible point is 25 and the CPU

time is 3,063 seconds. The number of iterations for the optimal point is 28 and the CPU time is 290 seconds. The starting point and optimum point are listed in the Appendix. The joint angle limits for head, arm, and spine are reduced to avoid redundancy and to carry the weapon. Symmetry condition constraint (step formulation) is imposed. The number of active constraints is 169. Active constraints and their Lagrange multipliers are also listed in the Appendix. The performance measure value is 12,168. The results show natural human running motion. Major contributions to the natural running motion are realistic joint torque constraints, the rate of angular momentum in the ZMP constraint, and the impulse term in the performance measure.

Figure 8.1 Running snapshot (3.0 m/s)

8.1. Joint Torque Profiles

As described in Chapter 2, there are parent branch and child branches in current mechanical structure. The joint torque at the branch node which connects parent branch and child branches is calculated separately in terms of each child branch. Therefore, to impose joint torque limits, it is necessary to have a module to combine the joint torques which calculates the resultant torque. And also, the index of joint torque must be in same sequence with the corresponding DOF. Figure 8.2 shows the knee joint torque profiles of the simulation in one gait cycle with experiment results from literature (Novacheck, 1998). Although the match is not perfect, the general trend is reasonable.

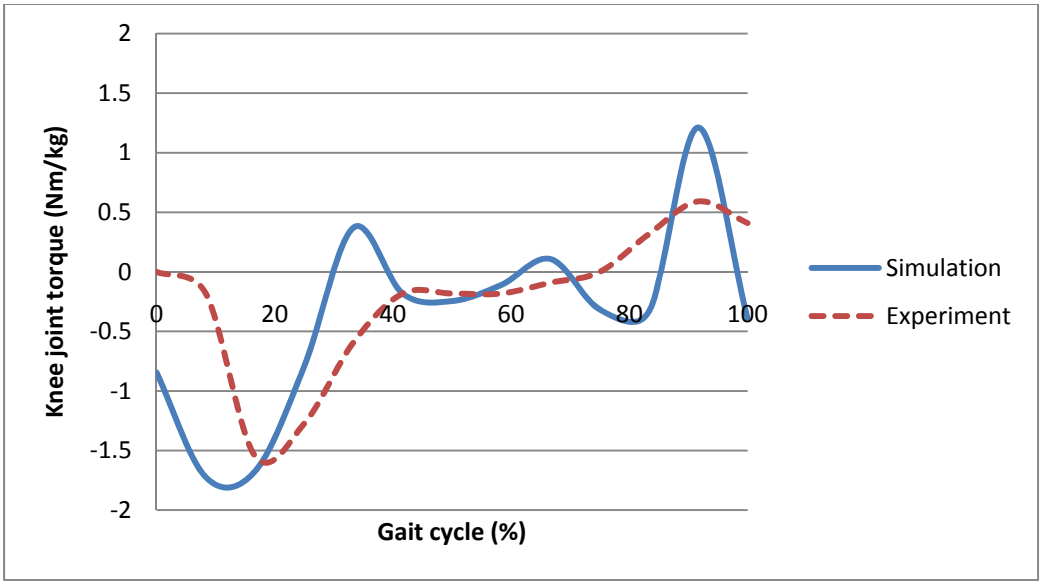

Figure 8.2 Knee joint torque profiles

8.2. Ground Reaction Force

Figure 8.3 shows that the vertical ground reaction force (corresponding to the global *y*-axis) results with 3.0 m/s running speed and 1.0962 m step length. The results

show that the shape of ground reaction force curve with the impact formulation is closer to the shape of the experimental data from the literatures (Õunpuu, 1994) compared to the simulation results without the impact formulation.

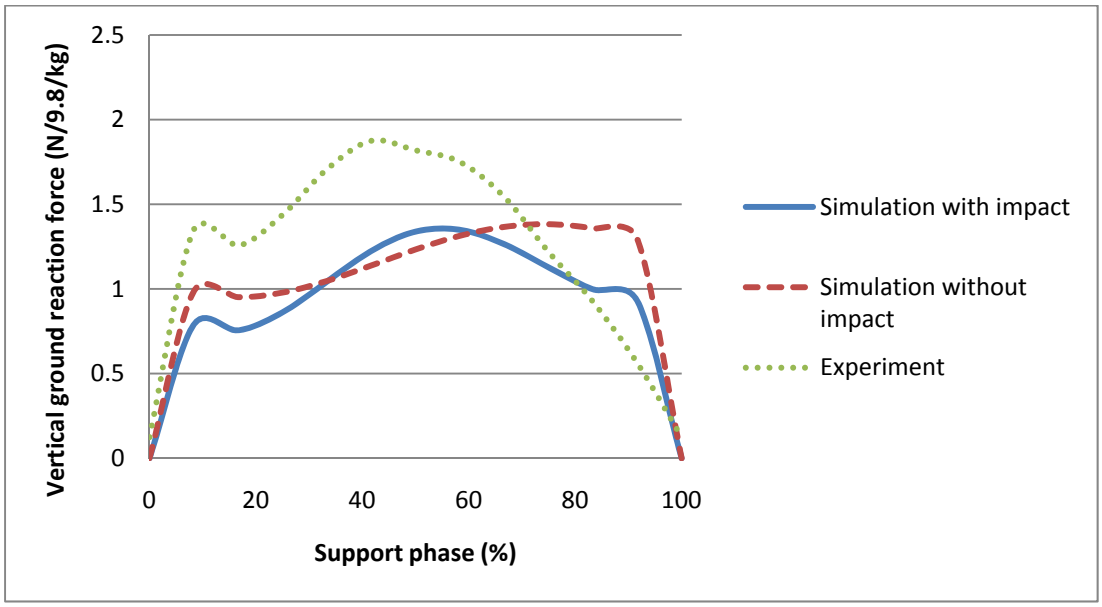

Figure 8.3 Vertical ground reaction force

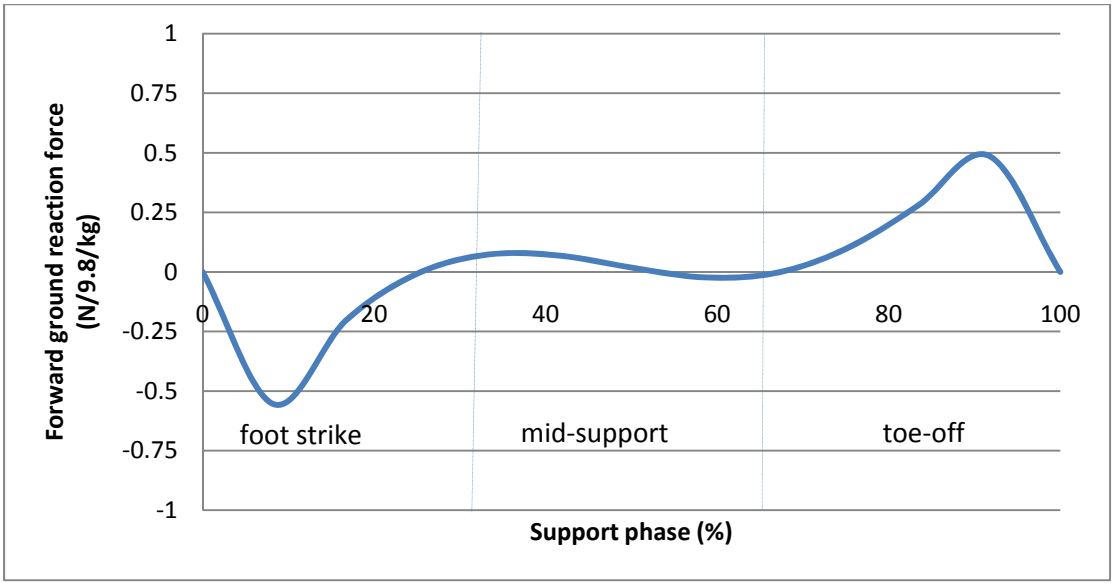

Figure 8.4 Forward ground reaction force

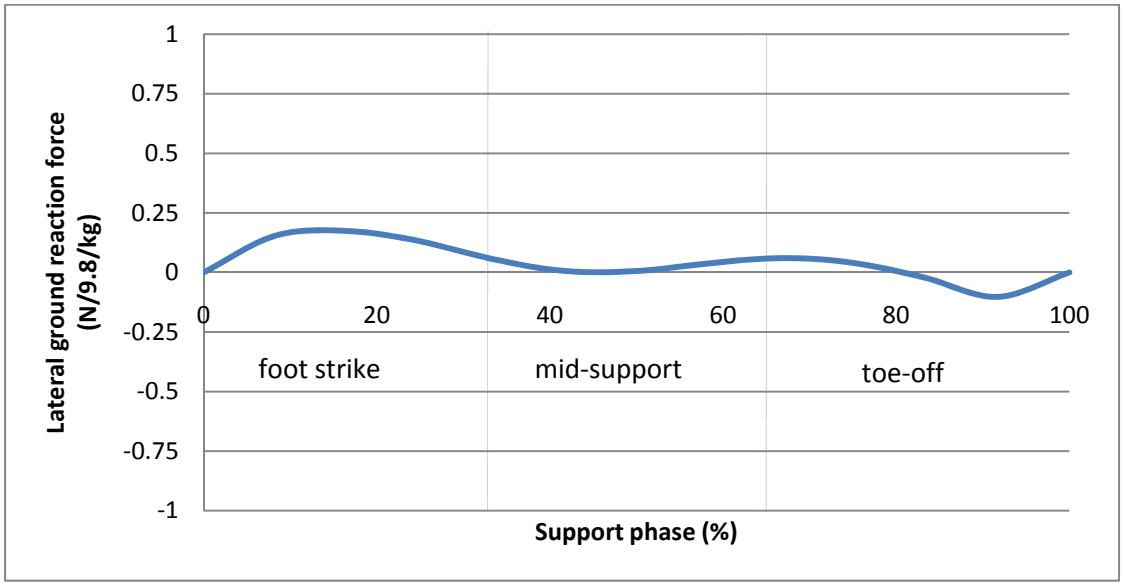

Figure 8.5 Lateral ground reaction force

In Figure 8.3, the simulation value is smaller than experiment value. Possible reason is that impulsive force at toe off phase is not modeled in the current formulation. Figure 8.4 shows the forward ground reaction force (corresponding to the global *z*-axis) and Figure 8.5 shows the lateral ground reaction force (corresponding to the global *x*-axis) respectively. The forward ground reaction force is acting in negative *z*-direction at foot strike phase and positive *z*-direction at toe off phase. In lateral ground force case, it is acting in positive *x*-direction at foot strike phase and negative *x*-direction at toe off phase.

8.3. Cause and Effect Case Study

8.3.1. Backpack Load

Figure 8.6 is the result of running without backpack. Only external load is weapon carried in hands (37.04 N). Figure 8.7 is the result of running with backpack (500 N) in

addition to the weapon in hands. We can see that the upper body leans more toward running direction when backpack is carried.

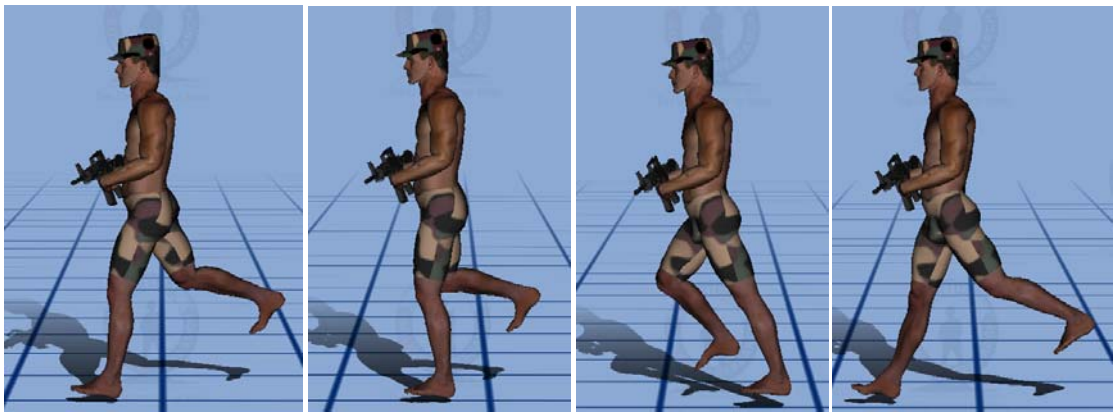

Figure 8.6 Running without backpack

Figure 8.7 Running with backpack

Figure 8.8 is the comparison of the knee joint torque between the case without backpack and with backpack. We can see that when the backpack is loaded, the more torque is produced at support phase. Figure 8.9 shows the vertical ground reaction forces comparison between the case without backpack and with backpack. It is observed that when the backpack is loaded the more ground reaction force is acting at foot strike phase

compared to the mid-support and toe off phases. Figure 8.10 shows the forward ground reaction force comparison and Figure 8.11 shows the lateral ground reaction force comparison respectively.

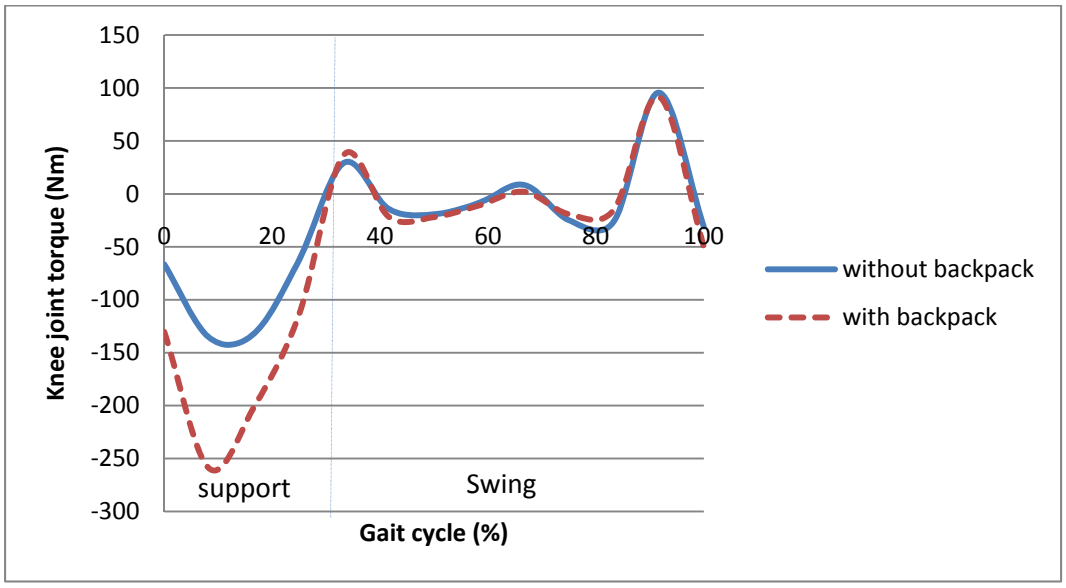

Figure 8.8 Knee joint torque comparison

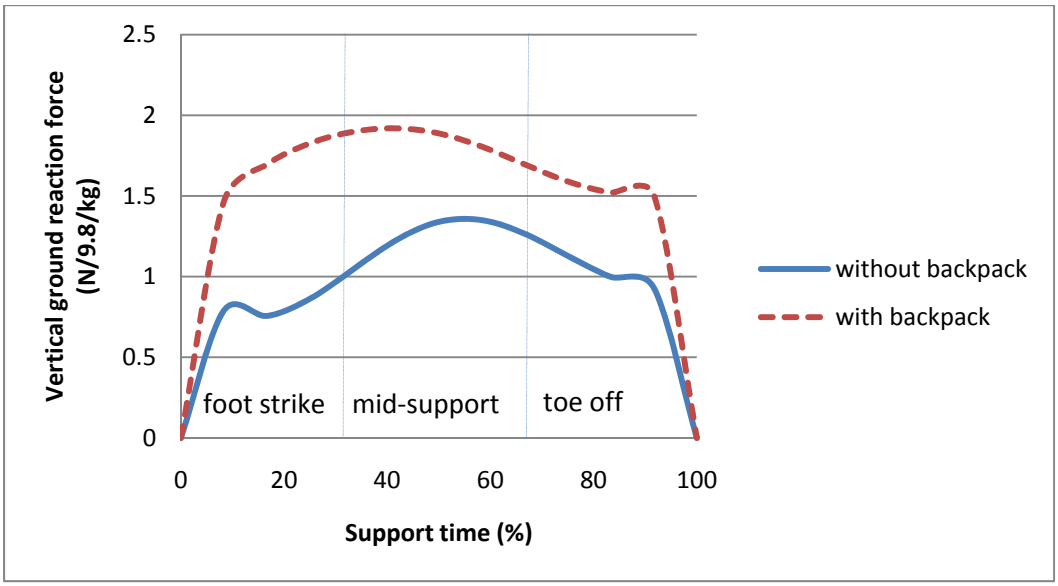

Figure 8.9 Vertical ground reaction force comparison

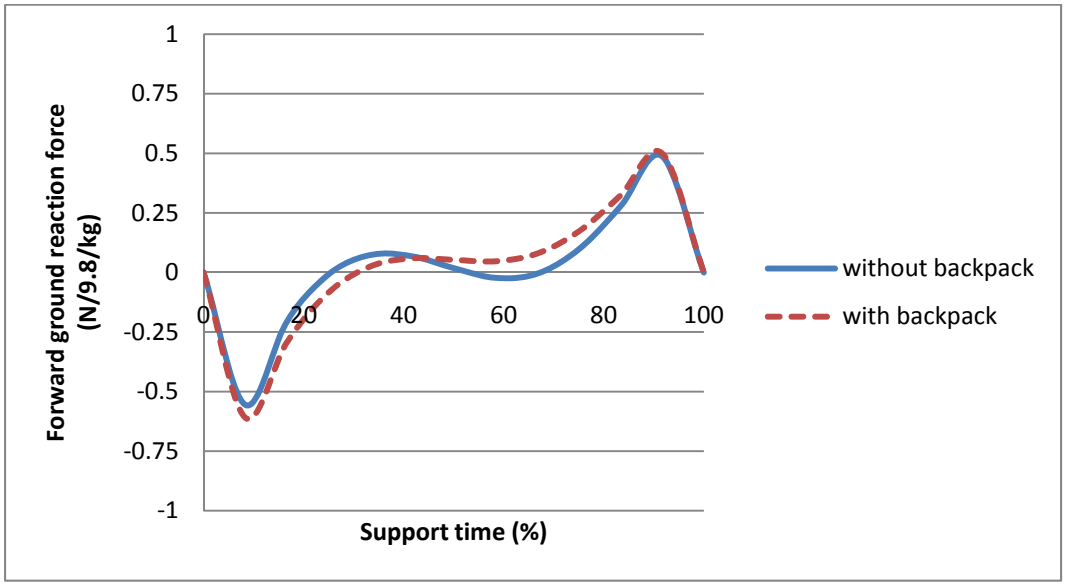

Figure 8.10 Forward ground reaction force comparison

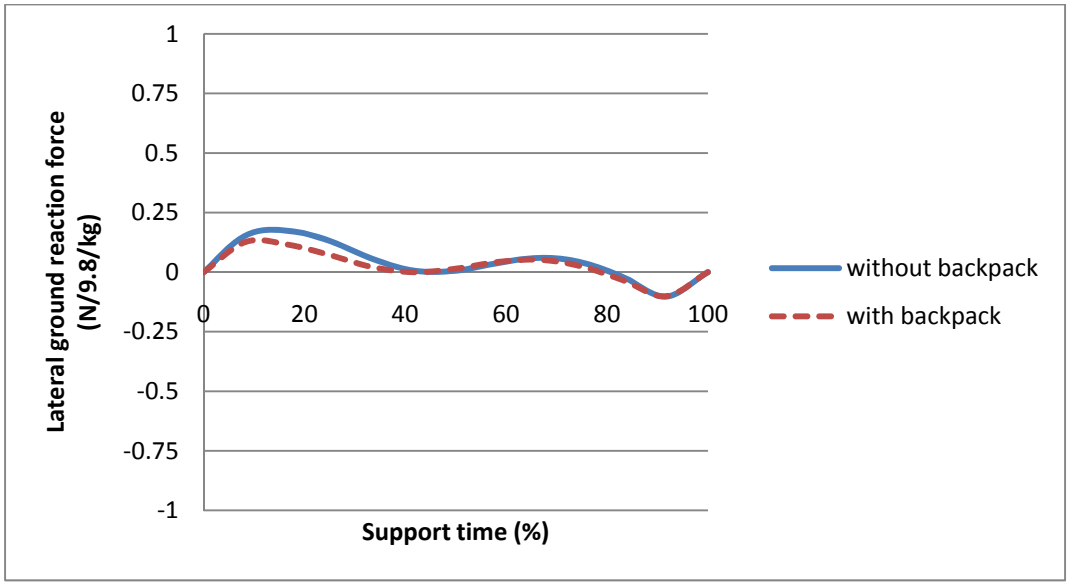

Figure 8.11 Lateral ground reaction force comparison

The forward ground reaction force slightly larger ground reaction force when the backpack is loaded.

8.3.2. Range of Motion – Armor Effect

Figure 8.12 depicts the armor at the back of thigh and shank. Santos™ have a capability to determine the range of motion for the given armor. Using that capability, we have new joint angle limits at knee joint which is reduced from 135º to only 71º. The weight of single armor is 3.19N, so the total weight of armor is 3.19×4 = 12.76N.

Figure 8.12 Armor attached at legs

Figure 8.13 shows the results of running without armor and Figure 8.14 shows the results of running with armor. It is obvious that the knee flexion with armor is smaller than that without armor.

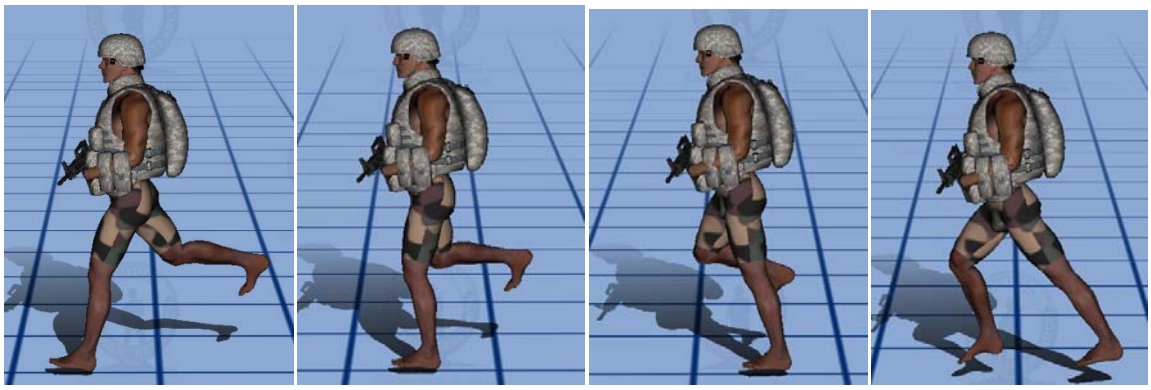

Figure 8.13 Running without armor

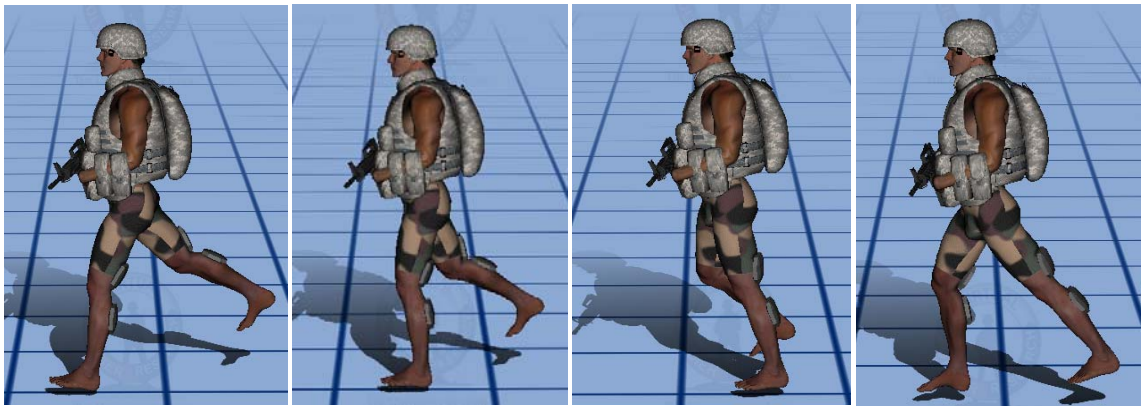

Figure 8.14 Running with armor

Figure 8.15 shows the comparison of joint angle profiles without armor and with armor. In the armor case, we can see that the joint angle limit constraint is active at 71º. And also, joint torque profile comparison is shown in Figure 8.16. It shows that the support leg produces more torque to help the swinging leg which is restricted by 71º. Figure 8.17 is the vertical ground reaction force results with and without armor. It shows that the impulse of with armor case is less minimized at the foot strike phase than without armor case due to the restriction of knee joint angle. Figure 8.18 shows the forward ground reaction force comparison and Figure 8.19 shows the lateral ground reaction force

comparison respectively.

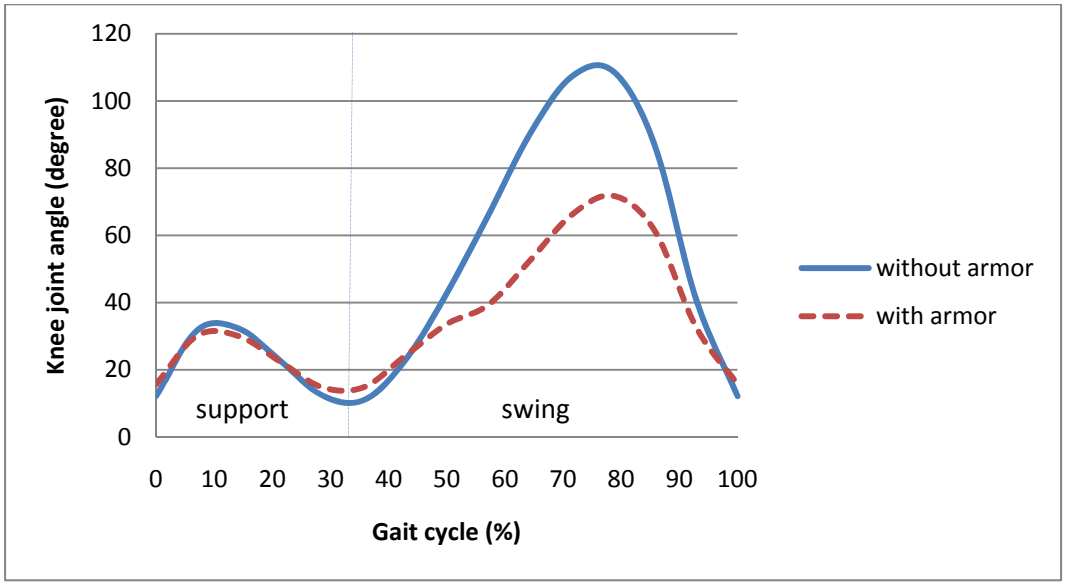

Figure 8.15 Knee joint angles with and without armor

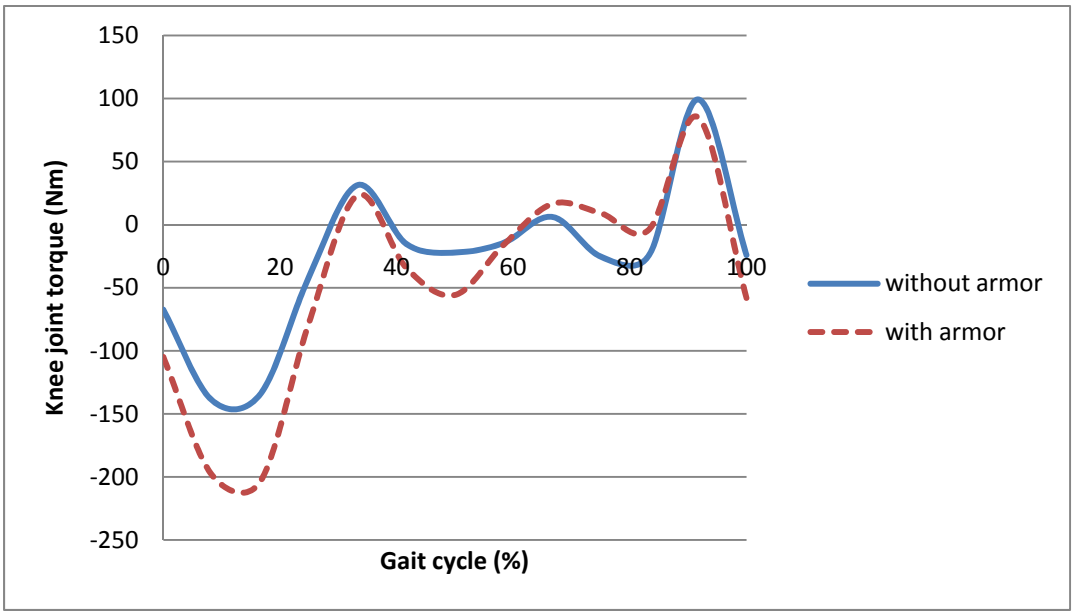

Figure 8.16 Knee joint torque with and without armor

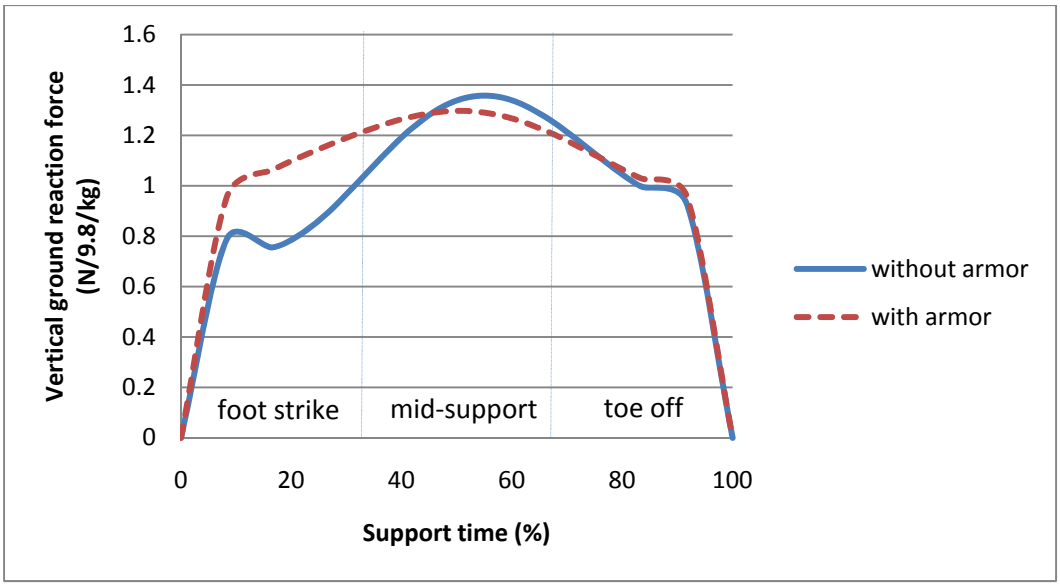

Figure 8.17 Vertical ground reaction force with and without armor

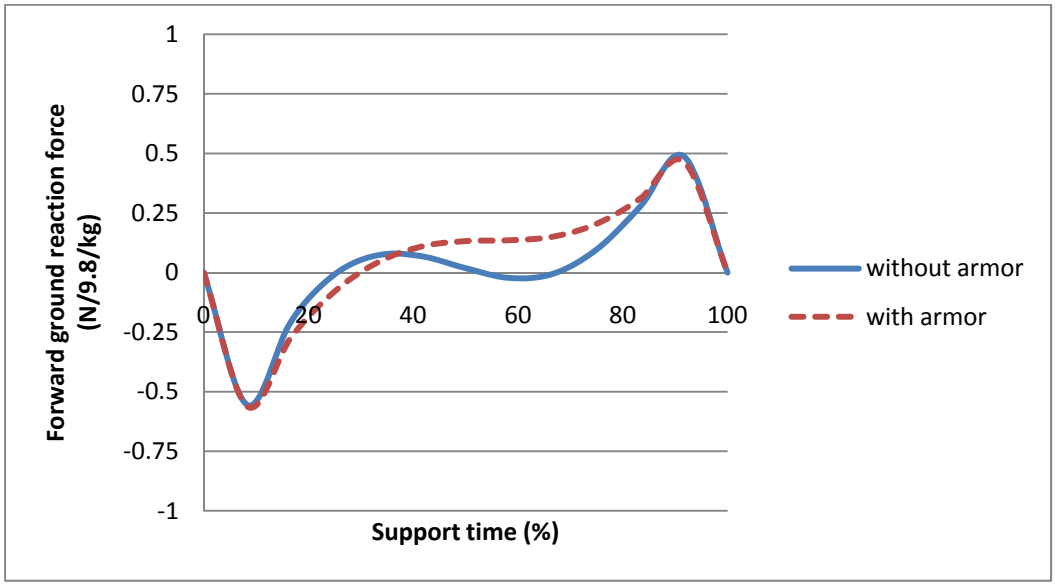

Figure 8.18 Forward ground reaction force with and without armor

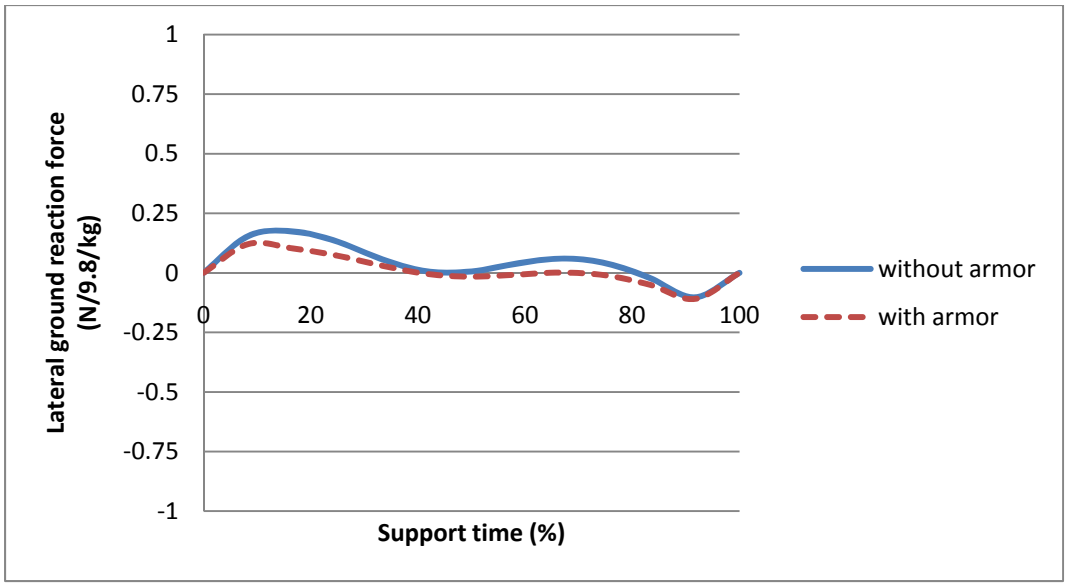

Figure 8.19 Lateral ground reaction force with and without armor

8.3.3. Different Running Speed

Figure 8.20 shows joint torques with different running speeds, 3.0 m/s, 3.5 m/s, and 4.0 m/s respectively. We can see that the joint torque gets larger when the running speed increases. Figure 8.21 shows the vertical ground reaction force for different running speeds. The results show that the ground reaction force becomes a little larger when the running speed is increased. Figure 8.22 is the results of forward ground reaction force for different running speeds. It shows also that the ground reaction force becomes a little larger when the running speed is increased. Figure 8.23 is the results of lateral ground reaction force for different running speeds.

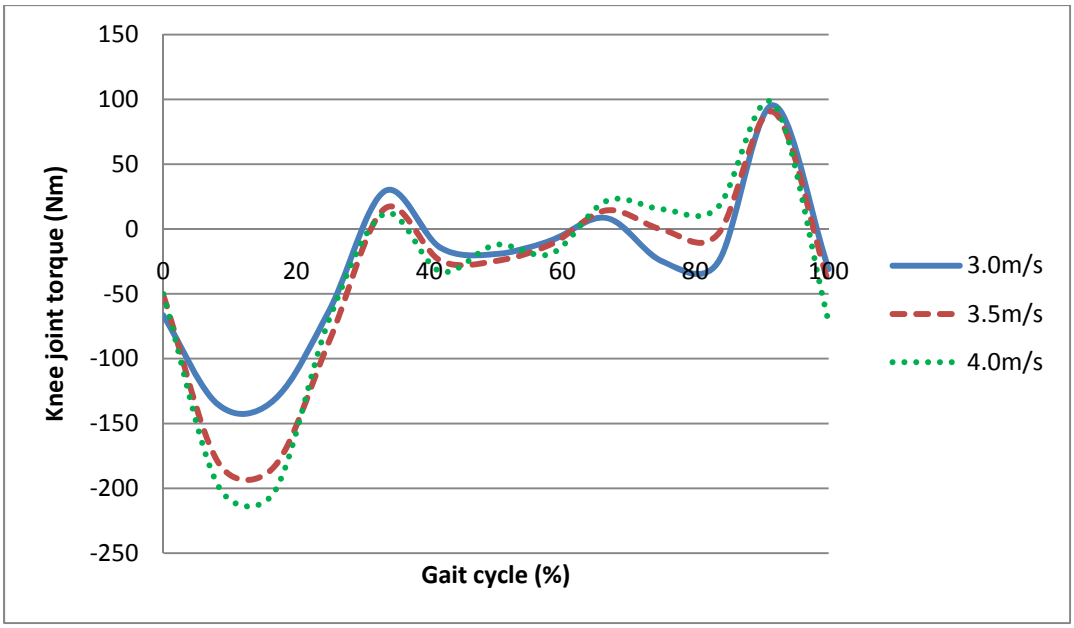

Figure 8.20 Knee joint torque in different running speed

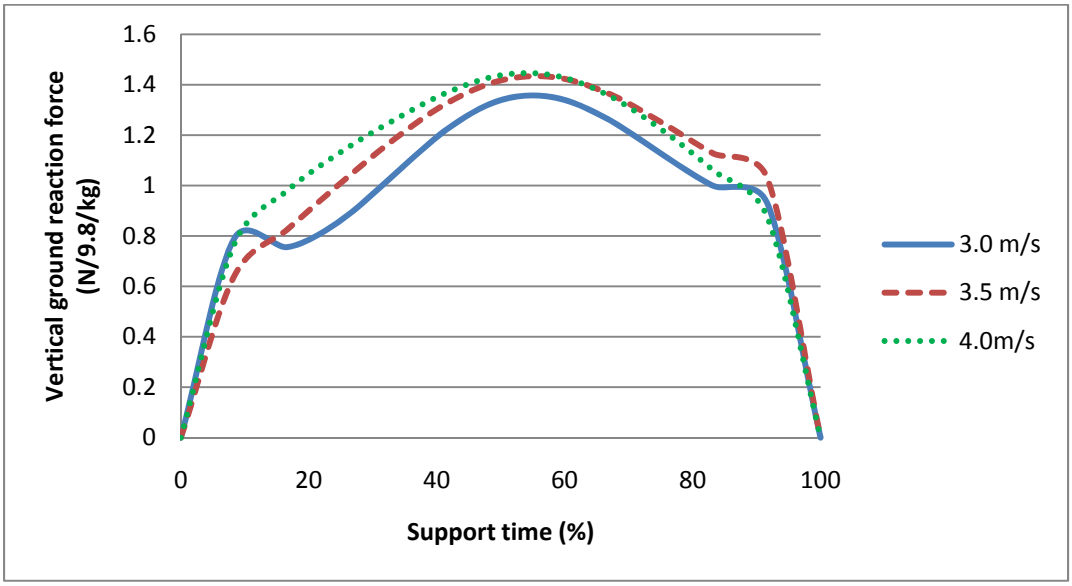

Figure 8.21 Vertical ground reaction force in different running speed

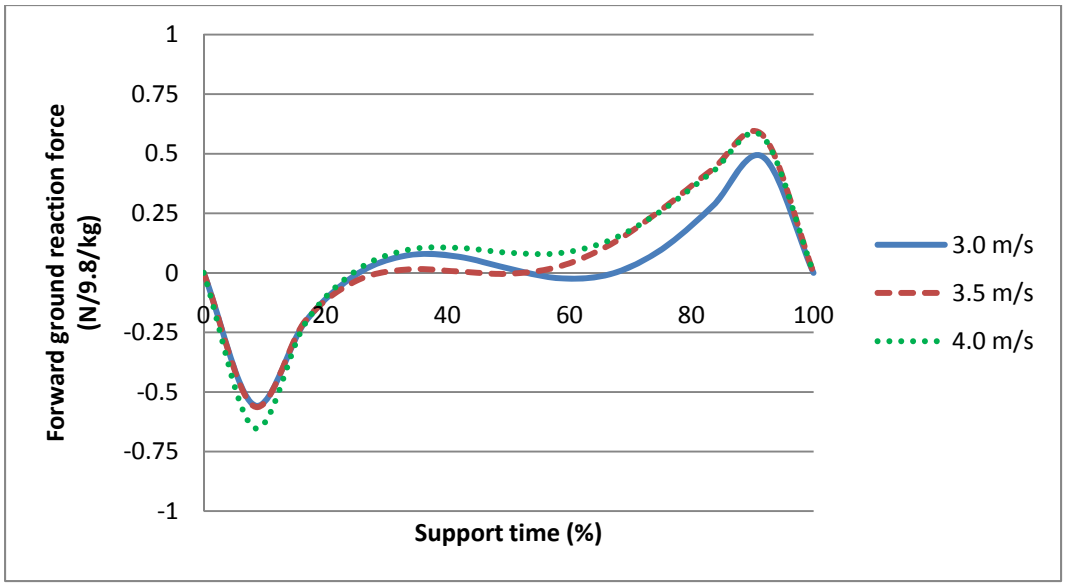

Figure 8.22 Forward ground reaction force in different running speed

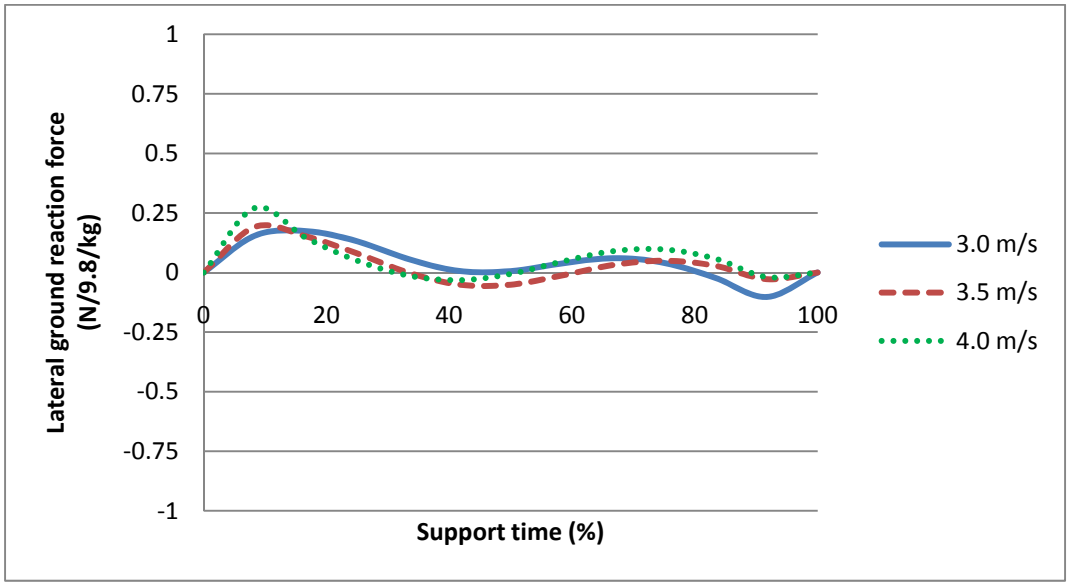

Figure 8.23 Lateral ground reaction force in different running speed

8.4. Discussion

The prediction results of digital human running are presented in this chapter. Total number of DOF is 55. The number of control points for each DOF is 5 and the

number of design variables is 275. The frozen degrees of freedom are the neck bend joint, clavicle joint, elbow joint, wrist joint, shoulder joint, and spine twist of the second, third, and fourth spine joints. The number of constraints is 1,046. The commercial software SNOPT is used to solve the nonlinear optimization problem of running. As mentioned in Chapter 7, we assumed that the mechanical structure of digital human is rigid body. Therefore, there is no wobbling mass effect. And also, mass moment of inertia of various segments is approximated. To obtain natural running motion, some parameters such as weight values in the performance measure are decided from numerical experiments. The numerical experiment was performed in many different cases and the results were compared. For example, one weight value is simulated in different running speeds and compared to the results from other weight values.

The joint torque profiles and ground reaction forces are presented as simulation results. As cause and effect case study, the backpack loading case, the range of motion restriction case and different running speed case are presented. Each case provides the joint torque profile comparison and ground reaction forces comparison. The summary of the results is given in Tables 8.1 and 8.2. In Table 8.1, FS stands for foot strike phase and TO stands for toe off phase. As already discussed before, we can easily see that the joint torque increases when the running speed increases or the backpack is loaded. The ground reaction force also increases when the running speed increases or the backpack is loaded. Table 8.2 shows the objective function values, the number of iterations, the number of active constraints, and the CPU time. Other performance quantities such as metabolic energy can be calculated once optimal solution is obtained. Table 8.3 shows the active constraints in each case.

Table 8.1 Summary of results – joint torque and ground reaction force

Cases	Peak value of knee joint torque (Nm)	Peak value of ground reaction force (N/9.8/kg)		
		Vertical	Forward (FS / TO)	Lateral
3.0 m/s	-135.7226	1.3499	-0.5556 / 0.4875	0.1738
3.5 m/s	-180.5822	1.4301	-0.5607 / 0.5775	0.1912
4.0 m/s	-198.9258	1.4380	-0.6509 / 0.5712	0.2708
Backpack	-259.3351	1.9192	-0.6098 / 0.4998	0.1271
Armor	-198.4213	1.2976	-0.5626 / 0.4649	0.1207

Table 8.2 Summary of results – optimization summary

Cases	Performance measure value	Number of iterations	Number of active constraints	CPU time (sec)
3.0 m/s	12,168	28	169	290
3.5 m/s	12,619	41	201	356
4.0 m/s	17,859	131	124	4,128
Backpack	14,801	57	157	427
Armor	14,494	34	204	460

Table 8.3 Summary of results – active constraints

Case	Active constraints
3.0 m/s	ground penetration, no slip, foot contact, symmetry conditions, joint angle limits (spine, clavicle, shoulder, elbow, wrist, knee, ankle), joint torque limits (ankle)
3.5 m/s	ground penetration, no slip, foot contact, ZMP, symmetry conditions, joint angle limits (spine, clavicle, shoulder, elbow, wrist, neck, hip, knee, toe)
4.0 m/s	ground penetration, no slip, foot contact, ZMP, symmetry conditions, joint angle limits (spine, clavicle, shoulder, elbow, wrist)
Backpack	ground penetration, no slip, foot contact, ZMP, symmetry conditions, joint angle limits (spine, clavicle, shoulder, elbow, wrist, hip, knee, ankle), joint torque limits (knee)
Armor	ground penetration, no slip, foot contact, ZMP, symmetry conditions, joint angle limits (spine, clavicle, shoulder, elbow, wrist, neck, knee, ankle, toe)

The results show that the presented formulation for digital human running is quite robust in terms of both kinematics and dynamics. The analytical gradients in the formulation also play significant role for the accuracy in terms of the optimization solution. Realistic joint torque constraints, the rate of angular momentum in the ZMP constraint, and the impact formulation are major contributions to the natural running motion.

CHAPTER 9

SLOW JOG ALONG CURVILINEAR PATHS

9.1. Problem Description

The formulation of running in Chapter 7 is for a straight path, there is an assumption that the motion is symmetric. However, slow jog along a curve is not a symmetric motion since the motion for the right and left parts of the body is not the same. Figure 9.1 depicts the running path of a slow jog along a circular path. The blue dot is a marker and the red curve is the circular path around the marker. Since it is a non-symmetric running motion, the right step and left step should be formulated and simulated separately (stride formulation).

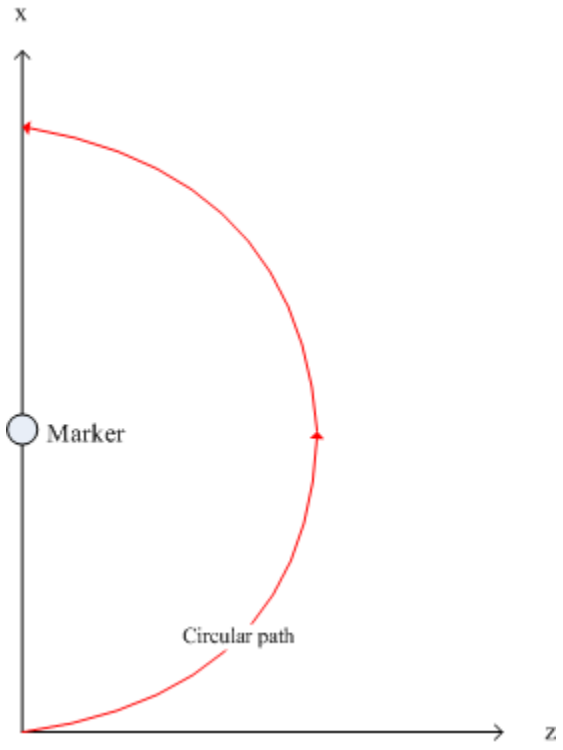

Figure 9.1 Circular path around marker

9.2. Formulation

9.2.1. Design Variables

The design variables are the joint angle profiles **q** parameterized using B-spline approximation.

$$DV : \mathbf{q} \tag{9.1}$$

The number of control points is 5 for each joint angle, and the number of degrees of freedom is 55. Therefore, the total number of design variables is 275.

9.2.2. Performance Measure

The same performance measure as in the normal running formulation is used:

$$f = w_\tau f_\tau + w_I f_I \tag{9.2a}$$

where

$$f_\tau = \int_0^t \boldsymbol{\tau}^T \boldsymbol{\tau} dt \tag{9.2b}$$

$$f_I = \mathbf{I}_{strk}^{\mathrm{T}} \mathbf{I}_{strk} \tag{9.2c}$$

$\boldsymbol{\tau}$ is joint torque, $\mathbf{I}_{strk}$ is the impulse at foot strike, and w_τ and w_I are the weighting parameters for the two objectives.

9.2.3. Constraints

The constraints for jog along the curves are as follows:

1) Joint angle limits
2) Joint torque limits

3) Ground penetration
4) Foot contact location constraint along the path
5) No slip constraint
6) ZMP during support phase
7) Initial foot location
8) Continuity condition constraint
9) Body rotation constraint

Most of the constraints are the same as for the normal running formulation in Chapter 7, except the foot location constraint along the path, the continuity condition constraint, and the body rotation constraint. The body rotation constraint enforces the condition where the global orientation of the body is the same as the tangential direction of the jogging path. This way, the human body is facing in the direction it is moving. Also, the neck joint, clavicle joint, shoulder joint, elbow joint, and spine tilt of the second, third, and fourth spine joint are frozen just as for the normal running formulation.

9.2.4. Continuity Condition

Figure 9.2 depicts the continuity constraint. This constraint is imposed at the beginning of each optimization so that the last posture of the previous optimization and the starting posture of the current optimization are matched. Thus, the continuity constraint is

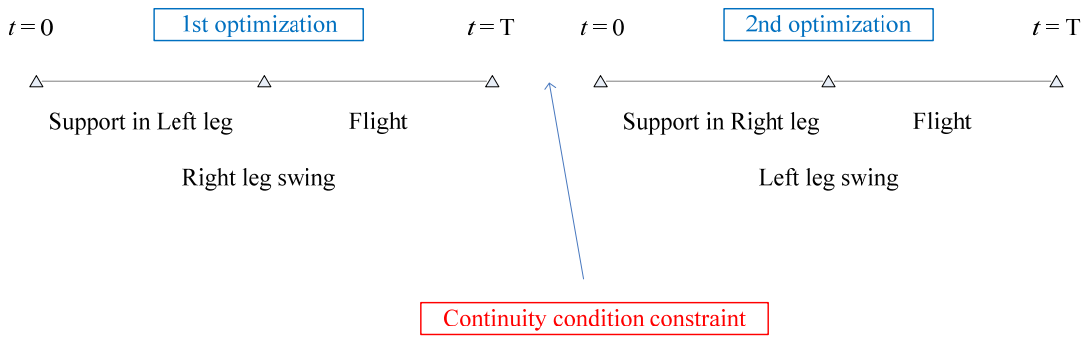

Figure 9.2 Continuity condition constraint

$$\mathbf{x}_{1st}(T) = \mathbf{x}_{2nd}(0) \tag{9.3}$$

where $\mathbf{x}_{1st}$ represents the control points of the first optimization problem and $\mathbf{x}_{2nd}$ represents the control points of the second optimization problem.

9.2.5. Foot Contact Location along the Path

For the problem of slow jog along curves, the foot contact locations depend on the running path. To impose a foot contact location constraint, we constrain three points at the foot – heel, mid foot, and toe – just as for the normal running formulation (Figure 9.3).

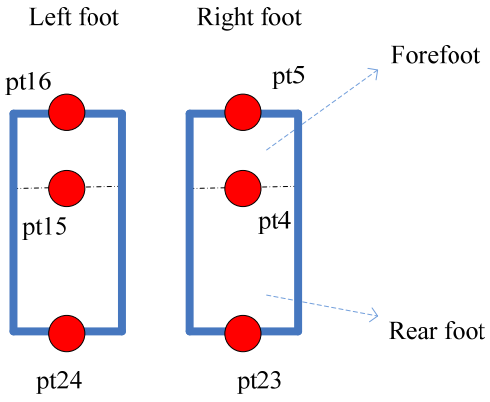

Figure 9.3 Key points for the foot location constraint

pt16: left toe center pt5: right toe center

pt15: left ball center pt4: right ball center

pt24: left heel center pt23: right heel center

To calculate the contacting location of these points, we need the step length and orientation of the foot. This orientation must be expressed in the inertial reference frame. Once we have the step length and the orientation of the foot, we can calculate the location of the three contact points – heel, mid foot, and toe.

Figure 9.4 depicts the foot location along the path. The blue box describes the foot on the ground. x-z is the inertial reference frame, and x_1-z_1 is the local reference frame for the foot. $\mathbf{r}_p$ is the vector from the origin of the inertial reference frame to the foot point p, which will be controlled in the local reference frame. $\mathbf{r}_1$ is the vector from the origin of the inertial reference frame to the origin of the local reference frame. $\mathbf{r}_{1p}$ is the vector from the origin of the local reference frame to the foot point p in the local reference frame. What we need is $\mathbf{r}_p$ since the foot location constraint is applied in the inertial reference frame.

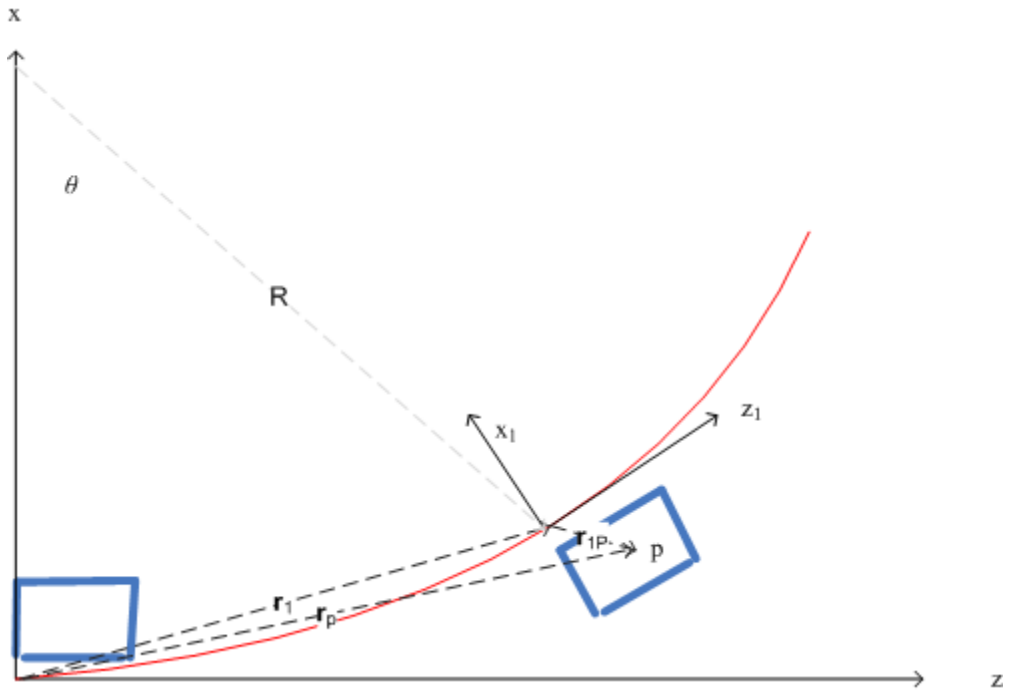

Figure 9.4 Foot location along the path

The vector $\mathbf{r}_1$ is determined by the step length and running curve:

$$\|\mathbf{r}_1\| = L \tag{9.4}$$

where L is step length. The angle θ, which is same as the orientation of the contacting foot, can be calculated from the marker position.

$$\theta = 2\sin^{-1}\left(\frac{L}{2R}\right) \tag{9.5}$$

Then the vector of point p can be written as:

$$\mathbf{r}_p = \mathbf{r}_1 + \mathbf{A}_1\mathbf{r}_{1p} \tag{9.6}$$

where $\mathbf{A}_1$ is the rotation matrix of the local reference frame.

Or,

$$\mathbf{r}_p = \begin{bmatrix} 2R\sin(\theta/2)\cos(\theta/2) + z_{1p}\cos\theta - x_{1p}\sin\theta \\ 2R\sin(\theta/2)\sin(\theta/2) + z_{1p}\sin\theta + x_{1p}\cos\theta \end{bmatrix} \tag{9.7}$$

The point *p* is defined as heel, midpoint, and toe in the current formulation.

9.3. Results

The problem has been solved using the stride formulation. Therefore, there are two optimization processes – right step and left step. Once the solution has been obtained, the motion is repeated along the running path. Figure 9.5 is a snapshot of postures for a 2.35 m/s slow jog around maker. Step length is 0.889 m. The number of constraints is 994. The feasible point from normal running in Chapter 8 was used as the starting point for optimization. The number of iterations for the optimal point is 16, and the CPU time is 244 seconds for the first step – the right step. For the second step – the left step – the number of iterations is 25 and the CPU time is 923 seconds. The performance measure value is 3,736 for the first step and 3,023 for the second step. The weight values for impact formulation are set to 1.0 for the torque square term and 0.5 for the impulse term. As mentioned in Chapter 8, these values are determined by numerical experimentation.

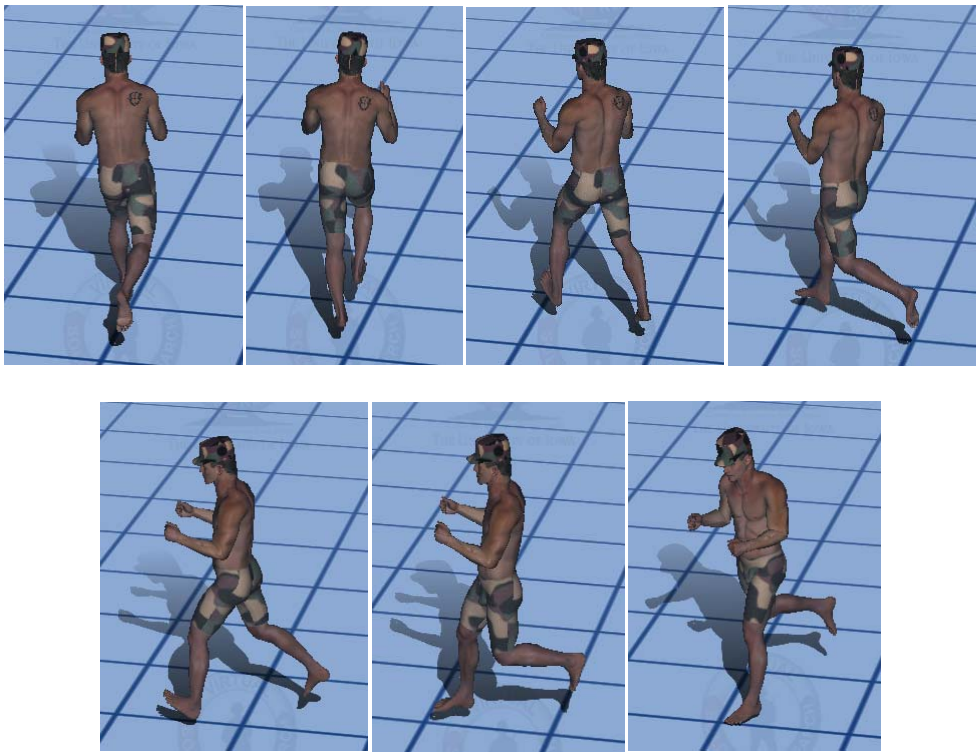

Figure 9.5 Slow jog along curve snapshot

Figures 9.6-9.8 show the results of the ground reaction forces.

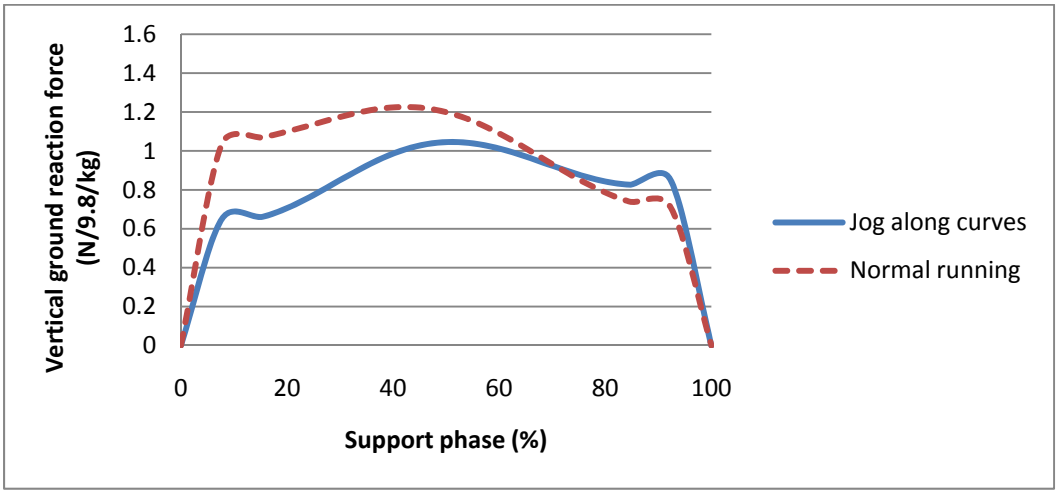

Figure 9.6 Vertical ground reaction force

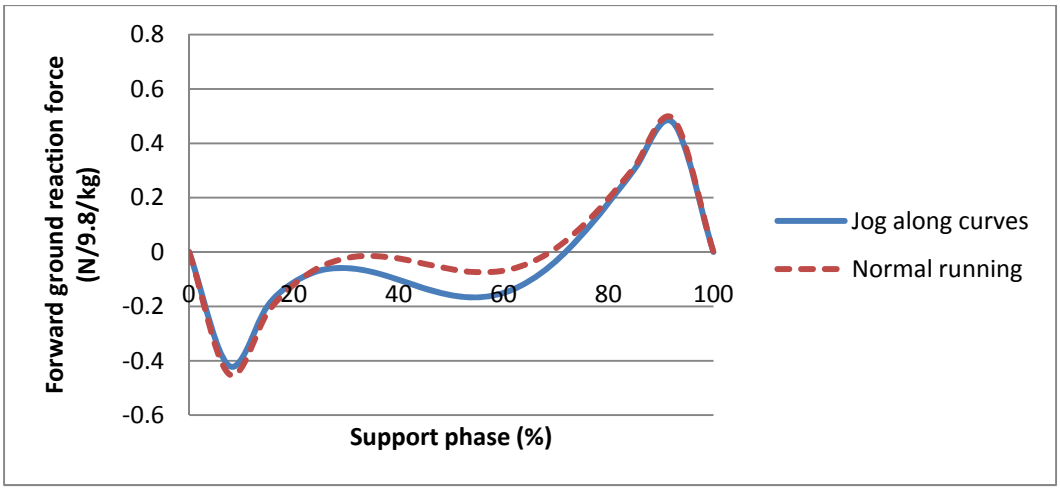

Figure 9.7 Forward ground reaction force

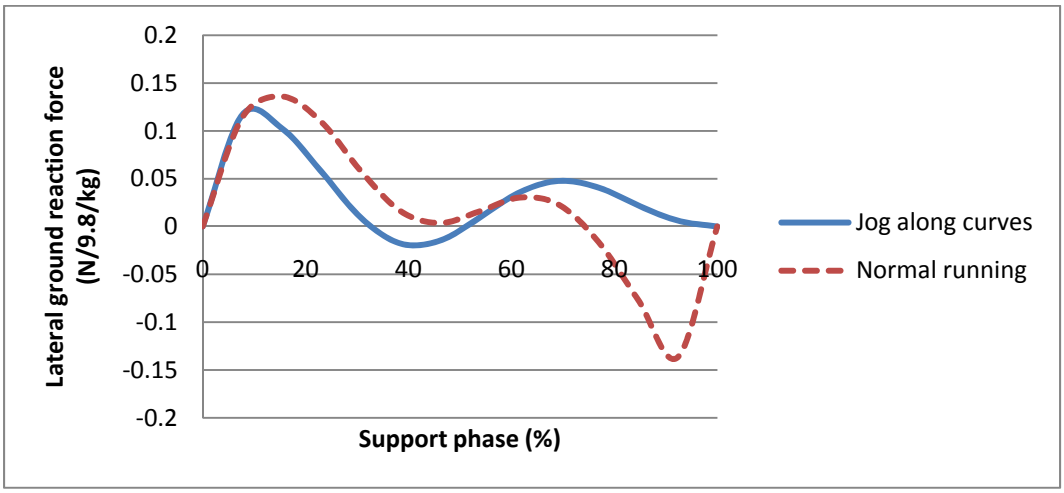

Figure 9.8 Lateral ground reaction force

Results show that the trends of the vertical and forward ground reaction forces of a slow jog along a curve are similar to the normal running case. However, the lateral ground reaction force is quite different. Most of the ground reaction force for a jog along a curve is in a positive area. This shows that the lateral ground reaction force is produced to turn the body in the direction of the motion.

9.4. Discussion

In this chapter, the problem of a slow jog along curved paths has been formulated. It is a non-symmetric running motion, so the stride formulation has been used. Jogging path is defined as a circular curve around the marker with a given radius. Most of the constraints are the same as for the normal running case. The body rotation constraint, continuity constraint, and foot location constraint are added for the slow jog formulation. The body rotation constraint is imposed so that the body faces the jogging direction. The continuity constraint is imposed between the first step optimization and the second step optimization. The foot contacting location is calculated from the step length, and the foot orientation along the path. The ground reaction forces show reasonable trends for the turning motion.

CHAPTER 10

STUDY OF UPPER BODY MOTION

10.1. Motivation

Upper-body motion is very important and difficult to predict for the running problem. First of all, the physics behind upper-body motion is not yet completely understood. Second, upper-body motion varies depending on input parameters such as running speed or backpack weight. For these reasons, it is very difficult to formulate the upper-body motion for running simulation. However, there is literature that can guide us on how to formulate upper-body motion. Kim et al. (2005) studied yawing moment cancelation and ZMP compensation for the humanoid robot (HanSaRam) to avoid the possible slipping on the ground caused by the yawing moment. So, they postulated that the upper-body motion of the robot should compensate for the yawing moment at the foot. This idea of compensation between yawing moment and upper-body motion is used in the current one-step running formulation.

10.2. Formulation with Upper-Body Motion

10.2.1. Design Variables

The design variables are the joint angle profiles **q** parameterized using B-spline approximation.

$$DV : \mathbf{q} \tag{10.1}$$

The number of control points is 5 for each joint angle and the number of degrees of freedom is 55. Therefore, the total number of design variables is 275.

10.2.2. Performance Measure

The performance measure can be modified to predict the upper-body motion. The idea is that the upper-body motion should compensate for the ground reaction moment during the running motion. In other words, if we minimize the ground reaction moment about the vertical axis, we can predict the upper-body motion that compensates for the ground reaction moment.

The modified performance measure for upper-body motion is

$$f = w_\tau f_\tau + w_I f_I + w_Y f_Y \tag{10.2a}$$

where

$$f_\tau = \int_0^T \boldsymbol{\tau}^{\mathrm{T}} \boldsymbol{\tau} dt \tag{10.2b}$$

$$f_I = \mathbf{I}_{strk}^{\mathrm{T}} \mathbf{I}_{strk} \tag{10.2c}$$

$$f_Y = \int_0^T M_{yGRF}^2 dt \tag{10.2d}$$

w_τ, w_I, w_Y are the weight values, $\mathbf{I}_{strk}$ is the impulse at foot strike, and M_{yGRF} is the ground reaction moment about the y-axis (vertical axis).

10.2.3. Constraints

The constraints for the upper-body motion formulation are as follows:

1) Joint angle limits
2) Joint torque limits
3) Ground penetration constraint
4) Foot location constraint - ground contact points

5) Initial posture constraint of foot location - initial rear heel position
6) No slip constraint
7) ZMP constraint during support phase
8) Arm-leg coupling constraint
9) Symmetry condition

The constraints for upper-body motion formulation are the same as for the normal running formulation in Chapter 7 except arm-leg coupling constraint. However, the ranges of the task-specific joint angle limits are different. Some of the degrees of freedom were frozen in the previous formulation. In this chapter, the ranges of the joint angle limits of the spine, shoulder, and elbow are relaxed for the upper-body motion formulation. Therefore, 44 active degrees of freedom are used for this formulation. Modified task-specific joint angle limits are listed in Table 10.1.

Table 10.1 Modified task-specific joint angle limits (degrees)

DOF	Without upper-body formulation		With upper-body formulation		Motion direction	
	Lower	Upper	Lower	Upper		
Q06	-1.0	1.0	-15.0	15.0	Spine	Joint2 twist
Q09	-1.0	1.0	-15.0	15.0		Joint3 twist
Q12	-1.0	1.0	-15.0	15.0		Joint4 twist
Q15	-0.5730	0.5730	-10.0	-0.5730	Right shoulder	Abduction/adduction
Q16	-1.0	1.0	-30.0	30.0		Extension/flexion
Q17	-6.5	-5.5	-6.5	6.5		Internal/external rotation
Q18	-91.0	-89.9427	-120.0	-89.9427	Right elbow	Flexion/extension
Q24	-0.5730	0.5730	-10.0	-0.5730	Left shoulder	Abduction/adduction
Q25	-1.0	1.0	-30.0	30.0		Extension/flexion
Q26	-6.5	-5.5	-6.5	6.5		Internal/external rotation
Q27	-91.0	-89.9427	-120.0	-89.9427	Left elbow	Flexion/extension

Arm-leg coupling constraint: It is considered that the arm swing motion helps running motion in terms of efficiency and comfortableness. In general, the left arm moves forward while the right leg moves forward, and the left arm moves backward while the right leg moves backward. Therefore, we constrain these arm-leg coupling directions in the sagittal plane (*z*-*y* plane) for upper-body motion. Figure 10.1 depicts the arm-leg coupling motion. $\mathbf{r}_1$ is the vector from left shoulder joint to left elbow joint, $\mathbf{r}_2$ is the vector from right hip joint to right knee joint, and $\mathbf{n}_z$ is the unit vector along *z*-direction.

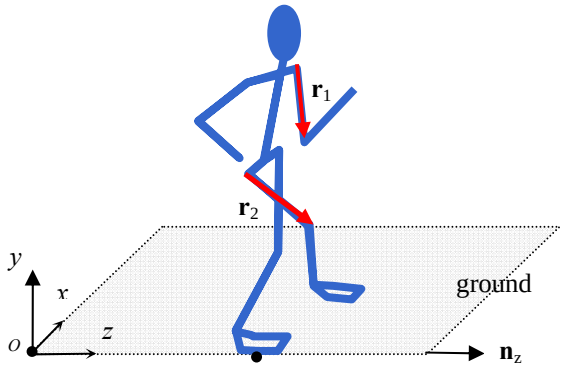

Figure 10.1 Arm-leg coupling motion

Then, the arm-leg coupling constraint is

$$(\mathbf{r}_1 \cdot \mathbf{n}_z)(\mathbf{r}_2 \cdot \mathbf{n}_z) \geq 0 \tag{10.3}$$

Note that the arm-leg coupling constraint has no relationship to obtain the swing angles of arm motion. It constrains only the swing direction of arm and the optimization process determines the swing angles.

10.3. Results

10.3.1. Comparison of Formulations

The total number of constraints is 1,060. Figures 10.2 and 10.3 are snapshots of the simulation for 3.0 m/s running with upper-body motion formulation. Step length is 1.096 m. Intel Core Duo 3.16 GHz CPU is used to obtain optimal solution. The number of iterations for obtaining the feasible point is 21 and the CPU time is 417 seconds. The number of iterations for the optimal point is 500, and the CPU time is 297 seconds.

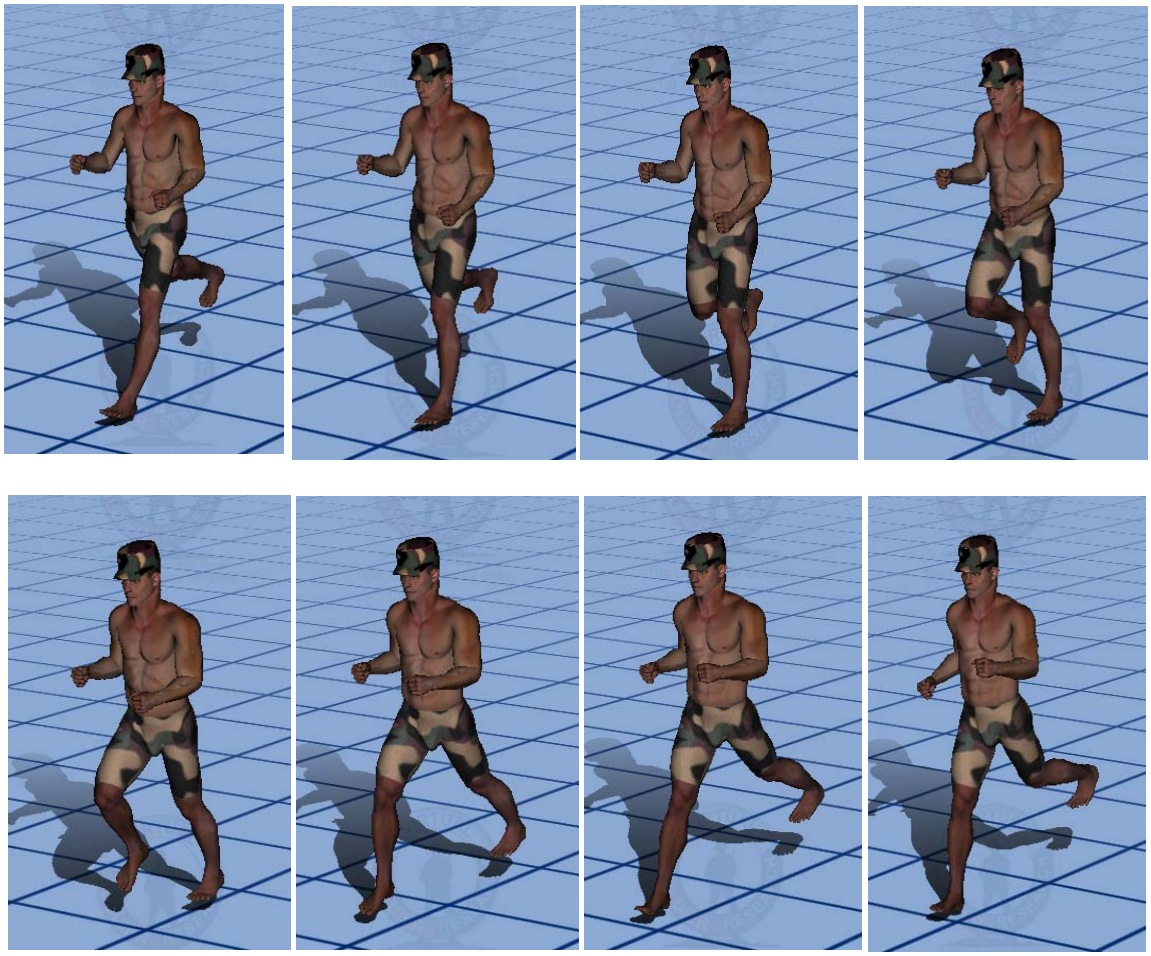

Figure 10.2 Snapshot with upper-body motion formulation

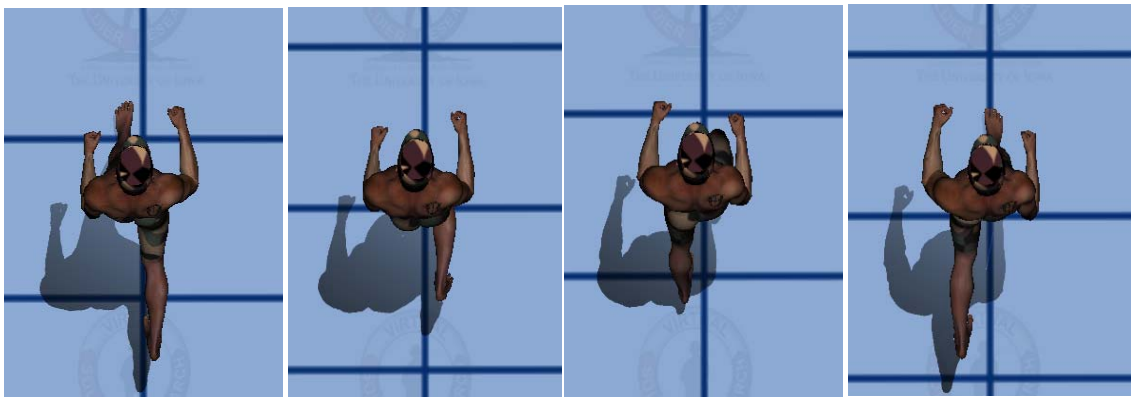

Figure 10.3 Snapshot with upper-body motion formulation – top view

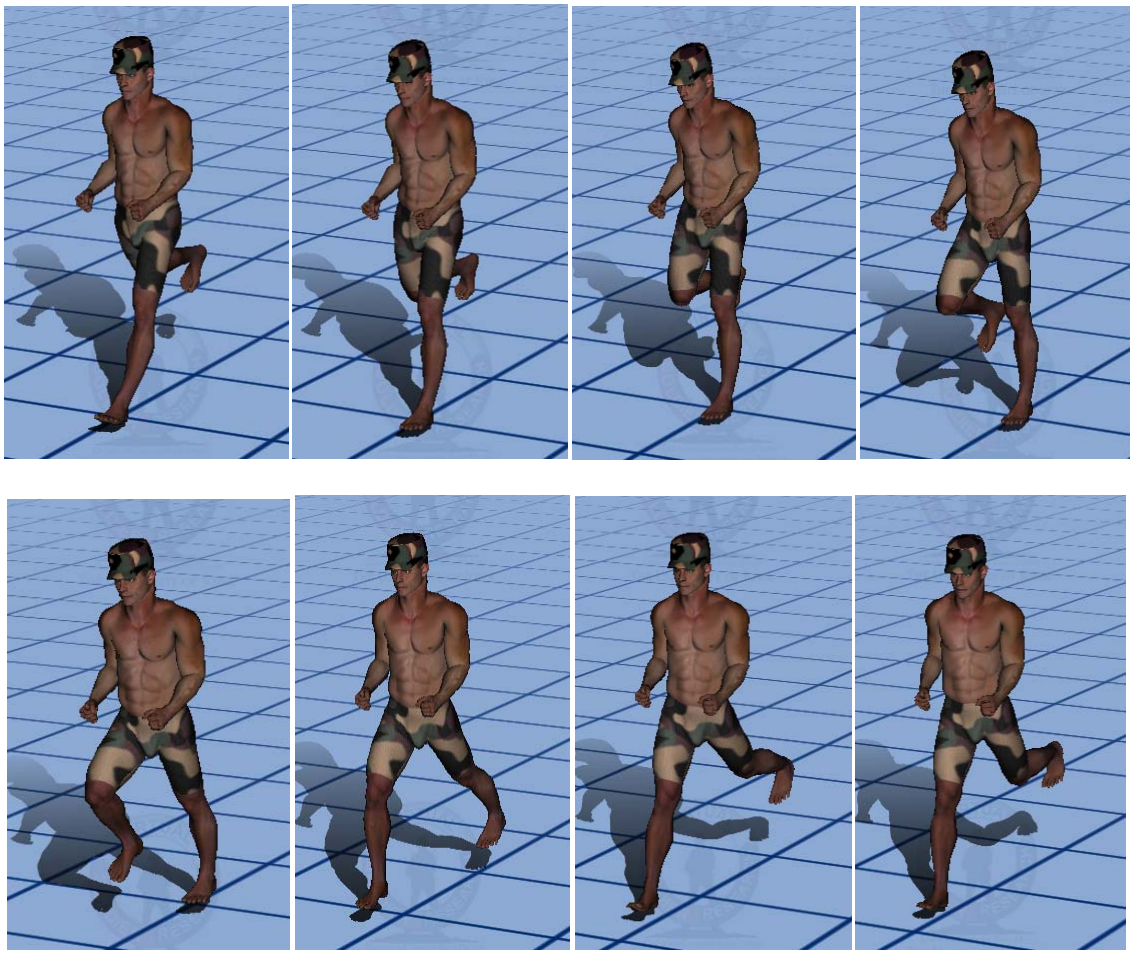

Figure 10.4 Snapshot without upper-body motion formulation

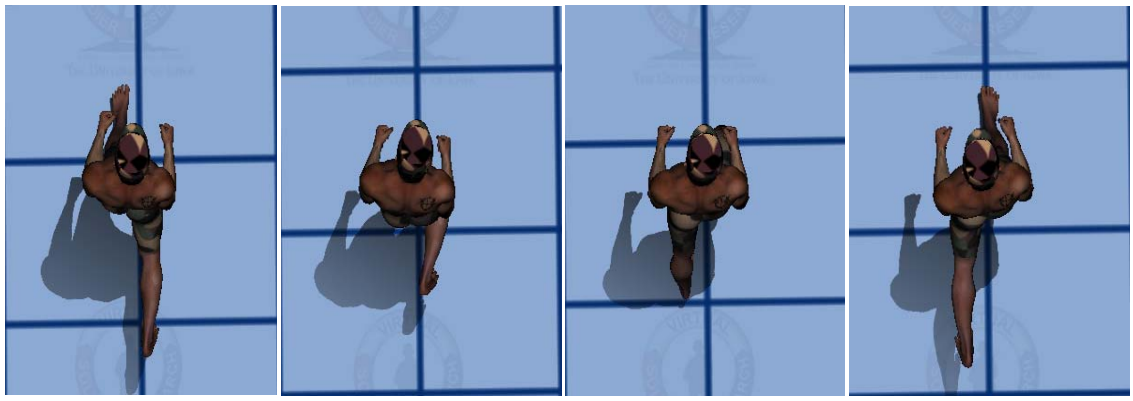

Figure 10.5 Snapshot without upper-body motion formulation – top view

The weight values in the performance measure are set to 1.0 for the torque square term,

0.5 for the impulse term, and 1.0×10^5 for the yawing moment term. As mentioned in Chapter 8, these values are determined by numerical experimentation. The performance measure value is 11,079. In Figure 10.3, the shoulder is rotating in the opposite direction of the legs or lower body. The active constraints are joint angle limits (spine, elbow and toe), joint torque limits (ankle), ground penetration, no slip, ZMP, foot location, arm-leg coupling and symmetry condition constraints.

Figures 10.4 and 10.5 are snapshots of the simulation from without upper-body motion formulation. In this case, the performance measure is the dynamics effort and impulse without yawing moment term which is the same as used in Chapter 8. The arm-leg coupling constraint is not included. However, the task-specific joint angle limits in Table 10.1 are used in this case. The active constraints are joint angle limits (elbow), ground penetration, no slip, foot location, and symmetry condition constraints. From the results, we can see that the right arm moves forward while the right leg moves forward, and the left arm moves backward while the left leg moves backward. Then, left right arm moves forward while the left leg also moves forward, and the right arm moves backward while the right leg also moves backward. This is opposite of what the natural motion should be. Therefore, the upper-body motion is not natural without the upper-body motion formulation.

Figures 10.6 and 10.7 show the knee joint angle profiles, the vertical ground reaction force results, and their comparisons with the results from without upper-body motion formulation (Figures 10.4 and 10.5). The trends of the results are similar to each other.

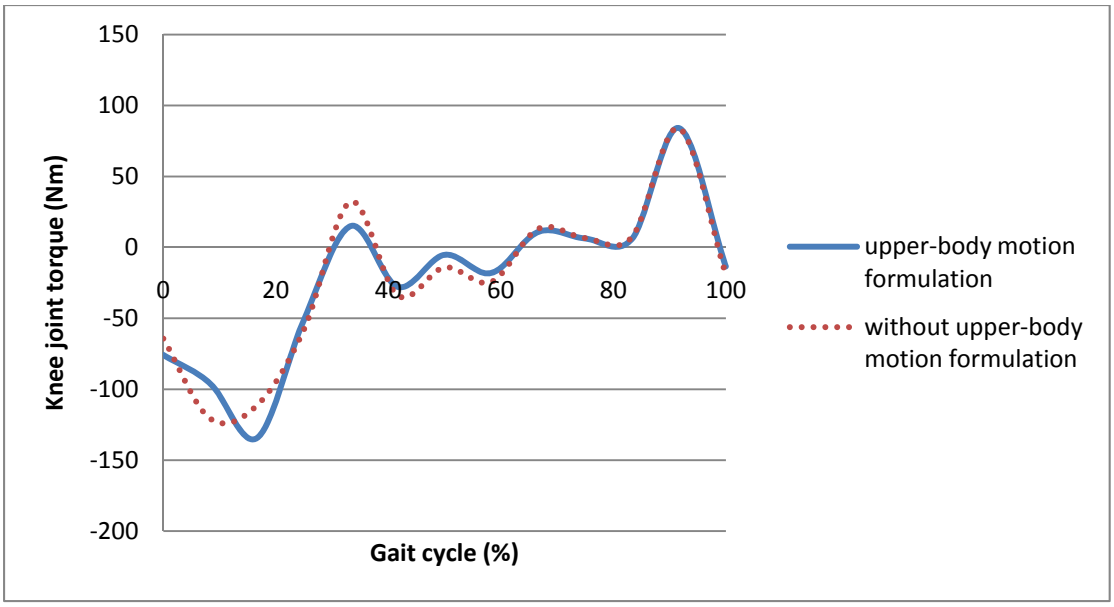

Figure 10.6 Knee joint torque profiles

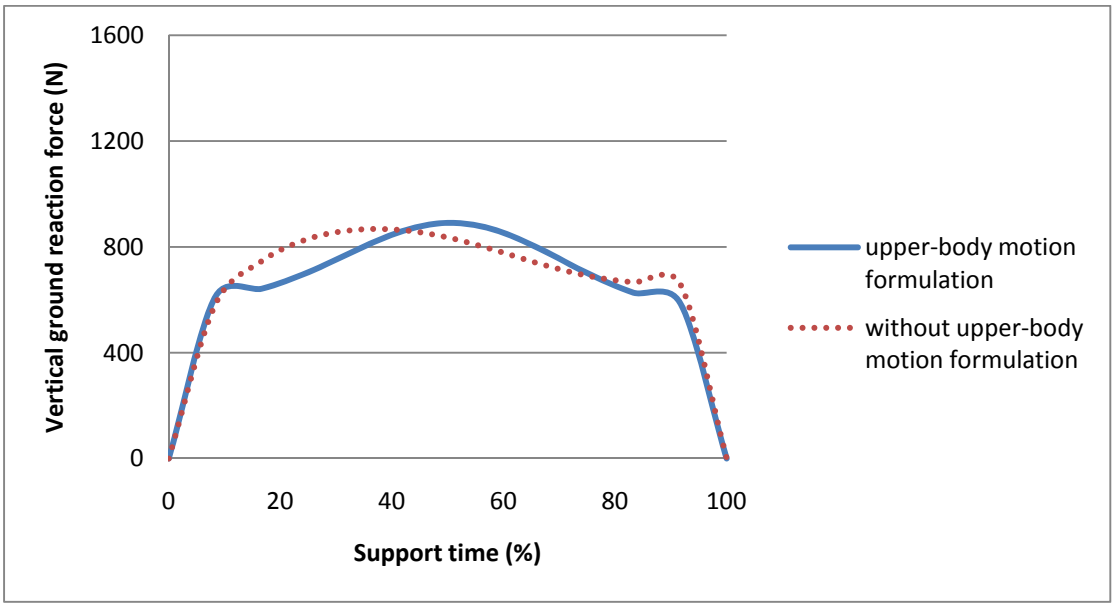

Figure 10.7 Vertical ground reaction force

Table 10.2 shows the comparison of the number of active degrees of freedom, the number of iterations, the performance measure values, the components values of the performance measure, the number of active constraints, peak value of knee joint torque, and peak

value of ground reaction forces.

Table 10.2 Comparison of results

Case		With upper-body motion formulation	Without upper-body motion formulation	Normal running with weapon
Active DOF		44	44	33
Number of iteration		500	162	28
Performance measure		11,079	12,391	12,168
Joint Torque part (f_τ)		8742	10,059	9,930
Impulse part (f_I)		4672	4,664	4,475
Yawing moment part (f_Y)		4×10^{-6}	125.80	67.57
Active constraints		146	121	169
Peak of knee torque (Nm)		-134.3013	-120.693656	-135.7226
Peak of GRF (N)	Vertical	891.06	864.17	1041.78
	Forward (FS/TO)	-289.89 / 372.23	-420.46 / 313.13	-428.78 / 376.22
	Lateral	74.14	140.46	134.13

Note that the yawing moment part of the performance measure in upper-body motion formulation is almost zero, implying that the ground reaction moment about the *y*-axis (vertical axis) is almost zero. In the other cases there is a large ground reaction moment about the *y*-axis.

10.3.2. Cause and Effect Case Study – Foot Locations

In this section, we study the effect of foot location from the center line of running, and determine if the foot location has an effect on natural running motion. Then, we can use the good results from this study in the later studies.

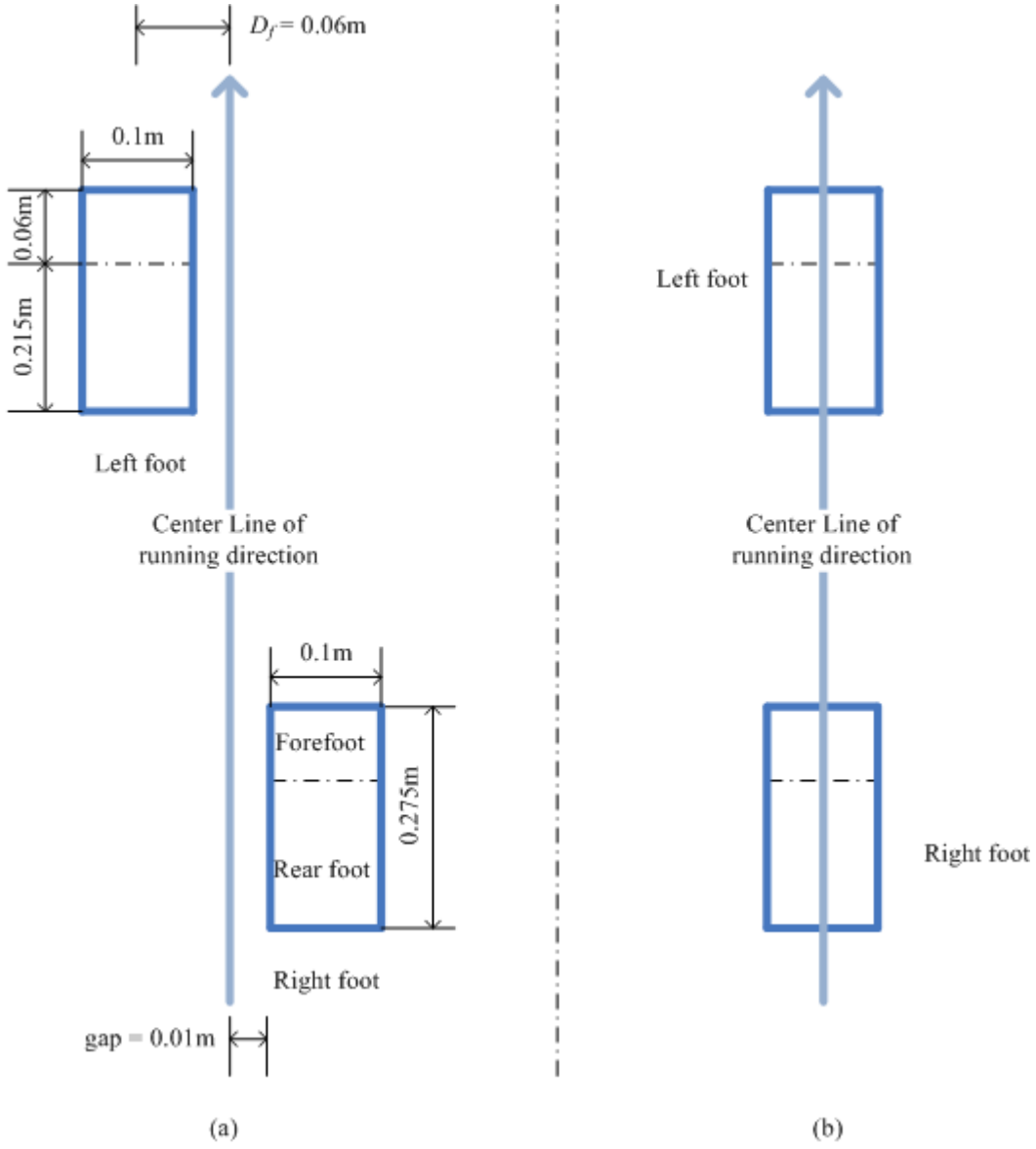

Figure 10.8 Foot locations in running

Figure 10.8 depicts the different foot location cases for the running formulation. D_f in Figure 10.8 (a) is the distance between the centerlines of foot and running direction. Figure 10.8 (b) is the case that the foot is located on the center line of running direction (D_f = 0.0m). Figures 10.9 and 10.10 are snapshots of running at 3.7 m/s with D_f as 0.06m and 0.0m, respectively.

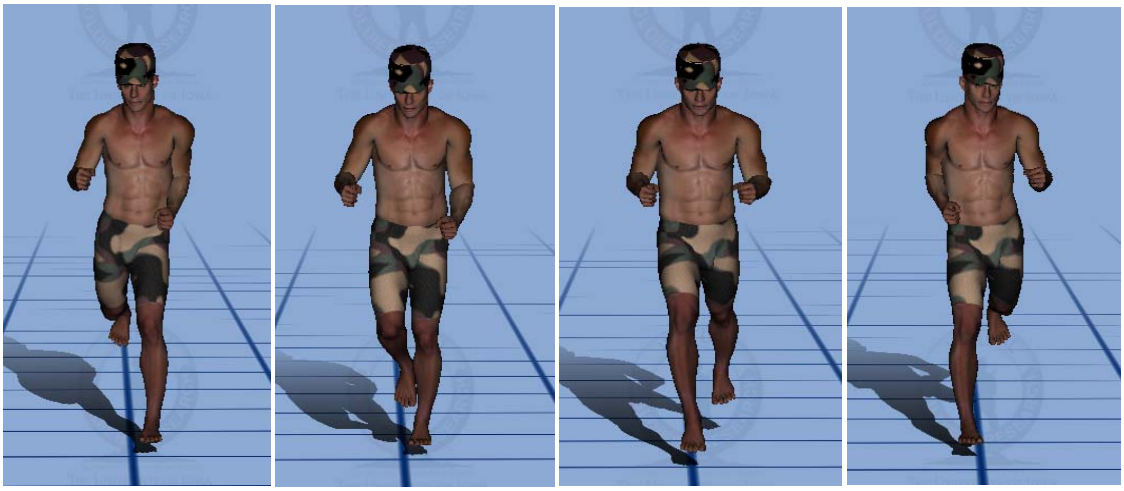

Figure 10.9 Snapshot of running at D_f = 0.06m

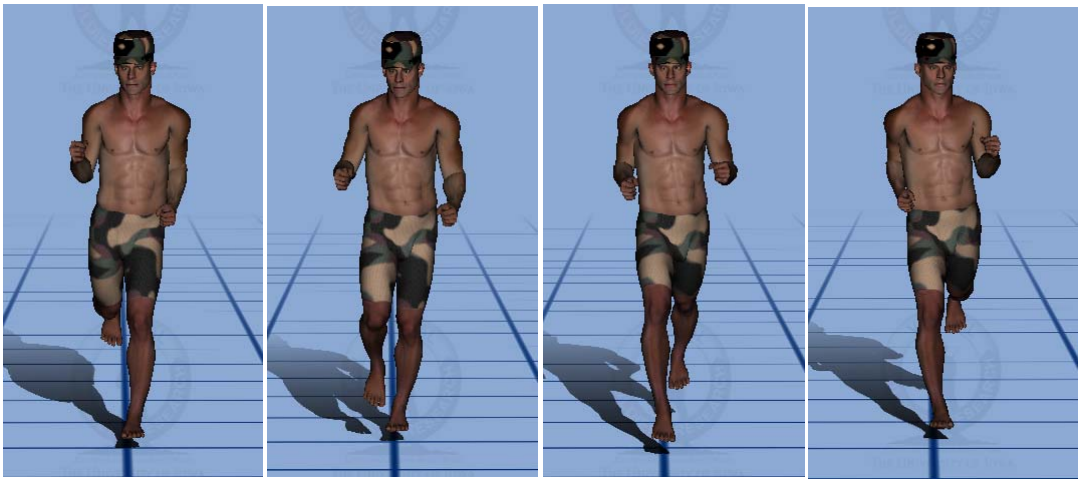

Figure 10.10 Snapshot of running at D_f = 0.0m

Figure 10.11 is snapshot of the results where D_f as 0.085m in Figure 10.8 (a).

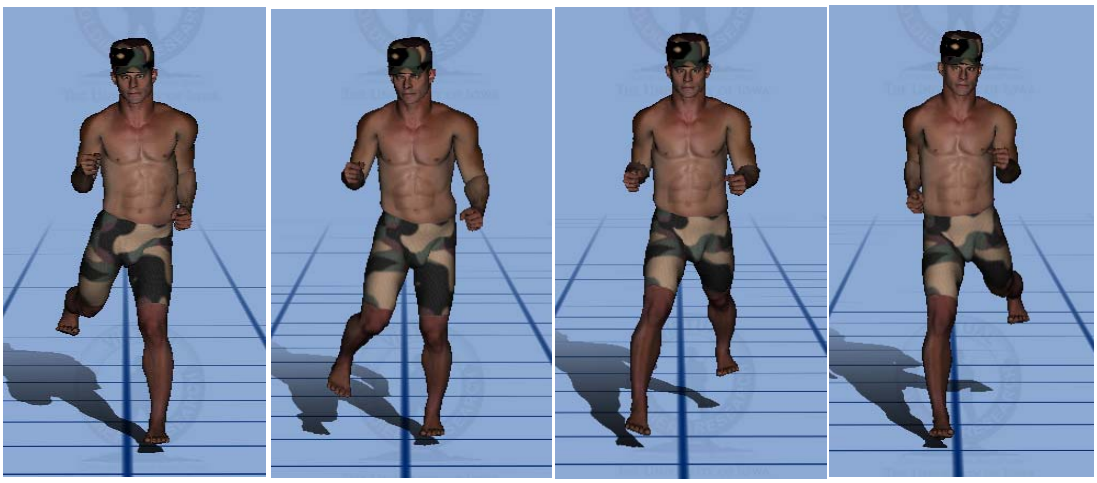

Figure 10.11 Snapshot of running at D_f = 0.085m

As an extreme case, D_f of 0.35m is specified. The optimization algorithm reports an infeasible problem with this constraint. The violated constraints are ZMP, foot location, and joint torque limits. For joint torque limit constraints, spine joint, right and left hip joints are violated. However, when the joint torque limits are relaxed to double of their normal values for all joints, optimal solution is found. Then, the active constraints are joint angle limits (right and left ankle), ground penetration, no slip, ZMP, foot location, arm-leg coupling, and symmetry condition constraints. Figure 10.12 is snapshot of the results. We can observe that the upper body is leaning toward to the next step for the stability in this case.

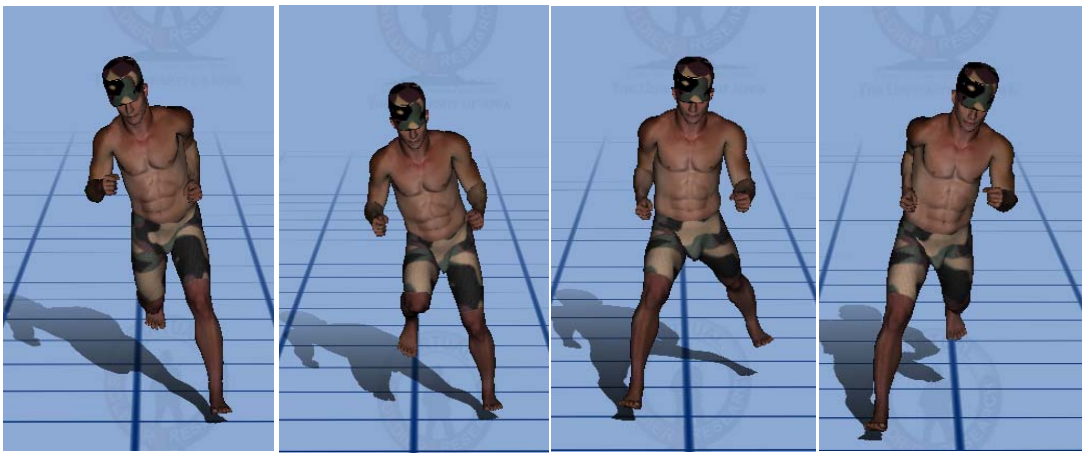

Figure 10.12 Snapshot of running at D_f = 0.35m

We can observe that the motion in Figure 10.9 is quite natural. Also, we can note that the hip is rotating too much when D_f as 0.0m in Figure 10.10. And the leg swings outward where D_f as 0.085m in Figure 10.11. Therefore, we can use D_f as 0.06m for later studies. Table 10.3 contains summary of results in this cause and effect case study – the foot locations.

Table 10.3 Summary of results – foot locations case study (running speed = 3.7 m/s)

Case		D_f = 0.06m	D_f = 0.0m	D_f = 0.085m	D_f = 0.35m
Number of iteration		24	201	359	85
Performance measure		15,921	19,466	15,624	45,662
Active constraints		191	189	207	144
Peak knee torque (Nm)		-200.10	-189.45	-192.70	-253.62
Peak GRF (N)	Vertical	944.41	974.18	880.11	1163.61
	Forward (FS/TO)	-475.24 / 349.73	-382.55 / 352.98	-422.25 / 304.18	-100.52 / 887.73
	Lateral	208.77	208.91	174.32	-759.90

10.3.3. Cause and Effect Case Study – Backpack Load

Figure 10.13 is snapshot of running without backpack. Figure 10.14 is snapshot of running with backpack (500N). The running speed is 3.0 m/s. We can observe that the upper body leans more toward running direction when backpack is carried.

Figure 10.13 Snapshot of running without backpack

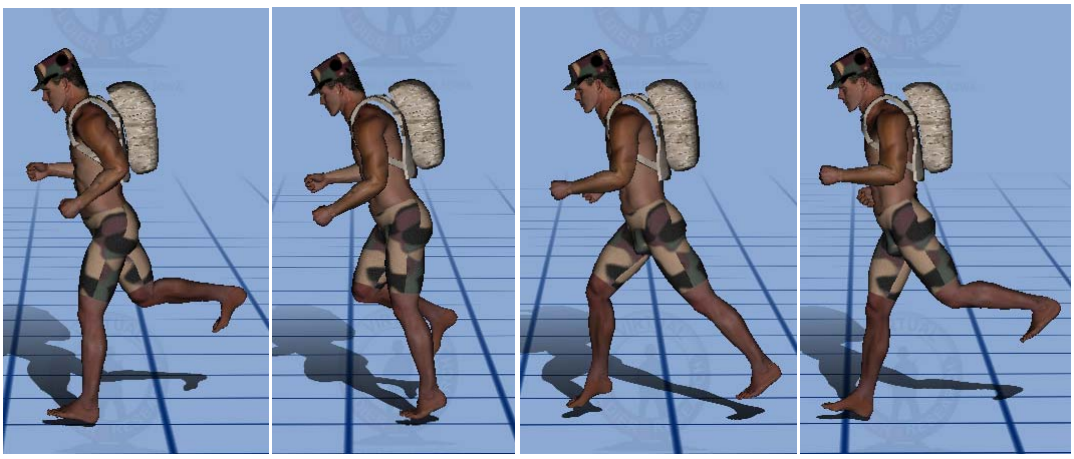

Figure 10.14 Snapshot of running with backpack (500N)

Figure 10.15 is a comparison of the knee joint torques for the cases without backpack and with backpack. We can see that when the backpack is loaded, the larger actuation torque is needed at the knee in the support phase.

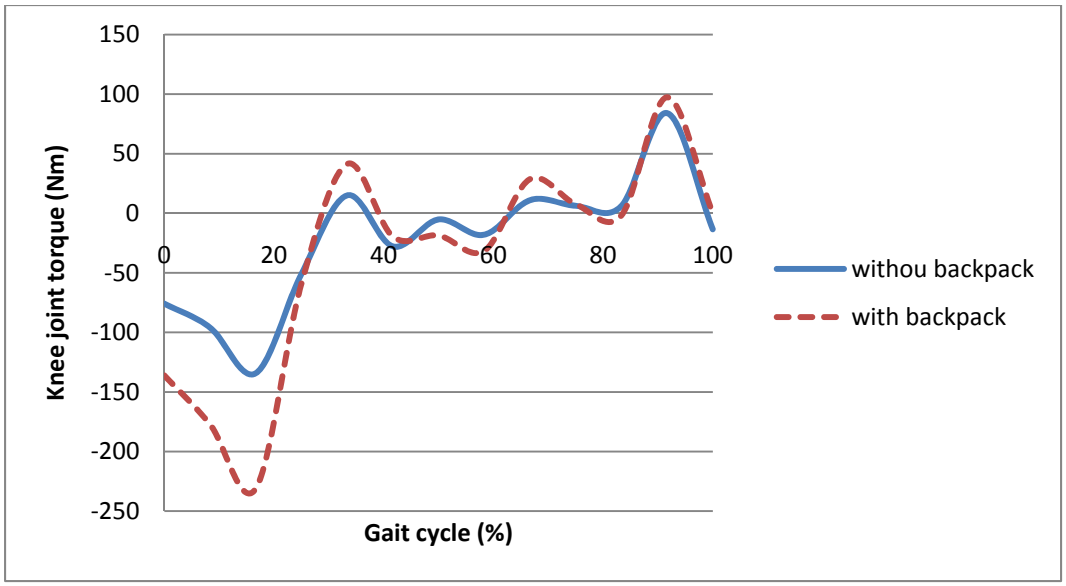

Figure 10.15 Knee joint torque comparison

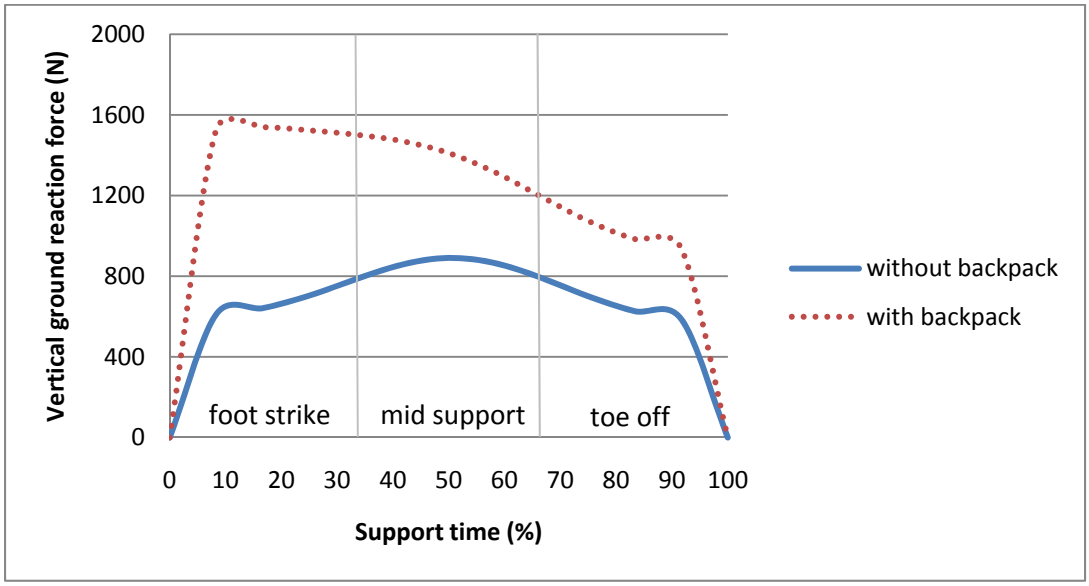

Figure 10.16 Vertical ground reaction force comparison

Figure 10.16 shows the vertical ground reaction force comparison for the cases without backpack and with backpack. We can see that larger ground reaction force acts at the foot strike compared to the mid-support and toe off phases.

As an extreme case, when 600N backpack is loaded, the optimization algorithm reports infeasible problem. The violated constraints are fourth spine joint torque limit, right and left knee joint torque limits. The active constraints are joint angle limits (knee, ankle, spine tilt), ground penetration, no slip, ZMP, foot location, arm-leg coupling and symmetry condition. However, when the joint torque limits are relaxed to double of their normal values for all joints, optimal solution is found. Table 10.4 shows the comparison of results in the cause and effect case study – the backpack load. In most cases, active constraints are the ground penetration, no slip, foot contact, ZMP, joint angle limits (spine, wrist, elbow, clavicle,), joint torque limits (ankle), arm-leg coupling, and symmetry conditions.

Table 10.4 Summary of results - backpack load case study (running speed = 3.0 m/s)

Case		No backpack	500N backpack	600N backpack
Number of iteration		500	478	352
Performance measure		11,079	15,324	15,492
Active constraints		146	177	195
Peak knee torque (Nm)		-134.3013	-231.1568	-351.8215
Peak GRF (N)	Vertical	891.06	1539.56	1619.18
	Forward (FS/TO)	-289.89 / 372.23	-572.77 / 222.90	-449.65 / 348.80
	Lateral	74.14	-135.51	-230.29

10.3.4. Cause and Effect Case Study – Running Speed

Figure 10.17 shows the knee joint torques with different running speeds, 3.0 m/s, 3.5 m/s, and 4.0 m/s respectively. From the figure, we can observe that the peak value of joint torque gets larger when the running speed increases.

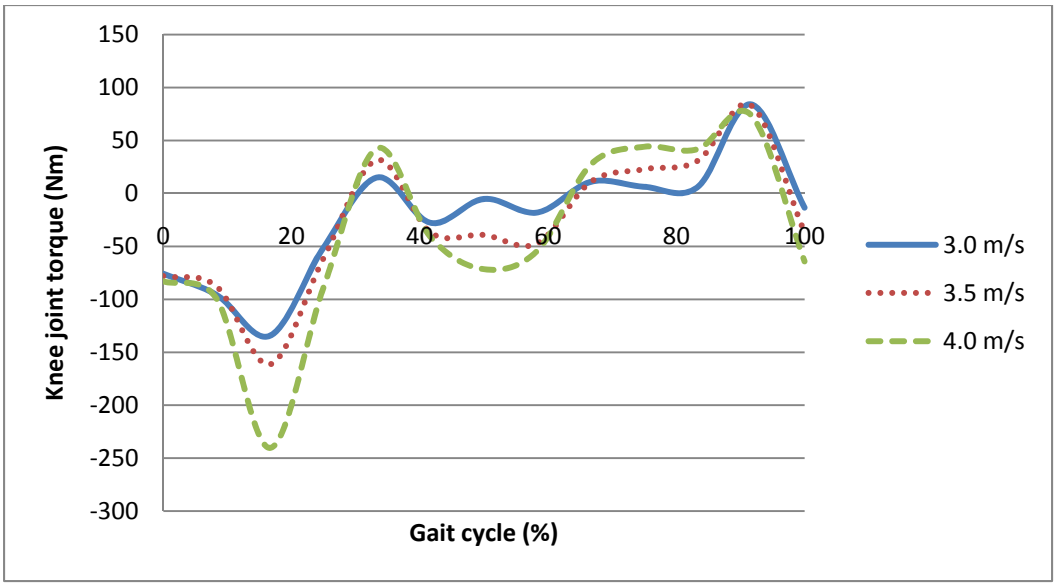

Figure 10.17 Knee joint torque in different running speed

Figure 10.18 shows the vertical ground reaction force for different running speeds. Also, it is observed that the peak value of ground reaction force gets larger when the running speed increases.

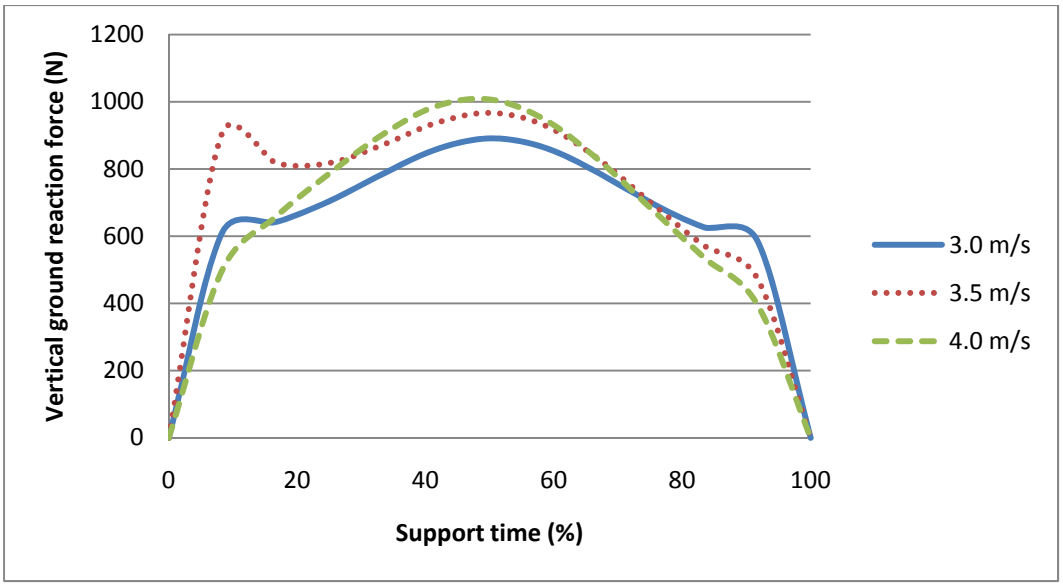

Figure 10.18 Vertical ground reaction force in different running speed

Common active constraints for all the cases are the ground penetration, no slip, foot contact, ZMP, arm-leg coupling, and symmetry conditions. For 3.0 m/s, spine, elbow, and toe joint angle limit constraints and the ankle torque limit constraint are active. For 3.5 m/s, spine, elbow, shoulder, hip joint, knee, and toe joint angle limit constraints and the knee joint torque limit constraint are active. For 4.0 m/s, spine, elbow, shoulder, hip joint, knee, and toe joint angle limit constraints and the hip and knee joint torque limit constraints are active.Table 10.5 shows the summary of results in the cause and effect case study – the running speed.

Table 10.5 Summary of results – running speed case study

Case		3.0 m/s	3.5 m/s	4.0 m/s
Number of iteration		500	324	354
Performance measure		11,079	13,665	20,713
Active constraints		146	191	189
Peak knee torque (Nm)		-134.30	-161.39	-240.30
Peak GRF (N)	Vertical	891.06	967.12	1007.02
	Forward (FS/TO)	-289.89 / 372.23	-470.87 / 369.99	-361.41 / 383.39
	Lateral	74.14	162.03	243.43

Figure 10.19 shows the performance measure values for different running speeds. We can observe that the performance measure value gradually increases when the running speed increases.

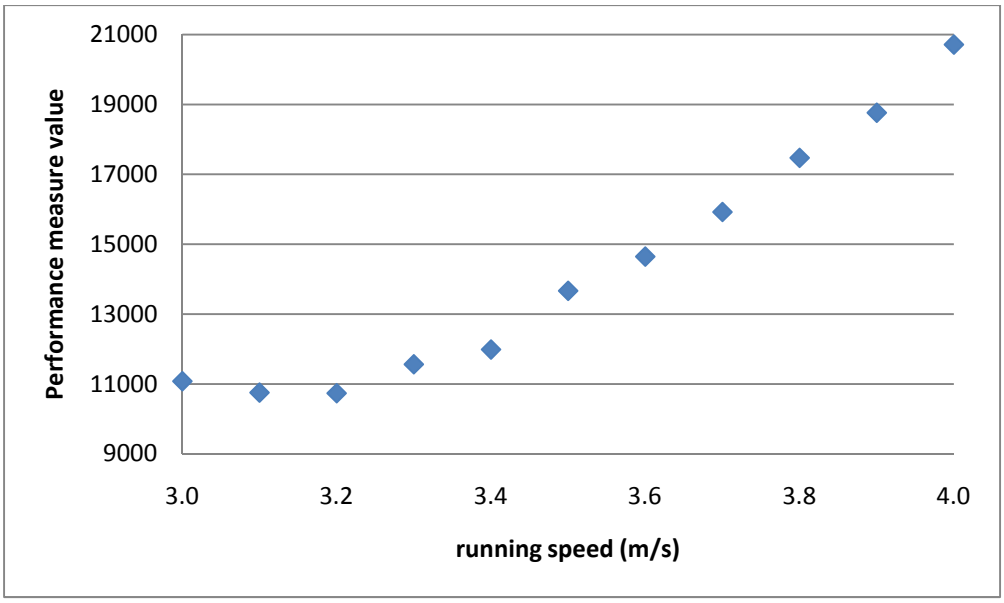

Figure 10.19 Performance measure values in different running speed

As an extreme case, when running speed is 3.0 m/s, the joint torque limits are reduced to half of their normal values for all joints. Then, the optimization algorithm reports infeasible problem. The violated constraints are foot location, no slip, ZMP, and joint torque limits. For joint torque limit constraints, spine, right and left hip, left ankle, right knee joint torque limits are violated. However, when the joint torque limits are reduced by just one fourth of their normal values, the optimization algorithm could find optimal solution.

10.4. Validation

Six determinants (hip flexion/extension, knee flexion/extension, ankle flexion/extension, pelvic tilt, pelvic rotation, and lateral pelvic displacement) are chosen to validate the running simulation. Experiments have been performed by VSR validation group and the data are obtained for two healthy male subjects. Each subject ran at various

running speeds. These results are normalized for the running cycle. The running speed of simulation is 3.0 m/s. Figure 10.20 shows the validation results.

In Figure 10.20, the blue dotted curves are 95% confident region of the statistical means, the black curves are mean value of experimental data, and the red curves are the simulation results. Pelvic displacement is the displacement of lateral pelvic movement. In general, the trend of red curves (simulation) follows the experimental results.

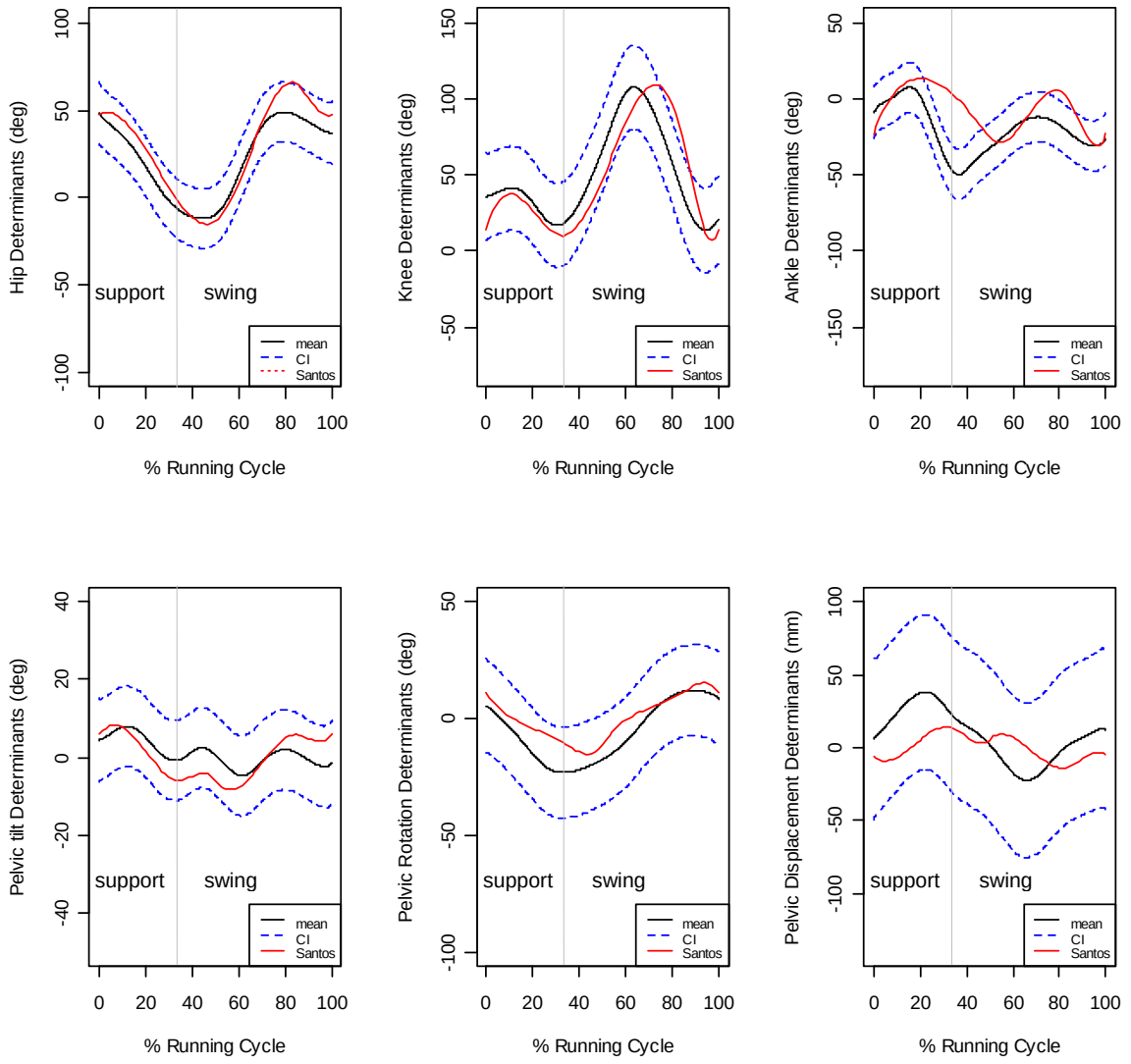

Figure 10.20 Validation – six determinants

10.5. Discussion

In this chapter, the upper-body motion has been investigated. A performance measure and arm-leg coupling constraint have been proposed to predict upper-body motion for running. The ground reaction motion is minimized in the performance measure so that we can predict the upper-body motion that compensates for the ground reaction moment. Also, task-specific joint angle limits are changed. In the previous chapter, 22 degrees of freedom were frozen and 33 active degrees of freedom were used for the running simulation. In this chapter, 44 active degrees of freedom are used. With the upper-body motion formulation, simulation results for running motion have improved and have become more natural. The upper-body motion has been improved. Results show that the shoulder is rotating in the opposite direction from the lower-body movement. Also, the right arm moves backward while the right leg moves forward, and the left arm moves forward while the left leg moves backward. However, the formulation for the upper-body motion still needs to be improved because the yawing motion is smaller than what is typical for a human. Possible reasons for the small yawing motion are approximated mass moment of inertia properties.

CHAPTER 11

STUDY OF SPARSITY OF THE FORMULATION

11.1. Motivation

The purpose of this chapter is to study how the sparsity of the Jacobian matrix of the current formulation affects the calculation time of the optimization process. If the Jacobian is very sparse, we may have the opportunity to reduce the calculation time. As mentioned in Chapter 8, we have used the NPOPT optimization solver, which is for dense optimization problems, for all the problems. There are a couple of other solvers in SNOPT that take advantage of the sparsity structure of the problem. The SNOPT B interface has the capability to handle the sparsity, so we can analyze effect of the sparsity using the SNOPT B solver.

11.2. Sparsity of the Formulation

11.2.1. SNOPT B Interface

SNOPT B (also known as SNOPT) has the capability for sparsity, but there are some limitations in its use. The constraints must be ordered in a specific way. Therefore, it is difficult to add or delete constraints. Also, indexing of the arrays is complex and therefore error prone. The solver was originally developed in Fortran, so even though we are using library files that have been converted from Fortran to C interface, the Fortran style for indexing of arrays must be used. For example, the indices of the array itself start at zero (as in C interface), but the coordinates of the elements or contents of the indicator start at one (as in Fortran).

In SNOPT B, only non-zero values in Jacobian are stored as a column vector. So, we need a separate generalized module that indicates the non-zero values in the Jacobian of the current formulation. Figure 11.1 depicts the algorithms that show the differences between NPOPT solver and SNOPT B solver.

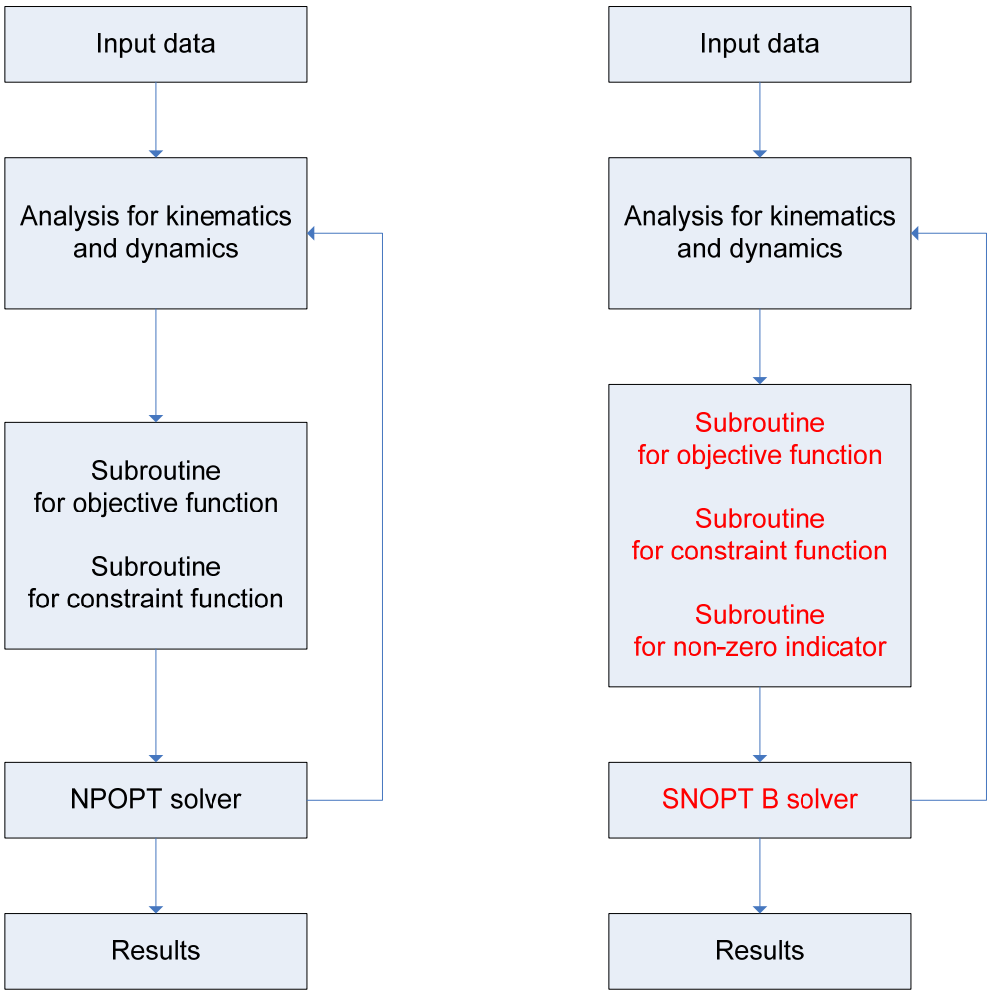

Figure 11.1 Algorithms for NPOPT solver and SNOPT B solver

Subroutines for the objective function, constraint functions, and non-zero indicator (red highlighted part) are modeled and implemented to study the sparsity of the formulation with SNOPT B interface.

11.2.2. Formulation

The running formulation to study sparsity structure of the problem is defined as follows:

11.2.2.1. Design variables

The design variables are the joint angle profiles **q** parameterized using B-spline approximation.

$$DV : \mathbf{q} \tag{11.1}$$

The number of control points is 5 for each joint angle and the number of degrees of freedom is 55. Therefore, the total number of design variables is 275.

11.2.2.2. Performance measure

The dynamic effort is used for the performance measure:

$$f = \int_0^T \boldsymbol{\tau}^T \boldsymbol{\tau} dt \tag{11.2}$$

11.2.2.3. Constraints

All constraints are treated as non-linear constraints in the previous formulation. However, the joint angle limit constraints are separated as linear constraints in the SNOPT B interface to improve the efficiency of optimization. The order of constraints is important because non-linear constraints must come first in SNOPT B. Table 11.1 shows the list of constraints. Constraints on the joint torques are not included in this study.

Table 11.1 List of constraints in SNOPT B interface

Order of constraints	In SNOPT B
1. Ground penetration	Treated as non-linear constraints
2. No slip constraints	
3. ZMP constraints	
4. Foot contacting position	
5. Joint angle limit constraints	Treated as linear constraints

The sparsity in the formulation only exists in the joint angle limit constraints. The reason is that DH transformation matrices are involved in the non-linear constraints and they contain sinusoidal functions. Therefore, it is almost impossible to indicate non-zero value location in the subroutine for non-zero indicator. Thus, in the formulation, linear constraints (385) are treated as sparse and non-linear constraints (161) are treated as dense.

11.3. Results and Discussion

The SNOPT B solver and NPOPT solver are used for the normal running problem with the same conditions – running speed, performance measure, constraints, and starting points for optimization. Table 11.2 shows CPU time with the SNOPT B and NPOPT solvers. It is seen that that the calculation time is not improved when the SNOPT B solver is used. Table 11.3 shows that sparsity of the formulation is 69%.

Table 11.2 CPU times with SNOPT B and NPOPT solvers

Solver	CPU time
SNOPT B	286.33 seconds
NPOPT	222.62 seconds

Table 11.3 Number of non-zero entries in the Jacobian

The number of constraints	546
The number of element in Jacobian	150150
The number of non-zero element in Jacobian	46200 (31% of total)

If the torque limit constraints are included, the sparsity will be 41%. In general, it is believed that 90% sparsity can improve calculation time. The results show that the sparsity of the formulation with SNOPT B does not improve the calculation time. Furthermore, it becomes quite tedious to modify the model, i.e., add and delete constraints. Therefore, it is not beneficial to use the sparsity of the formulation with SNOPT B for the current optimization formulation of the problem.

CHAPTER 12

CONCLUSIONS AND FUTURE RESEARCH

12.1. Conclusions

The optimization-based dynamic prediction of 3D human running motion has been studied in this dissertation. The predictive dynamics method is used to formulate the running problem. An algorithm based on the sequential quadratic programming approach is used to solve the nonlinear optimization problem. And analytical gradients for the optimization process are calculated. Denavit-Hartenberg method is used for kinematics analysis. The recursive Lagrangian formulation is used for the equations of motion which is derived using the energy methods. B-spline interpolation is used for time discretization. The control points for the joint angle profiles are treated as design variables. The dynamic effort is used as the performance measure. A minimal set of constraints is imposed in the formulation of the problem to simulate natural running motion. Zero moment point (ZMP) constraint is used for the dynamic stability in the support phase. The impulse at the foot strike is included in the performance measure. The joint angle profiles, joint torque profiles are calculated for the full body human model. The ground reaction force is determined. Several cause and effect cases are studied such as backpack loading, range of motion restriction by armor component, and different running speed. In addition to straight running motion, slow jog along curves has been simulated. Also, the formulation for upper-body yawing motion has been proposed.

In conclusion, the proposed formulation can predict 3D human running motion. It can predict not only the displacement field such as joint angles but also the force field

such as joint torques and ground reaction forces. The results obtained with the formulation are validated with the experimental data. Furthermore, it is found that the current formulation is robust and gives natural motion of human running.

12.2. Future Research

In future research, a shoe model with multi-body dynamics, wobbling masses effects, and a musculoskeletal model can be studied.

12.2.1. Shoe Model with Multi-Body Dynamics

A shoe model is not included in the current running formulation; it is a bare foot of rigid body. However, humans almost always run with shoes, and the running motion will be affected by the shoes. Rigid shoes, soft shoes, heavy shoes, and light shoes would give different results in running because the shoes will tend to mitigate the impact effect during foot strike. To incorporate a shoe model, a multi-body dynamics approach combined with predictive dynamics could be used. In this case, the spring-damper system will be modeled as a shoe. Then, the external force due to this spring damper system can be applied to the predictive dynamics model.

12.2.2. Wobbling Masses Effects and Musculoskeletal Model

We have used a rigid body assumption in the running formulation, and there is no muscle and tissue model. However, wobbling masses (muscles and tissues) effects are significant in human running. It affects not only kinematics results but also dynamics results. Therefore, a wobbling masses model should be included somehow in the future.

Also, a musculoskeletal model should be developed as a real human model for running so that muscle forces can be obtained instead of joint torques. Finally, a more accurate anthropometric data should be developed for better and more natural results in the running simulation.

APPENDIX

OPTIMIZATION DATA FOR 3 m/s NORMAL RUNNING

WITHOUT UPPER BODY MOTION

Table A.1 Starting control points

GT1	0.84997003562164 1.10505412775351 1.37614025787281 1.89523918824184 2.03231221436286
GT2	0.00248269965752 -0.02516060478073 0.02611604661562 -0.01832313795649 -0.00348269965752
GT3	0.01415504226172 0.05225195792225 0.09278364238798 -0.00547480591221 0.01499449996798
GR1	-0.04090408915706 -0.27994365560652 0.20693633439651 -0.08885394148351 0.03990408915706
GR2	0.01745329222222 -0.01438840266169 0.16285503887013 0.03455440229962 0.01745329222222
GR3	-0.13603393060447 0.09779866275732 0.05584745896381 0.26098820650552 0.13503393060447

Table A.1 Continued

Q01	0.02779463380737 0.03629046001669 0.05317403719813 -0.02426437609294 -0.02879463380709
Q02	0.02405830736763 0.04715079487682 0.02385141070336 0.01257947307967 0.02505830736779
Q03	0.04146602031833 -0.25546273328432 -0.02742594246914 -0.20230631585966 -0.04246602031833
Q04	-0.00980251494296 0.12849225999707 -0.18868380544847 0.08322451428133 0.00880251494295
Q05	0.01750041611122 0.01750396941386 0.01779623083139 0.01745408485722 0.01750041611104
Q06	0.00389351834580 0.05233670943638 -0.07192656435848 0.02123569479412 -0.00489351834551
Q07	-0.00882760589799 0.12705829872377 -0.18618803110858 0.08095252121885 0.00782760589799

Table A.1 Continued

Q08	0.01750041611122 0.01775575295685 0.01865027848653 0.01731850910349 0.01750041611122
Q09	0.01634106401306 0.03642889597462 -0.04014333197458 -0.00656895704748 -0.01734106401285
Q10	0.03392527712166 0.03068616168927 0.06142246027132 -0.03671383413772 -0.03492527712173
Q11	0.02016552716011 0.05822614139738 0.11186740215980 0.00062693232618 0.02116552716019
Q12	0.01645329222222 -0.00254992007598 0.05043896948810 -0.02773020908886 -0.01745329222204
Q13	0.00073422142605 -0.00396546834093 0.00565058209340 -0.00256845286738 0.00012126451915
Q14	-0.00100007364433 -0.00117679636369 0.00410317894825 -0.00171056857412 -0.00100007364433

Table A.1 Continued

Q15	0.00321605435117 -0.03654969024377 0.05374399415754 -0.02361051797274 -0.00218447154719
Q16	-0.01745329222216 0.01330097624474 0.02735844701899 0.00799012837539 -0.01296715422291
Q17	-0.10601903031049 -0.11698374734004 -0.11793325249362 -0.08875711565113 -0.10342823820177
Q18	-1.57317968467760 -1.60155229379731 -1.57177715519754 -1.59558462286753 -1.57834102446559
Q19	-0.00960188277943 -0.02444874916919 0.04881625856357 -0.02216842224814 -0.00373829758518
Q20	-0.00240125533922 0.03456947822747 -0.04825614868724 0.01827467485562 0.01000073644333
Q21	-0.00155119474744 0.01729483410089 0.00957276261733 -0.01239223017500 -0.01000073644333

Table A.1 Continued

Q22	-0.00087873548085 0.00403396349680 -0.00560177933762 0.00249603651076 0.00000985226555
Q23	-0.00100007364434 0.00023692648510 -0.00146055596251 -0.00086049731997 -0.00100007364432
Q24	-0.00318447154719 0.03652426707438 -0.05371686486100 0.02358867302212 0.00222076694648
Q25	-0.01196715422290 -0.05080533145098 0.08292313462048 -0.03326173000546 -0.01674615722953
Q26	-0.10242823820177 -0.12959211819850 -0.08214997578584 -0.10115936984698 -0.10701903031049
Q27	-1.57934102446559 -1.54739968931642 -1.62645761648575 -1.55894654385785 -1.57417968467760
Q28	-0.00473829758518 0.02940658633441 -0.02513030858040 -0.00205068786279 -0.01000073644333

Table A.1 Continued

Q29	0.00900073644333 -0.00644763963393 0.03542629977265 -0.02135299135060 -0.00140125533922
Q30	-0.00971165108556 -0.00535279603834 0.03188540971329 -0.01074347437201 -0.00055119474744
Q31	-0.00512092518627 0.06665664197016 0.00398837433402 0.04272596648734 0.00412092518627
Q32	-0.08688684625306 -0.08272839129289 -0.08602879519123 -0.08817043224582 -0.08588684625331
Q33	0.08726646111111 0.07917043473994 -0.01889435365353 -0.09067027786344 -0.08626646111118
Q34	-0.00267409080677 -0.10936405349131 0.15613650707763 -0.05381876857577 0.00367409080677
Q35	-0.00459819607796 0.03758723056670 -0.00658780922306 -0.02635784374672 -0.00359819607796

Table A.1 Continued

Q36	-0.09964932974848 0.26141790522039 -0.78369537363484 0.03383685433375 -0.06011989356094
Q37	0.40742890955931 0.21826187620772 -1.57040445642095 -0.39519856191948 -0.42692556572569
Q38	0.16545332637954 -0.15881906177663 -0.46263215760096 -0.27001069135906 -0.14345508511251
Q39	1.10927999914858 1.66587605237633 3.18698551122149 -0.25261622355293 0.17553292222222
Q40	-0.20502270814461 0.50175694481330 -0.84368161355552 1.02043490614325 0.59986574233778
Q41	-0.03956013761686 -0.14534103527674 0.07679735572825 -0.03666231285970 -0.04285445006652
Q42	-0.48611918715936 -2.15452204640424 1.38606034198253 -0.86705047225004 -0.57838171074149

Table A.1 Continued

Q43	-0.06111989356094 -0.23552850633948 0.29985201374256 -0.29302573064080 -0.09864932974841
Q44	-0.42792556572569 -0.48676465376848 0.34943939997859 0.50824366342699 0.40642890955931
Q45	-0.14445508511251 0.09049426460520 0.10333032107753 0.34110595332373 0.16645332637955
Q46	0.17453292222222 0.96974954054482 -0.63013258779589 0.81053001408902 1.11027999914866
Q47	0.59886574233778 -0.18227376661255 0.70868301179415 -0.58455194949263 -0.20402270814462
Q48	-0.04248365125991 -0.05406582509847 -0.01254422443112 0.01844322521394 -0.03856013761685
Q49	-0.57938171074149 -0.04336507268005 -1.11505553399342 0.41329600114029 -0.48511918715936

Table A.2 Optimum control points

GT1	0.89538780050841 1.13152618709349 1.38893609636305 1.86083683064535 1.98813480780975
GT2	-0.00976331011939 -0.04479366427848 0.03576995025107 -0.01005655605143 0.00876331011939
GT3	-0.00631839005266 0.01567300711992 0.05413065581941 -0.01738401075654 -0.00558512142460
GR1	-0.14272531280230 -0.39084122306135 0.28585760304941 0.01008180582490 0.14372531280230
GR2	0.01745329222222 -0.03350741778841 0.20091277764065 0.04485104231311 0.01745329222222
GR3	-0.14146225070588 0.07068807542924 0.08696234884286 0.25473967392424 0.14046225070588
Q01	0.05218180108066 -0.19459002357053 0.03257167950421 -0.18610156965393 -0.05318180108076

Table A.2 Continued

Q02	0.01750041611122 0.01775421090483 0.01761294515803 0.01742834583720 0.01760763679475
Q03	0.06297176830462 -0.06362026851431 -0.07290134304350 -0.13209407898452 -0.06397176830456
Q04	0.05734154794640 0.32694612839502 -0.21608298319729 0.08678751699642 -0.05834154794569
Q05	0.01750041611096 0.02050496009343 0.01844458849774 0.01683995251320 0.01850041611091
Q06	0.01645329222244 0.02627744025446 -0.02965212463635 -0.01212073413652 -0.01745329222244
Q07	0.03151339620673 0.44636396680906 -0.23168083202578 0.19091031249398 -0.03251339620674
Q08	0.01776217092438 0.02156457934715 0.01864659493204 0.01667208801277 0.01876217092449

Table A.2 Continued

Q09	0.01156128056179 -0.01757263348797 0.01743462216583 -0.02629140496493 -0.01056128056176
Q10	0.01724995264636 -0.08938598089600 0.07403000083437 -0.07571193369943 -0.01824995264640
Q11	0.03625980631416 0.08915823904690 0.02523424711799 0.00873340262044 0.03725980631445
Q12	0.01673967049056 -0.01012210182482 0.05855742366240 -0.03024633395984 -0.01573967049056
Q13	0.00091103633109 -0.00407524685492 0.00568477640108 -0.00257344823284 0.00012221680274
Q14	-0.00100007364424 0.00012972025887 0.00291778410183 -0.00202001792245 -0.00018763437118
Q15	0.00321839292068 -0.03655103260166 0.05374405023368 -0.02361018915746 -0.00218513978677

Table A.2 Continued

Q16	-0.01714369622087 0.01516569554389 0.02797579603647 -0.00035887473655 -0.01745329222222
Q17	-0.11074282738309 -0.08549306102488 -0.14761144825775 -0.08459941457216 -0.10291497504657
Q18	-1.57587204801162 -1.61226026447457 -1.53137670362639 -1.60058094704015 -1.58088589022197
Q19	-0.00189733263878 -0.03329221612178 0.05245597128565 -0.02316789116383 -0.00272608632603
Q20	-0.00306599330376 0.03571915890796 -0.05104912147682 0.02094915233731 0.00676653166953
Q21	0.00392868587817 0.01265737763051 0.01488263005415 -0.01477635571841 -0.00855105828794
Q22	-0.00087778319726 0.00404927774126 -0.00565909962204 0.00255332582411 -0.00008896366891

Table A.2 Continued

Q23	-0.00100007364433 0.00232375025189 0.00058127275599 -0.00136900180572 -0.00080328346504
Q24	-0.00318513978680 0.03652506348836 -0.05371837345467 0.02359006674870 0.00221839292074
Q25	-0.01645329222222 -0.04812089342519 0.08242019303865 -0.03349842879474 -0.01614369622087
Q26	-0.10191497504661 -0.13585041322866 -0.06049869206767 -0.12338148764466 -0.10974282738310
Q27	-1.58188589022189 -1.54538853025853 -1.62850849255382 -1.55732102521562 -1.57687204801161
Q28	-0.00372608632603 0.03415809138804 -0.04406086820359 0.01396497239877 -0.00289733263878
Q29	0.00576653166937 -0.02065179512690 0.04866541762684 -0.02299293825563 -0.00206599330371

Table A.2 Continued

Q30	-0.00955105828794 0.00193103424109 0.02306006428906 -0.00172341894097 0.00301927807128
Q31	-0.02969430808868 -0.03329476785321 -0.03038988145438 0.02671296676198 0.02869430808849
Q32	-0.08381693526199 -0.07604776466440 -0.08972608822292 -0.08704296703706 -0.08281693526199
Q33	0.08581391253817 0.06268965232758 -0.03798499720602 -0.09730806948948 -0.08481391253817
Q34	0.00768207463849 -0.12252323520200 0.17705607530711 -0.07674999386868 -0.00668207463864
Q35	-0.00811662500546 0.00942525347229 -0.02399070211080 -0.01660488410062 -0.00711662500546
Q36	0.03407355288516 0.50522341192108 -0.73095698096426 -0.08289438885459 -0.18573731516069

Table A.2 Continued

Q37	0.61121128371901 0.45291790365286 -1.60761311404865 -0.39299518791835 -0.44953326154569
Q38	0.19170901494200 -0.17289335662749 -0.29425633528547 -0.24335947334807 -0.11916743911679
Q39	0.80122868550153 1.41925819671311 3.11414820696360 -0.27074410283914 0.20507540377296
Q40	-0.32145370593117 0.14993969980615 -0.51388859131094 1.13795210477267 0.61654724050478
Q41	-0.01974111426238 -0.06590321774779 0.02781842421357 -0.00085754634061 -0.00596138051892
Q42	-0.72457694806582 -2.04936727336890 0.70500372896559 -0.99888167931527 -0.62694313203832
Q43	-0.18673731516071 -0.37765214703018 0.43156797573884 -0.21857989283478 0.03507355288510

Table A.2 Continued

Q44	-0.45053326154569 -0.55545336701177 0.18984154628230 0.69540354845520 0.61021128371903
Q45	-0.12016743911679 0.11039573604230 0.08005693306543 0.38907600108657 0.19270901494200
Q46	0.20407540377296 1.08781937589440 -0.34515790117474 0.46940093185719 0.80222868550134
Q47	0.61554724050478 -0.35285525297743 0.97836030157116 -0.57423829218258 -0.32045370593117
Q48	-0.00496138051892 -0.01436075557965 -0.05424538458800 0.00615803522153 -0.01874111426238
Q49	-0.62594313203832 0.06472071020561 -1.36064306292761 -0.01027094358668 -0.72357694806582

Table A.3 Active constraints

Active constraint	Time (s)	Lagr multiplier
Joint limit global_rotate_x	0	9.7824E-03
Joint limit spine_1_2	0	2.2812E-03
Joint limit spine_2_2	0	2.0250E-03
Joint limit right_clavicle_2	0	2.1842E-04
Joint limit left_clavicle_2	0	1.0340E-03
Joint limit spine_3_1	0.0792	-3.1286E-03
Joint limit right_clavicle_1	0.0792	1.7424E-03
Joint limit right_shoulder_1	0.0792	1.5412E-03
Joint limit right_elbow_1	0.0792	6.3154E-04
Joint limit right_elbow_2	0.0792	1.4363E-04
Joint limit right_wrist_1	0.0792	-2.2833E-04
Joint limit right_wrist_2	0.0792	-2.2276E-05
Joint limit left_clavicle_1	0.0792	-2.3620E-03
Joint limit left_shoulder_1	0.0792	-1.4652E-03
Joint limit left_shoulder_2	0.0792	1.3197E-03
Joint limit left_shoulder_3	0.0792	8.3414E-04
Joint limit left_elbow_1	0.0792	-1.6342E-03
Joint limit left_elbow_2	0.0792	-1.1947E-04
Joint limit head_2_1	0.0792	4.6168E-04
Joint limit right_clavicle_2	0.1583	-2.3792E-04

Table A.3 Continued

Joint limit right_shoulder_2	0.1583	-1.7350E-03
Joint limit left_clavicle_2	0.1583	-4.5130E-04
Joint limit left_wrist_2	0.1583	-6.9214E-05
Joint limit right_clavicle_1	0.2375	-2.6581E-03
Joint limit right_shoulder_1	0.2375	-1.8904E-03
Joint limit right_elbow_2	0.2375	-1.8131E-04
Joint limit right_wrist_1	0.2375	1.1809E-04
Joint limit left_clavicle_1	0.2375	8.0753E-04
Joint limit left_shoulder_1	0.2375	9.3232E-04
Joint limit left_elbow_1	0.2375	4.8875E-04
Joint limit left_wrist_2	0.2375	-4.1186E-05
Joint limit left_knee	0.2375	3.5847E-03
Joint limit spine_1_2	0.2802	3.1036E-03
Joint limit spine_2_2	0.2802	4.4268E-03
Joint limit spine_3_2	0.2802	4.3339E-03
Joint limit spine_3_2	0.2802	5.7777E-03
Joint limit head_1_2	0.2802	9.8041E-04
Joint limit spine_1_2	0.3228	6.7603E-03
Joint limit spine_2_2	0.3228	3.0499E-03
Joint limit spine_3_2	0.3228	2.1281E-03
Joint limit spine_3_3	0.3228	2.7685E-03

Table A.3 Continued

Joint limit spine_4_3	0.3228	1.4323E-03
Joint limit right clavicle_1	0.3228	2.9841E-03
Joint limit right clavicle_2	0.3228	8.4929E-04
Joint limit right shoulder_1	0.3228	1.8377E-03
Joint limit right shoulder_3	0.3228	-8.2682E-04
Joint limit right_elbow_1	0.3228	1.2073E-03
Joint limit right_elbow_2	0.3228	1.7394E-04
Joint limit right_wrist_1	0.3228	-1.9130E-05
Joint limit right_wrist_2	0.3228	8.3437E-05
Joint limit left_clavicle_1	0.3228	-1.3365E-03
Joint limit left_clavicle_2	0.3228	6.0432E-04
Joint limit left_shoulder_1	0.3228	-1.5554E-03
Joint limit left_shoulder_3	0.3228	4.9127E-04
Joint limit left_elbow_1	0.3228	-8.5494E-04
Joint limit left_wrist_1	0.3228	2.9739E-04
Joint limit head_1_3	0.3228	7.7371E-05
Joint limit left_ankle_1	0.3228	1.6640E-03
Joint limit global_rotate_x	0.3654	2.3989E-03
Joint limit spine_2_3	0.3654	1.1680E-03
Joint limit right_shoulder_2	0.3654	2.5954E-03
Ground penetration	0	-3.1974E-02

Table A.3 Continued

Ground penetration	0.0792	-3.5833E-03
Ground penetration	0.0792	5.0929E-02
Ground penetration	0.0792	-1.7611E-02
Ground penetration	0.1583	2.0897E-02
Ground penetration	0.3654	-4.6264E-03
Ground penetration	0.3654	-1.7257E-02
No slip constraint	0	-2.0903E-02
No slip constraint	0	-1.4112E-02
No slip constraint	0.0792	-5.1721E-05
No slip constraint	0.0792	-2.8788E-02
No slip constraint	0.1583	-3.4695E-02
No slip constraint	0.3654	-1.9707E-02
No slip constraint	0.3654	9.9564E-15
Foot location	0.0792	-3.7259E-01
Foot location	0.3654	-1.1364E-02
Initial rear heel position	0	-3.7856E-02
Torque limit left_ankle_1	0.1583	-4.1415E-05
Symm q global_trans_x	0	1.0076E-03
Symm q global_rotate_z	0	-5.0680E-04
Symm q global_rotate_y	0	1.5378E-02
Symm q spine_1_1	0	6.0983E-03

Table A.3 Continued

Symm q spine_1_2	0	-3.1469E-03
Symm q spine_1_3	0	5.5009E-04
Symm q spine_2_1	0	6.4966E-04
Symm q spine_2_2	0	3.2699E-03
Symm q spine_2_3	0	1.2387E-04
Symm q spine_3_1	0	1.0953E-03
Symm q spine_3_2	0	8.7787E-04
Symm q spine_3_3	0	1.1207E-02
Symm q spine_4_1	0	4.3543E-04
Symm q spine_4_2	0	5.2742E-03
Symm q right_clavicle_1	0	-3.9946E-04
Symm q right_clavicle_2	0	-2.0285E-04
Symm q right_shoulder_1	0	4.0611E-03
Symm q right_shoulder_3	0	1.1830E-02
Symm q right_elbow_1	0	2.4317E-03
Symm q right_wrist_1	0	5.0117E-03
Symm q right_wrist_2	0	3.4483E-03
Symm q left_clavicle_2	0	-4.4704E-03
Symm q left_shoulder_1	0	1.1893E-03
Symm q left_shoulder_2	0	1.2475E-03
Symm q left_shoulder_3	0	-1.3449E-03

Table A.3 Continued

Symm q left_elbow_1	0	-1.0464E-03
Symm q left_wrist_1	0	-1.0449E-03
Symm q head_1_1	0	3.3266E-04
Symm q head_1_2	0	-6.6836E-04
Symm q head_1_3	0	-5.6923E-05
Symm q head_2_1	0	1.5212E-04
Symm q right_hip_1	0	1.8021E-03
Symm q right_hip_3	0	1.0628E-03
Symm q right_knee	0	-1.0659E-04
Symm q right_ankle_1	0	-8.3438E-04
Symm q right_ankle_2	0	1.2332E-03
Symm q right_toe	0	7.1506E-05
Symm q left_hip_1	0	1.9970E-05
Symm q left_hip_2	0	6.4310E-05
Symm q left_hip_3	0	1.8560E-04
Symm q left_knee	0	3.8131E-04
Symm q left_ankle_1	0	-5.5286E-04
Symm q left_ankle_2	0	-1.4251E-04
Symm q left_toe	0	3.1911E-04
Symm v global_trans_y	0	-4.3310E-03
Symm v global_rotate_z	0	-5.3951E-04

Table A.3 Continued

Symm v global_rotate_x	0	3.6748E-03
Symm v global_rotate_y	0	5.0364E-04
Symm v spine_1_1	0	-1.5847E-04
Symm v spine_1_2	0	1.2321E-03
Symm v spine_1_3	0	-4.4475E-05
Symm v spine_2_1	0	2.7693E-04
Symm v spine_2_2	0	-2.7258E-05
Symm v spine_2_3	0	-4.4886E-07
Symm v spine_3_1	0	1.0670E-05
Symm v spine_3_2	0	-5.8049E-06
Symm v spine_4_3	0	1.0338E-04
Symm v right_clavicle_2	0	1.9852E-05
Symm v right_shoulder_1	0	-7.9663E-05
Symm v right_shoulder_2	0	1.6681E-03
Symm v right_shoulder_3	0	6.8531E-04
Symm v right_elbow_1	0	-1.1558E-05
Symm v right_elbow_2	0	1.6889E-03
Symm v right_wrist_1	0	2.1134E-04
Symm v right_wrist_2	0	7.6615E-05
Symm v left_clavicle_1	0	1.4803E-03
Symm v left_clavicle_2	0	-2.9351E-04

Table A.3 Continued

Symm v left_shoulder_2	0	1.3170E-03
Symm v left_shoulder_3	0	-1.8952E-04
Symm v left_elbow_1	0	9.8427E-05
Symm v left_elbow_2	0	-1.2531E-05
Symm v left_wrist_1	0	2.4691E-05
Symm v left_wrist_2	0	-8.9922E-05
Symm v head_1_2	0	1.0674E-04
Symm v head_1_3	0	4.3029E-06
Symm v head_2_1	0	3.4824E-05
Symm v head_2_2	0	1.0672E-06
Symm v right_hip_1	0	1.2068E-04
Symm v right_hip_2	0	9.7770E-05
Symm v right_hip_3	0	4.2799E-05
Symm v right_knee	0	-8.3998E-05
Symm v right_ankle_1	0	-6.2447E-05
Symm v right_ankle_2	0	1.2426E-04
Symm v right_toe	0	2.9802E-06
Symm v left_hip_1	0	2.9183E-05
Symm v left_hip_2	0	9.9260E-06
Symm v left_knee	0	4.1759E-04
Symm v left_ankle_1	0	-3.7906E-05

Table A.3 Continued

Symm v left_ankle_2	0	1.8023E-05
Symm v left_toe	0	3.0074E-04

REFERENCES

1. Alexander, R. M. 1984. "Walking and running." *American Scientist*, 72, 348-354

2. Arora, J. 2004. *Introduction to Optimum Design 2nd edition*. San Diego, California: Elsevier Academic Press.

3. Atkinson, Kendall E. 1988. *Introduction to Numerical Analysis 2nd edition*. John Wiley & Sons, Inc.

4. Ayoub, M. M. and Lin, C. J. 1995 "Biomechanics of manual material handling through simulation: Computational aspects." *Computers and Industrial Engineering*, 29(1), 427-431.

5. Azevedo, C. Poignet, P. and Espiau, B. 2002. "Moving horizon control for biped robots without reference trajectory." *Proceedings of the IEEE international Conference on Robotics and Automation*, vol. 3, 2762-2767.

6. Bedford, A. and Fowler, W. 2002. *Engineering Mechanics: Dynamics 3rd edition*. Upper Saddle River, New Jersey: Prentice Hall.

7. Bessonnet, G., Sardain, P. and Chessé, S. 2002. "Optimal motion synthesis – dynamic modeling and numerical solving aspects." *Multibody System Dynamics*, 8, 257-278.

8. Bottasso, C., Prilutsky, B. Croce, A. Imberti, E., and Sartirana, S. 2006. "A numerical procedure for inferring from experimental data the optimization cost functions using a Multibody model of the neuro-musculoskeletal system." *Multibody System Dynamics*, 16, 123-154.

9. Bruderlin, A. and Calvert, T. 1996. "Knowledge-driven, interactive animation of human running." *Proceedings of the Conference on Graphics Interface*, 213-221.

10. Cavanagh, P. 1990. *Biomechanics of distance running*. Champaign: Human Kinetics Publishers.

11. Cavanagh, P. and Lafortune, M. 1980. "Ground reaction forces in distance running." *Journal of biomechanics*, 13, 397-406.

12. Chaffin, D. B. and Andersson, G. B. J. 1984. *Occupational Biomechanics*. New York: John Wiley & Sons, Inc.

13. Chevallereau, C. and Aoustin, Y. 2001. "Optimal reference trajectories for walking and running of a biped robot." *Robotica*, 19, 557-569.

14. Chung, H. J., Xiang, Y. Mathai, A., Rahmatalla, S., Kim, J., Marler, T., Beck, S., Yang, J., Arora, J. Abdel-Malek, K. and Obusek, J. 2007. "A robust formulation for

prediction of human running.' *Proceedings of the Digital Human Modeling Conference*.

15. Collins, S., Adamczyk, P., and Kuo, A. 2009. "Dynamic arm swinging in human walking." *Proceedings of the Royal Society - Biological Sciences*, 3679-3688.

16. Craig, J. 1986 *Introduction to Robotics: Mechanics & Control*. Addison-Wesley Publishing Company.

17. De Boor, C. 2001. *A Practical Guide to Splines. revised edition*. New York: Springer.

18. Denavit, J. and Hartenberg, R. S. 1955. "A kinematic notation for lower-pair mechanisms based on matrices." *ASME Journal of Applied Mechanics*, 22, 215–221.

19. Dillman, C. 1975. "Kinematic analysis of running." *Exercise and Sport Sciences Reviews 3*, 193-218.

20. François, C. and Samson, C. 1994. "Running with constant energy." *IEEE International Conference on Robotics and Automation*, 1, 131-136.

21. Fujimoto, Y. 2004. "Trajectory generation of biped running robot with minimum energy consumption." *Proceedings of the IEEE international Conference on Robotics and Automation*, vol. 4, 3803-3808.

22. Fujimoto, Y. 2004. "Minimum energy biped running gait and development of energy regeneration leg." *The 8th IEEE International Workshop on Advanced Motion Control*, 415-420.

23. Gienger, M., Löffler, K., Pfeiffer, F. 2000. "A biped robot that jogs." *IEEE International Conference on Robotics and Automation*.

24. Gill, P. E., Murray, W. and Wright, M. H. 1981. *Practical Optimization*. New York: Academic Press.

25. Greenwood, D. T. 1977. *Classical Dynamics*. Englewood Cliffs, N.J.: Prentice Hall.

26. Haug, Edward J. 1989. Computer Aided Kinematics and Dynamics of Mechanical System. Boston: Allyn and Bacon.

27. Hamill, J., Derrick, T. R. and Holt, K. G. 1995. "Shock attenuation and stride frequency during running." *Human Movement Science*, vol. 14, 45-60.

28. Hardin, E. C., Van Den Bogert, A. J. and Hamill, J. 2004. "Kinematic adaptations during running: effects of footwear, surface, and duration." *Medicine and Science in Sports and Exercese*, vol. 36, no. 5, 838-844.

29. Hirai, K., Hirose, M., Haikawa, Y., and Takenaka, T. 1998. "The development of Honda humanoid robot." *Proceedings of the IEEE international Conference on Robotics and Automation*, vol. 2, 1321-1326.

30. Hodgins, J. K., and Raibert, M. N. 1991. "Adjusting step length for rough terrain locomotion." *IEEE Transactions on Robotics and Automation*, vol. 7(3), 289-298

31. Hodgins, J. 1996. "Three-dimensional human running." *Proceedings of the International Conference on Robotics and Automation*. vol. 4, 3271-3276.

32. Högberg, P. 1952. "Length of stride, stride frequency, "flight" period and maximum distance between the feet during running with different speed." *Arbeitsphysiologie 14*, 431-436.

33. Hollerbach, J. 1980. "A recursive Lagrangian formulation of manipulator dynamics and a comparative study of dynamics formulation complexity." *IEEE Trans. Systems, Man, and Cybernetics*, 10, 730-736.

34. Hurmuzlu, Y. 1993. "Dynamics of bipedal gait: part 1 – objective functions and the contact event of a planar five-link biped." *Journal of Applied Mechanics*, 60, 331-336.

35. Kajita, S., Nagasaki, T., Kaneko, K., Yokoi, K. and Tanie, K. 2005. "A running controller of humanoid biped HRP-2LR" *Proceedings of the IEEE International Conference on Robotics and Automation*, 616-622.

36. Kajita, S., Kaneko, K., Morisawa, M., Nakaoka, S., and Hirukawa, H. 2007. "ZMP-based Biped Running Enhanced by Toe Spring" *Proceedings of the IEEE International conference on Robotics and Automation*, 3963-3969.

37. Kajita, S., Nagasaki, T., Kaneko, K., and Hirukawa, H. 2007. "ZMP-based Biped Running Control" *IEEE Robotics and Automation Magagine*, 63-72.

38. Kang, Y., Cho, H. and Lee, E. 1999. "An efficient control over human running animation with extension of planar hopper model." The Journal of Visualization and Computer Animation, 10, 215-224.

39. Kawamura, A., Sugio, K., Suzuki, K. and Zhu, C. 2004. "Simulation study on one leg jumping for biped running", *The 8th IEEE International Workshop on Advanced Motion Control*, 433-438.

40. Kim, H., Horn, E., Xiang, Y., Malek, K. and Arora, J. 2004. "Digital human modeling and virtual reality for FCS: Dynamic motion prediction of gait and lifting." Technical Report, Virtual Soldier Research Lab, The University of Iowa.

41. Kim, Y., Lee, B., Yoo, J., Choi, S. and Kim, J. 2005. "Humanoid Robot HanSaRam: Yawing moment cancellation and ZMP compensation." *Proceedings of the Second American University of Sharjah International Symposium on Mechatronics.*

42. Lo, J., Huang, G. and Metaxas, D. 2002. "Human motion planning based on recursive dynamics and optimal control techniques." *Multibody System Dynamics*, 8, 433-458.

43. McKerrow, P. 1991. *Introduction to Robotics*. Addison-Wesley Publishing Company.

44. McMahon, T. A., Valiant, G. and Frederick E. C. 1987. "Groucho running." *Journal of Applied Physiology*, 63 (6), 2141-2542.

45. Munro, C., Miller, D., and Fuglevand, A. 1987. "Ground reaction forces in running: a reexamination." *Journal of Biomechanics*, 20(2), 147-155.

46. Nagasaka, K., Kuroki, Y., Suzuki, S., Itoh, Y. and Yamaguchi, J. 2004. "Integrated motion control for walking, jumping and running on a small bipedal entertainment robot." *Proceedings of the IEEE International Conference on Robotics and Automation*, vol. 4, 3189-3194.

47. Nagasaki, T., Kajita, S., Yokoi, K., Kaneko, K. and Tanie, K. 2003. "Running pattern generation and its evaluation using a realistic humanoid model." *Proceedings of the IEEE International Conference on Robotics and Automation*, vol. 1, 1336-1342.

48. Nilsson, J., Thorstensson, A. and Harbertsma, J. 1985. "Changes in leg movements and muscle activity with speed of locomotion and mode of progression in humans." *Acta Physiologica Scandinavica*, 123(4), 457-475.

49. Norkin, C. C. and White, D. J. 2003. *Measurement of Joint Motion: A Guide to Goniometry, 3rd Edition.* Philadelphia: F. A. Davis Co.

50. Novacheck, T. 1998. "Review paper: The biomechanics of running." Gait and Posture, 7, 77-95.

51. Õunpuu, S. 1994. "The biomechanics of walking and running." *Clinics in Sports Medicine*, 13(4), 843-863.

52. Park, J. and Kwon, O. 2003. "Impedance control for running of biped robots." *Proceedings of the IEEE/ASME International Conference on Advanced Intelligent Mechatronics*, 2, 944-949.

53. Patla, A. E., Robinson, C., Samways, M., and Armstrong, C. J. 1989. "Visual control of step length during overground locomotion: task-specific modulation of the locomotor synergy." *Journal of Experimental Psychology*, Vol. 15, No. 3, 603-617.

54. Perry, J. 1992. *Gait Analysis: Normal and Pathological Function.* Thorofare, NJ: Slack Inc.

55. Prautzsch, H., Boehm, W. and Paluszny, M. 2002. *Bézier and B-spline Techniques*. Berlin; New York: Springer.

56. Raibert, M. H. 1986. *Legged Robots that Balance*. Cambridge, Mass.: MIT Press.

57. Ren, L, Jones, R. K., and Howard, D. 2007. "Predictive modelling of human walking over a complete gait cycle." *Journal of Biomechanics*, 40, 1567-1574.

58. Roussel, L., Canuda-de-Wit, C. and Goswami, A. 1998. "Generation of energy optimal complete gait cycles for biped robots." *Proceedings of the IEEE International Conference on Robotics and Automation*, 3, 2036-2041.

59. Sardain, P. and Bessonnet, G. 2004. "Forces acting on a biped robot. Center of pressure – Zero moment point." *IEEE Transaction on Systems, Man, and Cybernetics – Part A: Systems and Humans*, 3(5), 630-637.

60. Shin, H. and Park, J. 2008. "ZMP-based biped running pattern generation with contact transition of foot." *Proceedings of 2008 IEEE/ASME International Conferece on Advanced Intelligent Mechatronics*, 916-921.

61. Simpson, K. and Bates, B. 1990. "The effects of running speed on lower extremity joint moments generated during the support phase." *International Journal of Sport Biomechanics*, 6, 309-324.

62. Toogood, R.W. 1989. "Efficient robot inverse and direct dynamics algorithms using micro-computer based symbolic generation." *Proceedings of IEEE International Conference on Robotics and Automation*, 3, 1827-1832.

63. Uicker, J. J. 1965. "On the dynamic analysis of spatial linkages using 4 × 4 matrices." *Ph.D. Dissertation, Northwestern University.*

64. Vukobratović, M., Borovac, B., Surla, D. and Stokić, D. 1990. *Scientific Fundamentals of Robots 7: Biped Locomotion – Dynamics, Stability, Control and Application*. Berlin; New York: Springer-Verlag.

65. Vukobratović, M. and Borovac, B. 2004. "Zero-moment point – thirty five years of its life." *International Journal of Humanoid Robotics*, 1(1), 157-173.

66. Warren, W. H. Jr., and Yaffe, D. M. 1989. "Dynamics of step length adjustment during running: a comment on Patla, Robinson, Samways, and Armstrong." *Journal of Experimental Psychology*, 15 (3), 618-623.

67. Waters, R. C. 1979. "Mechanical arm control." M.I.T. Artivicial Intelligence Lab. Memo. 549.

68. Westervelt, E. R. and Grizzle, J. W. 2003. "Hybrid zero dynamics of planar biped walkers." *The University of Pennsylvania, Department of Electrical and Systems Engineering, Departmental Paper*.

69. Williams, K. R. and Cavanagh, P. R. 1987. "Relationship between distance running mechanics, running economy, and performance." *Journal of Applied Physiology*, 63 (3), 1236-1245.

70. Winter, D. 2005. *Biomechanics and Motor Control of Human Movement. 3rd edition.* Hoboken, New Jersey: John Wiley & Sons, Inc.

71. Witkin, A. and Kass, M. 1988. "Spacetime constraints." Computer Graphics, vol. 22(4), 159-168.

72. Xiang, Y., Chung, H. J., Mathai, A., Rahmatalla, S., Kim, J., Marler, T., Beck, S., Yang, J., Arora, J. S. and Abdel-Malek, K. 2007. "Optimization-based dynamic human walking prediction." *Proceedings of the Digital Human Modeling Conference*.

73. Xiang, Y., Arora, J., Rahmatalla, S., and Abdel-Malek, K. 2009. "Optimization-based dynamic human walking prediction: One step formulation." *International Journal for Numerical Methods in Engineering*, vol. 79, 667-695.

74. Xiang, Y., Chung, H. J., Kim, J. H, Bhatt, R., Rahmatalla, S., Yang, J., Marler, T., Arora, J., Abdel-Malek, K. 2009. "Predictive dynamics: an optimization-based novel approach for human motion simulation." *Structural and Multidisciplinary Optimization*.

75. Zheng, Y. F. and Hemami, H. 1984. "Impact effects of biped contact with environment." *IEEE Transactions on Systems, Man, and Cybernetics*, SMC-14(3), 437-443.